The mechanism of the ferrous iron transport system (Feo): interaction of FeoC with the C-terminal region of FeoB

A thesis submitted for the degree of Doctor of Philosophy

By
Othman Abdulrahman Althobaiti
Student ID: 27831621

Supervision by
Professor Simon C. Andrews

Division of Biomedical Science & Biomedical Engineering
School of Biological Sciences
The University of Reading
UK
October 2025

Dedication

I would like to dedicate this thesis to my beloved family, my parents for their love and guidance, my siblings for their support, my wife for her patience and encouragement; my son and my twin daughters whose joy inspires me every day.

Declaration

I declare that the work presented in this thesis is my own work and all sources of information, data and ideas that are not my own have been fully acknowledged and referenced according to academic standards.

Signed: Othman Abdulrahman Othman Althobaiti

Date: 29 October 2025

Acknowledgments

بسم الله الرحمن الرحيم

(In the name of Allah, the most beneficent, the most merciful)

Firstly, I would like to thank **Allah** who has provided me with good health and ability to complete this work.

I am extremely gratitude and appreciation to my supervisor, **Prof Simon C Andrews** for his continuous help, support, patience, valuable guidance, encouragement during my PhD journey. Also, I would like to say that I am very delighted and proud to have had the chance to work under his supervision.

I would like to thank my supervisory committee members, **Dr. Simon Clarke** and **Dr. Glyn Barrett** for their academic guidance and valuable comments in this research. Also, I would like to thank **Dr. Jay Mulley** to be as second supervisor.

I would like to express my deepest thankfulness and love to all **my family** for their support through my PhD journey. I extend my gratitude to **my wife** for her patience and continuous help during this journey. My heartfelt thanks go to my son (**Abdulrahman**), and my twin daughters (**Elan and Layan**) whose happiness and laughter are a daily source of inspiration and strength.

I gratefully acknowledge the **Ministry of Education in Saudi Arabia** and **Taif University** for giving me the opportunity to complete this work and their support and financial assistance during this journey.

Lastly, I would like to thank **all** who have helped me throughout this journey.

Abstract

Iron is an essential element, but can also be toxic aerobically through the production of oxidizing free radicals. Two major types of iron are found in biological systems, the ferrous (Fe^{2+}) and ferric (Fe^{3+}) forms. The *feo* operon, found in many bacteria, encodes a ferrous-iron uptake pathway that functions under anaerobic conditions. The *feoABC* operon of *Escherichia coli* specifies three components: FeoA, a small cytosolic protein absolutely required for FeoB activity; FeoB, the major component consisting of an N-terminal G-protein domain in the cytoplasm and a C-terminal ferrous-permease domain embedded in the cytoplasmic membrane; and FeoC, a small Fe-S protein reported to control FeoB stability in response to oxygen and mainly only associated with the FeoAB system of facultative Enterobacteriaceae. This work consists of three results chapters. The first results chapter explores the role of FeoC on the iron-uptake activity of the Feo system by performing growth comparison of an iron-uptake mutant, aerobically and anaerobically, under a range of iron-restriction conditions in the presence and absence of induced *feoAB* or *feoABC*. The results showed a clear role of FeoC in supporting iron-uptake activity under aerobic reducing conditions in the presence of DTPA for strains producing FeoAB as the sole dedicated iron uptake pathway. However, the results with single-gene D*feoA*, D*feoB* and D*feoC* mutants did not show any distinct role of *feoC* in supporting Feo-dependent under iron-restricted growth aerobically; all the mutants gave similar strong growth restrictions under low-iron conditions both aerobically and anaerobically with reductant, buffer at pH 6 and chelator. Under anaerobic conditions in the presence or absence of iron, the *feoAB*/*ABC* constructs and the mutants (Δ*feoA*, Δ*feoB* and Δ*feoC*) showed no role for FeoC in supporting FeoAB-mediated iron uptake. The second results chapter focused on the role of the C-terminal region of FeoB (which is largely unique to the Enterobacteriaceae) in supporting FeoC-dependent enhanced Feo iron-uptake activity through protein-protein interaction. The research was divided into two parts. Firstly, introduction of a series of truncations in the C-terminal region of FeoB (CFeoB) using pBADara-*feoAB*/*ABC* constructs subjected to site-directed mutagenesis. The mutants were tested under iron-restricted growth aerobically. The results illustrated that the unmutated *feoABC* construct provides a clear growth advantage with respect to *feoAB* and the vector control under aerobic iron-restricted conditions with DTPA and MES. The CFeoB truncations had an overall negative impact on Feo-dependent growth for both the FeoAB and FeoABC strains. In the second part, the CFeoB region was expressed from pBADrha in three formats; Flag tag-CFeoB; CFeoB-Flag tag; CFeoB without any Flag tag. All the Flag tag versions were transferred into the pBADara-

feoAB/*feoABC* to determine any effect of CFeoB expression on FeoAB-dependent aerobic and iron-restricted growth in the presence and absence of FeoC. The results showed that in the presence of DTPA, clear growth advantage for the FeoABC strain which indicates to the role of FeoC-enhancement of the Feo activity. The CFeoB constructs caused a reduction in the growth of the FeoABC strain which was significant in two cases. CFeoB also caused a slight overall reduction in the FeoAB-supported growth. The findings suggest that the FeoC enhancement of FeoAB dependent aerobic, iron-restricted growth can be inhibited by provision of CFeoB in Flag tagged form. This is consistent with the proposed interaction of FeoC with the CFeoB region of FeoB. In the third results chapter, the impact of FeoC (and FeoAB) on global gene expression was explored by RNAseq in the absence of iron but with ascorbate and with iron but without ascorbate, at two time points (OD 0.5. and 0.8/1.0). With ascorbate at OD 0.5, FeoAB-induced 13 genes involved in anaerobic nitrite/nitrate respiration and repressed eight and seven genes for tRNA and amino acid biosynthesis, respectively. At OD 0.8 with ascorbate, FeoAB induced nine and eight genes involved in amino acid generation and carbon catabolism, respectively, and 16 and eight genes involved in amino acid biosynthesis and nucleotide metabolism, respectively. With iron at OD 0.5, FeoAB induced 17 genes related to anaerobic energy generation and repressed 32 genes involved in combating iron restriction. At OD 1.0 with iron, FeoAB induced 12 genes involved in anaerobic energy generation and repressed 25 genes involved in combating iron restriction. The results obtained for FeoABC-dependent global expression were generally similar to those for FeoAB, and together clearly indicated that *feoAB*/*feoABC* induction promotes large scale changes in the expression of genes involved in iron homeostasis in the presence of iron suggesting that Feo induction promotes excess iron accumulation resulting in enhanced Fe-Fur regulatory activity.

Differential expression between the *feoAB* and *feoABC* strains allowed the effect of *feoC* on expression to be considered. With ascorbate at OD 0.5, FeoC induced three genes involved in carbon metabolism and repressed 13 genes involved in anaerobic energy generation, whereas at OD 0.8 three genes involved in amino acid metabolism were induced and cold shock genes were repressed. At OD 0.5 with iron, FeoC induced six genes involved in amino acid metabolism and carbon metabolism, and repressed seven and four genes involved in cysteine biosynthesis (and sulphur assimilation) and motility, respectively. At OD 1.0 FeoC induced seven genes involved in amino acid metabolism and repressed six genes associated with combating iron restriction. In summary, the results suggest that the Feo system may influence the regulation of genes involved in anerobic energy generation, in particular those associated

nitrate/nitrite respiration. The impact of FeoC on Fur-dependent gene control may be related to its role in enhancing FeoAB iron uptake activity.

Table of Contents

List of Figures

List of tables

Chapter 1: Background

1.1 *Escherichia coli*

1.1.1 History of *E. coli*

Escherichia coli is a Gram-negative, rod-shaped bacterium that is able to grow without oxygen, and is thus a facultative anaerobe (Lim, Yoon and Hovde, 2010). Theodor Escherich, a German microbiologist and doctor, began researching gut microorganisms in new-borns and their function in digestion and disease in 1884. During his research, he found *Bacterium coli commune*, a quick-growing bacterium that is now known as *Escherichia coli*. The advantages of *E. coli* for biological research are it is easy to work with and can grow rapidly in various media or environments. This species has become a popular bacterium that is used in microbiology applications as well as it can be used in the microbiology teaching laboratory. As a result, when early 20th century microbiologists were looking for a model organism, *E. coli* was one of the most popular options (Blount, 2015).

E. coli is a common member of the gut microbiota for humans and animals. Many *E. coli* strains are classified as safe bacteria as they do not cause disease in humans and animals when colonising their gastrointestinal tracts. But other strains can cause disease and are therefore classified as harmful or pathogenic bacteria. These pathogenic *E. coli* strains can infect humans and animals, and often have developed their pathogenic capacity through horizontal acquisition of virulence factors carried by plasmids and/or bacteriophages. Such pathogenic strains are classified through serotyping, according to the manner in which they infect their hosts and treatment required, the resulting disease symptoms, or the virulence factors carried (Nataro and Kaper, 1998).

1.1.2 General features of *E. coli*

E. coli is commonly employed as a model organism for understanding biological mechanisms and is utilised universally as a cloning host in recombinant DNA technology. The reasons for

its popularity as an experimental aid are related to the advantages that it offers with respect to other bacteria: it is easy to propagate; its genome sequence was obtained early; many genetic tools are now available; it is well studied and understood; and it grows both aerobically and anaerobically. These advantages have led to its adoption as a host organism for use in biotechnology, manufacture and medical research. *E. coli* can be grown at various temperatures, from 20 to 40 °C (Kumar and Libchaber, 2013), with 37 °C considered the optimum (Noor *et al.*, 2013).

1.1.3 The taxonomy of *E. coli*

E. coli strains were initially identified serologically according to the O (lipopolysaccharide, LPS), H (flagellar) and K (capsule) antigens (Allocati *et al.*, 2013). Presently, serotyping of *E. coli* has found 53 and 67 types of H and K antigens, respectively, with around 186 O serotypes (Denamur *et al.*, 2021). *E. coli* is also classified by phylotyping, using methods such as restriction digestion, multiplex PCR and multi-locus sequencing typing (MLST). Such approaches have led to recognition of eight major phylotypes for *E. coli*: A, B1, B2, C, D, E, F and G that differ in their ecology, pathogenicity and host preferences, with phylotypes B2 and D those most commonly associated with humans (Lu *et al.*, 2016).

The *Escherichia* genus now consists of three recognised species: *E. albertii*, *E. fergusonii* and *E. coli*. For the classic *E. coli* strains, five phylogenetic clades are recognised, categorized as I–V, that are distinguished on the basis of nucleotide sequence. Clade III-IV and clade V are considered to represent two new *Escherichia* species, and clade II may also form a distinct species. Most classical *E. coli* strains fall into clade I, which also represents a new suggested *Escherichia* species designation called '*E. coli sensu lato*'. The clade I strains can be further classified into two subspecies consisting of phylogroups A, B1, C and E, and B2, D, F, G and H (Denamur *et al.*, 2021).

1.1.4 Pathotypes of *E. coli* strains and serotypes

As indicated above, some strains can cause serious diseases and indeed *E. coli* is one of the most common bacterial mediators of disease for humans and animals (Kaper et al., 2004). There are seven types of enteric *E. coli* strains that cause disease (Table 1.1) and three extraintestinal pathogenic *E. coli* (ExPEC) strains (Table 1.1) (Kaper *et al.,* 2004). Gut pathogenic strains are generally spread through faecal contamination of food and water.

1.1.4.1 Enteric *E. coli* strains

Enteropathogenic *E. coli* (EPEC) strains cause diarrhoea especially in babies in poor countries and animals, which is often related to poor sanitation conditions (Kaper *et al.,* 2004). EPEC carry a pathogenicity island of ~35 kb called the locus of enterocyte effacement (LEE). This locus encodes the type III secretion system which mediates the characteristic attaching and effacement (AE) lesions within the intestinal epithelium. There is a classification for EPEC based on the presence or absence of the '*E. coli* adherence factor' (EAF) plasmid which encodes bundle-forming pilus (*bfp*). Typical EPEC (tEPEC) are BFP-positive, whereas atypical EPEC BFP-negative (aEPEC) (Croxen and Finlay, 2010). EPEC is regularly found in livestock and wild animals (Denamur *et al.*, 2021).

Enterohemorrhagic *E. coli* (EHEC) generates a toxin called Shiga toxin (Stx). EHEC can cause diseases in humans known as haemorrhagic colitis (HC) and haemolytic uremic syndrome (HUS). EHEC was first identified in 1982 (Lim, Yoon and Hovde, 2010). EHEC can infect man, particularly the large intestine. EHEC releases Shiga toxin, which enters into the bloodstream, spreading the toxin around the body. It binds with globotriaosylceramide-3 (Gb3) on endothelial cells; subsequent internalisation results in inhibition of translation. The human renal glomerular endothelium displays high amounts of Gb3, such that Shiga toxin production causes serious renal failure, thrombocytopenia and microangiopathic haemolytic anaemia, all of which are symptoms of HUS. The Gb3 receptor is absent in cattle, the major reservoir species, and so EHEC colonisation tends to be asymptomatic. The infection

symptoms of the *E. coli* O157:H7 EHEC serotype are stomach discomfort, blood in diarrhoea and the deadly HUS.

Enterotoxigenic *E. coli* (ETEC) is a common cause of infections in tourists (traveller's diarrhoea) leading to light or critical diarrhoea for children, young and old people (Al-Abri, Beeching and Nye, 2005; Qadri *et al.*, 2005). ETEC strains are distinguished by plasmid-encoded heat-labile (LT) and/or heat-stable (ST) enterotoxins. ETEC is the most frequent pathotype of *E. coli* that causes new-born diarrhoea and is the major cause of traveller's diarrhoea in poor countries (Croxen and Finlay, 2010; Aslani *et al.*, 2011). ETEC is found in livestock and wild animals (Denamur *et al.*, 2021).

Enteroaggregative *E. coli* (EAEC) leads to persistent diarrhoea in humans, particularly in babies in poor countries and those with HIV (Nataro and Kaper, 1998; Weintraub, 2007). However, such strains can persist in the intestine without showing any symptoms. EAEC is considered the second most common cause of traveller's diarrhoea, after ETEC. EAEC is characterised by the 'stacked bricks' morphology of cells seen during adherence to HEp-2 cells. Its pathogenicity phenotype is dependent upon its ability to adhere to and aggregate upon the intestinal mucosa and then produce harmful toxins that cause the diarrhoea symptoms. Pathogenicity is linked to a plasmid (pAA) that encodes a number of virulence genes, such as an anti-aggregation protein transporter (CVD432), aggregative adherence fimbria (AAF), and the *aggR* gene, which controls fimbria production (Aslani *et al.*, 2011; Canizalez-Roman *et al.*, 2013).

Diffusely-adherent *E. coli* (DAEC) leads to symptoms of diarrhoea especially for babies (Servin, 2005). A key virulence factor is the fimbrial adhesion systems (Afa, Dr and F1845 adhesins). DAEC is a heterogeneous group characterised by a specific diffuse pattern of adherence (DA) to HeLa and HEp-2 cells (Bautista-De León *et al.*, 2013).

Enteroinvasive *E. coli* (EIEC) causes disease in all ages resulting in liquid diarrhoea and sometimes dysentery (Kaper *et al.,* 2004). EIEC is able to invade colonic epithelial cells, replicate intracellularly and then move into adjacent cells. Its virulence is mechanistically very similar to that of *Shigella* producing invasive and dysenteric diarrhoea in humans and is dependent on the *ipaH* and *virF* genes (Canizalez-Roman *et al.*, 2013). EIEC infects only humans, no animal reservoir is known (Denamur *et al.*, 2021).

Adherent invasive *E. coli* (AIEC) is linked to inflammatory bowel disease (IBD) (Darfeuille-Michaud, 2002; Negroni *et al.*, 2012). AIEC have the ability to attach to and enter intestinal epithelial cells, as well as live and reproduce within macrophages (Chervy, Barnich and Denizot, 2020). AIEC strains identified to infect only humans (Denamur *et al.*, 2021).

Verocytoxin-producing *E. coli* (VTEC) or Shiga-toxin-producing *E. coli* (STEC) are strains producing Shiga toxin or Shiga-like toxin. VTEC infects animals through the oral route. More than 380 VTEC serotypes have been extracted from humans and animals, although only a few serotypes have been associated with human illnesses (known as EHEC). The best-known serotypes of VTEC are *E. coli* O157:H7 (also an EHEC strain) and O104:H4 (also an EHEC and EAEC strain). Such strains are common causes of foodborne infection resulting in gastroenteritis and bloody diarrhoea, and sometimes HUS. Shiga toxins (Stx1 and Stx2) are produced by *Shigella dysenteriae* and VTEC, and consist of two subunit types in AB_5 format. The *stx* genes are carried by lambdoid-type prophages, and are thus readily subject to horizontal gene transfer.

1.1.4.2 Extraintestinal Pathogenic *E. coli* (ExPEC)

ExPEC cause non-intestinal infections and are linked to infections in hospital environments as well as society. **Uropathogenic *E. coli*** (UPEC) is the most common pathotype in this group and causes urinary tract infections (UTI) in humans, being responsible for 80% of UTI cases (Johnson and Stell, 2000; Kaper *et al.,* 2004). **Neonatal meningitis *E. coli*** (NMEC) causes bacterial meningitis in new-borns in poor countries and (like UPEC) is derived from the

gastrointestinal tract (Gaschignard *et al.*, 2011; Pouillot *et al.*, 2012). **Avian pathogenic *E. coli*** (APEC) strains infect birds, causing respiratory and systemic disease. It can also act as a foodborne zoonotic pathogen in man, and displays genetic similarity with other ExPEC types (UPEC and NMEC) (Kathayat *et al.*, 2021).

Table 1.1. Intestinal and Extraintestinal pathogenic *E. coli* strains

Strains that cause illness	Illness caused	Disease signs	Virulence factors	References
Intestinal Pathogenic *E. coli* strains				
Enteropathogenic *E. coli* (EPEC)	Lead to diarrhoea in babies	Caused liquid diarrhoea and puke	Bfp, Intimin, LEE	(Kaper *et al.,* 2004)
Enterohaemorrhagic *E. coli* (EHEC)	inflammation in colon, HUS	Caused blood in diarrhoea	Shiga toxins, Intimin, Bfp	(Kaper *et al.,* 2004) and (Bilinski *et al.*, 2012)
Enterotoxigenic *E. coli* (ETEC)	Caused diarrhoea in tourists	Caused liquid diarrhoea and puke	Heat-labile and sheat-stable toxins, CFAs	(Qadri *et al.*, 2005) and (Al-Abri, Beeching and Nye, 2005)
Enteroaggregative *E. coli* (EAEC)	Lead to diarrhoea in babies	Caused mucus in diarrhoea and puke	AAFs, cytotoxins	(Nataro *et al.,* 1998) and (Weintraub, 2007)
Diffusely Adherent *E. coli* (DAEC)	severe diarrhoea in babies	Caused liquid diarrhoea, and Urinary tract infections (UTIs)	Daa, AIDA	(Servin, 2005)
Entero-invasive *E. coli* (EIEC)	shigella infection	Caused liquid diarrhoea	Shiga toxin, hemolysin, Cellular invasion, Ipa	(Kaper *et al.,* 2004) and (Nataro, Steiner and Guerrant, 1998)
Adherent Invasive *E. coli* (AIEC)	Crohn's disease	Caused inflammation in the digestive tract continuously	Type 1 fimbriae, Cellular invasion	(Darfeuille-Michaud, 2002) and (Negroni *et al.*, 2012)
Extraintestinal Pathogenic *E. coli* (ExPEC)				
Uropathogenic *E. coli* (UPEC)	Urinary tract infections (UTIs) and other infections in whole body.	Caused inflammation in bladder, and kidney infection	Type 1 and P fimbriae; AAFs, hemolysin	(Kaper *et al.,* 2004) and (Johnson and Stell, 2000)
Neonatal Meningitis *E. coli* (NMEC)	Neonatal meningitis	Caused severe meningitis, sepsis	S fimbrie; K1 capsule	(Gaschignard *et al.*, 2011) and (Pouillot *et al.*, 2012)
Avian pathogenic *E. coli* (APEC)	cause disease by the food	-	Type 1 and P fimbriae; K1 capsule	(Johnson *et al.*, 2007) and (Rodriguez-Siek *et al.*, 2005)

Bfp: Bundle-forming pili; LEE: Locus for enterocyte effacement; HUS: haemolytic-uraemic syndrome; CFA: colonization factor antigen; AAF: aggregative adherence fimbria; Daa: diffuse adhesin; AIDA: adhesin involved in diffuse adherence; Ipa: Invasion plasmid antigen. Adapted from Allocati *et al.* (2013).

1.1.5 The *E. coli* genome

The *E. coli* genome is made up of a circular chromosome and plasmids. The genome size of *E. coli* strains ranges from 4.2 to 6.0 Mbp. This corresponds to around 3,900–5,800 genes. The smallest genomes in *E. coli* strains are in phylogroup A and B1, and the phylogroup E have the biggest genomes. About 2,000 genes of the core genome contribute to almost all the *E. coli* strains. The pangenome size was estimated to be as high as 75,000 (Bergthorsson and Ochman, 1998; Rasko *et al.*, 2008; Touchon *et al.*, 2009, 2020; Lukjancenko, Wassenaar and Ussery, 2010; Kallonen *et al.*, 2017). *E. coli* genomes exhibit considerable variation due to deletions and horizontally-acquired DNA transfer events scattered throughout the chromosome, with recombination hot spots at the *fim* operon and O-antigen gene cluster (Touchon *et al.*, 2009; Didelot *et al.*, 2012). The sizes of inserted DNA fragments are generally between 50 bp and 2–4 kb but can be as large as 100 kb. In addition, plasmids (typically 2-4 types) are found in most strains of *E. coli* which are variable but tend to be strain specific. Larger plasmids (up to 300 kb) are generally conjugative plasmids, smaller plasmids (<30 kb) are generally non-transferable (Denamur *et al.*, 2021).

1.2 The function of iron in bacteria

There are two main types of the iron in biology, the ferrous (Fe^{2+}) and ferric (Fe^{3+}) forms which are interchangeable through redox processes. Because of these characteristics, iron can be used as a biocatalyst or an electron transporter in proteins. Iron has multiple purposes in bacterial cells and is essential in nearly all known cases. Indeed, iron contributes to several key aspects of bacterial function, including cell structure, primary and secondary metabolism, the activity

of iron-dependent enzymes and various cellular reactions (Table 1.2) (Andrews *et al.,* 2003, 2013).

Table 1.2. Examples of functions of iron in bacteria. Adapted from Andrews *et al.* (2003; 2013).

Influenced Domain	Impacts
Major physiological impacts	Low iron can lead to problems related to intracellular processes: • Inhibition of growth. • Reduction of cellular DNA and RNA levels. • Inhibition of sporulation. • Modifications in morphology in cells of bacteria.
Major metabolic processes	Metabolic pathways that are iron dependent: • The Krebs cycle. • Electron transport. • Oxidative phosphorylation • Nitrogen fixation. • Biosynthesis of aromatic compounds - iron is needed for aromatic biosynthesis in *E. coli* bacteria. For example, 3-deoxy-D-arabino-heptulosonate-7-phosphate (DAHP) was the first enzyme of aromatic pathway and it contains per molecule of enzyme one atom of iron.
Metabolic products	• Major biosynthetic products that are affected by the iron regime: Porphyrins, Toxins, Vitamins, Antibiotics, Hydroxamates, Cytochromes, Pigments, Siderophores, Aromatic compounds, DNA and RNA
Important proteins and enzymes that are iron dependent	• Peroxidase, Superoxide dismutase, Nitrogenase, Hydrogenase, Glutamate synthase, Cytochromes, Ferredoxins, Flavoproteins, Ferritin.

The main biological purpose of iron is as a mediator of protein function, rather than a cellular structural component. Iron-containing enzymes are important for oxidative metabolism as driven by the tricarboxylic acid (TCA) cycle due (for example) to the role of enzymes such as aconitase (an Fe-S protein), and cytochromes and Fe-S cluster proteins that act to mediate electron transport in respiratory pathways. Facultative anaerobes like *E. coli* can lower the

amount of iron required by switching metabolism from respiration to fermentation (via glycolysis) to reduce utilization of the iron-demanding TCA cycle and respiratory chain (glycolytic enzymes are not iron requiring). Therefore, substrate-level phosphorylation may be used as the major source of energy instead of oxidative phosphorylation under iron restriction (Andrews *et al.,* 2003).

Aerobically, the presence of oxygen results in the unavoidable generation of toxic peroxides and superoxide radicals through reductive activities within bacterial cells. Such harmful redox products can be degraded by peroxidases, catalases and superoxide dismutases which are often haem or iron dependent. Iron also has a fundamental function in the repair of the cell. Iron has a key role in cell synthesis processes, for instance the B2 subunit of the major ribonucleotide diphosphate reductase of *E. coli* is an iron-dependent enzyme; this enzyme reduces ribonucleotides to deoxyribonucleotides that are required for the DNA manufacture. Iron also plays a role in numerous phases of nitrogen assimilation. The nitrogenase enzyme that is present in nitrogen-fixing prokaryotes reduces atmospheric dinitrogen to ammonia and is composed of both an "iron-molybdenum" and "iron-protein" component. Further, electrons required for the nitrogen-fixing reaction are delivered by a Fe-S containing ferredoxin. Glutamate synthase is another iron-dependent enzyme required for nitrogen assimilation. Another example of an important iron-requiring process is the generation of aromatic compounds by *E. coli*. For example, 3-deoxy-D-arabino-heptulosonate-7-phosphate (DAHP) is the first enzyme of the aromatic pathway, and it can bind one atom of iron per molecule (Messenger and Barclay, 1983).

1.2.1 The properties of iron

The relative levels of the ferrous and ferric forms are dictated by environmental factors. Iron can be found in mineral form and is relatively abundant being the fourth most common element in the Earth’s crust. Because of its desirable properties, iron is considered to have been a

suitable element for integration into proteins as a cofactor during the development of early life under oxygen-free conditions. The biological function of iron relies on its integration into proteins which can be in several main forms: mono- or bi-nuclear iron; iron-sulphur cluster; or haem (Andrews *et al.,* 2003).

During the evolution of life on Earth, the development of aerogenic photosynthesis resulted in the generation of molecular oxygen which began to build up in the atmosphere during the "Great Oxidation Event" ~2.2-2.4 billion years ago reaching current levels of ~21% ~400-420 million years ago. Until this point, iron would have been a "safe" metal and would have persisted in the highly soluble (0.1 M at pH 7.0) ferrous form. However, as the atmosphere became oxygenated the predominant oxidation state for iron is thought to have switched into the insoluble (10^{-18} M at pH 7.0) ferric form (Cartron *et al.*, 2006) leading to bioavailability issues. In addition, the presence of abundant atmospheric oxygen rendered iron as a potentially toxic substance, due to is tendency to mediate generation of reactive oxygen species (ROS). Thus, aerobically, iron is both potentially toxic and of low bioavailability. For these reasons, effective iron homeostasis mechanisms are considered a requirement to enable aerobic and aerotolerant organisms to balance their need to gain iron from their environment whilst ensuring that toxicity does not arise (Andrews *et al.,* 2003).

1.2.2 Iron homeostasis in bacteria

Iron homeostasis in bacteria is managed by five fundamental strategies: (Andrews *et al.,* 2003)

1. Deployment of efficient iron-uptake systems that enable acquisition of the available forms of iron from the corresponding environment.
2. Accumulation of iron stores inside the cell which as an endogenous source of iron for use when environmental iron availability is insufficient.

3. Iron-toxicity resistance systems that enable redox stress stimulated by iron to be effectively managed; this includes the decomposition of reactive oxygen species (ROS).
4. Management of iron utilisation in a process known as iron rationing or iron sparing. This involves the regulation of expression of iron-containing proteins in response to iron availability and the utilisation of alternative non-iron dependent isoenzymes and/or metabolic pathways.
5. A global regulatory system that is responsible for controlling iron homeostasis in response to iron regime and other relevant environmental factors (such as redox stress and growth phase).

1.3 Iron and bacterial pathogenicity

The most plentiful metal in the host is iron. However, a major part of the body's approach to resisting bacterial infection is known as "nutritional immunity" whereby iron availability is tightly restricted in order to exert a bacteriostatic influence on invading pathogens. A major component of the nutritional immunity process is the tight binding of extracellular ferric iron by transferrin, which is abundant in extracellular fluids such as the serum and serves to transport iron around the body. The partial saturation of transferrin ensures that there is essentially no free iron within extracellular fluids for utilisation by microorganisms. Further, the related protein, lactoferrin, is produced in response to infection and exhibits an even higher ferric-iron affinity. Lactoferrin is a strictly antimicrobial component found in secretions such as milk, saliva and tears, and is produced by neutrophils at mucosal surfaces (Johnson and Wessling-Resnick, 2012).

Some bacteria can utilise haem as a source of iron. Haem is abundant in blood as part of haemoglobin within red blood cells, representing ~25% of total body iron. Some bacterial pathogens can induce haemolysis that releases haemoglobin from red blood cells and secrete

proteases that release haem from haemoglobin. However, haemoglobin and haem are rapidly cleared from circulation by haptoglobin and haemopexin, respectively, thus limiting the availability of haem as an iron source for pathogens (Johnson and Wessling-Resnick, 2012). Further, infection induces the acute-phase response (APR) which initiates a further retention of iron by the host to reduce iron supply to pathogens. Interleukin-6 is the major cytokine responsible for inducing the APR in response to Pathogen-Associated Molecular Patterns (PAMPs) (e.g. LPS) that are sensed by pattern recognition receptors (PRRs) on immune cells, resulting in an inflammatory response. One of the APR products is hepcidin which is a peptide hormone that down regulates the absorption of iron from the gut, prevents release of iron from macrophages of the reticuloendothelial system and upregulates intracellular iron storage by ferritin (Parrow *et al.,* 2013). These processes thus further lower the availability of extracellular iron during infection.

Since iron availability is strictly limited within the host, pathogenic bacteria generally require specific mechanisms to acquire the iron they require in order to mount an effective infection. These mechanisms include: production and utilisation of high-affinity, low molecular weight iron chelators (siderophores); direct acquisition of iron from host sources such as haem, haemoglobin and transferrin (Mey *et al.,* 2021). These and other iron uptake mechanisms are described below (section 1.4).

1.4 How bacteria acquire iron

1.4.1 Introduction

The content of iron in *E. coli* is 10^5 to 10^6 atoms per cell. However, the ferric ion is only soluble at 10^{-17} M at pH 7 – equivalent to 6 x 10^6 iron atoms per litre which is far lower than required by *E. coli* during growth in liquid culture. Bacteria can overcome this "concentration gap" by solubilisation of ferric iron, which can be achieved by reduction to the more soluble ferrous from, acidification of the medium (thus raising solubility) or deploying ferric ion chelators

(known as siderophores). In practice, reduction and ferric ion chelation are the most common approaches (Andrews *et al.,* 2003).

1.4.2 Siderophore systems

Many bacteria (as well as fungi and plants) can produce high-affinity extracellular ferric chelators known as siderophores (or phytosiderophores in the case of plants) (Andrews *et al.,* 2013). The function of siderophores is to solubilise ferric iron to enable its uptake. Ferri-siderophore complexes can cross into Gram-negative bacteria by specific receptors in the outer membrane (OM). This uptake across the OM is assisted by the pmf energy-transducing TonB-ExbBD system which is located in the cytosolic membrane (CM) and includes a component (TonB) that spans the periplasm to make contact with OM receptors (Andrews *et al.*, 2003; 2013). Once internalised into the periplasm, ferri-siderophore complexes are bound to periplasmic binding proteins which deliver the complex to ATP-binding cassette (ABC) permeases in the CM. Once the ferri-siderophores reach the cytosol, the iron is released from the siderophore via reduction and/or siderophore degradation (Fig. 1.1A). In Gram-positive bacteria, there is no OM and so OM receptors and TonB-ExbB-ExbD systems are not required. Ferri-siderophores are transported across the CM by binding-protein-dependent ABC permeases. These systems are similar to those used in Gram-positive bacteria except that the binding protein is commonly a lipoprotein that is physically tethered to the outer surface of the cytosolic membrane, and no OM component is required (Fig. 1.1B) (Andrews *et al.*, 2003; 2013).

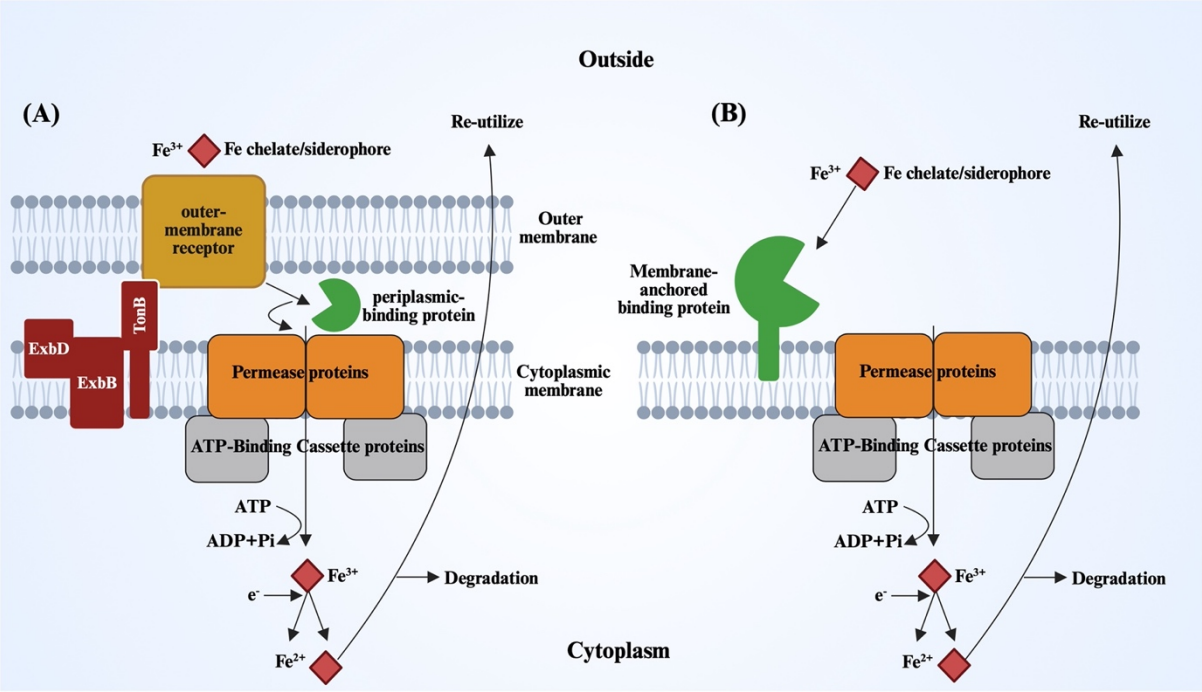

Figure 1.1: Schematic representation of ferrisiderophore uptake in Gram-negative and -positive bacteria. (A) Shows how ferri-siderophores cross the OM and CM in Gram-negative bacteria. **(B)** Illustrates that there is no OM in Gram-positive bacteria but ferri-siderophores can be transferred to the CM by using "binding-protein-dependent ABC permeases". Adapted from Andrews *et al.* (2003) and created using BioRender.

The molecular mass for siderophores is generally too high to allow passive diffusion through porins in the OM. They tend to exhibit high affinity and selectivity for ferric iron, which are advantages in their role in iron scavenging. Their function is to assist iron uptake when iron is growth limiting. Some siderophores, such as mycobactins of mycobacteria, are linked to the envelope for the cell, but most are secreted in free form into the environment. Siderophores are typically hexadentate, binding ferric iron in an octahedral coordination geometry. Functional groups commonly deployed as Fe^{3+} ligands are hydroxamates, α-hydroxy-carboxylates and catechols (Andrews *et al.,* 2013). More than 500 different types of siderophore have been distinguished. Examples of well-studied siderophores that represent the three different ligand types are enterobactin (a catecholate produced by Enterobacteriaceae, including *E. coli*), ferrichrome (a hydroxamate produced by fungi such as *Aspergillus*) and rhizoferrin (an α-hydroxycarboxylate produced by some fungal species) (Fig. 1.2). Very often, siderophores are

composed of peptides that may be arranged in a cyclic format and such siderophores are generated by non-ribosomal peptide synthetases (such enzymes are also employed for biosynthesis in peptide antibiotics such as β-lactams). Siderophores are produced within the cytosol and are then exported via dedicated CM transport proteins as siderophores are commonly polar. For example, the EntS protein exports the enterobactin from *E. coli* (Andrews *et al.,* 2013).

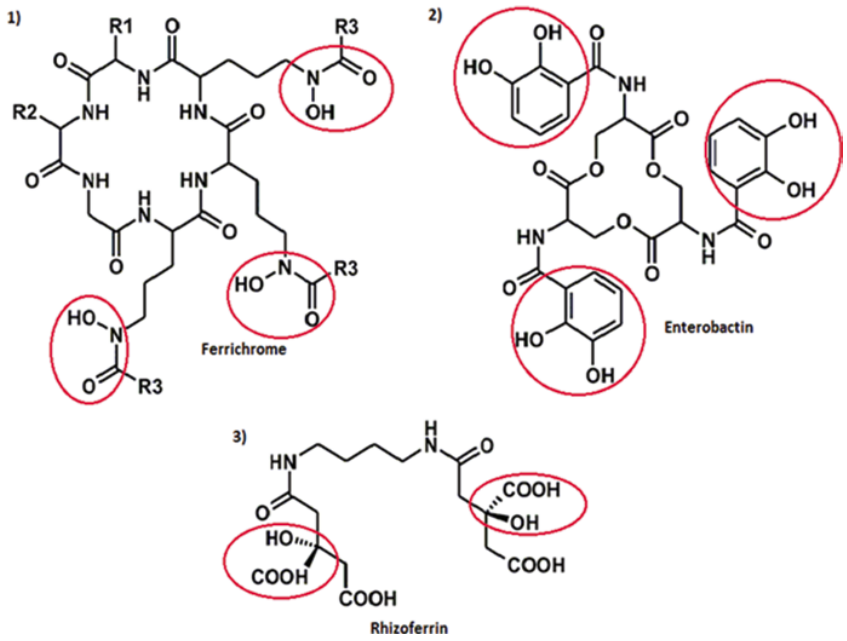

Figure 1.2: Examples of three siderophores for each of the three major functional group types. The chemical structures are shown in this diagram. (1) Shows the chemical structure for ferrichrome with hydroxmate groups. (2) Indicates the chemical structure for enterobactin with catecholate groups. (3) Illustrates the chemical structure for rhizoferrin with α-hydroxycarboxylates groups (Krewulak and Vogel, 2008). Ferric iron ligands are circled in red.

1.4.3 Ferric iron transporters (ferric di-citrate)

The ferric di-citrate uptake system (Fec) was identified in *E. coli* K-12 as a citrate inducible ferric iron transport system and it was shown that *E. coli* can use ferric citrate as a source of iron thanks to the presence of the Fec transporter system. Ferric citrate is taken across the outer membrane by the TonB-dependent FecA receptor. The periplasmic binding protein FecB then

collects the ferric citrate and delivers it to an ABC transporter (FecCDE) in the cytoplasmic membrane. The *fec* genes are regulated by the presence of extracellular ferric citrate bound to FecA which stimulates activation of FecR that in turn activates FecI (Fig 1.3). FecI is a extracytoplasmic-function (ECF) sigma factor and FecR works as anti-FecI-sigma factor (Fig. 1.3). When ferric citrate binds FecA, FecA works to transfer ferric citrate and stimulate release of FecI by FecR so that FecI can bind to RNA polymerase. Thus, the *fecABCDE* operon is induced by the presence of ferric citrate in the environment (Fig. 1.3). *fecABCDE* and *fecIR* genes are repressed in the presence of iron by Fur, and therefor are induced by iron restriction. The *fec* genes are not common in enteric *E. coli*, but are common in UPEC and bacteraemic strains (Mey *et al.,* 2021).

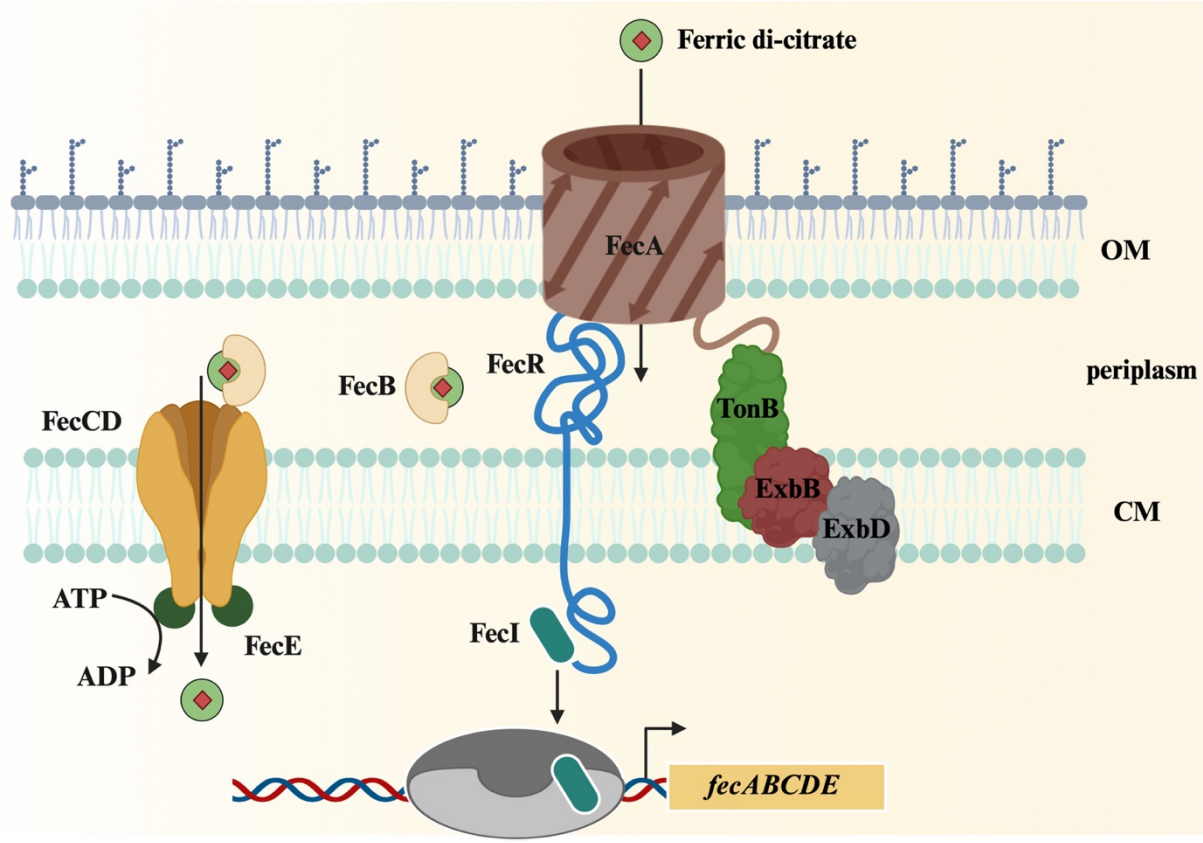

Figure 1.3: The ferric dicitrate transport system (Fec). The figure shows the elements of the Fec system and their cellular regions. Ferric dicitrate is moved through the outer membrane via TonB-depndent FecA and then is carried by FecB to the cytoplasmic membrane permease, FecCDE, for ATP-dependent transfer it to the cytoplasm. When bound to ferric dicitrate, FecA deactivates the anti-sigma factor FecR resulting in release of the sigma factor FecI. Then FecI

combines with RNA polymerase to allow the *fecABCDE* operon to be transcribed. Adapted from Mey *et al.* (2021) and created using BioRender.

1.4.4 Haem transport

Haem contains iron and is mainly found in haemoglobin in the host. Haem is considered to be the most abundant source of iron in mammalian hosts and pathogenic bacteria can benefit from this molecule. Several strains of the *Enterobacteriaceae* can induce haemolysis which releases haemoglobin from erythrocytes. Related haem transporters have been described in *S. dysenteriae* and EHEC (known as Shu and Chu, respectively) and have been found in other pathogenic *E. coli* strains (EIEC, EPEC, UPEC and NMEC). These haem transporters in Shigella include: ShuA (TonB-dependent outer membrane haem receptor); ShuT (periplasmic haem binding protein); ShuU and ShuV (inner membrane haem permease complex); ShuS cytoplasmic (haem oxygenase, releasing iron from haem); an ShuW, ShuX and ShuY (acting to help the haem degradation under anaerobically) (Fig. 1.4) (Mey *et al.,* 2021).

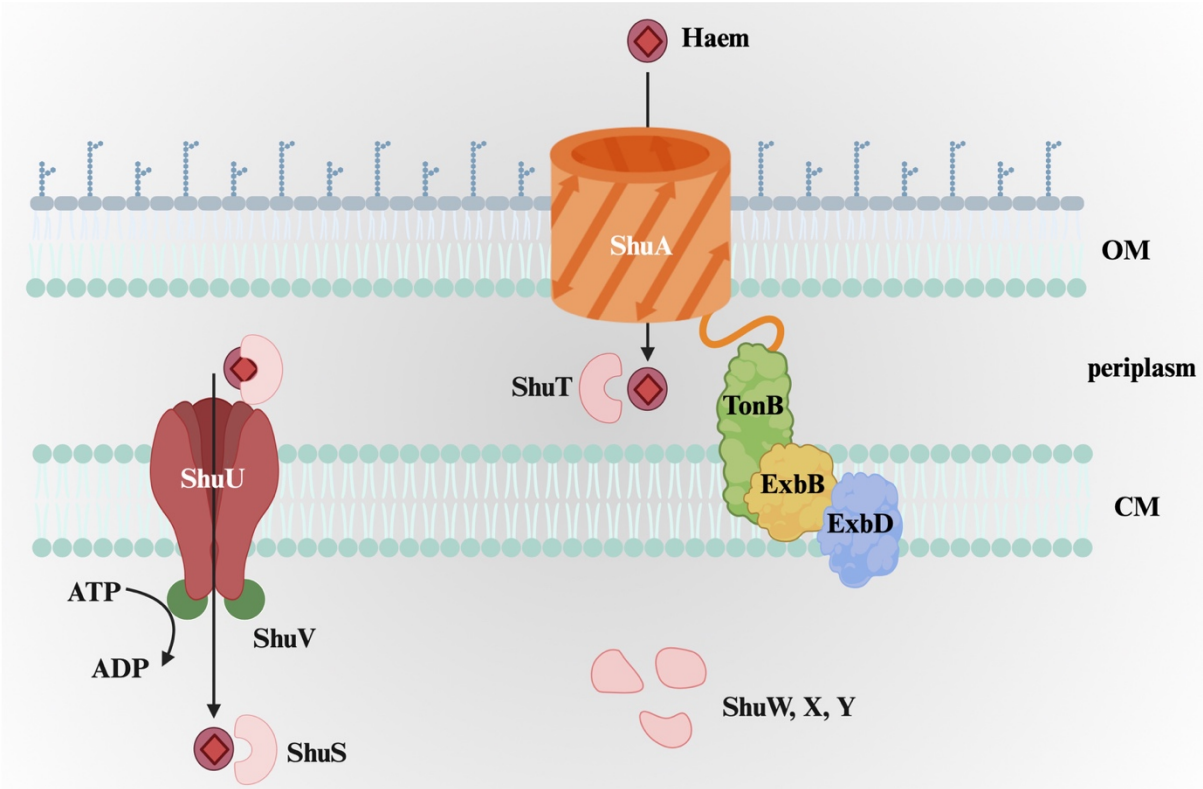

Figure 1.4: The Haem transport system (Shu). The Shu component and their cellular regions are shown. Adapted from Mey *et al.* (2021) and created using BioRender.

1.4.5 Ferrous iron transport in bacteria

1.4.5.1 Introduction

Ferrous iron is believed to pass easily through the porins of the Gram-negative OM, into the periplasm, where it can then be imported into the cytoplasm through several alternative transport systems (Ge and Sun, 2012). Different systems have been identified in previous studies for transport of ferrous iron into bacteria across the cytoplasmic membrane. These are exemplified by the following transporters: EfeUOB, MntH, ZupT, FeoABC, YfeABCDE and Fut (Lau *et al.,* 2015).

EfeUOB. The EfeUOB and FeoABC transporters are most likely the only bacterial transport systems capable of transporting ferrous iron in *E. coli*. EfeU is a protein that belongs to the yeast iron permease family, Ftr1p; and EfeO and EfeB are periplasmic proteins. The permease EfeU is responsible for iron transfer into the cell. The system is functional in *E. coli* O157:H7 but contains a frameshift mutation that inactivates the system in the non-pathogenic *E. coli* K-12 (Lau *et al.,* 2015).

MntH. MntH consists of a single protein composed of 11 transmembrane helices. MntH belongs to the "natural resistance-associated macrophage protein" (NRAMP) family of transporters. MntH of *E. coli* is a divalent metal ion/proton symporter with highly conserved residues in its trans-membrane regions that aid in divalent ion transport into the cell. MntH can transport both Fe^{2+} and Mn^{2+} but has preference for Mn^{2+}, although the related NRAMP1 and 2 of eukaryotes have preference for iron (Lau *et al.,* 2015).

ZupT. ZupT of *E. coli* is a member of the Zip family of transporters which are common in eukaryotes. The function of Zip proteins is to transport divalent metals. The precise function of ZupT is not known as yet but it is suggested that it could be specific for several metals: Zn^{2+}, Co^{2+}, Mn^{2+} and Fe^{2+} (Lau *et al.,* 2015).

FeoABC. The Feo system is the primary ferrous-iron transport system found in both pathogenic and non-pathogenic bacteria (Lau *et al.,* 2015). This is described in detail below.

YfeABCDE. The YfeABCD system is an ABC system that was identified in *Yersinia pestis*, and is not found in *E. coli.* However, it is present in the closely-related *Salmonella* spp. where it is designated as SitABCD and exhibits preference for Mn^{2+} over Fe^{2+} (Lau *et al.,* 2015).

Fut. Fut was discovered in the cyanobacterium, *Synechocystis* PCC6803. It consists of 4 protein components: FutA1, FutA2, FutB and FutC. FutA1 and FutA2 are two proteins in the periplasm (52% sequence similarity, partially redundant), FutB is a membrane permease and FutC is ABC protein and thus provides energy for the uptake process. Initially, the Fut system was believed to function as a ferric iron transporter, but later research found that FutA1 and FutA2 bind ferrous iron (Lau *et al.,* 2015).

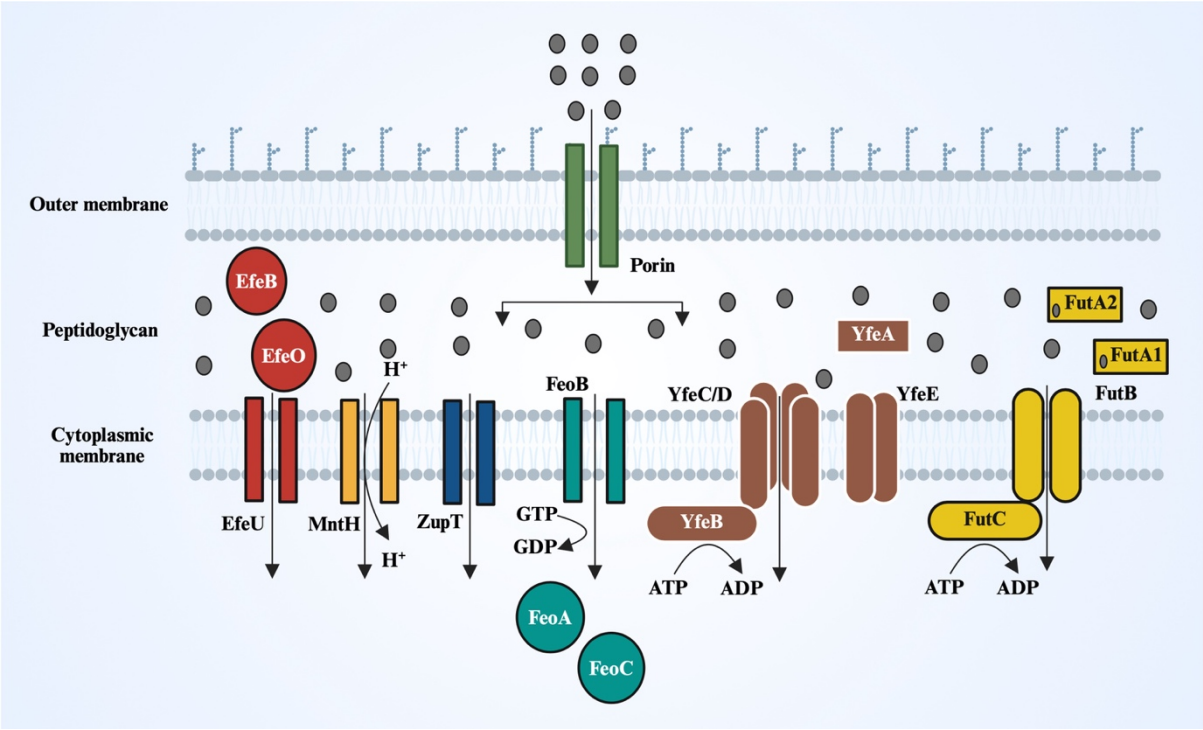

Figure 1.5: The major bacterial ferrous iron transport systems. These systems have been found in different Gram-negative bacteria. *E. coli* possesses the ferrous iron transport systems EfeUOB and FeoABC, as well as the manganese transport system MntH which has capacity for ferrous iron uptake. Rectangles show the permeases, ovals indicate ABC transporters and circles represent periplasmic-binding proteins. Adapted from Lau *et al.* (2015) and generated using BioRender.

1.4.5.2 Feo system

1.4.5.3 How the *feo* system was discovered

The *feo* operon was identified in *E. coli* K-12 through complementation of mutants with defects in ferrous iron transport. *feo* mutants were initially recognized by their resistance to streptonigrin; this antibiotic induces intracellular free radicals in the presence of iron. The Str^R mutants were shown to accumulate lower levels of iron anaerobically suggesting a ferrous-iron uptake (*feo*) defect. Complementation of the mutant allowed cloning and sequencing of the *feo* locus. The locus consists of three conserved genes forming an operon: *feoABC* (Hantke, 2003). *feoA* of *E. coli* encodes of 75-residue cytoplasmic proteins of 8.4 kDa; *feoB* specifies of 773 amino-acid residue, polytopic, CM-embedded protein of 84 kDa; and *feoC* also encodes a small cytoplasmic protein (78 amino acid residues). Although *feoA* and *feoB* are highly conserved in bacteria, *feoC* is less well conserved and is largely restricted to the Enterobacteriaceae (Lau *et al.,* 2015).

1.4.5.4 *feo* regulation

Fur and Fnr have been shown to be transcriptional regulators for *feo* operon expression in response to iron (repression) and anaerobiosis (induction), respectively, in *E. coli*. Fnr is a global regulator of anaerobic gene expression. It directly senses oxygen via its O_2-sensitive Fe_4-S_4 cluster which is degraded by oxygen converting Fnr into an inactive (non-DNA binding) state. Thus, the *feo* operon is induced in the absence of oxygen and iron (Lau *et al.,* 2015).

1.4.5.5 The significance of the Feo system

When there is a lack of oxygen, iron is mostly found in its ferrous state. Under such conditions, Feo is considered the major route for iron uptake in *E. coli* and many other bacteria. Thus, mutation of *feo* in both pathogenic and non-pathogenic bacteria can have a major impact on gut colonisation and/or virulence. Bacterial species where Feo has been shown to be important for *in vivo* survival and/or colonization include *E. coli* K-12 and pathogens such as *Salmonella enterica*, *Helicobacter pylori*, *Campylobacter jejuni*, *Vibrio cholerae* and *Porphyromonas*

gingivalis. In *E. coli*, iron transport studies have shown that Δ*feo* strains are unable to take up ferrous iron. Furthermore, these mutants are unable to colonize the gut of mouse effectively. However, corresponding mutants with ferric-iron transport defects, e.g. in enterobactin-dependent iron uptake, remain capable of colonizing the mouse gut. Thus, the ability of *E. coli* to colonize is the gut appears to be dependent on ferrous, rather than ferric, iron absorption. In *H. pylori*, loss of *feo* also resulted in failure to colonize the mouse gut. FeoB was also shown to be necessary for ferrous-iron uptake in *C. jejuni* and for colonizing in the intestine (Lau *et al.,* 2015).

1.4.5.6 The components of the Feo system

FeoA: The FeoA protein is a small 75-85 amino acid residue protein that is soluble and cytoplasmic, and has a high pI (9.4 for *E. coli*) (Cartron *et al.*, 2006; Lau *et al.,* 2015). The precise function of FeoA in ferrous iron transport is not yet known but it is absolutely required for uptake in *E. coli* (Al-Aidy, 2020) and is thus considered an essential Feo component, likely interacting with FeoB (Cartron *et al.*, 2006). Indeed, the high pI of FeoA may assist in interaction with FeoB in the membrane (Cartron *et al.*, 2006). FeoA has also been shown to be important in Feo-mediated iron uptake in *Vibrio cholerae* (Weaver *et al.*, 2013).

Eight FeoA forms have been structurally defined, most using solution state NMR spectroscopy and others using protein X-ray crystallography. The NMR solution structures converge well and showed FeoA to be monomeric, while the crystal structures showed a dimeric or octameric structure, perhaps due to crystallisation circumstances. The *E. coli* FeoA solution structure is one of the eight so far defined (PDB id:f2lx9) (Lau *et al.*, 2013). FeoA consists of two to three α-helixes and five to six β-strands forming a β-barre1 (Lau *et al.,* 2015). FeoA has been found to be identical in fold to the SH3-like domain within the DtxR-like bacterial metal-binding transcriptional regulators, for instance ScaR from *Streptococcus*, IdeR of *Mycobacterium* and DtxR of *Corynebacterium diphtheriae*. The role of the SH3-like domains in DtxR and its

homologues is unknown, but they can provide metal-binding ligands to the other two domains of these proteins. The DtxR-like proteins have three distinct domains: the dimerization, DNA-binding and SH3-like domains. These domains play a part in transcriptional control as well as metal binding. FeoA has been suggested to operate as a GAP (GTPase-activating protein) in the activation of FeoB (Lau *et al.,* 2015).

FeoB: The FeoB protein is considered to act as the ferrous iron permease. It consists of 3 major domains: the G-protein domain at the N-terminus; followed by the GDI (guanine-nucleotide dissociation inhibitor) domain; and the integral membrane permease domain (Lau *et al.,* 2015).

The G-Protein domain. FeoB was initially believed to be ATP dependent on the basis of perceived homology with ATPases in the nucleotide binding region. Also, ferrous iron uptake in *H. pylori* was found to be reduced by inhibition of ATPase activity, but not by dissipation of the proton motive force. However, it was later revealed that FeoB does not bear similarity to ATPases, but instead carries a cytosolic N-terminal G-protein domain with GTPase activity. G-proteins contain five motifs which are linked with GTP and hydrolysis. In *E. coli*, the location of the five motifs is at residues 1-170: the G1 (GxxxxGK(S/T)) motif at residue 10–17; the G2 (T) motif at residue 37; the G3 (DXXG) motif at position 56-59; the G4 (NXXD) motif at residue 120-123; and the G5 (STRGRG) motif at position 150-155 (Lau *et al.,* 2015). The role of the G1 motif is to bind the alpha and beta phosphates of GTP. The G2 and G3 motifs interact with the lambda phosphate and magnesium. The G4 motif provides hydrogen bonds connecting to the guanine nucleotide and the G5 motif helps to position the nucleotide. The G-protein domain consists of two 'switch' regions which help bind the nucleotide and responsible for supplying interaction sites to the signal transduction pathway's effectors (Lau *et al.,* 2015).

The GDI domain. The GDI domain (residues 171–276) acts as a linker between the G-protein and transmembrane domains. The GDI domain is hydrophilic and cytoplasmic, like the G-

protein domain, but its sequence is not well conserved between organisms. The GDI domain interacts with the switch I region of the G-domain and increases GDP binding without affecting GTP binding or the GTPase activity of the G-protein (Lau *et al.,* 2015).

The Gate motifs. The transmembrane domain is the third major domain of FeoB. This domain consists, approximately, of residues 277-773 for the *E. coli* FeoB. It is composed of 8-10 transmembrane helices located in the cytoplasmic membrane. This domain has been described as the most significant domain of the three. Presently, this domain is not defined structurally. The transmembrane domain is presumed to transfer ferrous iron from the periplasm to the cytoplasm. However, it is unclear how this iron permease domain regulates iron absorption in cells (Lau *et al.,* 2015).

C-terminal tail. The carboxy-terminal region on the *E. coli* FeoB protein is predicted to be cytoplasmic and possesses a segment that is rich in Cys and His residues. Its function is unclear, and it is only conserved within the γ-Proteobacteria (Cartron *et al.*, 2006; Orzel *et al.*, 2025). The protein's Core CFeoB, positioned between Gate motifs, may also bind metal in the transmembrane domain (Orzel *et al.*, 2025).

It was found that FeoA is needed for FeoB to move Fe^{2+} in *S. enterica*, the same as it is in *E. coli.* FeoA binds with FeoB *in vivo*, as showed by a bacterial 2-hybrid assay (Kim *et al.,* 2012). *In V. cholera*, FeoA, combined with FeoC, is essential for the functionality of FeoB (Weaver *et al.*, 2013).

FeoC. In *E. coli*, *feoC* (or *yhgG*) is the third and final gene in the *feo* operon. The FeoC protein is only present in γ-Proteobacteria. FeoC is a small (78 residues), cytoplasmic protein of predicted pI, 7.7. Its structure has been solved for *K. pneumoniae* (4AWX; 2K02) and *E. coli* (1XN7) and shown to consists of a winged helix-turn-helix (HtH) motif similar to that of LysR (transcriptional regulator) (Cartron *et al.*, 2006; Lau *et al.,* 2015). Such HtH motifs typically

interact with DNA, with the third helix engaging the major groove in a sequence specific fashion. Some evidence for this view was obtained from studies on FeoC in *Y. pestis* which indicated a role in transcription control because *feoC* mutation resulted in increased expression of *feoAB* (Guo *et al.,* 2011), although a subsequent study refuted this claim (Fetherston *et al.*, 2012).

Loop 1 of the HtH wing region carries four conserved cysteines that provide a predicted Fe_4-S_4 cluster binding site (Lima *et al.*, 2009). Indeed, FeoC of *K. pneumoniae* was shown to be able to form an iron-sulphur cluster (Hsueh *et al.*, 2013). In anaerobic, iron-deficient conditions, FeoC appears to bind to FeoB to protect it from proteolytic degradation to the accumulation of FeoB as well as ferrous iron absorption (Guo *et al.,* 2011). In *V. cholerae* and *S. enterica*, FeoC has been found to interact with FeoB *in vivo* (Kim *et al.,* 2013; Weaver *et al.*, 2013). FeoC was discovered in *S. enterica* to protect FeoB from the FtsH protease, which interacts with its N-terminal domain (Kim *et al.,* 2013). FeoC is believed to contain its Fe-S cluster under anaerobic circumstances, making it less sensitive to Lon-mediated proteolysis. The Fe-S cluster of FeoC is believed to be oxidized as the environment becomes aerobic, rendering it more sensitive to Lon-mediated proteolysis. FtsH-mediated proteolysis then inactivates FeoB. Thus, when the environment changes from anaerobic to aerobic, proteolytic loss of FeoC results in FtsH-mediated destruction of FeoB and reduced absorption of ferrous iron (Kim *et al.,* 2015) (Fig. 1.6). FeoC has also been shown to interact with zinc via its Cys residues (Hung *et al.,* 2012; Lau *et al.,* 2015).

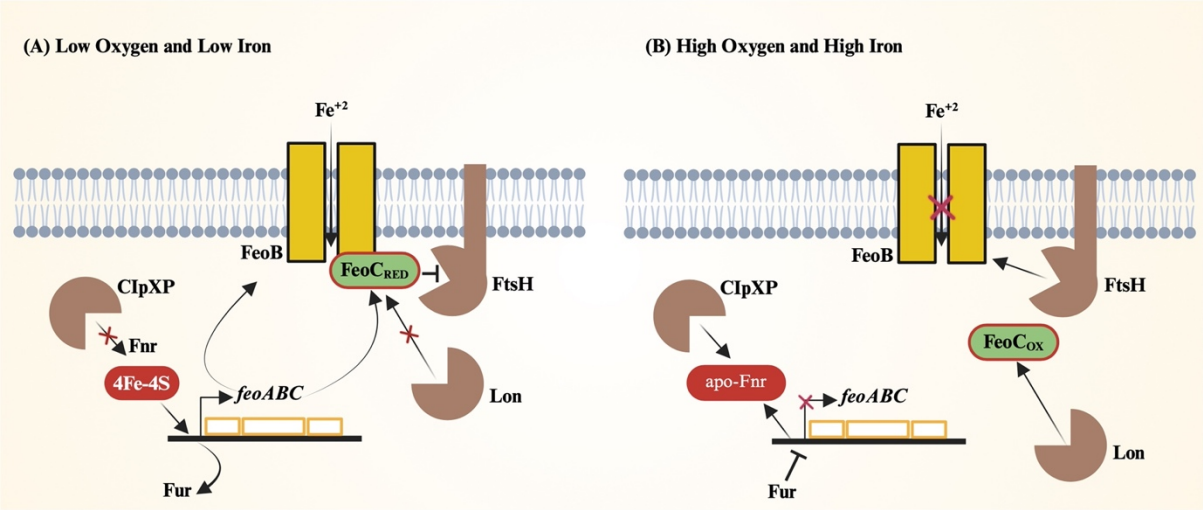

Figure 1.6: Schematic illustration of the regulation of FeoB-mediated absorption of Fe^{2+} in *Salmonella* via the proteolysis of FeoC. (A) Under low oxygen conditions, the Fnr regulator contains a 4Fe-4S cluster and is thus active; it is also able to evade ClpXP-mediated proteolysis. Consequently, it binds to the promoter of the *feo* operon, resulting in a significant rise in *feo* mRNA levels. The *feoC* protein may avoid Lon protease degradation due to the 4Fe-4S cluster ($FeoC_{RED}$). Subsequently, FeoC associates with FeoB, therefore protecting FeoB from FtsH-mediated proteolysis and enhancing FeoB accumulation and Fe^{2+} absorption under low iron and low O_2 conditions. Fur fails to repress under low iron conditions. **(B)** Under high iron, the Fe^{2+}-Fur regulator suppresses *feo* transcription. Fnr is inactive under high oxygen conditions due to loss of its 4Fe-4S cluster and degradation via the ClpXP protease. The FeoC Fe-S cluster is oxidized ($FeoC_{ox}$) resulting in raised sensitivity to the Lon protease. Subsequently, the FeoB transporter becomes exposed to FtsH protease activity due to the loss of protection from FeoC. Fe^{2+} uptake is thus diminished. Adapted from Kim et al. (2015) and created using BioRender.

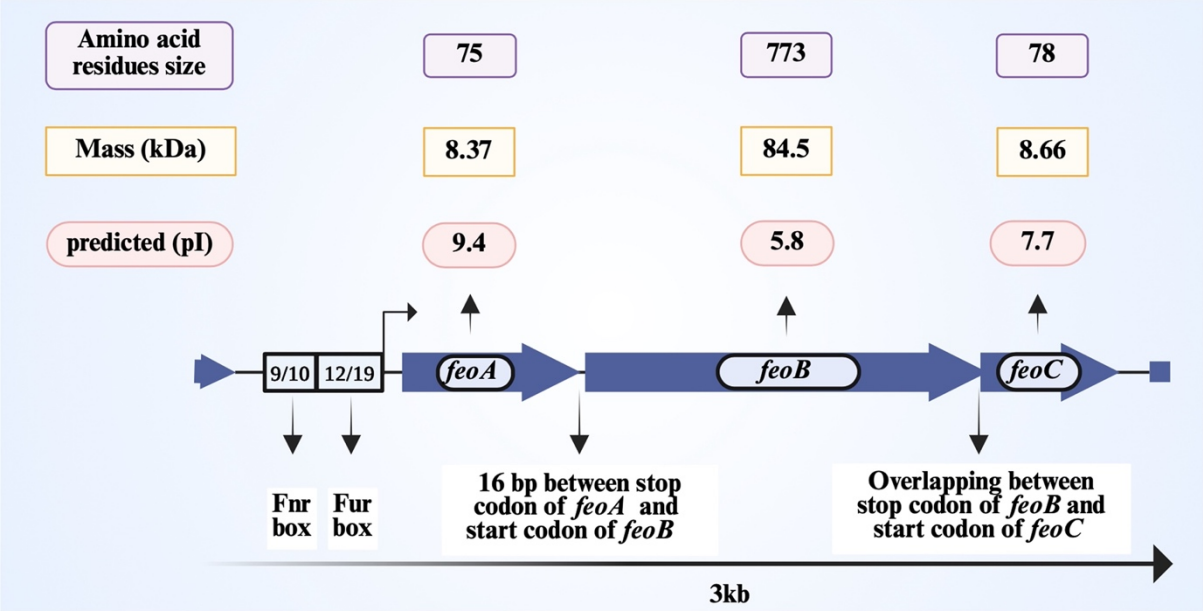

Figure 1.7: Schematic representation of the *feoABC* operon of *E. coli*. The lengths, mass and predicted pI of the Feo components are indicated. 16 bp is the distance between the *feoA* stop codon and the *feoB* start codon. There is overlap between the stop codons for *feoB* and the start codon for f*eoC*. Also, this figure indicates the binding sites for both Fnr and Fur modified adapted from Cartron *et al.* (2006) and generated by BioRender.

1.5 Ferric uptake regulator (Fur)

In Enterobacteria, including *E. coli*, Fur is the main iron regulator and thus controls iron uptake systems. Fur is an Fe-dependent repressor. The purpose of Fur is to repress transcription of genes under iron sufficiency, and to allow derepression under iron sufficiency. Fur is reported to control around 90 mRNA transcripts in response to iron status and thus can be considered a global regulator (Andrews *et al.,* 2003). Fur uses ferrous ion as a co-repressor to allow binding to operators called 'iron boxes' found in the promoter region of regulated genes. Fur is made up of two 17-kDa subunits that form a homodimer (Andrews *et al.,* 2003). Under the iron-rich conditions, some Fur-regulated genes are induced (Braun, 2001). In *E. coli*, this Fe-Fur induction depends on RyhB, a small non-encoding regulatory RNA which is subject to direct Fe-Fur repression. RyhB regulates some genes that encode iron-containing proteins. Under iron-rich conditions, RyhB expression is repressed by Fur, but if iron is limited then Fur repression is relieved such that RyhB can be expressed (Fig. 1.8). RyhB acts to reduce cellular

demand for iron under iron restriction by suppressing expression of target iron genes (promoting rapid turnover of corresponding transcripts in a Hfq-dependent fashion; Andrews *et al.,* 2003). Thus, Fur induces iron uptake under iron restriction and also (indirectly) reduces cellular iron demand.

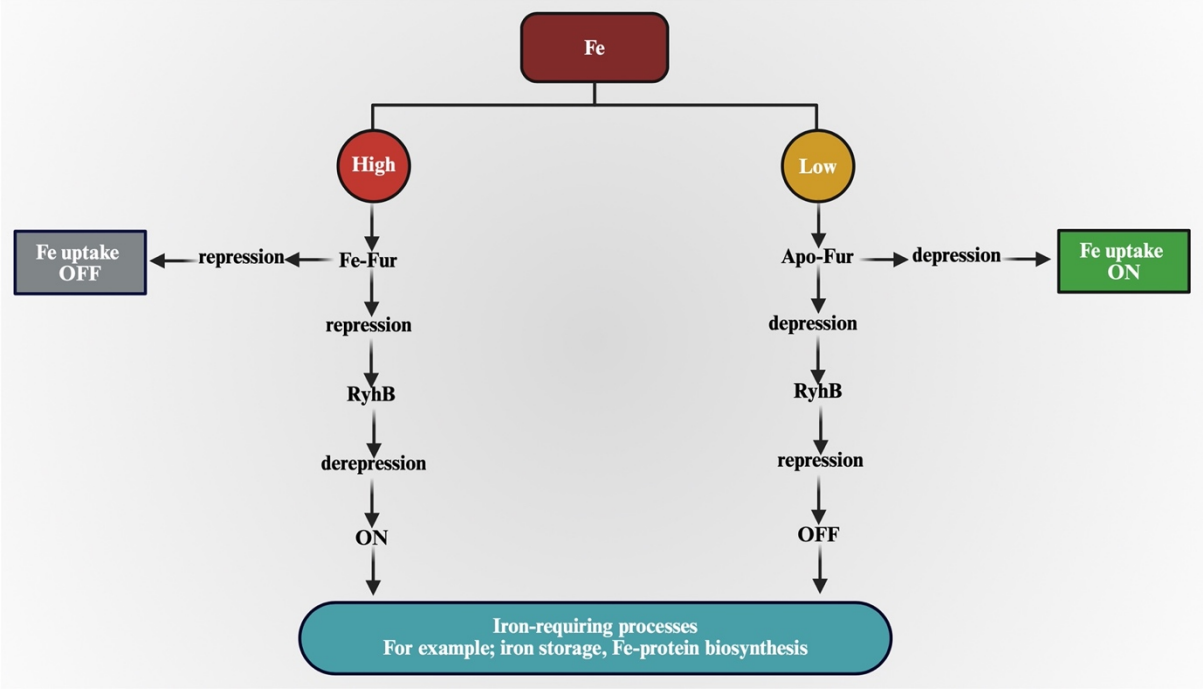

Figure 1.8: Schematic representation of Fur and RyhB control of iron-dependent gene regulation in *E. coli*. Adapted from Massé and Gottesman (2002) and created by BioRender.

1.6 Iron storage

Iron that is located outside of the cell is not the only source of iron available to bacteria. Many bacteria store iron intracellularly using iron-storage proteins (Andrews, 1998). Such iron stores can be used as a source of iron for growth when there is not enough iron in the environment. There are four kinds of iron-storage proteins known in bacteria: ferritins (Ftns); which are also common in eukaryotes; bacterioferritins (Bfrs), found only in prokaryotes and unlike ferritins contain haem as a prosthetic group; the DNA-binding protein from starved cells (Dps) found only in prokaryotes; and encapsulated ferritin-like proteins (FLPs), found in bacteria and more commonly in archaea (Eren *et al.*, 2024). These four kinds of proteins are evolutionarily related, and can be found in combinations in prokaryotes. Ferritin and bacterioferritin proteins

each consist of 24 identical (or closely similar) subunits whereas Dps proteins are smaller consisting of just 12 identical subunits. In each case, the subunits come together to form a roughly spherical protein shell encompassing a hollow centre that acts as an iron-storage reservoir. Each of the 12 or 24 subunits forms a four-α-helix bundle as the major structural motif. As the 24-meric ferritins and bacterioferritins are large proteins (~500 kDa), they can store about 2000-3000 ferric iron atoms per holomer. The Dps proteins are smaller (~250 kDa) and thus have a lower capacity for iron storage (~500 ferric iron atoms per holomer). These iron-storage proteins take up iron in the ferrous form which is then oxidised to the ferric form during the storage and iron-core formation process. The iron-storage process is catalytic requiring a ferroxidation step driven by specific catalytic sites (the ferroxidase centre) located in the centre of the 4-helix-bundle subunits (ferritin and bacterioferritin) or at the twofold interface between subunits (Dps proteins (Ilari *et al.*, 2000). Ferrous iron is bound at a di-iron site at the ferroxidase centre which is then subject to oxidation by O_2 which generates an oxo-bridged di-ferric intermediate. The ferric iron is then transferred into the hollow centre creating a ferrihydrite or ferric phosphate iron core. The Dps protein of *E. coli* is thought to primarily function in iron and redox-stress resistance, and DNA protection, rather than provision of iron stores (Andrews *et al.,* 2003), and utilises hydrogen peroxide as oxidant rather than oxygen. Indeed, Dps is a nucleoid protein that is highly abundant in stationary phase with a role in sequestering the chromosome. The encapsulated FLPs form large protein cages, and the iron is stored within the encapsulin cage while the FLP performs the ferroxidase function. The encapsulin-FLP system have a high iron-storage capacity (20,000 iron atoms per molecule) than Ftns, Bfrs and Dps (4,500, 4,500 and 500 iron atoms per molecule) due to their larger size (Eren *et al.*, 2024).

1.7 Aims

In a recent study by Al-Aidy (2020), it was found that in the presence of the reductant, ascorbate, FeoC increases Feo activity (Feo-dependent growth under iron restriction)

aerobically. However, in anaerobic conditions, with or without ascorbate, FeoC only had a minor effect on Feo activity. In the presence and absence of oxygen, FeoC had only a slight effect on the cellular levels of FeoB. Thus, FeoC seems to boost Feo activity activity under aerobic conditions with ascorbate without having a major impact on FeoA or FeoB levels (Al-Aidy, 2020). These findings are contradictory to those of Kim *et al.* (2013). Therefore, the aim of this research was to further understand the purpose of FeoC by investigating whether it directly interacts with the C-terminal tail of FeoB (like FeoC, the C-terminal tail is only found in the *Enterobacteriaceae*). This involved deleting the C-terminal tail and over-expressing the FeoB-C-terminal tail to determine any impact on the ability of FeoC to enhance FeoAB activity under reducing, aerobic conditions. Lastly, the impact on global expression of *feoAB* and *feoABC* induction from pBADara were compared in a *feoABC* mutant in order to deduce any regulatory impact of FeoC global gene expression by RNAseq.

Chapter 2: Materials and Methods

2.1 Preparing *E. coli* competent cells using the calcium chloride method

This method is quite simple and fast, and it presents good transformation efficiencies (~10^5-10^6 colonies per µg of DNA). All steps were performed aseptically. Firstly, a single colony was used to inoculate 5 ml of LB broth in a sterile test tube, and this was incubated overnight on a shaker at 37 °C and 250 rpm in an Eppendorf Innova S44i shaking incubator. Secondly, 0.5 ml of *E. coli* overnight culture were used to inoculate 50 ml LB broth in a 250 ml flask equipped with a cottonwool bung. Thirdly, the flask was incubated on a shaker at 250 rpm at 37 °C for 3-4 h and during this time samples were taken to record the optical density (OD) at 600 nm by cell density meter (WPA CO8000). Once the OD_{600nm} reached between 0.4-0.5, the culture was split into two 50 ml Falcon tubes and the cells were harvested by centrifugation for 5 min at 5000 rpm and 4 °C using an Eppendorf centrifuge 5804 R equipped with an Interchangeable centrifuge rotor. Fourthly, the supernatant was thoroughly removed, and the cell pellet was resuspended in 30 ml ice-cold 100 mM of $MgCl_2$ and left for 10 min on ice. Then, the suspension was centrifuged for 5 min at 5000 rpm (as before) and the supernatant was discarded. Fifthly, the cell pellet was resuspended in 30 ml ice cold 100 mM $CaCl_2$ and then this was incubated for 30 min on ice. The resuspended culture was then centrifuged, as before, and the cell pellet was resuspended in 4 ml ice-cold 100 mM $CaCl_2$ with 20% glycerol. Finally, 200 µl aliquots were distributed into Eppendorf tubes on ice and the tubes were immediately transferred to a -80 °C freezer (Sambrook and Russell, 2001).

2.2 Transformation of chemically-competent *E. coli*

Competent cells prepared as above were defrosted on ice. Then, 1 µl of plasmid DNA was added and mixed with the competent cell suspension on ice. After that, the tubes were maintained on ice for 30 min. Then, the tubes were placed into a water bath at 42 °C for 2.5 min. The tubes were then transferred on to ice for 5 min. Following this, 1 ml of fresh LB medium was added with brief mixing and all the samples were incubated at 37 °C for 1 h to allow

expression of antibiotic resistance. Then, 100 µl samples were plated out onto LB agar plates with an appropriate antibiotic. In the next step, the remaining ~1.1 ml of sample were microcentrifuged at ~12,000 rpm for 6 min and then ~800 µl of supernatant were removed. The cell pellets were resuspended with the residual supernatant to give ~100 µl total volume. Lastly, the ~100 µl sample was spread out as above (Sambrook and Russell, 2001).

Table 2.1: The *E. coli* stains used in this work

Strain name	Genotype	Reference
BW25113 Δ*feoA*::*kan*	F$^-$ Δ(*araD-araB*)*567* Δ*lacZ4787*(::*rrnB-3*) Δ*rph-1* Δ(*rhaD-rhaB*)*568 hsdR514* Δ*feoA*::*kan*	(Baba *et al.*, 2006)
BW25113 Δ*feoB*::*kan*	F$^-$ Δ(*araD-araB*)*567* Δ*lacZ4787*(::*rrnB-3*) Δ*rph-1* Δ(*rhaD-rhaB*)*568 hsdR514* Δ*feoB*::*kan*	(Baba *et al.*, 2006)
BW25113 Δ*feoC*::*kan*	F$^-$ Δ(*araD-araB*)*567* Δ*lacZ4787*(::*rrnB-3*) Δ*rph-1* Δ(*rhaD-rhaB*)*568 hsdR514* Δ*feoC*::*kan*	(Baba *et al.*, 2006)
E. coli BW25113	F$^-$Δ(*araD-araB*)*567* Δ*lacZ4787*(::*rrnB*-3) λ$^-$ *rph-1* Δ(*rhaD-rhaB*)*568 hsdR514*	(Baba *et al.*, 2006)
E. coli TOP10	*E. coli* F$^-$ *mcr*A Δ(*mrr-hsdRMS-mcrBC*) 80*lacZ*ΔM15 Δ*lacX74 nupG recA1 araD139* Δ(*ara- leu*)7697 *galE15 galK16 rpsL* (Str^R) *endA1* λ$^-$	Thermo Fisher Scientific
JC32	Derived from wild type (W3110) Δ*fecABCDE, ΔzupT, ΔmntH, ΔentC, ΔfeoABC, ΔefeU*	(Cao *et al.*, 2007)
JC32(pBADara-*feoAB*)	JC32 strain has pBADara plasmid carries *feoAB* gene	Lab stock
JC32(pBADara-*feoABC*)	JC32 strain has pBADara plasmid carries *feoABC* gene	Lab stock
JC32(pBADara)	JC32 strain has pBADara plasmid	Lab stock
JC32(pBADrha-*feoAB*)	JC32 strain has pBADrha plasmid carries *feoAB* gene	Lab stock

JC32(pBADrha-*feoABC*)	JC32 strain has pBADrha plasmid carries *feoABC* gene	Lab stock
JC32(pBADrha)	JC32 strain has pBADrha plasmid	Lab stock
TOP10(pBADara *feoABC*)	*E. coli* TOP10 strain has pBADara plasmid carries *feoABC* gene	Lab stock
TOP10(pBADara-*feoAB*)	*E. coli* TOP10 strain has pBADara plasmid carries *feoAB* gene	Lab stock
TOP10(pBADara)	*E. coli* TOP10 strain has pBADara plasmid	Lab stock
TOP10(pBADrha *feoAB*)	*E. coli* TOP10 strain has pBADrha plasmid carries *feoAB* gene	Lab stock
TOP10(pBADrha-*feoABC*)	*E. coli* TOP10 strain has pBADrha plasmid carries *feoABC* gene	Lab stock
TOP10(pBADrha)	*E. coli* TOP10 strain has pBADrha plasmid	Lab stock
W3110	Wild type F^- λ^- Δ(*rrnD-rrnE*)1 *rph*-1	(Bachmann, 1972) and (Hayashi *et al.*, 2006)

Table 2.2: The plasmids used in this work.

Plasmid name	Features	Reference/source
pBAD/His A (pBADara)	*araBAD* promoter allowing L-arabinose induction under AraC control, with a high-efficiencyT7 phage ribosome binding site. Multiple cloning site, Ap^R, medium copy (pBR322 *oriV*), *araC*-encoding, 4.1 kb. Used for tightly-controlled gene expression in *E. coli*.	Thermo Fisher Scientific
pBADrha	pBADrha is a vector and it has a cassette for chloramphenicol resistance as well as pSCrhaB2 can be used to active the rhamnose inducible promoter to regulate the gene expression. The vector contains *rhaR* and *rhaS*, genes regulator of rhamnose promoter, and the	(Ford *et al.*, 2014)

	transcriptional terminator (*rrnB*T1T2). In addition, the vector consists of two origins of replication, M13*ori* and p15A*ori*, and a multiple cloning site (MCS). The size of the plasmid is 6.1 kb.	
pBADara-*feoAB*	pBAD/His A expressing *feoAB* from *E. coli* K-12	(Al-Aidy, 2020)
pBADara-*feoABC*	pBAD/His A expressing *feoABC* from *E. coli* K-12	
pBADrha-*feoAB*	pBADrha consisting of *feoAB* from *E. coli* K-12	
pBADrha-*feoABC*	pBADrha consisting of *feoABC* from *E. coli* K-12	
pCP20	Knockout plasmid of ~9.4 kb. It is a temperature sensitive replicon and is used to remove the kanamycin-resistance cassette from the chromosome.	Datsenko and Wanner, 2000)
pMA:Flag-C*feoB*	pMA-T plasmid (2374 bp), Amp^R, with insert specifying the C-terminal domain (final 164 bp) of *feoB* (*E. coli*) with an N-terminal Flag- tag.	GeneArt
pMA:C*feoB*-Flag	As above, except that the Flag-tag is at the C-terminus	GeneArt
pMA:C*feoB*	As above, but no Flag-tag was included (final 140 bp)	GeneArt
pBADrha: Flag-*CfeoB*	pBADrha plasmid (6.1 kb), Cm^R, with insert specifying the C-terminal domain (final 164 bp) of *feoB* (*E. coli*) with an N-terminal Flag- tag.	This work
pBADrha: *CfeoB*-Flag	As above, except that the Flag-tag is at the C-terminus	This work
pBADrha: *CfeoB*	As above, but no Flag-tag was included (final 140 bp)	This work

Table 2.3: Primers used to confirm *feo* status. Tm was calculated by using the Sigma-Aldrich calculator

Gene	Direction of primers (F and R 5′ → 3′)	Melting Temperature (°C)	GC Content (%)	Primer Length
F-*feoABC*	AGCCACATCAACATT GAGTCAGAT	65.8	41.7	24
R-*feoABC*	TGTGTATTAGCGAGTT TTCATCCCT	65.4	40	25

Table 2.4: Primers used for site directed mutagenesis of the *feoB* gene for both plasmids pBADara-*feoAB* and pBADara-*feoABC* as indicated in the below (747- 750-755-760 and 765)

Gene	Direction of primers (F and R 5' → 3')	Melting Temperature (°C)	GC Content (%)	Primer Length
Change from serine (Ser) to stop codon (TAA) at ***feoB*** codon 747				
F-*feoB* S747*	CTG CGC CGC GCG CGT TAA CGG GTG GAT ATC GAA	88.7	63.6	33
R-*feoB*-S747*	TTC GAT ATC CAC CCG TTA ACG CGC GCG GCG CAG	88.7	63.6	33
Change from aspartate (Asp) to stop codon (TAA) at ***feoB*** codon 750				
F-*feoB*-D750*	GCG CGT AGC CGG GTG TAA ATC GAA CTG CTG GCA	85.50	60.61	33
R-*feoB*-D750*	TGC CAG CAG TTC GAT TTA CAC CCG GCT ACG CGC	85.50	60.61	33
Change from alanine (Ala) to stop codon (TAA) at ***feoB*** codon 755				
F-*feoB*-A755*	GTG GAT ATC GAA CTG CTG TAA ACC CGC AAG TCG GTA AGC	81.20	51.28	39
R-*feoB*-A755*	GCT TAC CGA CTT GCG GGT TTA CAG CAG TTC GAT ATC CAC	81.20	51.28	39
Change from valine (Val) to stop codon (TAA) at ***feoB*** codon 760				
F-*feoB*-V760*	GCA ACC CGC AAG TCG TAA AGC AGT TGC TGC GCA	85.40	57.58	33
R-*feoB*-V760*	TGC GCA GCA ACT GCT TTA CGA CTT GCG GGT TGC	85.40	57.58	33
Change from alanine (Ala) to stop codon (TAA) at ***feoB*** codon 765				
F-*feoB*-A765*	GTA AGC AGT TGC TGC TAA GCC AGC ACC ACC GGT	81.10	57.58	33
R-*feoB*-A765*	ACC GGT GGT GCT GGC TTA GCA GCA ACT GCT TAC	81.10	57.58	33

2.3 Preserving bacterial strains

Two methods were used to preserve bacterial strains. The first method involved inoculating a single colony into 5 ml of fresh LB in a test tube for incubation overnight on a shaker at 37 °C and 250 rpm. The following morning, 0.5 ml of the resulting overnight culture were transferred into a cryovial tube with 0.5 ml of sterile 50% glycerol. The second method was to streak the bacteria on to LB agar and, following incubation at 37 °C overnight, a single colony was

transferred into the cryovial tube with 0.5 ml of fresh LB and 0.5ml of 50% glycerol. For both methods, the cryovial tubes were stored at -80 °C (Sambrook and Russell, 2001).

2.4 Preparing LB broth and LB agar

To prepare the LB broth, 10 g of Oxoid tryptone, 5 g of Oxoid Yeast Extract and 5 g of sodium chloride were dissolved in 1 L of ultrapure water (18.2 Ω) in a 1 L Duran bottle. For the LB agar, 1 L of LB broth was combined with 15 g of Oxoid agar. Sterilisation was achieved by autoclaving (121 ˚C, 20 min) (Sambrook and Russell, 2001).

2.4.1 Preparing antibiotics

To prepare ampicillin at a 1000X stock concentration of 100 mg/ml, 1 g of sodium ampicillin was combined with 10 ml of ultrapure and sterile water (aseptically) and was then used at a working concentration 100 µg/ml. To prepare a chloramphenicol 1000X stock at 50 mg/ml, 0.5 g of chloramphenicol was combined with 10 ml 99% of absolute ethanol for use at a working concentration of 50 µg/ml. To prepare the 1000X kanamycin stock of 50 mg/ml, 0.5 g of kanamycin were added to 10 ml of ultrapure and sterile water for use at a working concentration of 50 µg/ml. These antibiotics were added to the media once the media had cooled down to <50 °C. All the antibiotics were sterilized using 0.22µm syringe filters and stored at -20 °C.

2.5 Preparing cultures in LB

Overnight cultures were prepared in 15 ml test tubes with 5 ml of LB broth, with or without suitable antibiotics (ampicillin at 100 µg/ml, for pBADara transformants; or chloramphenicol at 50 µg/ml for pBADrha transformants), by inoculation of a single colony from an L-agar plate. Incubation was at 250 rpm and 37 °C for around 16-18 h.

2.6 Preparing 0.4% glucose M9 minimal medium

A 200 ml volume of 5X M9 salts (Sigma-Aldrich), 2 ml of 1 M $MgSO_4$ (to give a final concentration 2 mM), 0.1 ml of 1 M $CaCl_2$ (to give a final concentration 0.1 mM), 10 ml of 10% thiamine (to give a final concentration 0.1% w/v), 40 ml of 20% w/v glucose (to give a final concentration 0.4%), 1 ml of 100 mg/ml ampicillin or 50 mg/ml chloramphenicol (to give

final concentration 100 and 50 μg/ml, respectively), and were combined with ultrapure sterilized water to give a total volume of 1 L. A 0.2 ml volume of 100 mM ferric citrate at pH ~7 (to give a final concentration 20 μM) and/or 10 ml of 20% w/v arabinose/rhamnose inducer (to give a final concentration 0.2%) were also included as required. Medium ingredients were sterilized by autoclave in 500 ml batches in acid-washed Duran bottles, or filter sterilised. Storage was at 4 °C.

2.7 Preparing 0.4% glucose M9 minimal agar plates

M9 agar plates were prepared by combining 160 ml of ultrapure H_2O with 3 g of agar per bottle and then the Duran bottles were autoclaved. After that, the following chemicals were added: 40 ml of autoclaved 5X M9 (to give 1X M9), 4 ml of 20% glucose (to give final concentration 0.4%), 0.4 ml of 1 M $MgSO_4$ (to give a final concentration 2 mM), 20 μl of 1 M $CaCl_2$ (to give a final concentration 0.1 mM), 2 ml of 10% thiamine (to give final concentration 0.1%), and 40 μl of 100 mM ferric citrate (to give a final concentration 20 μM). Suitable antibiotic was also added, and the agar was then carefully mixed and maintained at approximately 50 ˚C prior to pouring into Petri dishes. The plates were allowed to set and dry, and were then stored at 4 °C before use.

2.8 Aerobic bacterial growth experiments

An overnight pre-culture was prepared in test tubes with 5 ml of 0.4% glucose M9 minimal medium (plus 20 μM ferric citrate and antibiotics as required) by inoculation of a single colony from an M9 minimal agar plate. Test tubes were incubated at 250 rpm and 37 °C for around 16-18 h. Then, the pre-culture was harvested by centrifugation (an Eppendorf Centrifuge 5804 R) at 5000 rpm for 10 min 4 °C. In order to wash the pellet and remove the ferric citrate, the resulting pellet was resuspended in fresh (iron-free) M9 minimal medium and then re-centrifuged as above. The washing step was performed twice. The OD_{600} of the washed

preculture was determined and adjusted (with 0.4% M9 salts medium) to give a final OD of 1.0.

2.9 Anaerobic bacterial growth experiments

Overnight growth, harvesting and washing of preculture was as above (Methods 2.8). The growth medium (0.4% glucose M9 minimal medium) was inoculated to give a starting OD of 0.01. Then, 50 ml of inoculated medium were transferred to a 50 ml syringe equipped with needle. Any air was expelled and the needle aperture was sealed with a rubber bung to ensure an air-tight seal. The bacteria were then grown without shaking at 37 ˚C (up to 24 h) allowing anaerobiosis conditions to develop as residual oxygen is consumed. The OD was recorded every 2 h for 24 h by expelling 1 ml aliquots for measurement utilizing a WPA Colour wave CO7500 Colorimeter.

2.10 Preparing bacteria for growth using the Spark Tecan or Stratus Cerillo plate reader

High throughput growth comparisons were performed using a Spark Tecan plate reader at 37 ˚C, with 180 rpm shaking, over a 24 h period. Cultures, (prepared as in Methods 2.8) in 0.4% glucose minimal medium of 200 µl, were applied to the wells of a 96-well sterile plate (Nunclon Delta Surface, ThermoFisher Scientific) equipped with a lid. Ferric citrate (20 µM), diethylenetriamine pentaacetate (DTPA at pH 7; typically, at 1 µM), 100 mM MES buffer (pH 6), 2 mM ascorbate, antibiotic (Methods 2.4.1) and/or 0.02% arabinose were included in some cases. Growth comparisons were performed (in technical triplicate and biological duplicate) under aerobic conditions.

2.11 Plasmid DNA extraction (miniprep)

For this purpose, a GeneJET Plasmid Miniprep kit (Thermo Fisher Scientific) was used following the manufacturer's instructions, as follows. Firstly, a single *E. coli* transformant colony was inoculated into 5 ml of fresh LB in a bunged or capped test tube with the required concentration of antibiotic and the test tube was incubated overnight at 250 rpm and 37 ºC,

aseptically. Then, 1-5 ml (depending on plasmid copy number) of the overnight culture were centrifuged (microfuge at top speed for 5-10 min) and the resulting pelleted cells were resuspended in 250 µl of the Resuspension Solution with in a 2 ml Eppendorf tube. In this step it was important to make sure the bacteria were resuspended completely by vortexing or pipetting thoroughly. After this, 250 µl of the Lysis Solution (with SDS and NaOH/KOH) were added, with mixing by inverting the tube 4-6 times until the solution became clearer, indicating lysis had been achieved. Then, 350 µl of the Neutralization Solution were added with mixing as before, the samples were microcentrifuged for 5 min and the supernatant was transferred into a GeneJET spin column. The samples were then microcentrifuged for 1 min and the flow-through discarded. The column was placed back into the same tube and 500 µl of the Wash Solution were added followed by microcentrifugation for 1 min and removal of flow-through solution. In the last steps, the GeneJET spin column was transferred into a fresh 1.5 ml microcentrifuge tube and 50 µl of sterile ultrapure water were applied to the centre of the GeneJET spin column to elute the plasmid DNA. The samples were left at the room temperature for 2 min before microcentrifugation for 2 min. The column was removed and the 50 µl solution of purified plasmid was stored at -20 °C until required for further use.

2.12 Agarose gel electrophoresis

The agarose gel consisted of 0.7-1% agarose in 0.5X TBE buffer (5X TBE stock solution: 446 mM Tris base, 445 mM boric acid and 10 mM EDTA, pH 8.0). The agarose (0.7-1 g) was added to 80 ml of ultrapure water and was dissolved by heating to boiling point in a microwave oven; 20 ml of 5X TBE were added, and the solution was mixed and cooled to 50 °C. Then, 2 µl of gel red (Biotium) were added as nucleic acid stain. The agarose was poured into a UV-transparent gel tray, and the comb was placed in the top of the tray. Once the gel had set, the comb was removed, and the tray was placed in the gel tank with 0.5X TBE as running buffer. Samples (~10 µl) and DNA ladder (Fig. 2.1) were loaded into wells with DNA Gel Loading

Dye (Thermo Fisher scientific) included, and electrophoresis was performed at 90 V for 45 min.

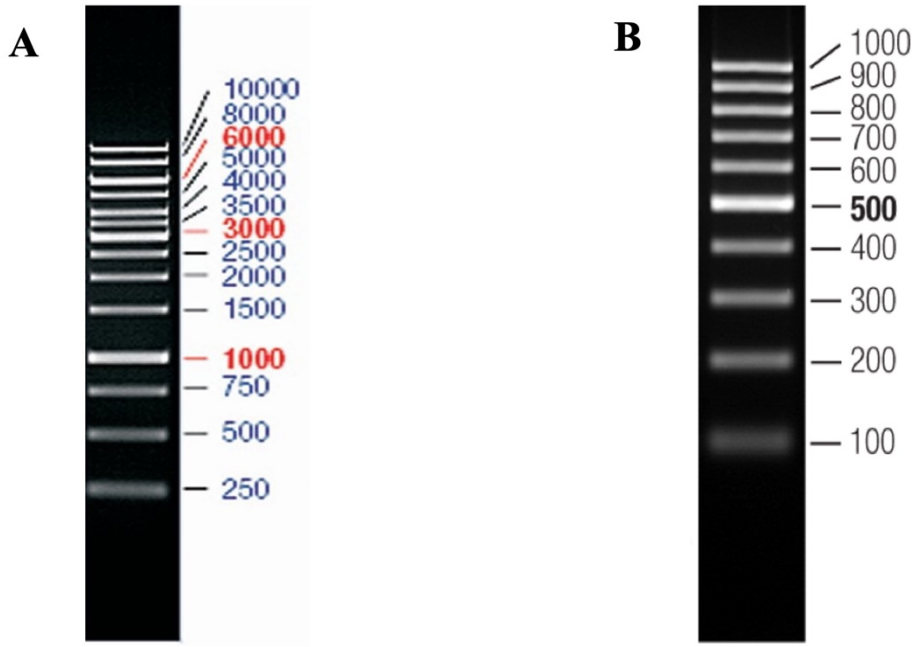

Figure 2.1: DNA size markers used in this study in agarose gel electrophoresis. (A) The GeneRuler 1kb ladder (from 250 bp to 10000 bp). **(B)** The GenRuler 100bp DNA ladder (from 100 bp to 1000 pb) (Thermo Fisher Scientific) that was utilized in. Typically, 3 µl were applied to each gel.

2.13 Plasmid digestion by using restriction enzymes

Plasmid DNA was digested by using the appropriate restriction enzyme(s) (Table 2.5) and by following the manufacturer's instructions. The digestion reaction was performed in total volume of 20 µl consisting of 100 ng/µl of plasmid, 2 µl of 10X Fast Digest Green Buffer, 1 µl of each enzyme and qH_2O up to a final volume of 20 µl. The reaction was incubated at 37 °C in water bath for 5 min and the digested plasmid was then subjected to agarose gel electrophoresis (Methods 2.12).

Table 2.5: Restriction enzymes used in this work

Restriction enzyme names	Restriction enzyme site	Purchased
*Hin*dIII	5'-A↓AGCTT-3' 3'-TTCGA↑A-5'	Thermo Fisher Scientific
*Bam*HI	5'-G↓GATCC-3' 3'-CCTAG↑G-5'	Thermo Fisher Scientific
*Nde*I	5'-CA↓TATG-3' 3'-GTAT↑AC-5'	Thermo Fisher Scientific
*Sal*I	5'-G↓TCGAC-3' 3'-CAGCT↑G-5'	Thermo Fisher Scientific
*Xho*I	5'-C↓TCGAG-3' 3'-GAGCT↑C-5'	Thermo Fisher Scientific
*Nco*I	5'-C↓CATGG-3' 3'-GGTAC↑C-5	Thermo Fisher Scientific

2.14 Genomic DNA purification from *E. coli*

For this purpose, a GeneJET Genomic DNA Purification Kit was used (Thermo Fisher Scientific) using the protocol provided, as follows. Firstly, an overnight culture was prepared in LB broth, as in (Methods 2.4). Next morning, 1 ml of the overnight culture was placed into a 1.5 ml Eppendorf tube and then micocentrifuged for 10 min at 5000 x g, and the pellet was retained. Then, the pellet was resuspended in 180 µl of Digestion solution, 20 µl of Proteinase K solution were added and the mixture was vortexed. The samples were then incubated at 56 °C for 30 min using the shaking water bath until the cells were fully lysed. Following this, 20 µl of RNase A solution were added, the sample was briefly vortexed and then incubated for 10 min at room temperature. Next, 200 µl of Lysis solution were added and the samples were vortexed for 15 s. Ethanol (400 µl of 50% v/v) was added to the samples which were then transferred into the GeneJET genomic DNA purification column placed within a collection tube. The samples were centrifuged for 1 min at 6000 x g. The collection tubes were removed and replaced by a new 2 ml GeneJET Genomic DNA purification column. Then, 500 µl of Wash Buffer I were applied and the samples were then centrifuged for 1 min at 8000 x g with discard of the flow-through and placement of the purification column back into the collection

tube. Wash Buffer II (500 µl) was then applied, and samples were centrifuged for 3 min at 12000 x g. Finally, 30 µl of sterile ultrapure water were applied to the centre of the GeneJET column membrane for 2 min at room temperature and the samples was then centrifuged for 1 min at 8000 x g to elute the DNA, which was stored at -20 °C.

2.15 Polymerase chain reaction (PCR)

A Phusion High Fidelity DNA Polymerase kit (Thermo Fisher Scientific) was used according to manufacturer's instructions. The PCR reaction consisted of a 20 µl total volume in a 50 or 20 µl PCR tube (4 µl of 5X Phusion GC buffer, 0.4 µl of 10 mM dNTP mix, 1 µl each of forward and reverse primer of 10 µM, 1 µl of template DNA, 0.5 µl of 50 mM $MgCl_2$, 1 µl of 100% DMSO, 0.2 µl of Phusion DNA polymerase and 10.9 µl of water). PCR reactions were performed using a 96-well T100 PCR thermal cycler machine using the conditions indicated (Table 2.6).

Table 2.6: PCR program used with the Phusion High Fidelity DNA Polymerase kit.

Phase	Temperature	Time	Number of cycles
Primary denaturation	98 ºC	3 min	1 cycle
Denaturation	98 ºC	30 s	30 cycles
Annealing	67 ºC	30 s	
Extension	72 ºC	5 min	
Last Extension	72 ºC	5 min	1 cycle

DreamTaq Green PCR Master Mix (2X) (Thermo Fisher Scientific) was also used in some cases, following the manufacturer's instructions. The PCR reaction contained 1 µl of template DNA, 1 µl of each primer (to give a final concentration of 0.5 µM), 12.5µl of Master Mix and 9.5 µl of, nuclease-free water (from the kit). All other details are as above apart from the PCR program (Table 2.7).

Table 2.7: PCR program used with DreamTaq Green PCR Master Mix (2X). The below conditions are as recommended by Thermo Fisher Scientific.

Phase	Temperature	Time	Number of cycles
Primary denaturation	95 ºC	3 minutes	1 cycle
Denaturation	95 ºC	30 seconds	30 cycles
Annealing	58-60 ºC	30 seconds	
Extension	72 ºC	1 minute	
Last Extension	72 ºC	5 minutes	1 cycle

2.16 Deleting the kanamycin cassette using plasmid pCP20

The pCP20 plasmid (from the lab stocks) was transformed into competent TOP10 (Methods 2.2) and fresh plasmid DNA was isolated (Methods 2.11). The identity of the isolated pCP20 plasmid was confirmed by double restriction digestion with *Bam*HI and *Nco*I, and single single digestion with *Xho*I. Once the plasmid was confirmed, it was introduced (by chemical transformation) into competent BW25113Δ*feoA*::*kan*, Δ*feoB*::*kan* and Δ*feoC*::*kan* to eliminate the kanamycin cassette, as follows. The Δ*feo*::*kan* transformants were selected on 100 µg/ml ampicillin at 30º C. Next day, some of the colonies were transferred in LB agar without antibiotic and incubated at 43 ºC for 16 h to induce FLP synthesis for removal of the kanamycin cassette and to inhibit further pCP20 replication. Resulting colonies were then isolated and screened for sensitivity to ampicillin, chloramphenicol and kanamycin to confirm that the plasmid (Amp^R/Cm^R) and Kan cassette had been lost. Strain identity was further confirmed by PCR (Methods 2.15).

2.17 Site-directed mutagenesis (SDM)

The Quikchange II XL Site-Directed Mutagenesis kit (Agilent) was employed according to the manufacturer's instructions. The primers (complementary forward and reverse) were designed to be 25-45 nucleotides in length, with the mismatch directing the corresponding mutation position in the middle. The GC content for the primers was above 40-60% and a 3 nucleotide 'GC clamp' was placed at the 3′ end. The Tm was >78 °C and was calculated using the

following equation: Tm = 81.5+0.41*(%GC)–675/N–'% mismatch' (where N is the length of primer), as recommended by the kit manufacturer. The PCR reactions for the control and the test samples for SDM were as follow: 5 µl of 10x reaction buffer; 2 µl (10 ng) of whitescript 4.5-kb control plasmid (5 ng/µl) or 5-50 ng of pBADara-*feo* DNA template; 1.25 µl (125 ng) of each primer; 1 µl of dNTP mix; 3 µl of QuikSolution reagent; 36.5 µl of double-distilled water (ddH_2O) to final volume of 50 µl; and 1 µl of *PfuUltra* HF DNA polymerase (2.5 U/µl). The PCR reaction conditions are indicated in (Table 2.8).

Table 2.8: The PCR's conditions used for SDM. Rate of PCR was 1 kb/min at 68 °C.

Step	Number of cycles	Temperature	Time
1	1	95°C	1 min
2	18	95°C	50 sec
		60°C	50 sec
		68°C	1 min/kb of plasmid length
3	1	68°C	7 min

PCR products were assessed by agarose electrophoresis. After the PCR the reaction, 1 µl of *Dpn*I (10 U/µl) was added to 10 µl of each PCR reaction, mixed and incubated it at 37 °C for 1 h to digest the methylated template DNA. The XL 10-Gold ultracompetent cells were carefully thawed on ice and then 45 µl of XL 10-Gold ultracompetent cells were transferred to a prechilled 14 ml BD Falcon polypropylene round-bottom tube for both control and samples. Then, 2 µl of β-mercaptoethanol were added to the 45 µl of cells, with carefully mixing. The reaction was incubated on ice for 10 min with gentle mixing every 2 min. Following this, 2 µl of *Dpn*I-treated PCR-amplified DNA was transferred into 45 µl aliquots of ultracompetent cells, with gentle mixing, and this was then incubated on ice for 30 min. Each tube was heated at 42 °C in a water bath for 30 sec, this step was critical in order to get a high efficiency of transformant bacteria. Tubes were then incubated on ice 2 min. A 0.5 ml volume of preheated NZY^+ broth (at 42 °C) (purchased from Sigma-Aldrich) was added to each tube and then tubes

were incubated at 37 °C for 1 h with shaking at 250 rpm. The transformation reactions were plated out on LB agar with appropriate antibiotic and incubated 16 h at 37 °C. Resultant transformants were subject to plasmid isolation using the GeneJET Plasmid Miniprep kit (Methods 2.11) and the isolated plasmid DNA was assessed by agarose gel electrophoresis. Samples that exhibited the expected size pattern were submitted to Eurofins Scientific for Sanger sequencing. The primers for forward and reversed were designed to be anneal at a 50 bp distance from the mutation site (Table 2.9).

Table 2.9: Primers used for Sanger sequencing to confirm the mutants.

Gene	Direction of primers (F and R 5′ → 3′)	Melting temperature (°C)	GC content (%)	Primer length (nucleotides)
F-*feoABC*	GCTGAATATCGCTTACTCAC	56.60	45	20
R-*feoABC*	GTAACGCCAGCAAATCG	60.40	52.94	17

2.18 Cloning the region of *feoB* encoding the C-terminal extension domain, with/without a Flag-tag, into pBADrha

2.18.1 Design and synthesis of *CfeoB*

The C-terminal extension domain of FeoB (C-FeoB) was identified by using PyMol to display the predicted structure (from Alpha Fold) of the *E. coli* FeoB protein. In addition, a multiple alignment of FeoB amino acid sequences from a diverse range of bacterial species was utilized to identify the C-FeoB region of FeoB from the Enterobacteriaceae. Alignment was achieved using the Geneious Alignment tool (part of the Geneious Prime package) with default parameters. The ~47 amino acid region thus identified (~140 bp) was synthesised by GeneArt in three formats: with an 8-codon Flag-tag sequence (DYKDDDDK) at the N-terminus and C-terminus with the Flag-tag sequence; and without any Flag-tag. All three synthetic *CfeoB* sequences included flanking regions to enable Gibson cloning into the multiple-cloning site of the inducible plasmid, pBADrha, in a format designed to allow expression of *CfeoB* from the rhamnose-inducible promoter. Thus, a start codon was included at the beginning of each *CfeoB* gene and two consecutive stop codons at the end. In addition, *Nde*I and *Hin*dIII sites were

included at the up- and down-stream flanking regions, respectively, for cloning and restriction mapping purposes. The synthetic constructs were received from GeneArt within the pMA-T vector (Amp^R) and were designated: pMA:Flag-*CfeoB* (Appendix Figs. A.1&A.2); pMA:*CfeoB*-Flag (Appendix Figs. A.3&A.4); and pMA:*CfeoB* (Appendix Figs. A.5&A.6). Each plasmid was used to transform TOP10 to enable isolation of plasmid DNA as a source of DNA for cloning purposes. The pBADrha plasmid was digested with *Nde*I and *Hin*dIII (Methods 2.13), and the linearised plasmid was then purified from an agarose gel (Methods 2.18.2).

2.18.2 Preparation of pBADrha

The pBADrha plasmid was digested and purified by gel electrophoresis using a GeneJET Gel Extraction kit (Thermo Fisher Scientific) according to the manufacturer's instructions. Thus, the linearised plasmid was electrophoresed in a 0.7% agarose gel at 80 V for 60 min. Low-energy UV light was used to observe the corresponding band (~6 kb) which was excised from the gel using a fresh scalpel blade. The gel slice was placed into a 1.5 ml Eppendorf tube and its weight was determined to calculate the volume of Binding Buffer required. The required volume of binding buffer was then applied to the tube containing the gel slice (1:1 w/v). The gel mixture was incubated at 50-60 °C for 10 min with occasional inversion making sure that the gel slice was totally dissolved. After the incubation period, the yellow colour was checked to indicate that an optimal pH for DNA binding was achieved. Following this, 800 µl of the mixture were transferred to the GeneJET purification column, and this was centrifuged for 1 min and the flow-through was removed. Then, 700 µl of Wash Buffer (containing ethanol) were added to the GeneJET purification column which was centrifuged for 1 min. The flow-through was discarded. The GeneJET purification column was centrifuged again to remove residual Wash Buffer. Finally, the GeneJET purification column was placed into 1.5 ml Eppendorf tube and 30 µl of sterile ultrapure water were added to the centre of the GeneJET

purification column membrane (to elute the plasmid). The column was centrifuged for 1 min and the purified DNA was stored at -20 °C. All purification steps were performed at room temperature using a microcentrifuge at 10000 rpm.

2.18.3 Ligation of *CfeoB* into pBADrha plasmid using T4 DNA ligase

Once the linearised, *Nde*I/*Hin*dIII-digested and purified pBADrha plasmid had been prepared, the *CfeoB* target genes (insert DNA) were also prepared for cloning by digestion with *Nde*I and *Hin*dIII. Ligation was then achieved with T4 DNA ligase by applying the manufacturer's (ThermoFisher) protocol for sticky-end ligation. The reaction mixture thus included the linearised vector (20-100 ng of DNA) and the insert DNA at 1:1, 3:1 and 5:1 molar ratios (insert: vector). In addition, 2 µl of 10X T4 ligase buffer and 1 Weiss U of T4 DNA ligase were added to the mixture, with nuclease-free water added to give a final volume of 20 µl. The ligation reactions were mixed and incubated for 1 h at 22 °C. Then the mixture was incubated at 65 °C for 10 min to inactivate the T4 DNA ligase. Following this, 2 µl volumes of the ligation reaction mixtures were used to transform competent TOP10 (Methods 2.2) and Cm^R transformants were selected. Several of the resultant Cm^R (Amp^S) transformants were then isolated and subjected to plasmid isolation (Methods 2.11). Plasmid identity was confirmed by restriction mapping and by NGS using the Nanopore 30 sequencing service (Source Bioscience).

2.19 Sodium dodecyl sulphate polyacrylamide gel electrophoresis (SDS-PAGE) and western blotting

2.19.1 Sample preparation

Cell pellets (0.5 OD) were collected from cultures when the bacterial growth reached an OD of 0.5. The residual supernatant was thoroughly removed, and pellets were stored at -20 °C for further work. Prior to electrophoresis, the pellets were defrosted on ice, resuspended in 100 µl of 1X digestion buffer (100 mM Tris-HCl, pH 6.8, 4% (w/v) SDS, 0.1% (w/v) bromophenol

blue, 200 mM DTT and 20% (v/v) glycerol in ultrapure water), heated at 100 °C for 10 min and then centrifuged at 13000 rpm for 5 min before loading into wells.

2.19.2 SDS-PAGE

SDS-PAGE was used to separate proteins using a BioRad MiniProtean III system following the manufacturer's guidance. Gels of 15% w/v acrylamide were freshly made in the laboratory and the resolving gel contained: 5 ml of 1.5 M Tris-HCl (pH 8.8); 10 ml of 30% w/v acrylamide (Bio-Rad); 100 µl of 10% of w/v fresh ammonium persulphate; 5 µl of TEMED; and 200 µl of 10% SDS. The 4% of stacking gel contained: 2.5 ml of 0.5 M Tris-HCl (pH 6.8); 1.5 ml of 30% w/v acrylamide; 10 µl of fresh 10% w/v ammonium persulphate; 5 µl of TEMED; and 35 µl of 10% SDS. Gels consisted of 4 ml of resolving gel followed by 2 ml of stacking gel. Isopropanol was layered on top of the resolving gel during setting to generate a smooth surface and support polymerisation. A comb was inserted into the stacking gel solution to form wells. Once set, the comb was removed, the wells were rinsed with qH_2O and the gel cassette was placed into the electrophoresis tank with running buffer (250 mM Tris, 1.9 M glycine, 1% w/v SDS). Samples (10 µl) were then applied to the wells and power was applied at a constant 30 mA/gel. Once the dye front had reached the bottom of the gel (~45 min), the power was disconnected and the gels were removed from the gel cassette and then stained with 0.2% Coomassie Brilliant Blue R-250 in destaining solution (30% v/v methanol and 10% v/v glacial acetic acid) for 1 h. The stain was then removed, the gels were rinsed in qH_2O and soaked in destaining solution until background stain was removed from the gel. Finally, the UVP GelDoc-it Bio-Imaging system was used to document the gel.

Premade gradient gels (4 to 20% acrylamide tris glycine) and 16% acrylamide Tris-Tricine gels (from BioRad) were also used following manufacturer's instructions.

2.19.3 Western blotting

2.19.3.1 Electrotransfer

Following SDS-PAGE, the unstained gel was used to transfer the resolved proteins to a nitrocellulose membrane using a BioRad Transblot Turbo following the manufacturer's guidance, as below. The gel cassette was washed with qH_2O to ensure remove residual running buffer. The nitrocellulose membrane was pre-soaked in transfer buffer (250 mM Tris, 1.9 M glycine, 20% methanol). After that, the gel was released from the cassette and the stacking gel was removed. Next, two soaked filter papers were placed on the base of the drawer of Transblot Turbo, the nitrocellulose membrane was then placed on the top of the filter paper, the resolving gel was placed on top of nitrocellulose membrane and two more filter papers were placed on top of the resolving gel. A roller was used to eliminate air bubbles. The drawer was locked and placed into Transblot Turbo, and the power was applied (25 V, 2.5 A, 30 min).

2.19.3.2 Blocking and washing steps

After the electrotransfer step, the nitrocellulose membrane was released from the Transblot system and treated by soaking in 1X Tris-buffered saline (TBS: 20 mM Tris; 150 mM NaCl; pH 7.6) with 5% non-fat dried milk (as blocking agent) at room temperature for 2 h (or at 4 °C overnight) with gentle shaking. Once the blocking step was complete, the nitrocellulose membrane was washed three times with TBS-T (100 ml of 10X TBS buffer and 1 ml of Tween 20 in 1000 ml).

2.19.3.3 Immunodetection

After the blocking and washing steps, the anti-Flag-tag primary antibody (purchased from Abcam) was applied (at 1:1000 dilution in blocking buffer) to the nitrocellulose membrane and incubated the membrane for 2 h at room temperature with shaking. The nitrocellulose membrane was then washed three times with TBS-T and the secondary antibody (Goat Anti-Mouse IgG H&L (HRP) was then applied (at a 1:2000 dilution in blocking buffer) for 1 h.

Following this, the nitrocellulose membrane was washed three times in TBS-T to remove any remaining Tween 20 detergent and then immune-positive bands were detected by adding the ECL substrate (Thermo Fisher). The blot was then observed and documented using a G:BOX Chemi XRQ (Syngene) system equipped with GeneSys software.

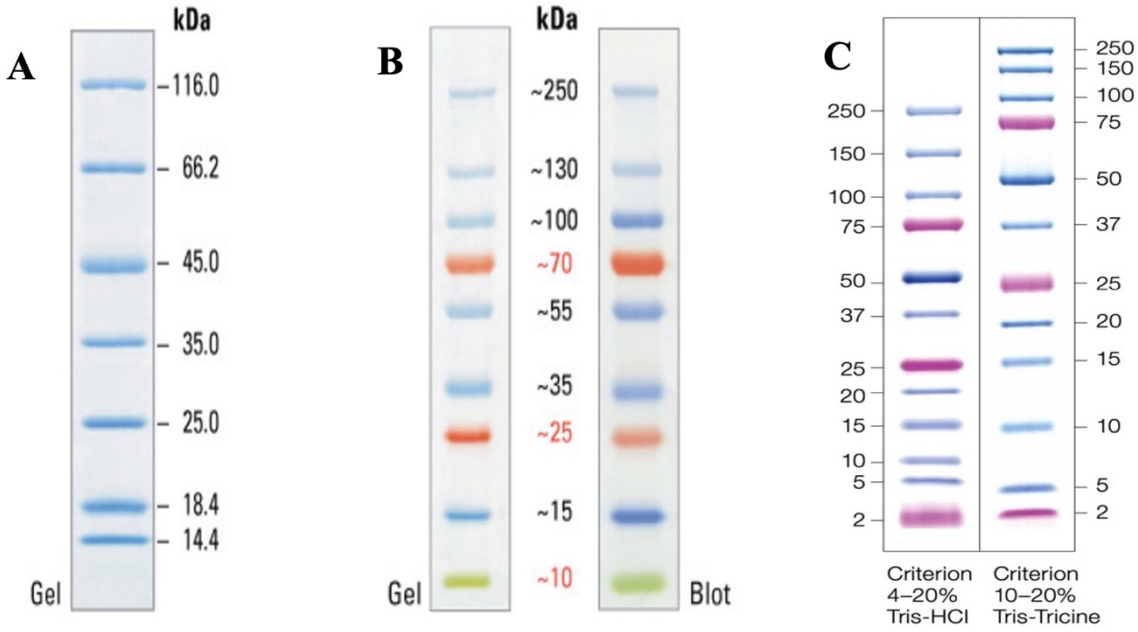

Figure 2.2: SDS-PAGE and western-blot size markers used in this study. **(A)** PageRuler™ Unstained Low Range Protein Ladder used for SDS-PAGE (ThermoFisher Scientific). **(B)** PageRuler™ Prestained protein ladder used for western blot experiment (ThermoFisher Scientific). **(C)** Precision Plus Protein™ Dual Xtra Prestained Protein Standards - a low range protein ladder (2 to 250 kDa) (from BioRad) used for western blotting.

2.20 RNA extraction from *E. coli*

2.20.1 Collection of samples

The samples were collected in RNA-free sterile 50 ml Falcon tubes and two volumes of RNA protector (Later) were added. The samples were then incubated at room temperature for 5 min and centrifuged at 5000 *g* and 4 °C for 10 min. Finally, the supernatant was discarded from each sample and the tubes were kept at -80 °C for RNA isolation according to Qiagen's protocols.

2.20.2 RNA isolation

The RNAprotect Bacteria Reagent kit (Qiagen) was used to isolate total RNA following the manufacturer's instructions. The samples were defrosted at room temperature and then 250 µl of TE buffer, lysozyme and proteinase K were added to each sample with vortexing for 10 s. The samples were then incubated at room temperature for 10 min with vortexing every 2 min for 10 s. A 700 µl volume of RLT and β-mercaptoehanol buffer were added to each sample with vortexing, 500 µl of absolute ethanol were added to each sample and the samples were mixed gently by pipetting. After this, 700 µl of the lysate mixture was transferred to a RNeasy mini spin column which was then centrifuged at >8000 *g* for 30 s and the flow-through was discarded. This step was repeated with a further 700 µl volume of lysate mixture. A 350 µl volume of RW1 buffer was added to each sample followed by centrifugation at >8000 *g* for 30 s. An 80 µl volume of DNase I in RDD was added to each sample followed by incubation at 30 °C in a thermomixer for 15 min. Again, 350 µl of RW1 buffer was added to each sample which was incubated at room temperature for 5 min and centrifuged at >8000 *g* for 30 s. Then, 500 µl of RPE buffer (with ethanol) were added to the spin column which was then centrifuged at >8000 *g* for 30 s, and the flow-through was discarded. Again, 500 µl of RPE buffer (with ethanol) were added to the spin column which was then centrifuged at >8000 *g* for 2 min. The column was placed into a new collection tube and centrifuged at >8000 *g* for 1 min to remove any remaining ethanol. The spin column was then placed into an RNase-free, sterile 1.5 ml Eppendorf tube and the RNA was eluted by adding 30 µl of RNase-free water into the middle of the spin column membrane, followed by incubation for 2-3 min and centrifugation the at >8000 *g* for 1 min. Following this, 20 µl of RNase-free water were applied to the middle of the spin column membrane (to elute any remaining RNA) with incubation for 2-3 min before centrifugation at >8000 *g* for 1 min. The resultant 50 µl RNA samples were then stored at -80 °C immediately.

2.20.3 TURBO DNA-free™ treatment of total RNA

A TURBO DNA-free™ DNase kit (Invitrogen) was used to remove any contaminating DNA from the total RNA samples generated as above. Firstly, each sample was diluted to 10 µg in 50 µl and then a 0.1 volume of 10X TURBO DNase™ buffer was added to each sample with mixing. After that, 2 µl of TURBO DNase™ enzyme were added to the samples with mixing and the samples were incubated at 37 °C using the Thermomixer for 30 min. Again, 2 µl of TURBO DNase™ enzyme were added to the samples with incubation at 37 °C for another 30 min. Then, a 0.2 volume of DNase Inactivation Reagent was added with mixing by vortex followed by incubation for 5 min at room temperature with intermittent mixing. Finally, the samples were centrifuged at 10,000 *g* for 1.5 min, the supernatant was transferred to an RNA-free sterile 1.5 ml Eppendorf tube and the RNA was stored at -80 °C.

2.20.4 Measure the quality of RNA with an Agilent 4200 TapeStation

The Agilent 4200 TapeStation was used to check the quality and quantity of RNA. RNA sample buffer was allowed to warm to room temperature for 30 min. Then the RNA ladder and the total RNA were thawed on ice. For the ladder, 5µl of RNA sample buffer was added to the tube strip along with 1µl of RNA ladder, for the samples 5µl of RNA sample buffer was added to the tube strip along with 1µl the sample (total RNA). After that, samples were mixed using an IKA vortex system at 2000 rpm for 1 min with spinning the ladder and samples down. Ladder and samples were heated to 72 °C to denaturation for 3 min and then the strip tube was placed on ice for 2 min with spinning the ladder and samples down. Then, the strip tube was loaded into the Agilent 4200 TapeStation and the cap of the tube strips was removed carefully. The ladder was placed into the A1 position on tube strip holder in the Tapestation instrument. In the next step, the RNA screenTape and tips were placed in the instrument. Once all the above steps were completed, the start button was clicked to run the instrument. Finally, once the run finished, the Agilent TapeStation analysis software opened the results. Following sample validation, the samples were submitted to Novogene for RNA sequencing.

2.20.5 RNA sequencing and data analysis

The methodology followed by Novogene is briefly described below. RNA integrity was confirmed using the Bioanalyzer 2100 system. Then, rRNA was removed from the total RNA followed by ethanol precipitation of the remaining RNA. After fragmentation, first strand cDNA was generated using reverse transcriptase and random hexamer primers. Second strand synthesis was achieved with DNA polymerase and the dUTPs were exchanged with dTTPs during the cDNA synthesis. The cDNA was then subjected to end repair, A-tailing, adapter ligation, size selection, amplification and purification. The quality of the resulting cDNA library was then confirmed Qubit, real-time PCR and Bioanalyzer analysis. The library preparations were then pooled and subjected to Illumina sequencing. The resulting sequence data were processed to remove adapter sequences and low-quality sequence data; only high-quality data were utilised for further analysis. Reads were aligned to the genome sequence using Bowtie 2-2.2.3. HTSeq v0.6.1 and FPKM were used to quantify reads per gene, and DESeq2 was used for differential expression analysis.

Chapter 3: Exploring the role of FeoC: complementation of *feo* mutants with inducible *feoAB* and *feoABC* constructs

3.1 Introduction

E. coli is a Gram-negative facultatively anaerobic bacterium (Lim, Yoon and Hovde, 2010). Aerobically at neutral to alkaline pH, iron is mainly in its oxidized ferric form. Under microaerobic/anaerobic conditions or low pH, iron is stable in its reduced ferrous form. Many bacteria can transport both ferric and ferrous iron using distinct uptake systems. Such ferrous uptake systems include the metal-ABC transporters MntH, ZupT, YfeABCD and FutABC, EfeUOB and Feo (Lau *et al.,* 2015). The Feo system was first found in *Escherichia coli* K-12 (Hantke, 1987; Cartron *et al.*, 2006). The Feo system of *E. coli* is encoded by three genes (*feoA*, *feoB* and *feoC*) that form an operon. The *feoA* gene encodes a 75 amino acid residue cytoplasmic protein that appears to interact with FeoB to stimulate its iron-uptake activity (Cartron *et al.*, 2006). FeoB is the main ferrous-iron transporter. It consists of 773 residues and contains two main regions: an N-terminal cytoplasmic G-protein domain and C-terminal polytopic transmembrane domain. FeoC is a 78 residue cytoplasmic protein consisting of a helix-turn-helix motif and an iron-sulphur cluster. It is reported to regulate FeoB stability in response to oxygen (Kim *et al.,* 2015). FeoC is found in the Feo systems of *Gammaproteobacteria* but is not otherwise normally found within bacterial Feo systems (Lau *et al.,* 2013; Gómez-Garzón *et al.,* 2022).

In the research described in this chapter, it was firstly important to confirm that the JC32 bacterium (derived from the wild type W3110 strain) is mutated in all relevant iron-transport systems. Additionally, it was necessary to test its iron-restriction phenotype. This was achieved through growth on M9 minimal medium with 0.4% glucose, with/without iron and with/without DTPA as ferric iron chelator (Paterson *et al.*, 2022) aerobically using 250 ml flasks and 96-well plates within a Spark Tecan multimode plate reader. Growth experiments

were also performed anaerobically using 50 ml syringes. PCR was used to confirm *feoABC* status. In addition, the genotype of JC32 was further confirmed by whole genome sequencing.

Secondly, once the genotype and phenotype of JC32 had been confirmed, pBADara-*feoAB* and pBADara-*feoABC* were obtained from the lab stocks and their identities were confirmed by *feoAB* and *feoABC* by restriction digestion and gel electrophoresis. They were then transferred into JC32 to enable growth tests aimed at exploring the function of FeoC under iron-restricted growth conditions, both aerobically and anaerobically, and in the presence and absence of reductant. Lastly, single Δ*feoA*, Δ*feoB* and Δ*feoC* mutants were obtained from the lab stocks and their phenotypes were tested under iron-restricted growth conditions with/without bipyridyl (Romeo *et al.*, 2001) with/without reductant and pH control via provision of a suitable buffer.

The aim of this chapter was thus to investigate the role of FeoC on the iron-uptake activity of the Feo system through performing growth comparisons under a range of iron-restriction conditions in the presence and absence of *feoC*.

3.2 Isolation and confirmation of the *feoAB* and *feoABC* inducible pBAD plasmids

In order to confirm that the *feoC* gene does indeed contribute to Feo-dependent growth under iron restriction (Al-Aidy, 2020), it was necessary to compare the growth of *E. coli* strains carrying *feoAB* with those bearing *feoABC*. To enable this, a set of corresponding pBADara and pBADrha plasmids was obtained from laboratory stocks (Table 2.2) as plasmid DNA samples. These were used to transform competent *E. coli* TOP10 and then plasmid DNA was isolated from the resulting Ap^R and Cm^R transformants. The identity of the isolated plasmids was confirmed by gel electrophoresis and restriction digestion (Methods 2.11, 2.12, 2.13; Fig. 3.1, 3.3).

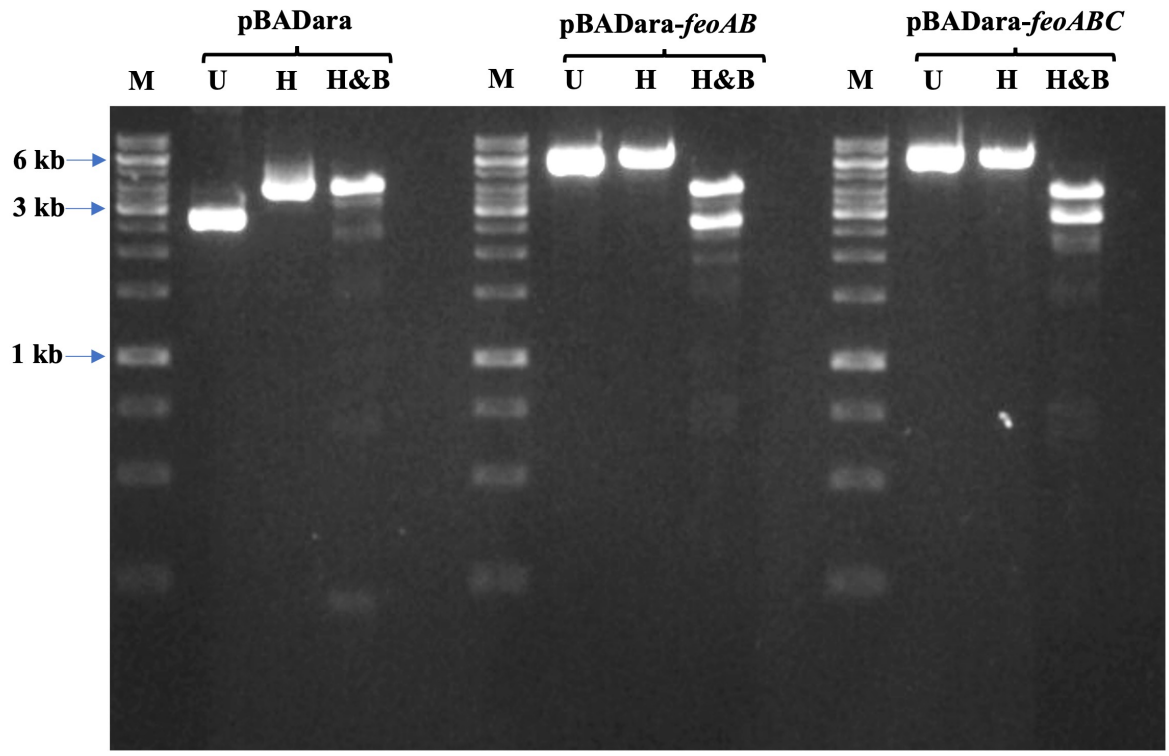

Figure 3.1: Agarose gel electrophoretic analysis of pBADara, pBADara-*feoAB* and pBADara-*feoABC* DNA with and without restriction digestion. M, GeneRule 1 kb ladder (Fig. 2.1); U, undigested; H, *Hin*dIII digested; and H&B, *Hin*dIII and *Bam*HI digested.

For the three pBADara/His plasmids (Fig. 3.1) the expected sizes were observed. The pBADara (4.1 kb) uncut DNA had a mobility similar to that of the 2.5 kb marker; covalently closed circular DNA generally runs at two-thirds of the linear form, so the observed mobility is as expected. *Hin*dIII and *Hin*dIII/*Bam*HI double digestion gave a band of ~4 kb, as expected for the linearised plasmid (Fig. 3.2A). The pBADara-*feoAB* (6.65 kb) and pBADara-*feoABC* (6.9 kb) samples gave linearized plasmid DNA bands of 6-7 kb, as expected, and the double digests released fragments matching the expected 2.5 and 2.8 kb *feoAB* and *feoABC* inserts (Fig. 3.2B, C), respectively. This confirms the identity of the three pBADara plasmids.

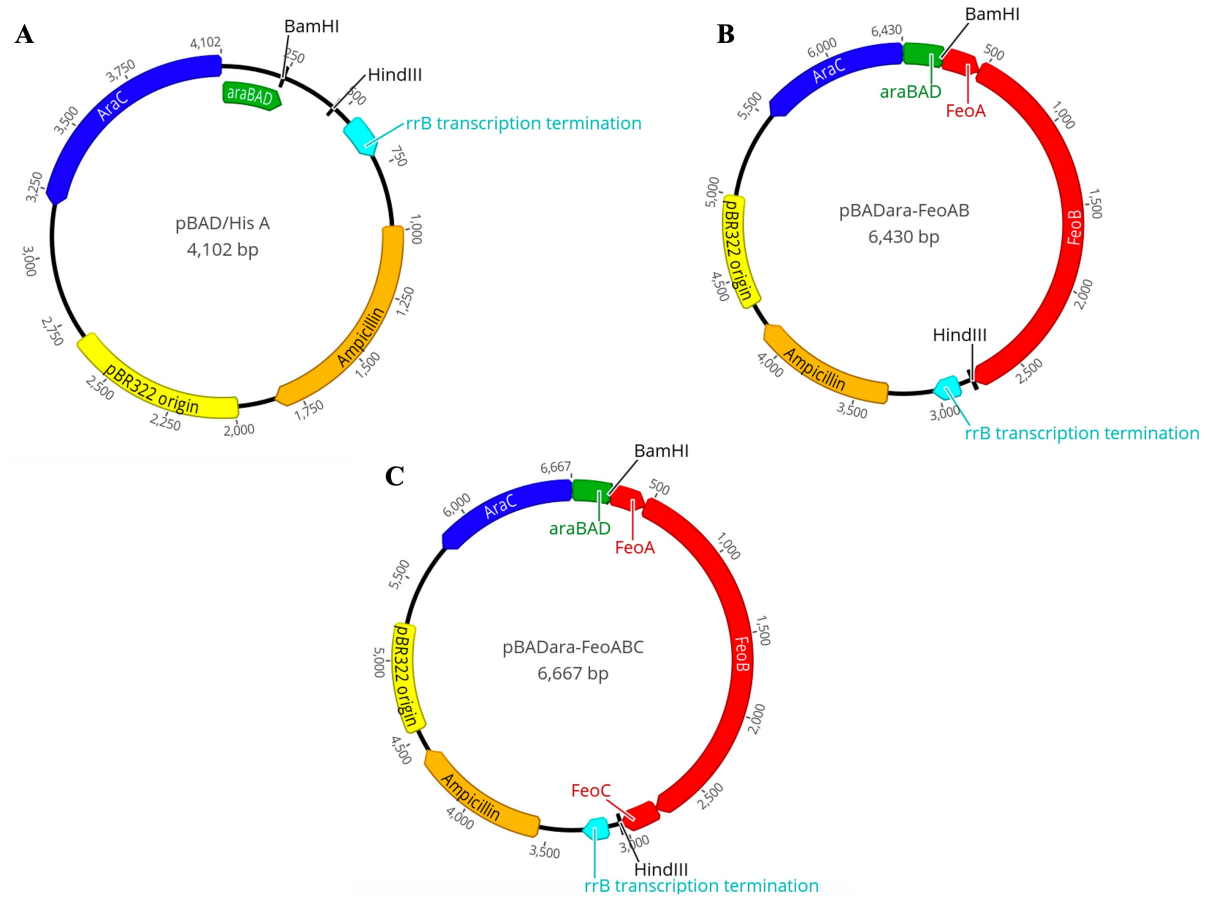

Figure 3.2: Genetic maps of pBADara, pBADara-*feoAB* and pBADara-*feoABC*. (A) For pBADara, loci shown include the multiple cloning site (MCS), the *araBAD* promotor (green), the *araC* gene and Amp^R locus. **(B)** For pBADara-*feoAB*, the *feoAB* locus inserted between *Bam*HI and *Hin*dIII is also shown. **(C)** For pBADara-*feoABC*, the *feoABC* operon inserted between *Bam*HI and *Hin*dIII is also indicated. Maps were generated using Geneious Prime.

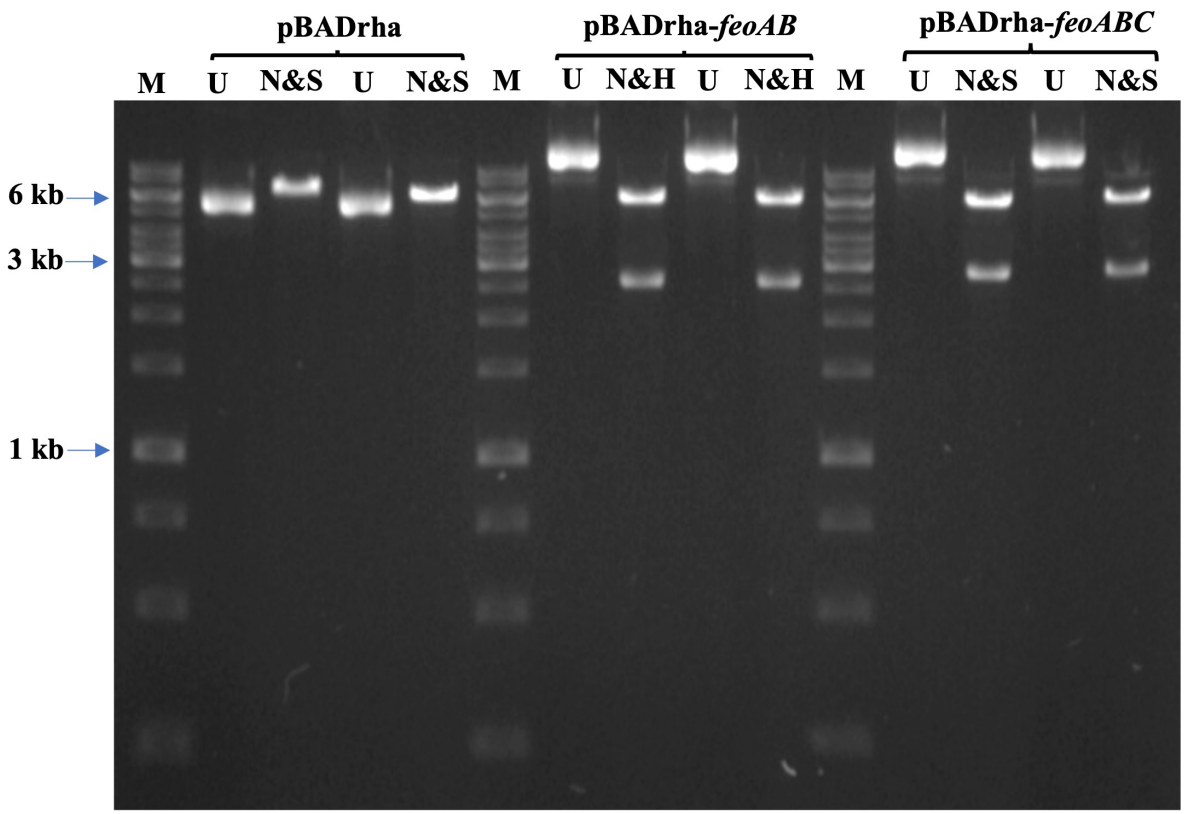

Figure 3.3: Agarose gel electrophoretic analysis of pBADrha, pBADrha-*feoAB* and pBADrha- *feoABC* DNA with and without restriction digestion. M, GeneRule 1 kb ladder (Fig. 2.1); U, undigested; N, *Nde*I digested; and N&S, *Nde*I and *Sal*I digested; N&H, *Nde*I and *Hin*dIII digested.

For the three pBADrha plasmids (Fig. 3.3), the expected sizes were obtained. The pBADrha (6.1 kb) uncut DNA gave the expected size for the uncut vector (slightly higher mobility with respect the expected size of the linearized plasmid). The *Nde*I and *Sal*I double digestion gave a band of ~6.1 kb, as expected for the linearised plasmid (Fig. 3.4A). The pBADrha-*feoAB* (8.65 kb) sample gave the expected size for the plasmid and the inserted gene (6.1 and 2.5 kb, respectively) by double digests with *Nde*I and *Hin*dIII (Fig. 3.4B). For the pBADrha-*feoABC* (8.9 kb) sample, the expected sizes for both plasmid and the inserted gene (6.1 and 2.8 kb, respectively) by double digests by *Nde*I and *Sal*I were obtained (Fig. 3.4C). This confirms the identity of the three pBADrha plasmids.

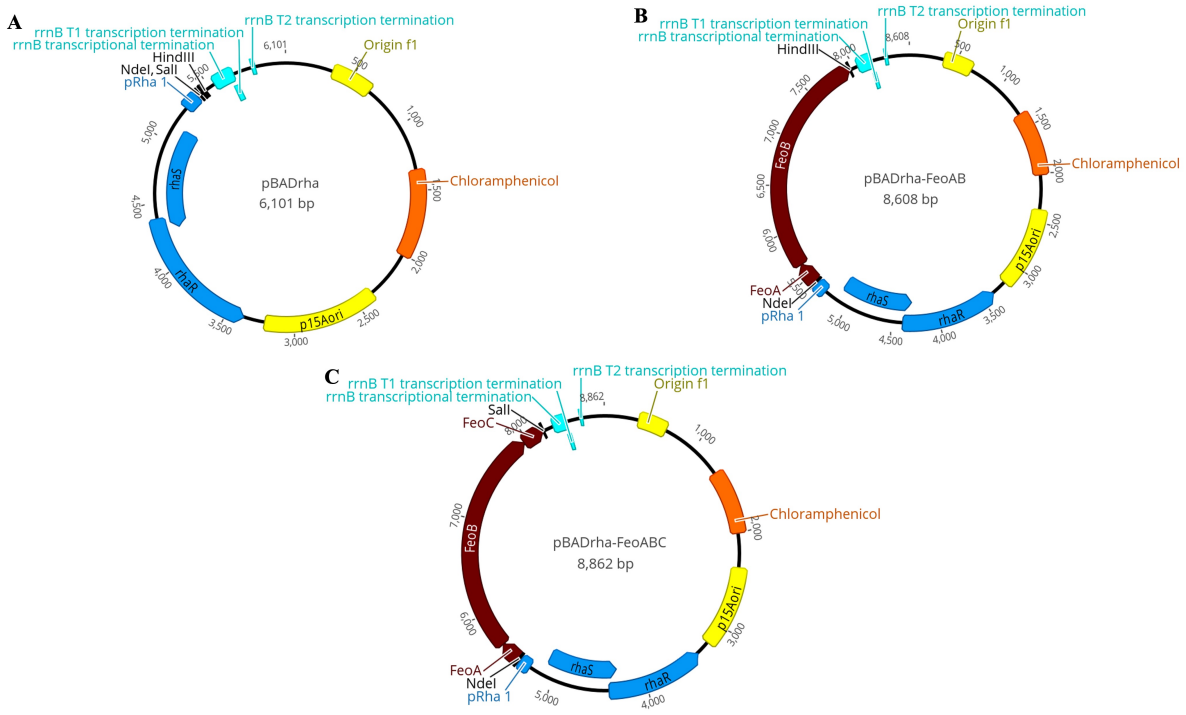

Figure 3.4: Genetic map of pBADrha, pBADrha-*feoAB* and pBADrha-*feoABC*. (A) For pBADrha, the map indicates the MCS, chloramphenicol resistance locus, the *ori* and the *rhaSR* locus. **(B)** For pBADrha-*feoAB*, the map additionally shows *feoAB* inserted between the *Hin*dIII and *Nde*I sites. **(C)** For pBADrha-*feoABC*, the map shows *feoABC* inserted between the *Nde*I and *Sal*I sites.

3.2.1 Confirmation of the aerobic iron-restriction phenotype of the iron-uptake mutant (JC32)

Once the *feoAB*- and *feoABC*-expressing plasmids had been confirmed, the next step was to introduce them into JC32 (Table 2.1). JC32 is an *E. coli* mutant lacking Feo, Ent, Fec, MntH, ZupT and EfeU dependent iron uptake systems and thus is reported to exhibit an iron-restricted phenotype (Cao *et al.*, 2007). Thus, it was first necessary to confirm the iron-restricted phenotype of JC32 with respect to the parent (wildtype) strain, W3110. This was important since future experiments depended on the ability of the *feo* plasmids to complement the iron-restricted growth of JC32. Therefore, both strains were grown aerobically in 250 ml acid-washed flasks containing 50 ml of M9 minimal medium with 0.4% glucose with/without 20 µM ferric citrate as iron source (Methods 2.6). As can be seen (Fig. 3.5A), when ferric citrate was included, W3110 and JC32 grew well in M9 medium, although W3110 exhibited

the better growth. After 8 h, the OD for W3110 and JC32 was 0.77 and 0.53 (1.5-fold difference), respectively, with little difference seen at 14-26 h. When ferric citrate was excluded from the growth medium, W3110 again showed better growth than the mutant, although overall growth was much weaker. After 8 h, the OD was 0.7 and 0.34 for the wildtype and JC32 (~twofold difference), respectively, and after 14-26 h growth was again similar. Thus, under aerobic growth conditions (in the absence of DTPA) the growth of JC32 was lower than the wildtype both with and without iron.

When DTPA was also included in the medium (as an iron chelator) along with excess iron (as ferric citrate), W3110 and JC32 exhibited strong growth (Fig. 3.5B) with little difference apparent. However, in the absence of ferric citrate and presence of DTPA, although W3110 showed a weaker growth than seen with ferric citrate, JC32 showed no growth over the course of the experiment (OD or 1.75 and 0.12 at 25 h, respectively). Thus, a major aerobic growth restriction was seen for the mutant with respect to the wildtype that was dependent on low iron and the presence of 1 µM DTPA, which is indicative of an iron-restriction growth defect for JC32.

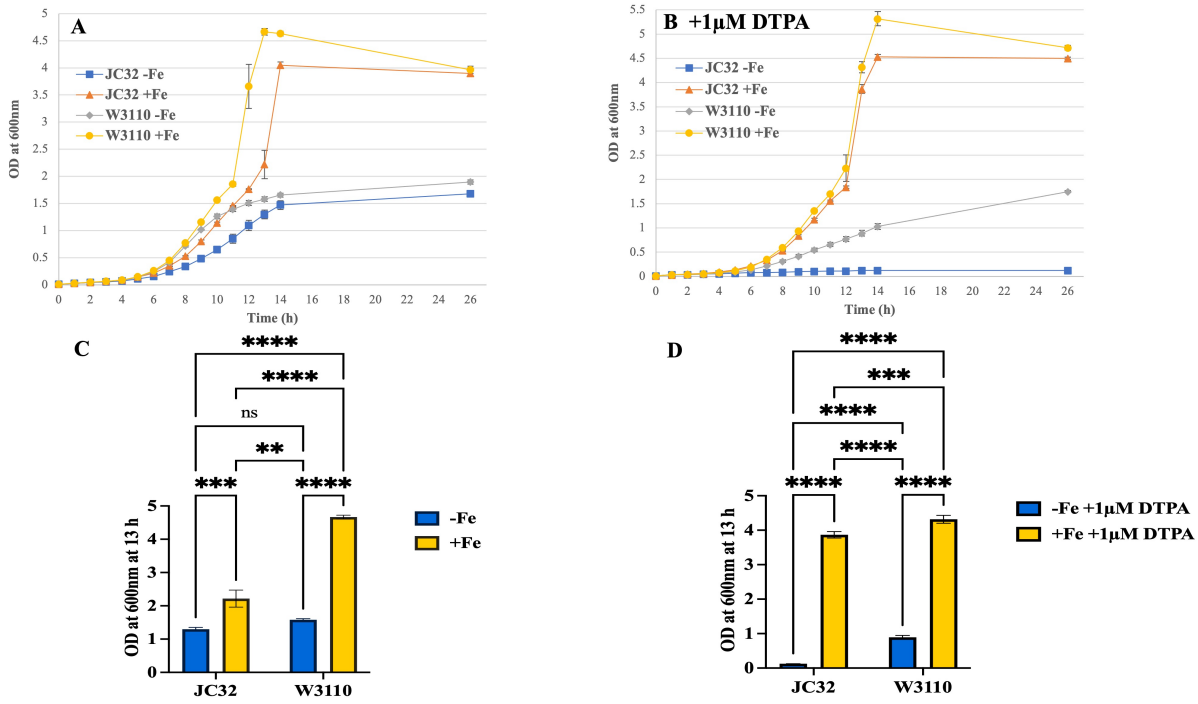

Figure 3.5: Growth comparison of the W3110 and JC32 under low/high iron, with /without DTPA under aerobic conditions in 250 ml flasks. Pre-cultures were grown overnight in 5 ml of M9 minimal medium with 0.4% glucose and 20 µM ferric citrate at 250 rpm and 37 °C. The cultures were washed with the fresh M9 twice to remove any residue iron. For the growth comparison (**A**), M9 minimal medium with 0.4% glucose, with/without 20 µM ferric citrate, was employed under aerobic condition in acid-washed flask, with starting OD of 0.01 and shaking at 250 rpm and 37 °C. Growths was performed in two flasks at the same time and repeated it three times. **(B)** The same conditions were employed as in (A), except that 1 µM DTPA was included in all growth comparison cultures. Standard deviation was calculated and displayed as error bars. **(C&D)** ODs at 13 h are presented from (A) and (B), respectively. P-values were calculated by two-way ANOVA and generated by GraphPad Prism; **, P <0.01; ***, P <0.001; ****, P <0.0001.

The growth comparisons performed above (Fig. 3.5AB) were repeated using 96-well microtiter plates in a Spark Tecan microtiter plate reader (Methods 2.10). The aim was to confirm the results previously obtained and to determine whether the microtiter plate approach would be suitable for future work, since this enables a greater number of cultures to be considered in parallel and eliminates the need for sampling. The results obtained were similar to those generated in 250 ml flasks – a strong growth defect was seen for the JC32 strain with respect to W3110 with 1 µM DTPA in the absence of iron (Fig. 3.6B); the wildtype increased in OD by ~0.75 units, whereas no notable increase was seen for the mutant. However, when iron was provided in the medium both strains achieved the same final OD although the growth of the mutant was ~2 h delayed with respect to the wildtype (Fig. 3.6AB). It should also be noted that JC32 displayed a reduced growth under iron- and DTPA free conditions with respect to W3110 (Fig. 3.6A) giving a lower final growth yield (of ~0.1 OD unit) and growth delay (of ~3 h). The results therefore confirm that JC32 exhibits a major iron-restricted aerobic growth phenotype in the presence of DTPA that can be explored using a microtiter plate reader.

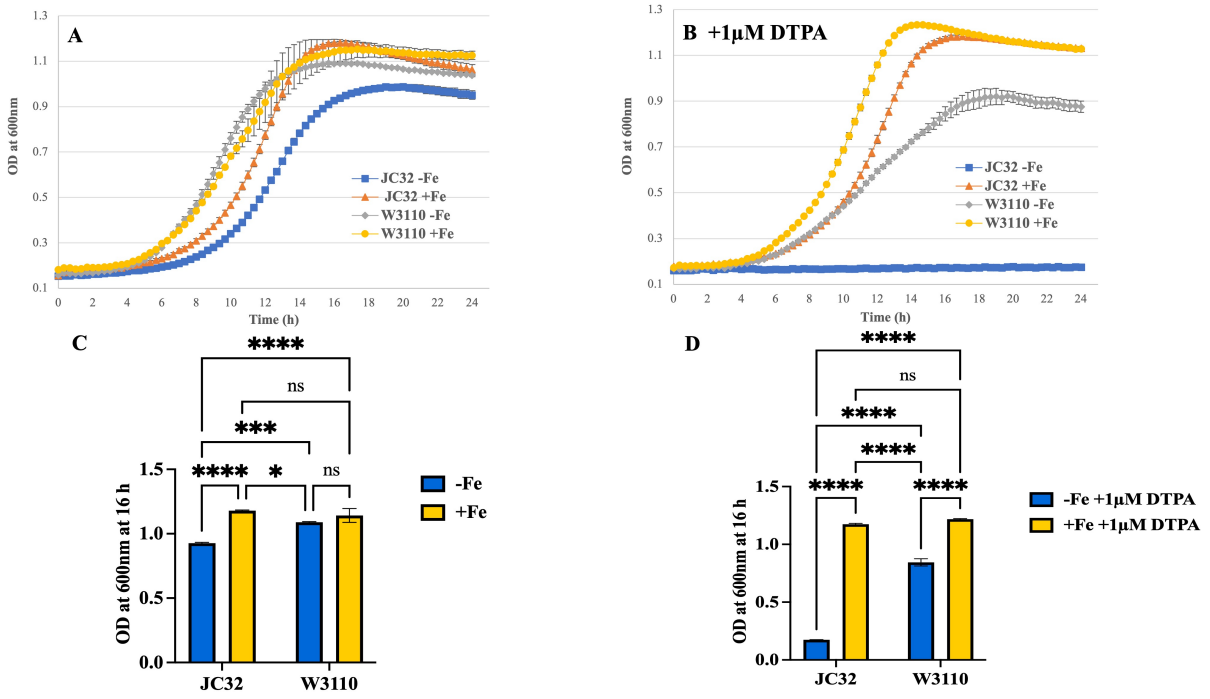

Figure 3.6: Growth comparison of W3110 and JC32 under high and low iron as well as with DTPA under aerobic conditions in 96-well plates. Details (**A&B**) are as for Fig. 3.5AB except that growths were achieved in 200 µl volumes using a 96-well plate within a Spark Tecan multimode plate reader. Starting OD was 0.01 and incubation was at 180 rpm at 37 °C with OD_{600} measurement every 20 min over 24 hours. Growths were performed in two wells at the same time and repeated it three times, and then the averages were taken from the three repetitions. Standard deviation was calculated and displayed as error bars. (**C&D**) ODs at 16 h are presented from (A) and (B), respectively. P-value were calculated by two-way ANOVA and generated by GraphPad Prism (*, P <0.05; ***, P <0.001; ****, P <0.0001).

3.2.2 Confirmation of the anaerobic iron-restriction phenotype of JC32

Since the Feo system is an anaerobic ferrous iron transporter, it was also considered necessary to confirm that the JC32 strain exhibits an iron-restricted phenotype (due to *feoABC* inactivation) anaerobically. To achieve anaerobiosis, growths were performed in 50 ml syringes containing 50 ml of M9 medium with 0.4% glucose, with/without ferric citrate as a source of iron (Methods 2.9). As can be seen in Fig. 3.7A, W3110 grew similarly in the presence or absence of ferric citrate, indicating that iron restriction had not been achieved. Also, the wildtype was little affected by the addition of 1 µM DTPA (Fig. 3.7B), which again

indicates that (for the wildtype) iron restriction had not been achieved. This likely reflects the greater availability of iron anaerobically (due to the high solubility of ferrous iron), the presence of a full complement of iron transporters and the lower overall growth achieved anaerobically compared that seen aerobically (maximum OD of ~0.76 cf. 5.3, respectively). For JC32, the addition of iron enabled a similar final growth yield (at ~13 h) as that obtained for the wildtype (Fig. 3.7AB), both with and without DTPA, although JC32 did display a growth delay with respect to W3100 (of ~1 h) in the presence of iron. In the absence of iron, both with and without DTPA, JC32 showed a clearly reduced growth with respect to W3110 (OD 0.26 and 0.71 at 12 h, respectively; Fig. 3.7B). This reduced growth, caused by lack of iron, was in contrast to the results obtained with the wildtype under the same conditions where no reduced growth was observed. Thus, JC32 displays a clear iron-restriction phenotype under anaerobiosis.

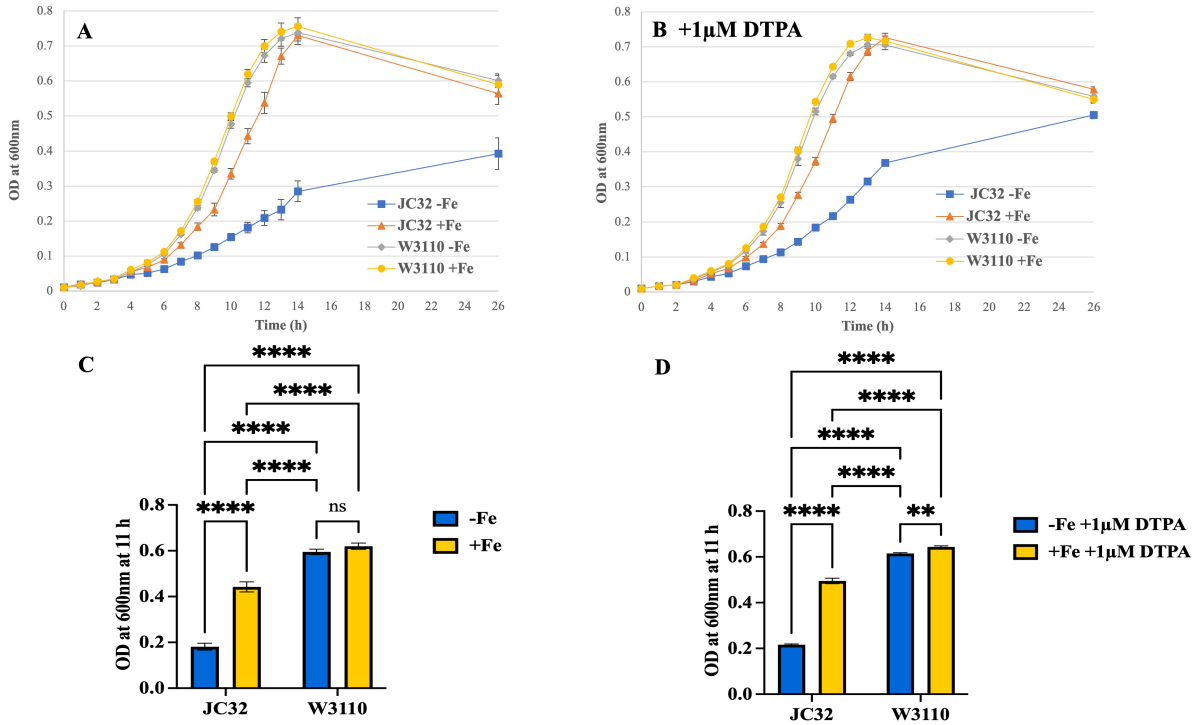

Figure 3.7: Growth comparison of W3110 and JC32 with high/low iron with/without DTPA under anaerobic conditions in 50 ml syringes. Growth details, without (**A**) and with (**B**) DTPA were as for Fig. 3.5, except for the use of anaerobic conditions. Growths were in duplicate and growth comparisons were repeated three times, and the averages were taken from

three repetition growths. Standard deviation was presented as error bars. (**C&D**) ODs at 11 h are presented from (A) and (B), respectively. P-values were calculated by two-way ANOVA and generated by GraphPad Prism (**, P <0.01; ****, P <0.0001).

3.2.3 Confirmation of *feoABC* status by PCR

The growth comparisons above confirmed the iron-restricted phenotype of JC32 (Cao *et al.*, 2007). However, it was also considered prudent to confirm the Δ*feoABC* status of JC32, to further ensure that *feo* complementation studies could be performed. Therefore, genomic DNA was extracted from W3110 and JC32 as template for diagnostic PCR amplification of the *feoABC* locus (Methods 2.14; Fig. 3.9AB). Following this, the *feoABC* locus of W3110 and JC32 was PCR amplified (Methods 2.15; Tables 2.6 & 2.7) and the PCR products were analysed by agarose electrophoresis (Methods 2.12; Fig. 3.10). PCR with DreamTaq gave the anticipated PCR product sizes of ~3 kb for the wildtype and ~0.5 kb for the *feoABC* mutant (Fig. 3.10), thus confirming the *feo* status of the corresponding stains. It should be noted that PCR analysis with Phusion polymerase gave similar results (not shown). Fig 3.8 shows the *feo* locus from *E. coli* K-12 and the primer positions, indicating the size of the locus as ~3 kb.

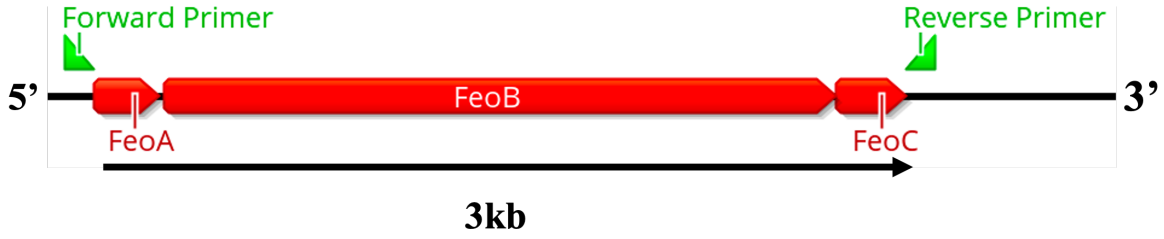

Figure 3.8: Genetic map of the *feo* locus of *E. coli* K-12. The PCR primer positions are also indicated. Obtained using Geneious Prime software.

The results for the genome sequencing of JC32 are summarised in (Fig. 3.9C) showing that all six iron-uptake loci possess the anticipated deletion.

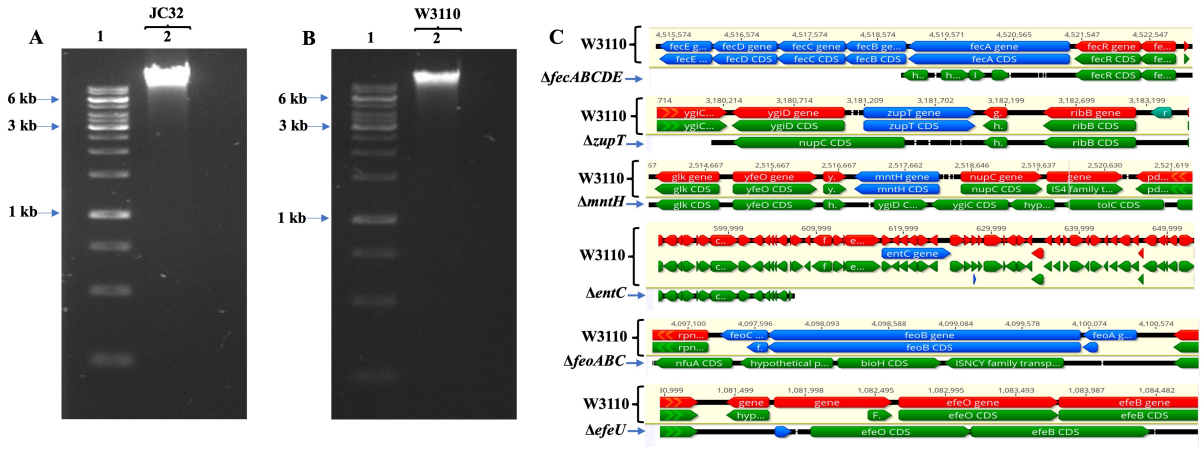

Figure 3.9: Purification of genomic DNA from the JC32 and W3110, and genome NGS analysis. Agarose gel electrophoretic analysis (Methods 2.12) of DNA isolated (Methods 2.14) from JC32 **(A)** and W3110 **(B)**. Lane 1 contains the GeneRuler 1kb ladder as marker; lane 2 contains genomic DNA from JC32 or W3110. **(C)** Summary of whole genome NGS for JC32 by MicrobesNG. Geneious Prime software was used to align the sequences of the relevant genomic loci (deleted genes shown in blue) of JC32 to those of the wildtype (W3110), the JC32 parent.

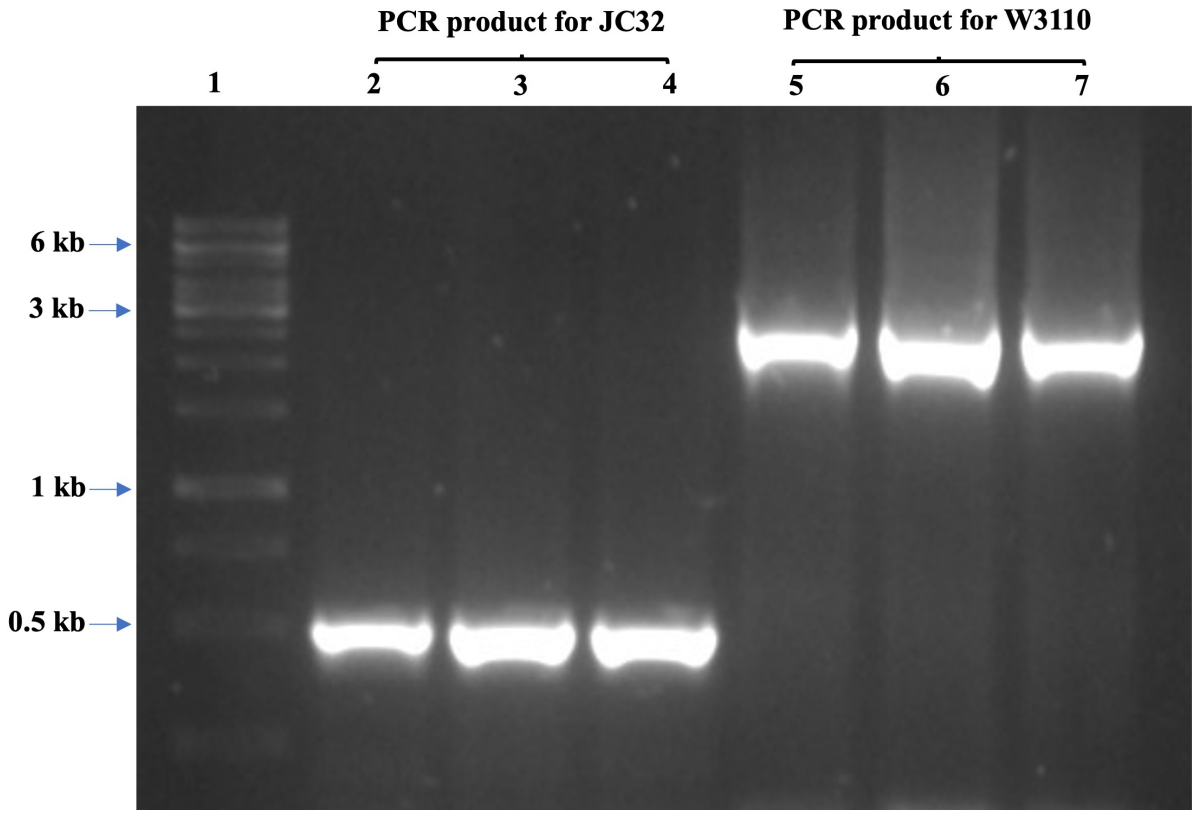

Figure 3.10: Agarose gel electrophoretic analysis of *feoABC* PCR amplification products from W3110 and JC32. PCR was performed using DreamTaq Green PCR Master Mix

(Methods 2.15) and the *feoABC*-F and -R primers (Table 2.3). Lane 1, 1 kb GeneRule DNA ladder; lanes 2, 3 and 4, PCR product for JC32; lane 5, 6 and 7, PCR product for W3110.

3.2.4 Complementation of JC32 with pBADara-*feoAB* and pBADara-*feoABC*: effect on iron-restricted growth with/without DTPA under aerobic conditions

To determine whether the inducible *feoABC* and *feoAB* plasmids can completement the iron-restriction *feo* defect of JC32, the corresponding transformants, containing pBADara, pBADara-*feoAB* and pBADara-*feoABC*, were grown under aerobic conditions in 96-well plates in 200 µl of M9 medium with 0.4% glucose with/without 20 µM ferric citrate (Fig. 3.11). The results illustrate that when iron was added, the three transformants grew well, although the pBADara transformant exhibited a slightly reduced growth (~0.1 OD unit, ~1 h delay) with respect to the pBADara-*feoAB* and pBADara-*feoAB* strains (Fig. 3.11A). A slightly enhanced growth of the pBADara-*feoABC* and pBADara-*feoAB* transformants with respect to the vector control was also observed in the absence of added iron (e.g. OD 0.55, 0.55 and 0.37, respectively, at 8 h) (Fig. 3.11B). Thus, a growth advantage for the *feoAB* and *feoABC* complemented strains was seen under both high and low iron conditions, although it was relatively modest.

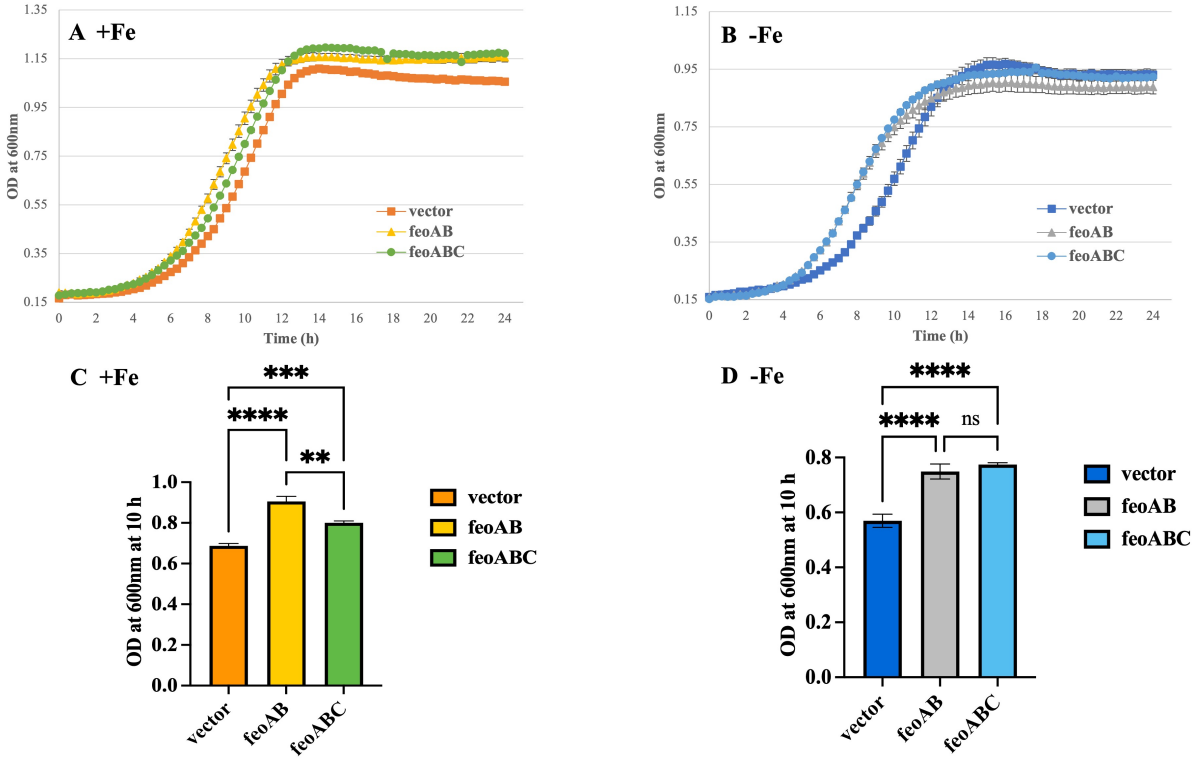

Figure 3.11: Effect of *feoAB*$^+$, *feoABC*$^+$ and Δ*feoABC* status on low-iron aerobic growth of *E. coli*. JC32 transformants carrying pBADara-*feoABC*, pBADara-*feoAB* and pBADara were grown overnight in 5 ml of M9 medium with 0.4% glucose containing 100 µg/ml ampicillin and 20 µM of ferric citrate in test tubes on a shaker at 37 °C and 250 rpm**.** Following day, the overnight cultures were harvested by centrifugation (an Eppendorf Centrifuge 5804 R) at 4 °C and 5000 rpm and then the pellets were washed twice with fresh M9 to remove any residue of iron. The washed overnight cultures where then used to inoculate fresh M9 minimal medium with 0.4% glucose, antibiotic and 0.2% arabinose, with/without 20 µM ferric citrate (**A/B**, respectively) under aerobic condition in a 96-well plate. See Methods 2.10 for further details. (**C&D**) ODs at 10 h are presented from (A) and (B), respectively. P-values were calculated by one-way ANOVA and generated by GraphPad Prism (**, P <0.01; ***, P <0.001; ****, P <0.0001).

The previous growth comparison of JC32 with W3110 showed a stronger phenotype when DTPA was included. Thus, a further set of growth comparisons was performed with the *feo* plasmid transformants as in Fig. 3.11, but with 1 µM DTPA included (Fig. 3.12). As before (Fig. 3.11), in the presence of iron, only a slight growth advantage was seen for the pBADara-*feoABC* and -*feoAB* transformants, with respect to the vector control (Fig. 3.12A). However,

with DTPA in the absence of added iron the *feo*-complemented strains showed a clear growth advantage (Fig. 3.12B). The *feoABC*-complemented strain exhibited an increase in growth of 0.23 OD units over 24 h, whereas the vector control only showed an increase of 0.02 OD units (11.5-fold difference). The *feoAB*-complemented strain showed a more modest threefold greater overall growth than the control. These results indicate that FeoABC is able to support iron-restricted growth when *feo* is induced under aerobic conditions. They also indicate that the absence of FeoC reduces this capacity substantially (~fourfold according to the results presented here; Fig. 3.12B). These findings are consistent with those of Al-Aidy (2020).

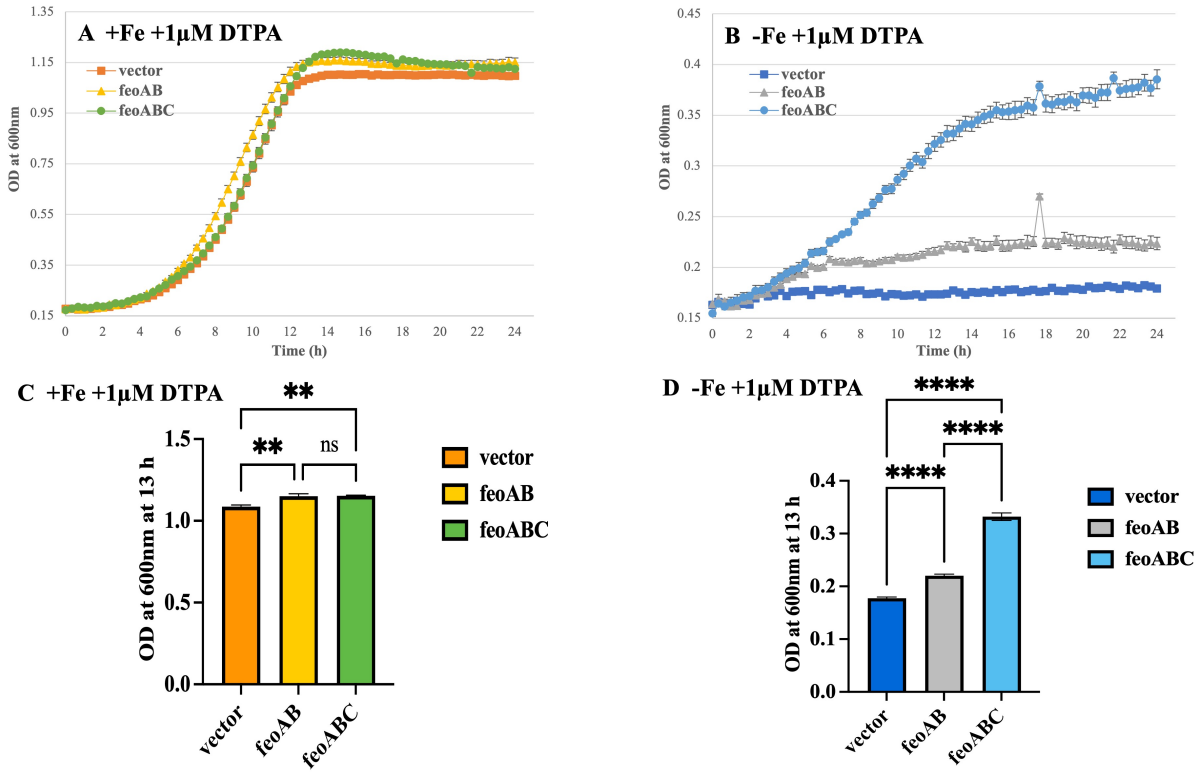

Figure 3.12: Effect of *feoAB*$^+$, *feoABC*$^+$ and Δ*feoABC* status on low-iron aerobic growth of *E. coli*, with DTPA. Details are as for Fig. 3.11, except for the inclusion of 1 µM DTPA for the growth comparisons in all cases. **A**. With 20 µM ferric citrate and 1 µM DTPA. **B**. With 1 µM DTPA, and no additional iron. (**C&D**) ODs at 13 h are presented from (A) and (B),

respectively. P-values were calculated by one-way ANOVA and generated by GraphPad Prism (**, P <0.01; ****, P <0.0001).

3.2.5 Complementation of JC32 with pBADara-*feoAB* and pBADara-*feoABC*: effect on iron-restricted growth with/without DTPA under anaerobic conditions

The above results show that *feoABC* complementation can greatly improve aerobic iron-restricted growth, and that this effect is very much enhanced by the presence of *feoC*. In order to determine whether the inducible *feo* constructs could also complement iron-restricted growth anaerobically, and if so whether this is also *feoC* dependent, growth comparisons were repeated under anaerobic conditions (Methods 2.9). Thus, growth was compared in the presence and absence of 20 μM ferric citrate, with and without DTPA (Fig. 3.13). The results show that in the presence of iron, both with and without 1 μM DTPA, there was little difference in growth between the *feo*-complemented strains and the vector control (Fig. 3.13). However, in the absence of added iron, both *feoAB*- and *feoABC*-complemented JC32 showed greater growth than the vector control (e.g. 0.63 cf. 0.41 OD units at 12 h for the *feoABC* bearing and vector control strain, respectively; Fig. 3.13A). This effect was little affected by 1 μM DTPA (Fig. 3.13B). Thus, *feoAB* and *feoABC* support anaerobic low-iron growth to a similar degree. This suggests that FeoC may not be important anaerobically but may instead have an aerobic function (as indicated above).

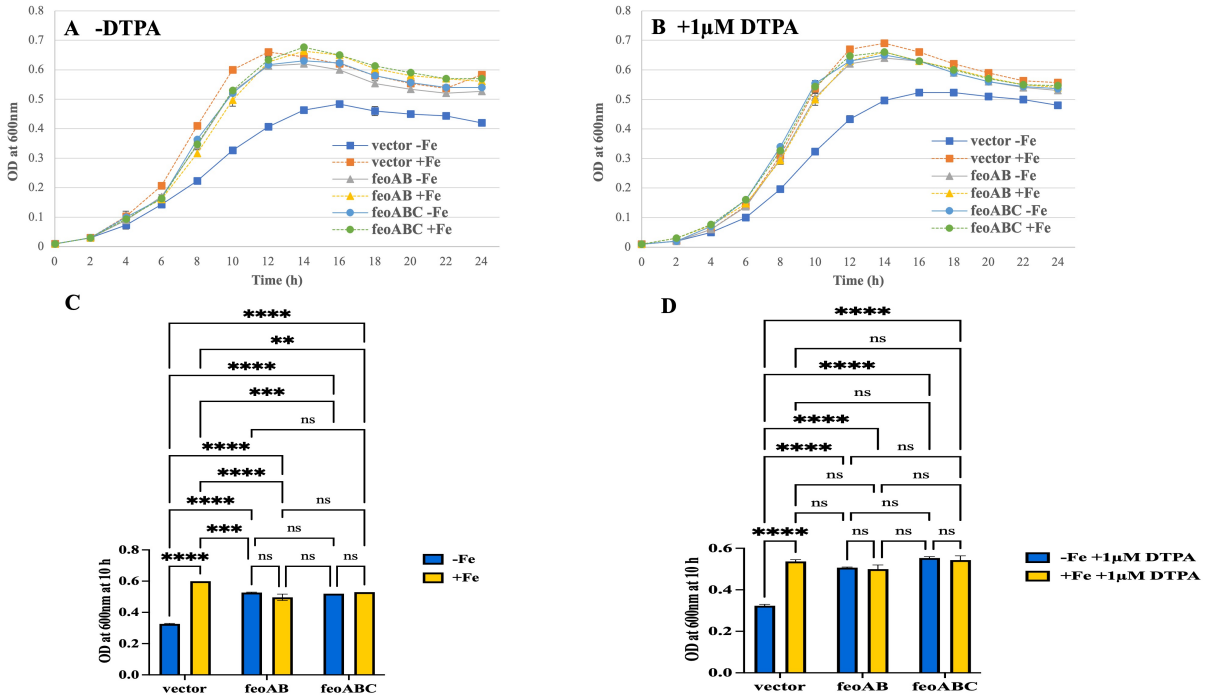

Figure 3.13: Effect of *feoAB*$^+$, *feoABC*$^+$ and Δ*feoABC* status on low-iron <u>anaerobic</u> growth of *E. coli*, with (B) and without (A) 1 µM DTPA. Details are as for Fig. 3.11 and 3.12, except for the use of anaerobic growth conditions (in 50 ml syringes; Methods 2.9). (**C&D**) ODs at 10 h are presented from (A) and (B), respectively. P-values were calculated by two-way ANOVA and generated by GraphPad Prism (**, P <0.01; ***, P <0.001; ****, P <0.0001).

The possibility that a higher level of DTPA might increase the low-iron growth differences seen between the *feo*-complement JC32 transformants and the vector control was tested using DTPA at 2 µM. However, this change had little impact on the results obtained (Fig. 3.14).

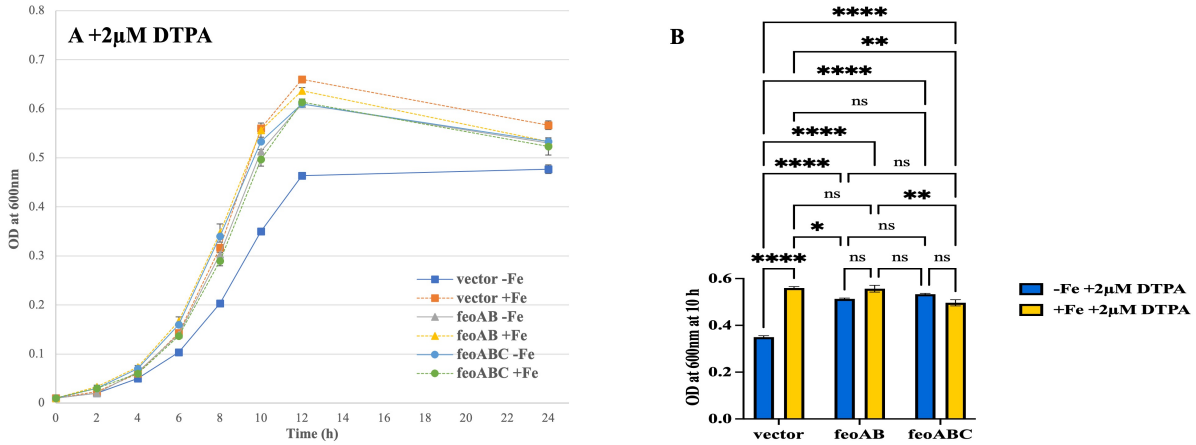

Figure 3.14: Effect of *feoAB*$^+$, *feoABC*$^+$ and Δ *feoABC* status on low-iron anaerobic growth of *E. coli*, with <u>2 µM DTPA</u>. Details are as for Fig. 3.13B, except that DTPA concentration

was raised to 2 μM. (**B**) OD at 10 h are presented from (A). P-value were calculated by two-way ANOVA and generated by GraphPad Prism (*, P <0.05; **, P <0.01; ****, P <0.0001).

3.2.6 Complementation of JC32 with pBADara-*feoAB* and pBADara-*feoABC*: effect on iron-restricted aerobic growth under reducing and buffered conditions

A clear iron-restricted growth difference was seen between the pBADara-*feoAB* and pBADara-*feoABC* transformants under low-iron, aerobic conditions with DTPA (Fig. 3.12B). To further explore this FeoC-dependent growth difference, the effect of controlling pH with a strong buffer was explored (Fig. 3.15A). The aim was to determine whether the acidification of the medium that occurs during glucose utilisation might play a part in the observed *feoC*-dependent phenotype. Thus, MES was included to stabilise the pH (Fig. 3.15B) and it was therefore necessary to account for any effect that MES might have on low-iron growth. MES was selected as the buffer to utilise since it is considered a biologically suitable buffering agent (Good and Izawa, 1972). Under low-iron conditions with MES (pH 6), there was a clear growth difference between the three transformants. The growth of the *feoABC*$^{+}$ strain was ~1 h advanced with respect to the *feoAB*$^{+}$ strain, and ~3 h advanced with respect to the vector control (Fig. 3.15A). Thus, a clear *feoC*-dependent phenotype was exhibited under low iron conditions even though DTPA was absent. This suggests that stabilising the pH during growth reduces iron availability (as is the case for DTPA) in way that enables the FeoC-dependent phenotype to be exhibited.

Ascorbic acid was also added to the growth medium (Fig. 3.15B) in order to determine any effect of reductant (e.g. through enhancing ferrous iron availability) on the FeoC-dependent low-iron growth effect. It was considered that the reducing agent would act to maintain iron in the reduced, ferrous state and might thus enhance the importance of the Feo system aerobically. Also, ascorbic acid is an antioxidant and may thus support Feo activity aerobically (FeoB is reported to be subject to H_2O_2-dependent proteolytic degradation under aerobiosis; (Kim *et al.,* 2013; Weaver *et al.*, 2013). Thus, ascorbic acid was included at 2 mM, along with

100 mM MES to stabilise the pH at 6. The results obtained resemble those achieved with 100 mM MES alone (Fig. 3.15A) except that the *feoAB*$^{+}$ strain grew similarly to the *feoABC*$^{+}$ strain, and that both complemented strains grew similarly to the wildtype. This suggests that under the conditions of Fig. 3.15B, the Feo system is the dominant high-affinity iron transporter. These results also indicate that the presence of reductant eliminates the FeoC-dependent growth difference seen under aerobic, low-iron conditions.

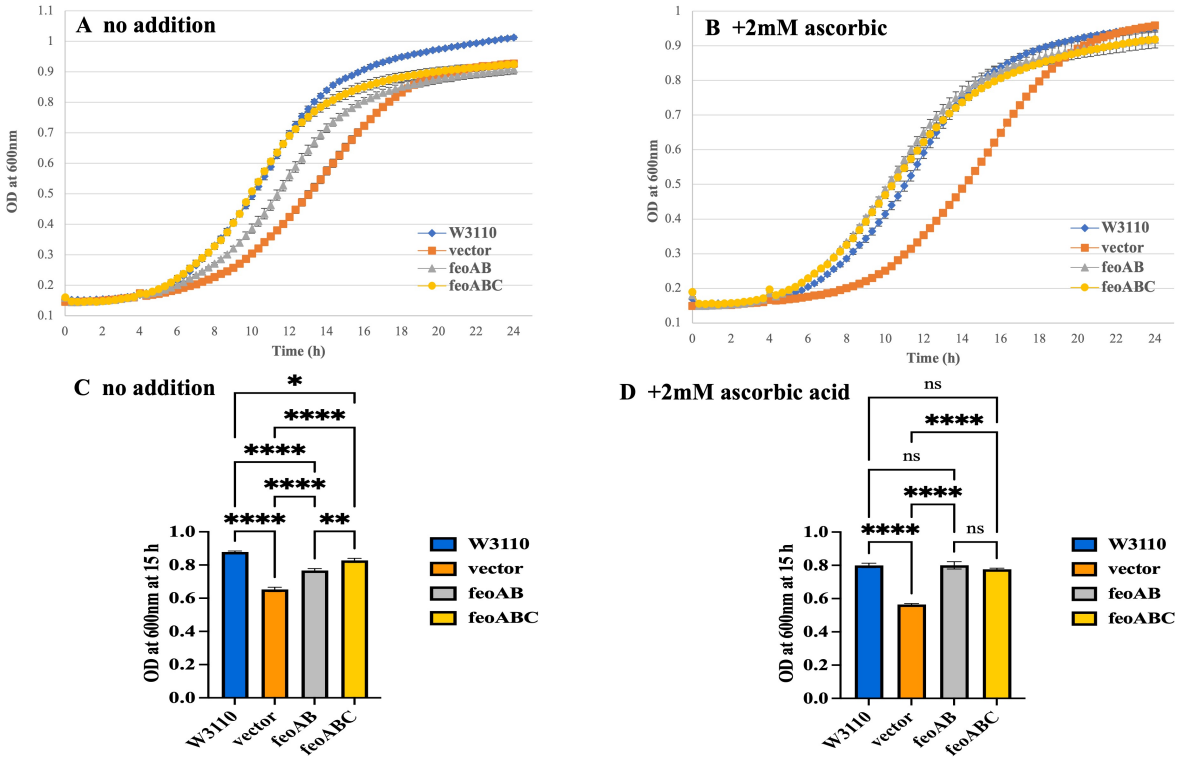

Figure 3.15: Effect of *feoAB*$^{+}$, *feoABC*$^{+}$ and Δ*feoABC* status on low-iron aerobic growth of *E. coli*, with 100 mM MES (pH 6) and 2 mM ascorbic acid. Details are as for Fig. 3.11, except for the inclusion of 100 mM MES (pH 6) in all cases and the exclusion (A) or inclusion (B) of 2 mM ascorbic acid. In addition, W3110 was included as a wildtype control. Growth medium was 200 µl of M9 minimal medium with 0.4% glucose, 100 mM MES (pH 6), 0.02% arabinose with/without 2 mM ascorbic acid (with antibiotic as required) and growths were performed in 96-well plates at 180 rpm and 37 °C using a Spark Tecan device. (**C&D**) ODs at

15 h are presented from (A) and (B), respectively. P-values were calculated by one-way ANOVA and generated by GraphPad Prism (*, P <0.05; **, P <0.01; ****, P <0.0001).

To further explore the effect of ascorbic acid and MES buffer on the FeoC-dependent growth phenotype, the experiment above (Fig. 3.12) was repeated in the presence of 1 μM DTPA, since previous results had shown a strong *feoC* phenotype aerobically under low iron when DTPA was included (Fig 3.12B). The results show that addition of 1 μM DTPA in the absence of ascorbate (Fig. 3.16A) results in a major growth reduction for the JC32 strains with respect to the wildtype (OD of 0.17-0.38 at 24 h for the JC32 transformants, cf. 0.87 for the wildtype). In addition, the *feoABC*$^{+}$ strain showed a clearly superior growth to the *feoAB*$^{+}$ strain, as seen before aerobically with 1 μM DTPA (Fig. 3.12B). However, when 2 mM ascorbic acid was also included, the growth of the *feoABC*$^{+}$ strain was greatly enhanced (from 0.38 to 0.98 OD units at 24 h; Fig. 3.16A & B) such that it matched that of the wildtype. In contrast, the growth of the *feoAB*$^{+}$ strain and vector control were little affected by the ascorbic acid (Fig. 3.16A & B). These results suggest that the presence of ascorbate along with MES buffer enhances the growth difference between the *feoABC*$^{+}$ and *feoAB*$^{+}$ strains as induced by DTPA under low-iron aerobic conditions (the growth difference seen at 24 h was 17-fold; increase of 0.83 and 0.05 OD units at 24 h, respectively). Thus, these conditions represent an excellent option for investigation of the environmental factors that elicit the FeoC growth phenotype exhibited here.

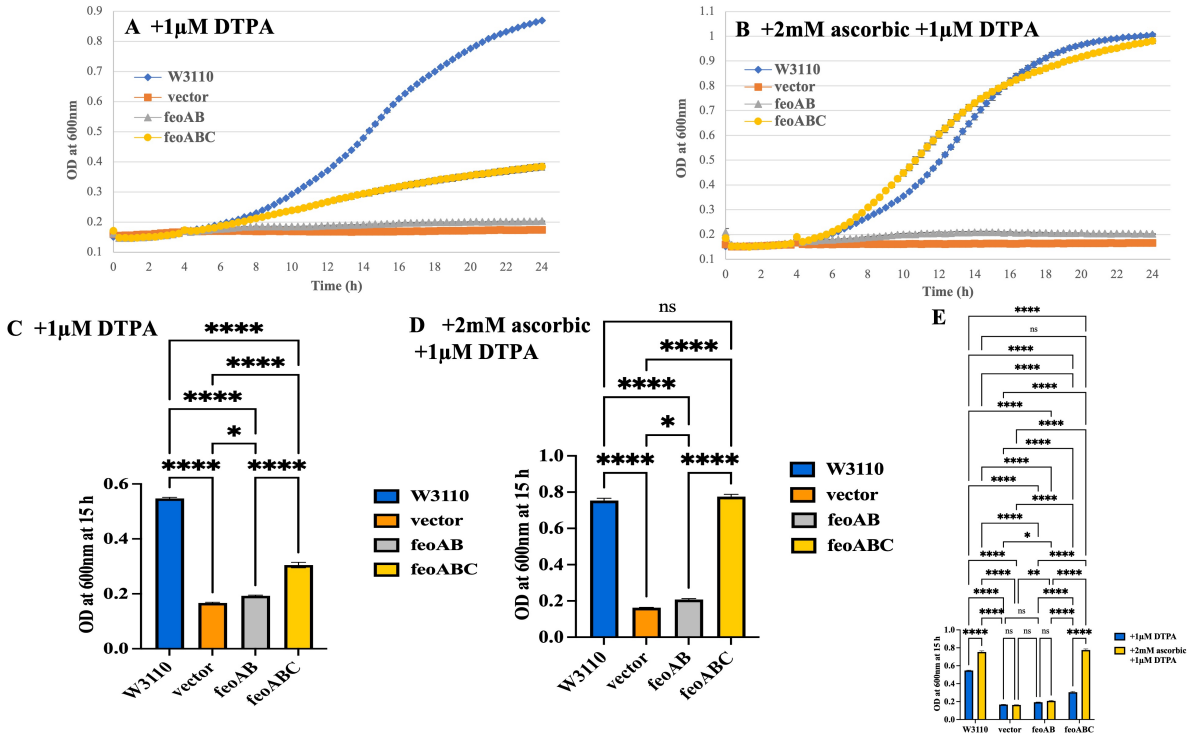

Figure 3.16: Effect of *feoAB*$^+$, *feoABC*$^+$ and Δ*feoABC* status on low-iron aerobic growth of *E. coli*, with <u>100 mM MES (pH 6)</u>, <u>2 mM ascorbic acid</u> and <u>1 µM DTPA</u>. Details are as for Fig. 3.15 except for the inclusion of 1 µM DTPA in all growth comparisons. A. No ascorbic acid. B. 2 mM ascorbic acid. (**C, D & E**) ODs at 15 h are presented from (A), (B) and (A) plus (B), respectively. P-values were calculated by one- (C & D) or two-way (E) ANOVA and generated by GraphPad Prism (*, P <0.05; **, P <0.01; ****, P <0.0001).

3.2.7 Phenotype of the wildtype BW25113 and Δ*feoA*::*kan*, Δ*feoB*::*kan* and Δ*feoC*::*kan* chromosomal mutants: effect on iron-restricted growth with/without DTPA under <u>aerobic</u> conditions

The previous results showed that there is an important role of FeoC under iron-restricted aerobic growth with DTPA (Fig 3.12B) which is enhanced by reducing, buffered (at pH 6) conditions (Fig.3.16B) during complementation of JC32 with pBADara-*feoAB* and pBADara-*feoABC*. In addition, it should be noted that FeoC may not be important anaerobically because there was no difference between *feoAB*- and *feoABC*-complemented JC32 (Fig. 3.13AB) even with increased concentration of DTPA to 2 µM (Fig. 3.14). Here, similar conditions were used to test the phenotypes of the three single mutants (Δ*feoA*::*kan*, Δ*feoB*::*kan* and Δ*feoC*::*kan*) and

the wildtype (BW25113) to determine whether the *feoC* phenotype can be replicated when iron transporters other than Feo remain in place.

Thus, BW25113 and the Δ*feoA*::*kan*, Δ*feoB*::*kan* and Δ*feoC*::*kan* mutants were grown under aerobic condition in 96-well plates in 200 µl of M9 medium with 0.4% glucose with/without 20 µM ferric citrate (Fig. 3.17). The results show that when the iron was added, all four strains grew well with little difference noticed (e.g. OD 1.12, 1.11, 1.10 and 1.06 respectively, at 10 h) (Fig. 3.17AC). When iron was excluded, no difference was again seen between the four stains, although growth was reduced similarly for all strains (e.g. OD 0.79, 0.79, 0.79 and 0.77 respectively, at 10 h) (Fig. 3.17 B&D).

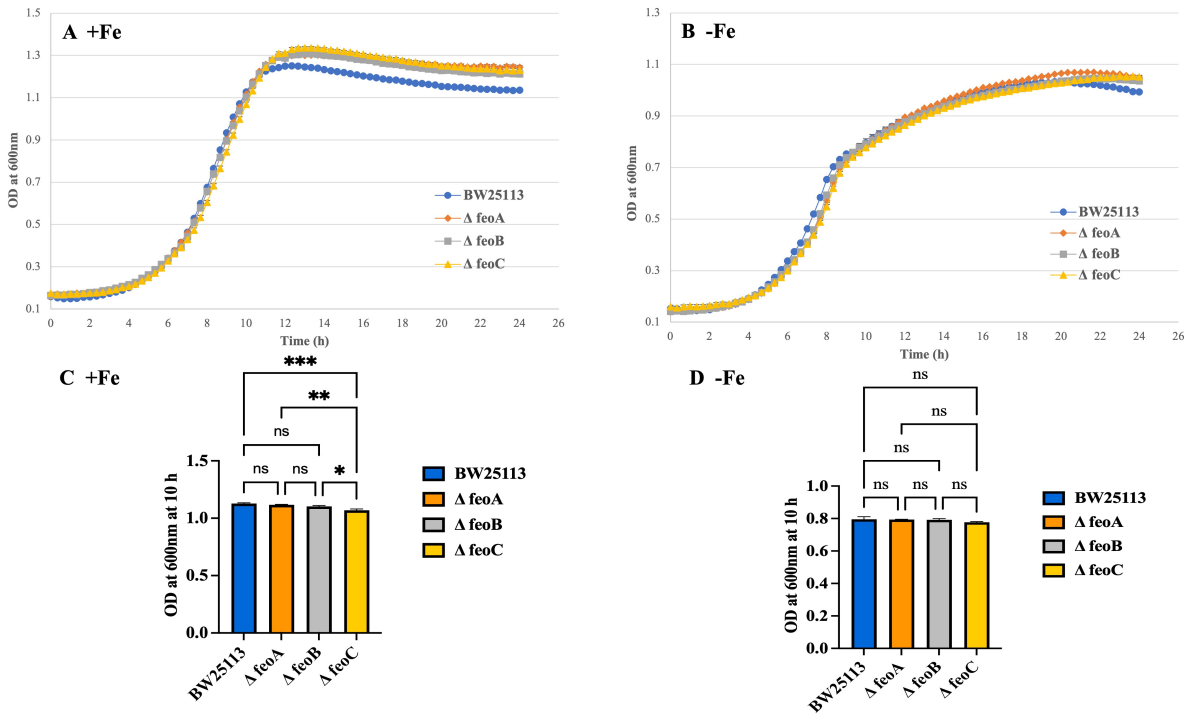

Figure 3.17: Effect of low-iron provision on the growth of BW25113 and the Δ*feoA*::*kan*, Δ*feoB*::*kan* and Δ*feoC*::*kan* strains under aerobic conditions. BW25113, and isogenic Δ*feoA*::*kan*, Δ*feoB*::*kan* and Δ*feoC*::*kan* mutants were grown overnight in 5 ml of M9 medium with 0.4% glucose and 20 µM of ferric citrate in test tubes on a shaker at 37 °C and 250 rpm. The following day, the overnight cultures were harvested by centrifugation (an Eppendorf Centrifuge 5804 R) at 4 °C and 5000 rpm, and the pellets were washed twice with fresh M9 to remove any residue of iron. The washed overnight cultures where then used to inoculate fresh M9 minimal medium with 0.4% glucose, with/without (**A/B**, respectively) 20 µM ferric citrate

under aerobic condition in a 96-well plate. (**C&D**) ODs at 10 h are presented from (A) and (B), respectively. P-values were calculated by one-way ANOVA and generated by GraphPad Prism (*, P <0.05; **, P <0.01; ***, P <0.001).

The previous growth comparison of pBADara, pBADara-*feoABC* and -*feoAB* transformants showed a stronger difference between them in the presence of DTPA and absence of additional iron (Fig. 3.12B). Therefore, a further set of growth comparison was performed with BW25113 the Δ*feoA*::*kan*, Δ*feoB*::*kan* and Δ*feoC*::*kan* mutants, as in Fig. 3.17, but with the addition of 1 µM DTPA (Fig. 3.18A). As before in the presence of iron all the stains grew well and only slight differences were seen (e.g. ODs of 1.11, 1.1.09, 1.08 and 1.06 respectively, at 10 h). However, a clear difference in growth was seen between BW25113 and the three mutants starting at 8 h such that BW25113 displayed an overall growth increase of ~0.37 OD units over 24 h whereas the mutants showed an increase of just ~0.17 OD units (~2.2-fold difference). (Fig. 3.18B)

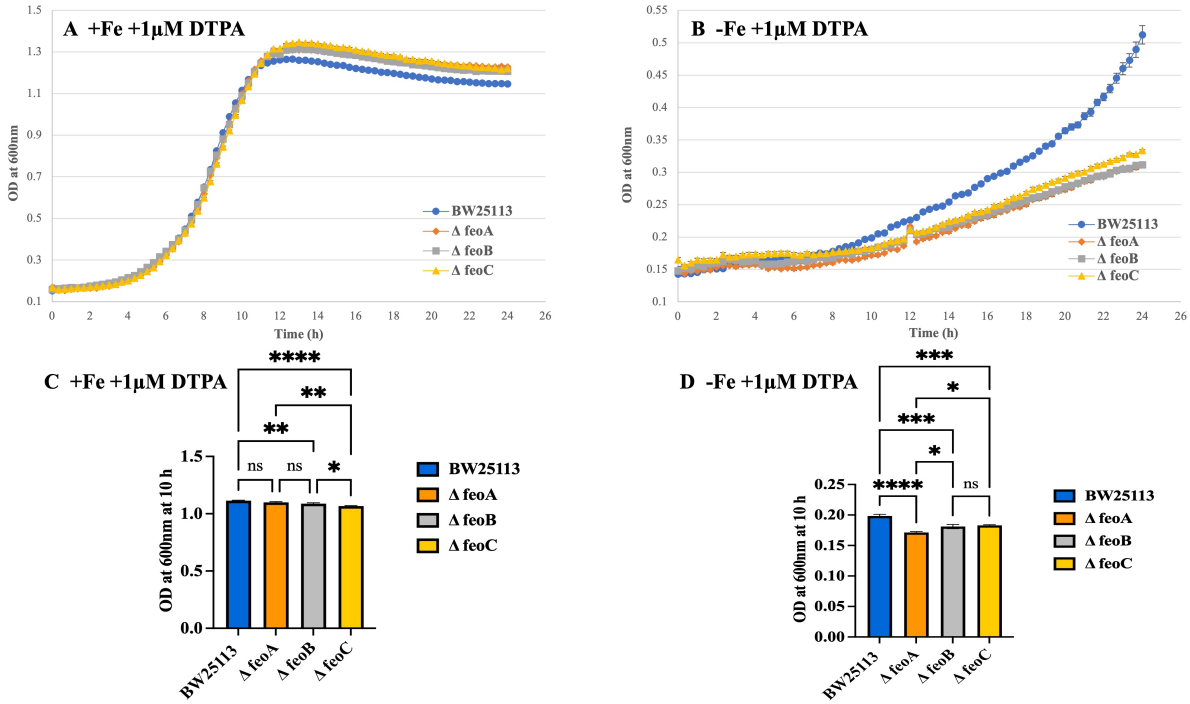

Figure 3.18: Effect of Δ*feoA*::*kan*, Δ*feoB*::*kan* and Δ*feoC*::*kan* status on low-iron aerobic growth of *E. coli*, with DTPA. Details are as for Fig. 3.17, except for the inclusion of 1 µM DTPA for the growth comparisons in all cases. (**A**) With 20 µM ferric citrate and 1 µM DTPA. (**B**) With 1 µM DTPA, and no additional iron. (**C&D**) ODs at 10 h are presented from (A) and

(B), respectively. P-values were calculated by one-way ANOVA and generated by GraphPad Prism (*, P <0.05; **, P <0.01; ***, P <0.001; ****, P <0.0001).

3.2.8 Effect of Δ*feoA*::*kan*, Δ*feoB*::*kan* and Δ*feoC*::*kan* mutations on iron-restricted aerobic growth under reducing and buffered conditions

A major *feoC*-dependent growth difference was observed when comparing pBADara, pBADara-*feoABC* and -*feoAB* transformants under reducing and buffered conditions aerobically (Fig. 3.15AB and Fig. 3.16AB). Therefore, a set of growth comparisons was performed with the Δ*feoA*::*kan*, Δ*feoB*::*kan* and Δ*feoC*::*kan* mutants to investigate whether such conditions could reveal a *feoC* phenotype (Fig. 3.19AB). The strains were grown aerobically in 96-well plates in 200 µl of M9 medium with 0.4% glucose with 100 mM MES (pH 6) with/without 2 mM ascorbic acid as reductant agent. The results showed that all stains grew well and followed very similar growth curves (Fig. 3.19AB). However, there were significant differences in growth at 10 h: the wildtype showed better growth than the mutants in the presence of ascorbate (at 10 h) (Fig. 3.19CD). However, the growth differences were modest.

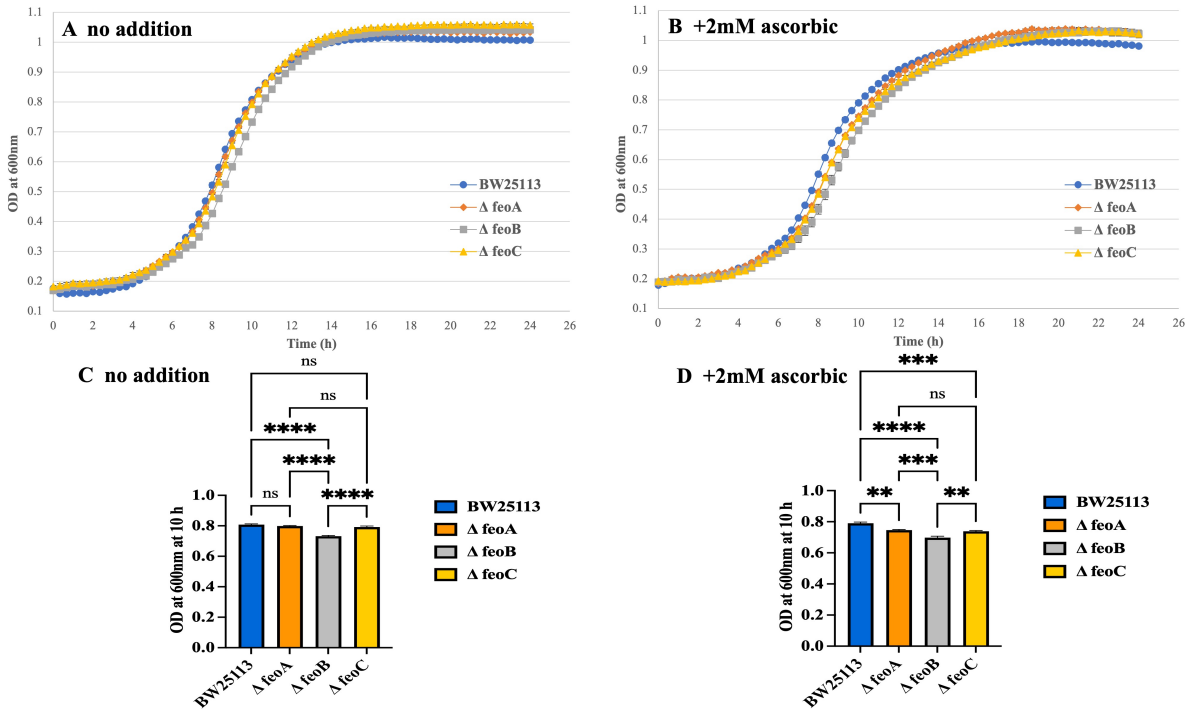

Figure 3.19: Effect of Δ*feoA*::*kan*, Δ*feoB*::*kan* and Δ*feoC*::*kan* status on low-iron aerobic growth of *E. coli*, with 100 mM MES (pH 6) and 2 mM ascorbic acid. Details are as for Fig. 3.17, except for the inclusion of 100 mM MES (pH 6) for the growth comparisons in all cases and the exclusion (**A**) or inclusion (**B**) of 2 mM ascorbic acid. Growth medium was 200 µl of M9 minimal medium with 0.4% glucose and growths were performed in 96-well plates at 180 rpm and 37 °C using a Spark Tecan device. (**C&D**) ODs at 10 h are presented from (A) and (B), respectively. P-values were calculated by one-way ANOVA and generated by GraphPad Prism (**, P <0.01; ***, P <0.001; ****, P <0.0001).

The previous growth comparison of pBADara-*feoABC* and pBADara-*feoAB* transformants showed a strong advantage for the strain with *feoC* when 1 µM DTPA was also included (Fig. 3.16AB). Therefore, the effect of Δ*feoA*::*kan*, Δ*feoB*::*kan* and Δ*feoC*::*kan* status was tested as above (Fig. 3.19) but with inclusion of 1 µM DTPA. The results showed a major growth advantage for BW25113 with respect to the *feo* mutants in the absence of ascorbate and presence of 1 µM DTPA: the BW25113 culture increased by 0.21 OD units over 24 h whereas the mutants showed an increase of only ~0.1 OD units (a ~2.1-fold difference) (Fig. 3.20A). The inclusion of ascorbate resulted in a major increase in growth for BW25113 (total growth of 0.56 OD units over 24 h) whereas the mutants showed an increase of just ~0.07 units (~8-

fold difference) (Fig. 3.20B). Thus, the greatest difference in aerobic growth was obtained under the same conditions that provided the maximum growth advantage for the *feoABC* transformant with respect to the *feoAB* transformant. It should be noted that although the wildtype showed a significant growth advantage with respect to the mutants, no significant difference was found between the mutants (Fig. 3.20CD).

In the *feoC* mutant the *feoAB* genes are expected to be functional so it was somewhat surprising that the *feoC* mutant did not show a clear advantage over the *feoA* and *feoB* mutants given the results obtained by *feo* complementation. This may be due to the presence of other iron transporters that may mask the impact of the presence of an active Feo system aerobically. It could be due to weak expression aerobically as *feoABC* is FNR controlled. Further, when *feoAB* and *feoABC* are provided on an inducible plasmid, this may be expected to increase overall Feo system levels due to a gene dosage effect such that a *feo*-dependent growth effect is more readily observed.

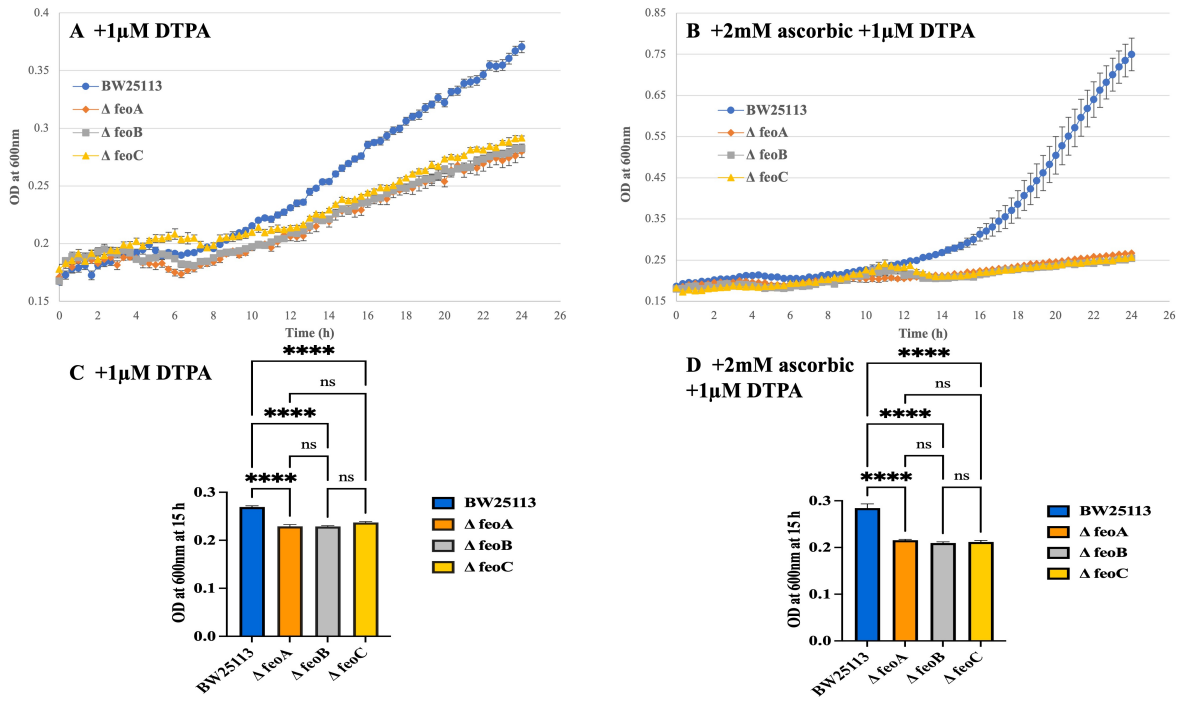

Figure 3.20: Effect of Δ*feoA*::*kan*, Δ*feoB*::*kan* and Δ*feoC*::*kan* status on low-iron aerobic growth of *E. coli*, with 100 mM MES (pH 6) and 2 mM ascorbic acid. Details are as for Fig. 3.19 except for the inclusion of 1 µM DTPA in all growth comparisons. (**A**) No ascorbic

acid. (**B**) 2 mM ascorbic acid. (**C&D**) ODs at 15 h are presented from (A) and (B), respectively. P-values were calculated by one-way ANOVA and generated by GraphPad Prism (****, P <0.0001).

3.2.9 Effect of Δ*feoA*::*kan*, Δ*feoB*::*kan* and Δ*feoC*::*kan* mutations on iron-restricted growth, under reducing and buffered conditions with/without Bipyridyl under anaerobic conditions

The above results showed that the BW25113 possesses a growth advantage over the Δ*feoA*::*kan*, Δ*feoB*::*kan* and Δ*feoC*::*kan* mutants under aerobic iron-restricted conditions but no difference between the three mutants was apparent suggesting that FeoC is an important part of the Feo system aerobically. Therefore, growth comparisons were performed under anaerobic conditions (Methods 2.9) in an attempt to identify a specific *feoC* phenotype. The results showed that in the presence and absence of iron, there is little difference in growth although a significantly reduced growth was observed for the Δ*feoB*::*kan* mutant during the rapid growth phase with iron (Fig. 3.21AC) and both the Δ*feoA*::*kan* and Δ*feoB*::*kan* mutants displayed this effect in the absence of iron Fig. 3.21BD) (a difference of ~0.07 OD units at 10 h; 3.21D). Thus, the *feoC* mutant showed a weak anaerobic iron-restriction advantage over the *feoA* and *feoB* mutants which is consistent with the view that FeoA and FeoB are the most important elements of the Feo iron uptake system.

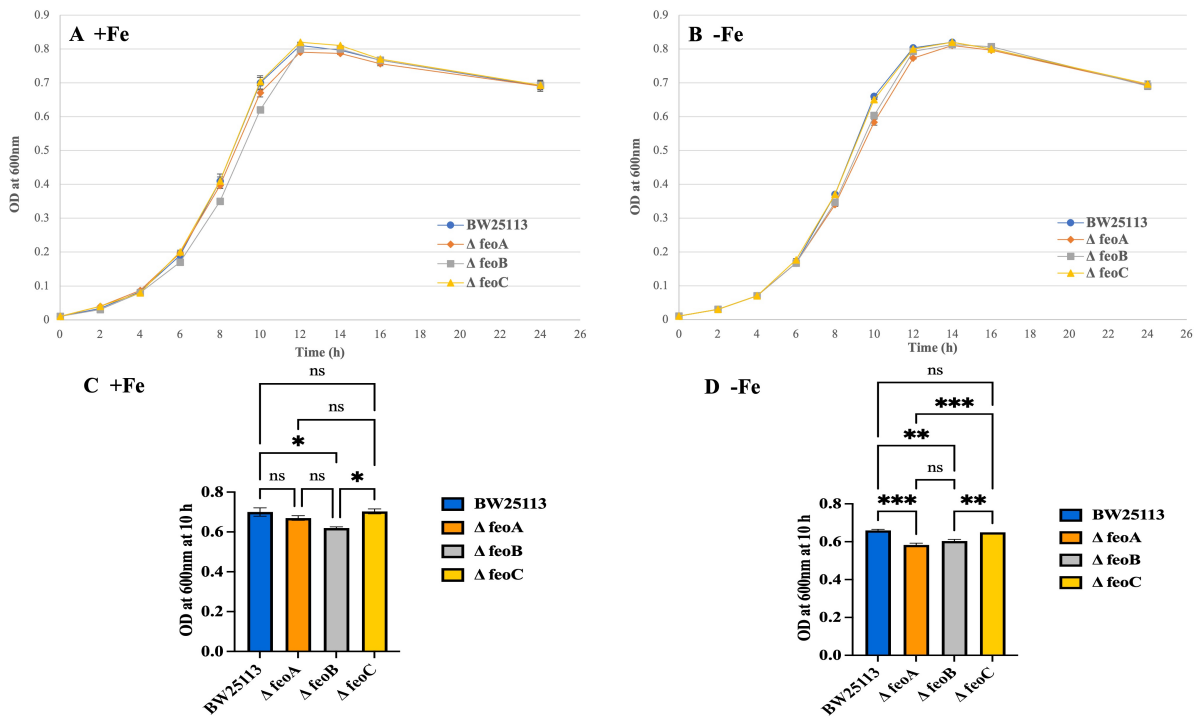

Figure 3.21: Effect of Δ*feoA*::*kan*, Δ*feoB*::*kan* and Δ*feoC*::*kan* status on low-iron <u>anaerobic</u> growth of *E. coli*. Details are as for Fig. 3.17, except for the use of anaerobic growth conditions (in 50 ml syringes; Methods 2.9). (**C&D**) ODs at 10 h are presented from (A) and (B), respectively. P-values were calculated by one-way ANOVA and generated by GraphPad Prism (*, P <0.05; **, P <0.01; ***, P <0.001).

The growth comparison was repeated in the presence of bipyridyl as a ferrous-iron chelator (Romeo *et al.*, 2001). The results showed a slight growth defect for the Δ*feoA*::*kan*, Δ*feoB*::*kan* and Δ*feoC*::*kan* mutants with respect to the wildtype, with little difference between the three mutants (Fig. 3.22). Thus, unlike the results in Fig. 3.21BD, the inclusion of bipyridyl did not provide a clear difference in phenotype between the *feoC* and the *feoA* and *feoB* mutants.

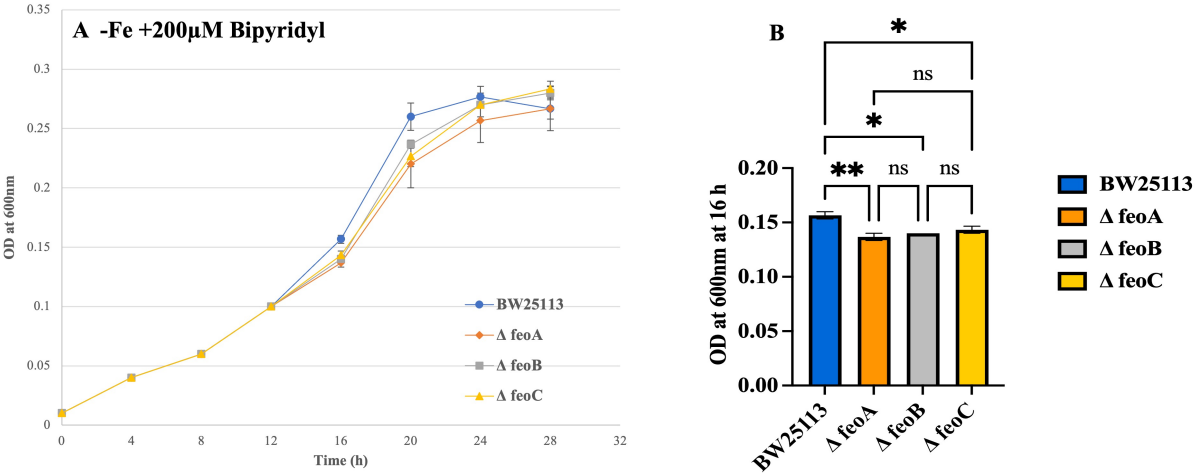

Figure 3.22: Effect of Δ*feoA*::*kan*, Δ*feoB*::*kan* and Δ*feoC*::*kan* status on low-iron anaerobic growth of *E. coli* with Bipyridyl. (A) Details are as for Fig. 3.21B except the inclusion of 200 µM of 2,2 Bipyridyl under anaerobic growth conditions (in 50 ml syringes). (**B**) ODs at 16 h are presented from (A). P-values were calculated by one-way ANOVA and generated by GraphPad Prism (*, P <0.05; **, P <0.01).

A possible role for ascorbate in enhancing the phenotype for the *feo* mutants was next explored (Fig. 3.23). The results showed that the *feoA* strain exhibited a slightly reduced growth under low iron without ascorbate at around 12 h (Fig. 3.23AC), and that both the *feoA* and *feoB* strains showed this effect when ascorbate was provided (Fig. 3.23BD). These results resemble those of Fig. 3.21 which also showed no anaerobic low-iron phenotype for the *feoC* mutant.

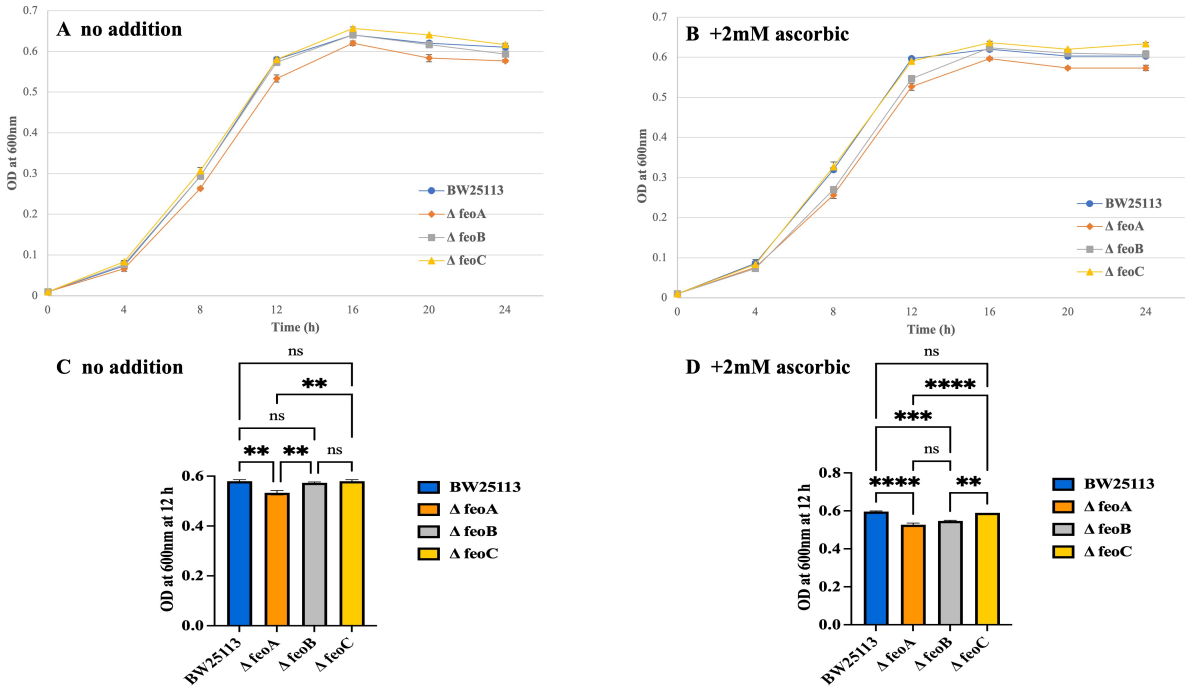

Figure 3.23: Effect of Δ*feoA*::*kan*, Δ*feoB*::*kan* and Δ*feoC*::*kan* status on low-iron <u>anaerobic</u> growth of *E. coli* with 2 mM ascorbate and 100 mM MES. Details are as for Fig. 3.19, except for the use of anaerobic growth conditions (in 50 ml syringes). (**A**) Without 2 mM ascorbate. (**B**) With 2 mM ascorbate. (**C&D**) Data comparison at 12 h from panels A and B, respectively. P-value were calculated by one-way ANOVA and generated by GraphPad Prism (**, P <0.01; ***, P <0.001; ****, P <0.0001).

In an attempt to achieve a strong iron-restricted growth phenotype for the *feo* mutants, growth comparison was repeated with the same condition above (100 mM MES and 2 mM ascorbate) with additional of 100 µM bipyridyl. A major growth difference between the wildtype and *feo* mutants was observed when bipyridyl was included (Fig. 3.24A): a 4.5- to 7.2-fold reduced growth for the *feo* mutants over 24 h; Fig. 3.24B). The *feoA* and *feoB* mutant anaerobic iron-restriction phenotypes are similar to those reported previously (Cartron *et al.*, 2006). However, this *feoC* phenotype was unexpected as the presence/absence of *feoC* had not shown any anaerobic effect on growth previously (Figs. 3.13 & 3.14) and other research suggests no anaerobic phenotype for a *feoC* mutant (Kim *et al.,* 2013).

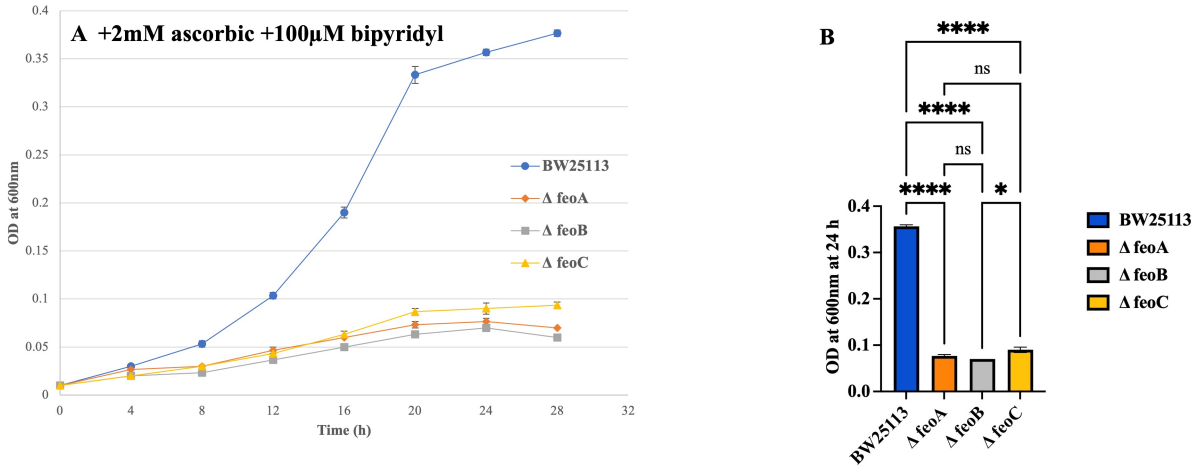

Figure 3.24: Effect of Δ*feoA*::*kan*, Δ*feoB*::*kan* and Δ*feoC*::*kan* status on low-iron anaerobic growth with ascorbate and Bipyridyl. (**A**) Details are as for Fig. 3.23, except for the inclusion of 100 µM of 2,2 bipyridyl (100 mM MES, pH 6, and 2 mM ascorbate were also included) during growth under anaerobic growth conditions (in 50 ml syringes). (**B**) Growth from (A) at 24 h is summarised. P-values were calculated by one-way ANOVA and generated by GraphPad Prism (*, P <0.05; ****, P <0.0001).

3.2.10 Effect of Δ*feoA*::*kan*, Δ*feoB*::*kan* and Δ*feoC*::*kan* mutations on iron-restricted growth under anaerobic respiration conditions with 0.4% glycerol and 50 mM sodium nitrate

The above anaerobic growths were under fermentative conditions. Thus, the growth comparison was repeated with 0.4% glycerol and 50 mM sodium nitrate (in place of 0.4% glucose) to enable anaerobic respiration, conditions that would be expected to raise iron demand since nitrate respiration systems are iron rich (Baez *et al.*, 2022). However, the results showed only a minor growth reduction for the *feo* mutants under low-iron anaerobic respiration conditions (Fig. 3.25), as was found for the *feoA* and *feoB* mutants under the equivalent anaerobic fermentative conditions (Fig. 3.21). Thus, any extra demand for iron imposed by anaerobic nitrate respiration failed to notably affect iron-restricted growth of the *feo* mutants.

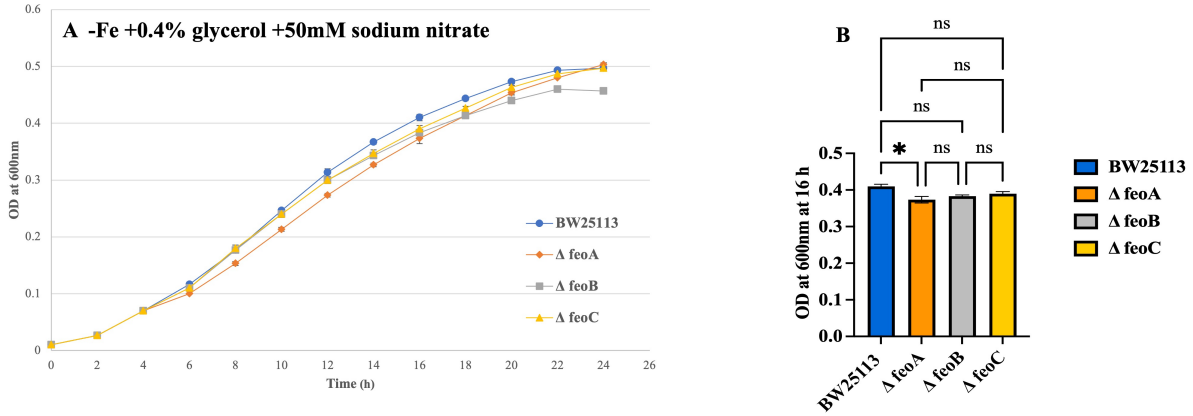

Figure 3.25: Effect of BW25113, Δ*feoA*::*kan*, Δ*feoB*::*kan* and Δ*feoC*::*kan* status on low-iron growth of *E. coli* under anaerobic respiration conditions. (**A**) Details are as for Fig. 3.21B, except for the inclusion of 0.4% glycerol and 50 mM sodium nitrate instead of 0.4% glucose. Growths were under low-iron anaerobic conditions (in 50 ml syringes). (**B**) Data from (A) at 16 h. P-value were calculated by one-way ANOVA and generated by GraphPad Prism (*, P <0.05).

3.2.11 Deletion of the kanamycin cassette of the Δ*feoA*::*kan*, Δ*feoB*::*kan* and Δ*feoC*::*kan* mutants

The kanamycin cassette of the *feo*::*kan* mutants was deleted (Methods 2.16) as it may affect the expression of downstream genes through polarity effects such that the phenotypes obtained are difficult to interpret (Liu *et al.*, 2020). Thus, the pCP20 plasmid was used to eliminate the Kan cassette. The pCP20 was obtained from the lab stock and then the plasmid was transferred into the TOP10 (Methods 2.2). Plasmid DNA then extracted from transformants using a GeneJET plasmid Miniprep kit (Methods 2.11). After that, the identity of the plasmid DNA confirmed by restriction analysis (Methods 2.12 and 2.13) (Fig. 3.26).

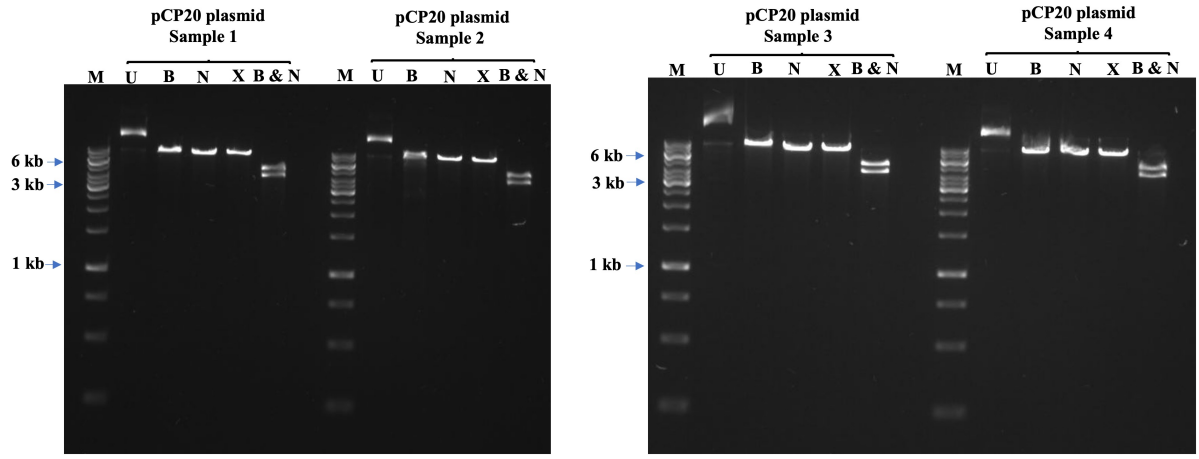

Figure 3.26: Agarose gel electrophoretic analysis of pCP20 plasmid DNA with and without restriction digestion. M, GeneRule 1 kb ladder; U, undigested; B, *Bam*HI digested, N, *Nco*I digested, X, *Xho*I and B&N, *Bam*HI and *Nco*I digested.

Fig. 3.26 shows the expected size of the pCP20, ~9.3 kb for the linearised form: *Bam*HI, *Nco*I and *Xho*I single digestions gave a band of ~9 kb as expected (Fig. 3.27). The uncut plasmid gave a lower than expected mobility indicating that it was in a concatenated state. The *Bam*HI and *Nco*I double digestions gave two bands of ~5 and 4 kb which is similar to the expected sizes (Fig. 3.27).

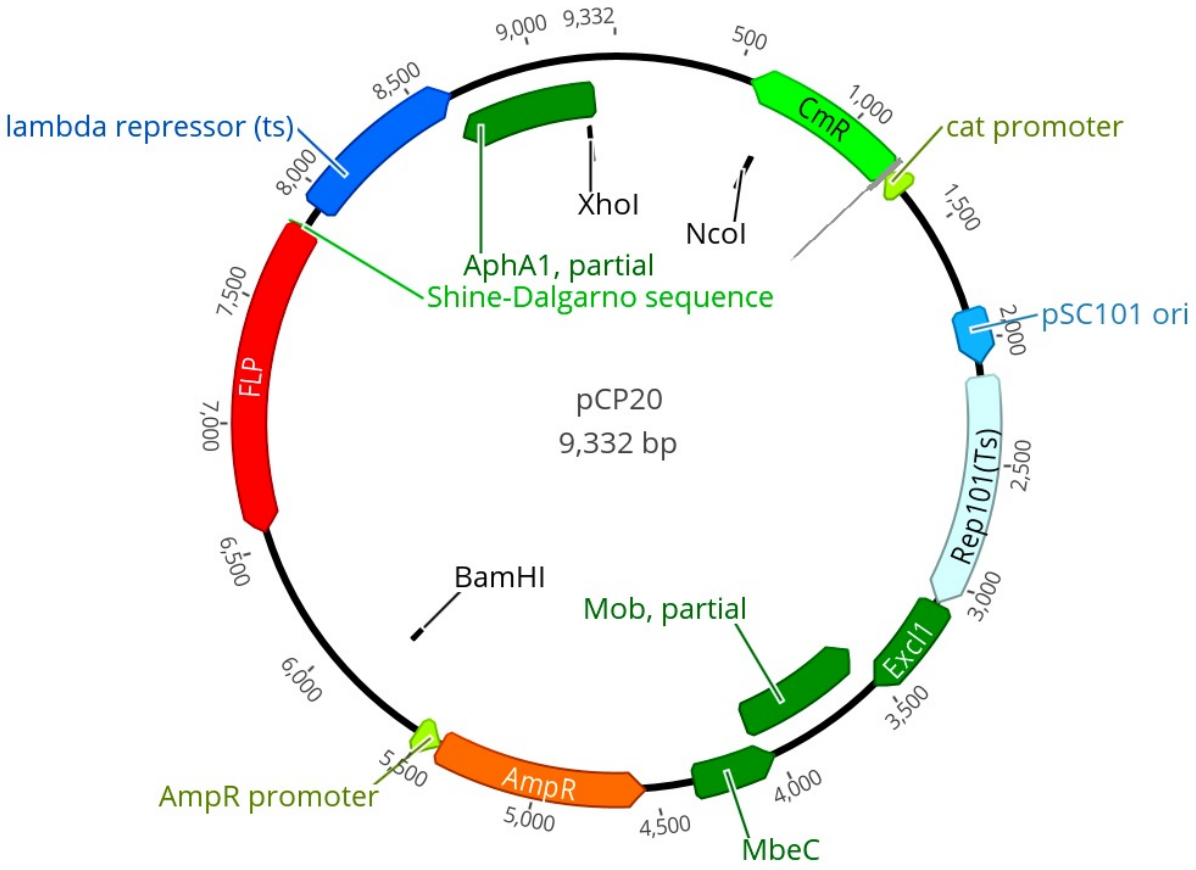

Figure 3.27: The genetic map of pCP20. The map indicates the chloramphenicol and ampicillin resistance loci (CmR and AmpR), the Ts pSC101 *ori* locus and the restriction enzymes *Bam*HI, *Nco*I and *Xho*I. This plasmid is described as a knockout plasmid. It is a temperature sensitive replicon and is used to remove the kanamycin-resistance cassette from the chromosome via expression of flippase (FLP).

Fig 3.28A shows that genomic DNA was successfully isolated from BW25113 and the Δ*feo*::*kan* mutants. This DNA was used as template for PCR amplification of the *feo* locus using DreamTaq Green PCR Master Mix (Methods 2.15) with the *feoABC*-F and -R primers (Table 2.3). In all cases, the expected sizes were obtained: BW25113 (*feoABC*), ~3 kb; Δ*feoA*::*kan*, ~4 kb (*feoBC* ~2.5 kb plus Kan cassette ~1.5 kb); Δ*feoB*::*kan* , ~ 2 kb (*feoAC* ~ 465 bp plus Kan cassette ~1.5 kb); and Δ*feoC*::*kan*, ~ 4 kb (*feoAB* ~ 2.5 kb plus Kan cassette ~1.5 kb) (Fig. 3.28B). Thus, the strains used appear to have the expected *feo* gene status.

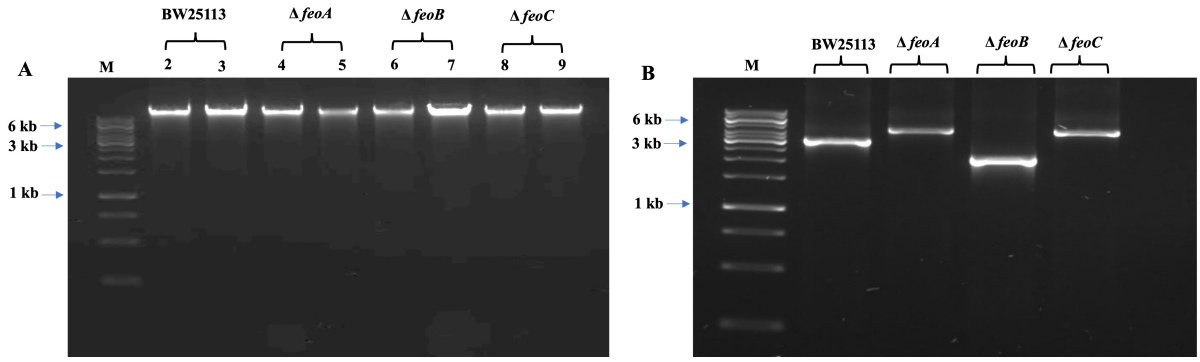

Figure 3.28: Purification of genomic DNA and *feo* amplification from the BW25113 and the Δ*feoA*::*kan*, Δ*feoB*::*kan* and Δ*feoC*::*kan* mutants. (**A**) Agarose gel electrophoretic analysis of isolated chromosomal DNA (lanes 2-9) with GeneRuler 1kb ladder in lane M. (**B**) Agarose gel electrophoretic analysis of the *feoABC* PCR amplification products for the wildtype and Δ*feoA::kan, ΔfeoB::kan and ΔfeoC::kan* mutants.

Following treatment with pCP20, six resulting Kan^S derivates for each *feo* mutation were analysed for the loss of the Kan cassette by PCR amplification of the *feo* locus, as above. The results show that in all cases the expected PCR fragment size was obtained indicating loss of the 1.5 kb Kan cassette (Fig 3.29). For Δ*feoA*, Δ*feoB* and Δ*feoC* the expected and observed sizes before/after *kan* deletion were: ~4/~2.5 kb (Fig 3.29A); ~2/~0.5 kb (Fig 3.29B); and ~4/~2.5 kb (Fig 3.29C).

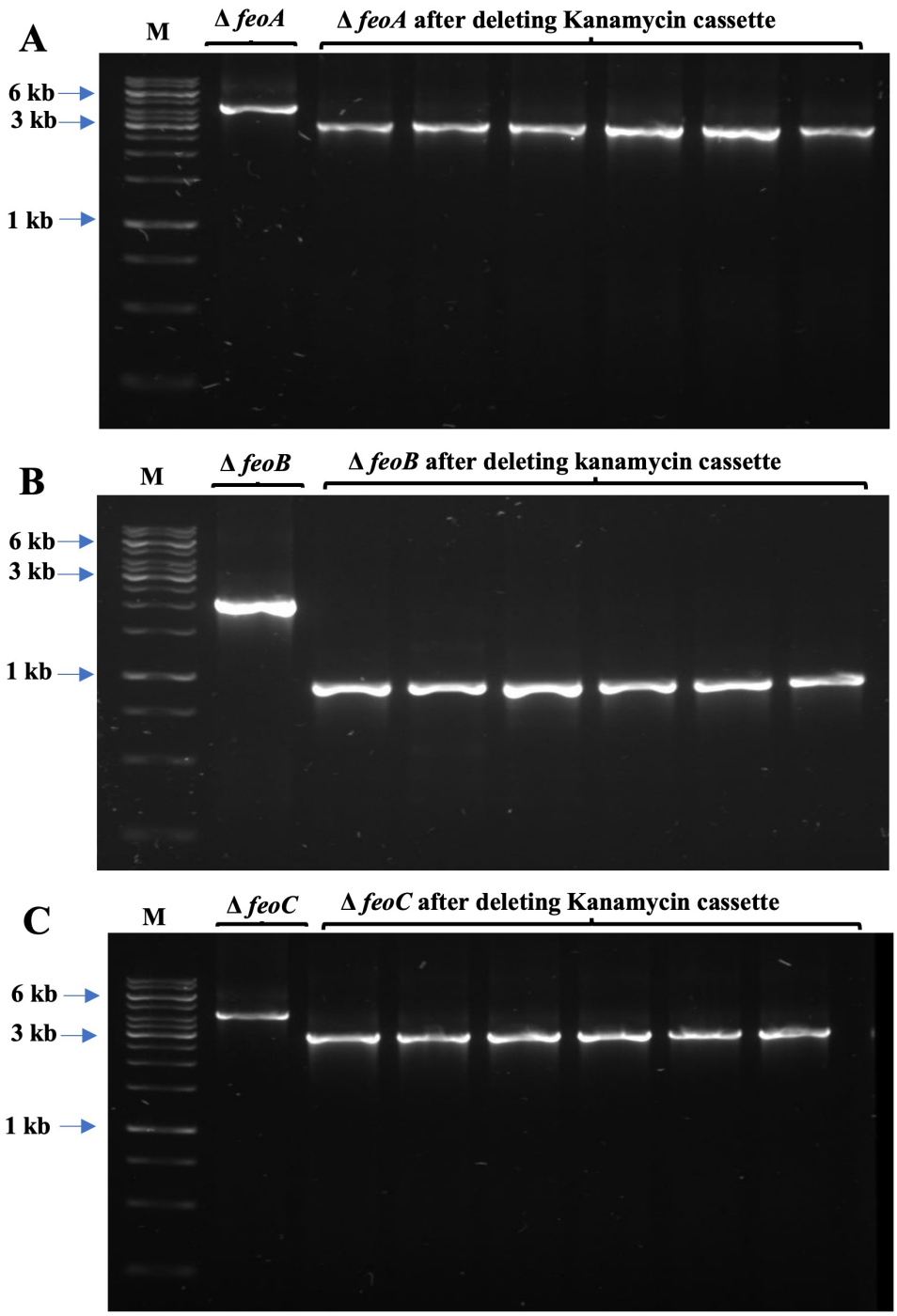

Figure 3.29: Agarose gel electrophoretic analysis of *feoABC* PCR amplification products from candidate Δ*feoA*, Δ*feoB* and Δ*feoC* isolates. (**A**) Δ*feoA* isolates, (**B**) Δ*feoB* isolates and (**C**) Δ*feoC* isolates. The PCR product obtained with the corresponding parent is also shown. M indicates the 1 kb GeneRuler DNA ladder.

3.2.12 Effect of the Δ*feoA*, Δ*feoB* and Δ*feoC* mutations on iron-restricted growth with/without DTPA under aerobic conditions

Once the kanamycin cassette had been deleted for all mutants, the growth comparison was repeated with same conditions as above. Initially, the strains were compared under aerobic conditions in 96-well plates in M9 medium with 0.4% glucose with/without 20 µM ferric citrate (Fig. 3.30). The results showed that when iron was present, all the strains grew well with little difference noted, although the wildtype and *feoA* mutant had a very minor growth advantage (Fig. 3.30AC). When iron was absent, growth was slightly reduced (~0.2 OD unit lower maximum growth) but there was no statistical difference seen between them (Fig. 3.30BD). It should be noted that these results are similar to those obtained above with kanamycin cassette present (Fig. 3.17AB) and indicate no notable growth differences between the mutants and wildtype.

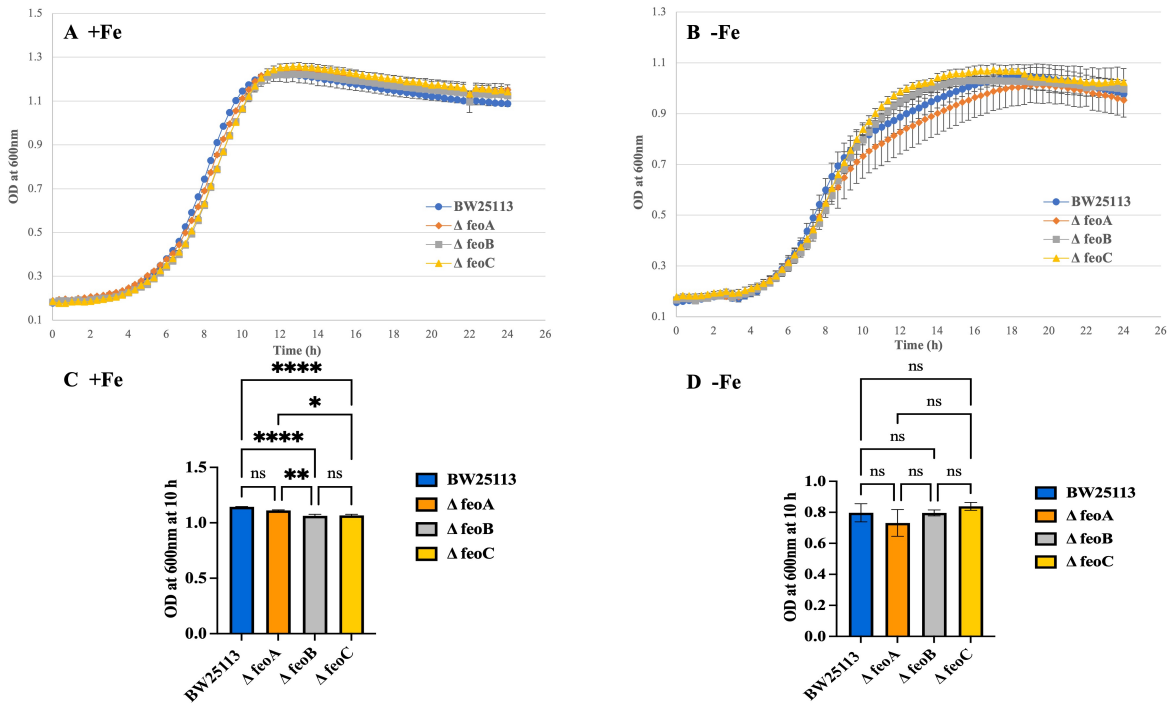

Figure 3.30: Effect of Δ*feoA*, Δ*feoB* and Δ*feoC* status on low-iron aerobic growth of *E. coli*. BW25113 and the Δ*feoA*, Δ*feoB* and Δ*feoC* strains were grown overnight in 5 ml of M9 medium with 0.4% glucose and 20 µM of ferric citrate in test tubes on a shaker at 37 °C and 250 rpm. The following day, the washed cell pellets were used to inoculate fresh M9 minimal medium with 0.4% glucose, with/without (**A**/**B**) 20 µM ferric citrate, under aerobic

conditions in a 96-well plate (Methods 2.10). (**C&D**) OD values at 10 h for (A) and (B) respectively. P-value were calculated by one-way ANOVA and generated by GraphPad Prism (*, P <0.05; **, P <0.01; ****, P <0.0001).

The growth comparison was repeated as above but with DTPA included. The results show that when iron was added along with 1 µM DTPA, all strains grew well and showed similar growth (Fig 3.31AC). However, when iron was excluded and 1 µM DTPA was included, the Δ*feoA*, Δ*feoB* and Δ*feoC* mutants showed a major growth defect with respect to the wildtype: BW25113 showed an increased growth of ~ 0.9 OD units over 24 h whereas the Δ*feoA*, Δ*feoB* and Δ*feoC* mutants showed increases of ~0.6, 0.5 and 0.8 (1.5-, 1.8- and 1.125-fold difference, respectively) (Fig. 3.31BD). Thus, the Δ*feoB* mutant showed a greater defect than the other two mutants, and the *feoC* mutant showed the weakest growth defect. These results are consistent with the notion that FeoC supports Feo activity aerobically. In addition, the results are similar to those obtained with the *kan*-cassette substitution mutants (Fig. 3.18) whereby all three mutants showed significantly reduced growth.

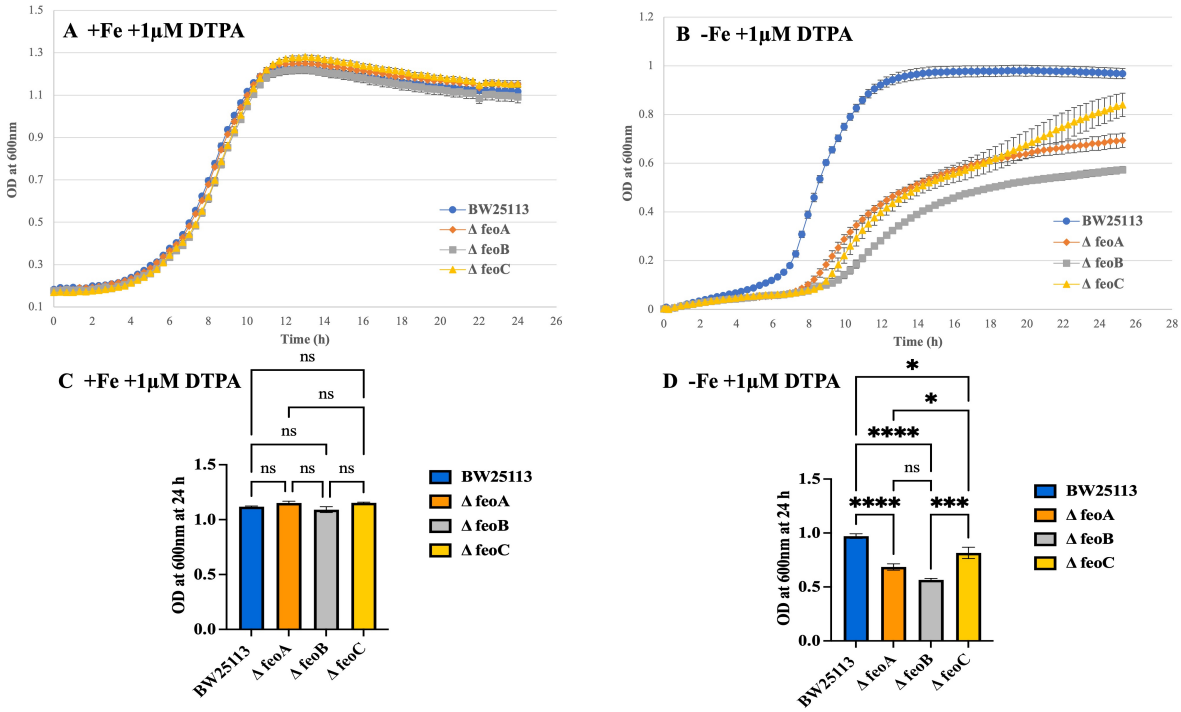

Figure 3.31: Effect of Δ*feoA*, Δ*feoB* and Δ*feoC* status on low-iron aerobic growth of *E. coli*, with <u>DTPA</u>. Details are as for Fig. 3.30, except for the inclusion of 1 µM DTPA for the

growth comparisons in all cases. (**A**) With 20 µM ferric citrate and 1 µM DTPA. (**B**) With 1 µM DTPA, and no additional iron. (**C&D**) OD values at 10 h for (A) and (B) respectively. P-value were calculated by one-way ANOVA and generated by GraphPad Prism (*, P <0.05; ***, P <0.001; ****, P <0.0001).

3.2.13 Effect of Δ*feoA*, Δ*feoB* and Δ*feoC* mutation on low-iron aerobic growth with 100 mM MES (pH 6) and 2 mM ascorbic acid

Again, growth comparison was repeated aerobically, this time with reductant and MES buffer (pH 6). The results show that all strains grew well and similarly without 2 mM ascorbic but with ascorbate the wildtype showed a minor advantage with respect to the *feo* mutants which was significant for the *feoC* mutant (Fig. 3.32). These results are similar to those seen for the Δ*feo*::*kan* mutants where little difference in growth was observed (Fig. 3.19).

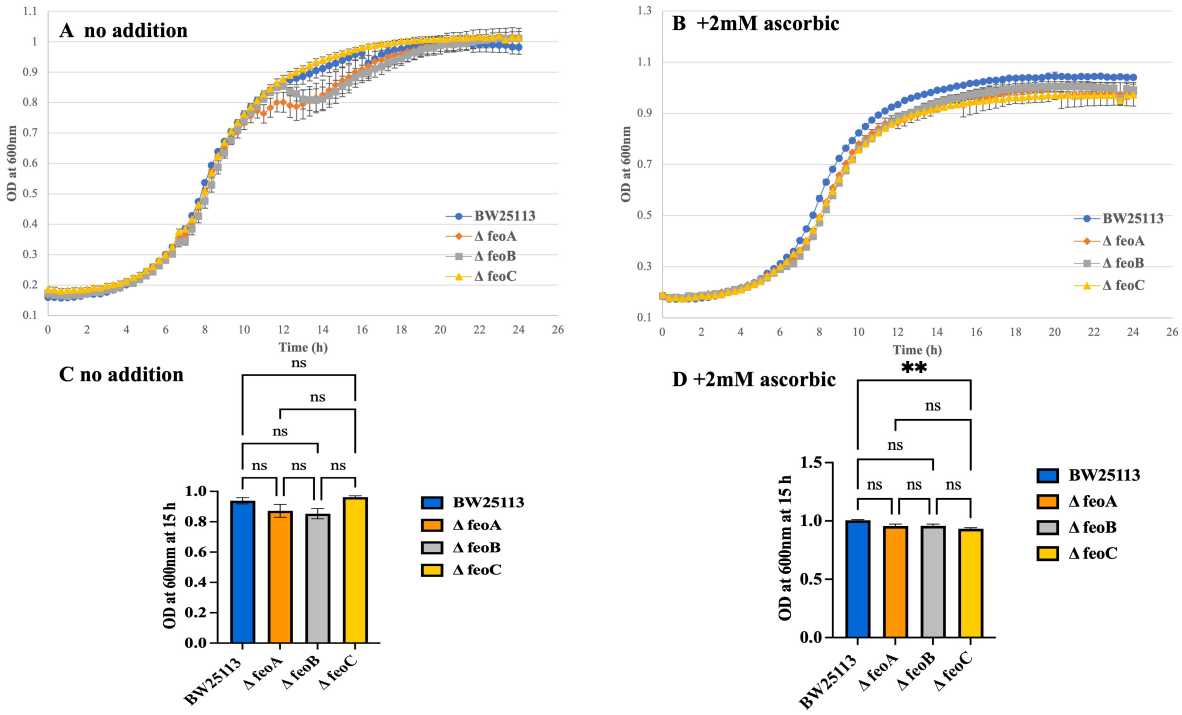

Figure 3.32: Effect of BW25113, Δ*feoA*, Δ*feoB* and Δ*feoC* status on low-iron aerobic growth of *E. coli*, with 100 mM MES (pH 6) and 2 mM ascorbic acid. Details are as for Fig. 3.30, except for the inclusion of 100 mM MES (pH 6) for the growth comparisons in all cases and the exclusion (**A**) or inclusion (**B**) of 2 mM ascorbic acid. Growth medium was 200 µl of M9 minimal medium with 0.4% glucose, 100 mM MES (pH 6), with/without 2 mM ascorbic acid and growths were performed in 96-well plates at 180 rpm and 37 °C using a Spark Tecan

device. (**C&D**) The OD values at 15 h for (A) and (B), respectively. P-values were calculated by one-way ANOVA and generated by GraphPad Prism (**, P <0.01).

A further growth comparison was performed, as in Fig. 3.20B, under aerobic iron-restricted conditions in the presence of DTPA, ascorbate and MES (pH 6) (Fig. 3.33). The wildtype showed much better growth than the wildtype (~twofold at 24 h): BW25113 and the Δ*feoA*, Δ*feoB* and Δ*feoC* mutants displayed increases in growth over 24 h of 0.79, 0.35, 0.24 and 0.31 OD units, respectively (Fig. 3.33A) which corresponds to 2.5-, 3.29- and 2.55-fold reductions for Δ*feoA*, Δ*feoB* and Δ*feoC* mutants, respectively (Fig. 3.33B). Although all three mutants showed significantly weaker growth than the wildtype, the was no significant difference between the three mutants (Fig. 3.32B). Thus, as for the data presented above (Figs 3.18, 3.20 and 3.31), the *feoC* mutant displays a strong aerobic growth defect under DTPA-induced iron restriction, similar to that of the *feoA* and *feoB* mutants.

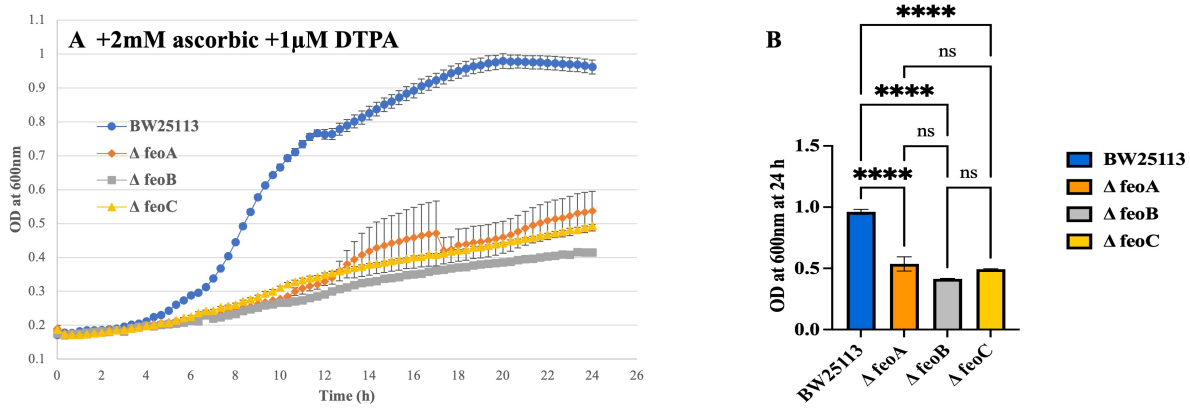

Figure 3.33: Effect of Δ*feoA*, Δ*feoB* and Δ*feoC* status on iron-restricted aerobic growth of *E. coli*, with DTPA, MES (pH 6) and ascorbic acid. Details are as for Fig. 3.32 except for the inclusion of 1 μM DTPA in all growth comparisons. (**A**) Growth with 2 mM ascorbic acid, 100 mM MES (pH 6) and 1 μM DTPA. (**B**) OD values at 24 h. P-values were calculated by one-way ANOVA and generated by GraphPad Prism (****, P <0.0001).

3.2.14 Effect of Δ*feoA*, Δ*feoB* and Δ*feoC* mutation on iron-restricted growth with/without Bipyridyl under anaerobic conditions

A growth comparison was also performed, as in Fig. 3.21 for the Δ*feo*::*kan* strains, under anaerobic, low-iron conditions with bipyridyl (Fig. 3.34). The results obtained were similar to

those obtained previously for the *kan*-replacement mutants (Fig. 3.21) in that the presence and absence of iron made little difference to growth ant the mutants grew similarly to the wildtype. However, slight and significant differences were seen, albeit the effect were weak (Fig. 3.34)

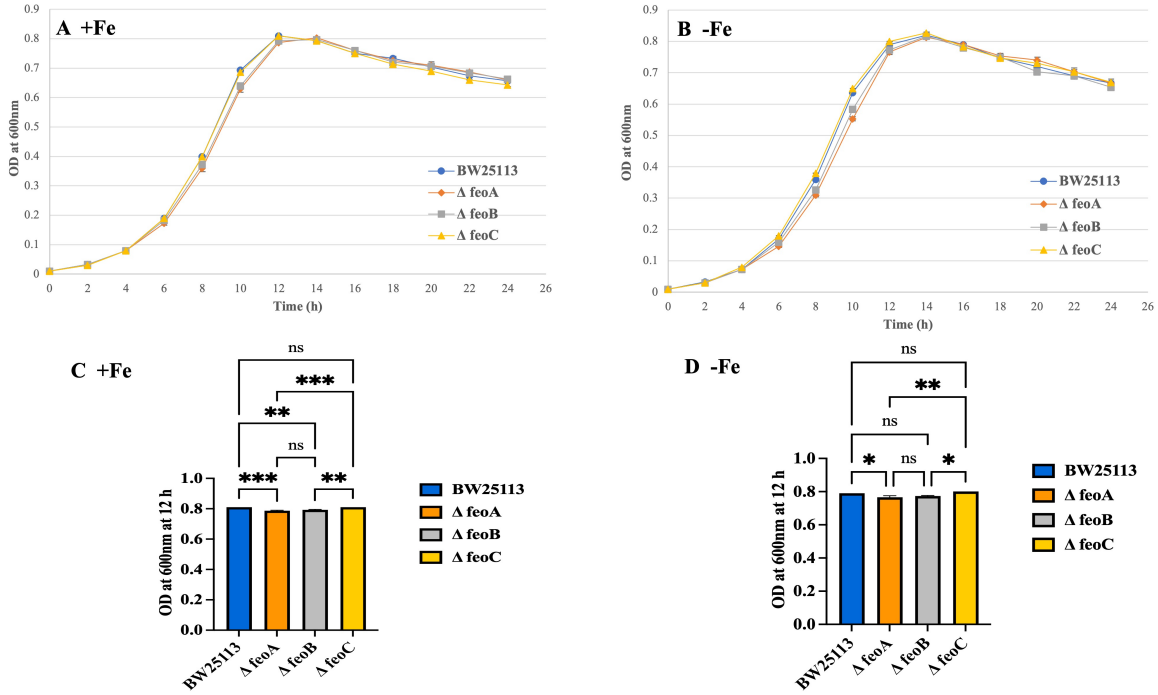

Figure 3.34: Effect of Δ*feoA*, Δ*feoB* and Δ*feoC* status on low-iron anaerobic growth of *E. coli*. Details are as for Fig. 3.30, except for the use of anaerobic growth conditions (in 50 ml syringes; Methods 2.9). (**A**&**B**) Growths with and without 20 µM ferric citrate, respectively. (**C**&**D**) OD at 12 h for (A) and (B), respectively. P-values were calculated by one-way ANOVA and generated by GraphPad Prism (*, P <0.05; **, P <0.01; ***, P <0.001).

A further anaerobic growth comparison was performed, as in the Fig. 3.22, and again the results were similar to those achieved with the *kan* replacement mutants (Fig. 3.22) where a weak reduction in growth was observed for the *feo* mutants. The presence of 200 µM bipyridyl resulted in reduced growth for all three Δ*feo* mutants (Fig. 3.35A), and the differences were significant (Fig. 3.35B). Indeed, at 22 h, the Δ*feoA*, Δ*feoB* and Δ*feoC* mutants showed ~1.42, 1.26 and 1.17-fold lower growth than the parent strain but the Δ*feoC* mutant showed slightly better growth than the other *feo* mutants, consistent with the main role in anaerobic Feo iron uptake being mediated by FeoAB. Nevertheless, a clearly reduced anaerobic growth was

observed for the *feoC* mutant which was unexpected given that previous work indicates no phenotype anaerobically (Kim *et al.,* 2013).

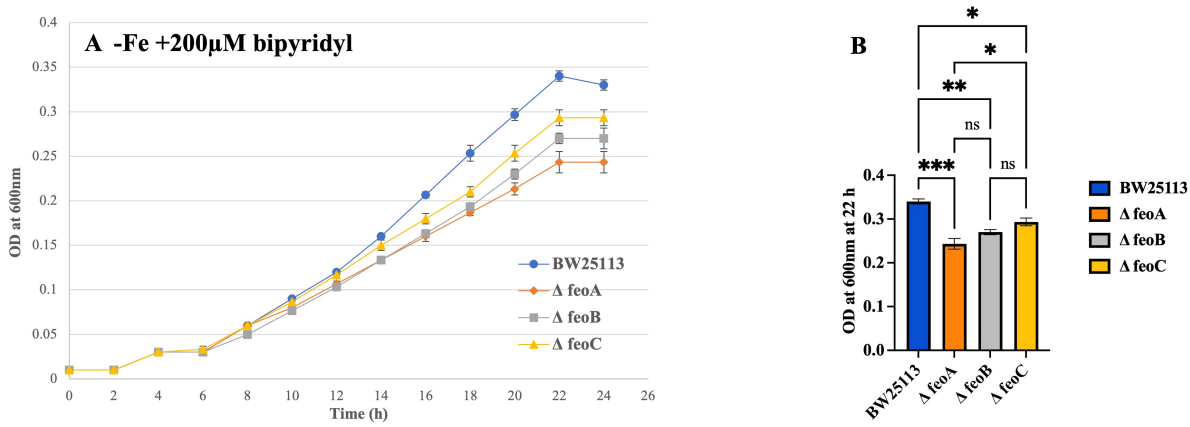

Figure 3.35: Effect of Δ*feoA*, Δ*feoB* and Δ*feoC* status on low-iron anaerobic growth of *E. coli* with Bipyridyl. (**A**) Details are as for Fig. 3.34B, except for the inclusion of 200 µM of 2,2 bipyridyl as chelator under anaerobic growth conditions (in 50 ml syringes). (**B**) OD values at 22 h. P-values were calculated by one-way ANOVA and generated by GraphPad Prism (*, P <0.05; **, P <0.01; ***, P <0.001).

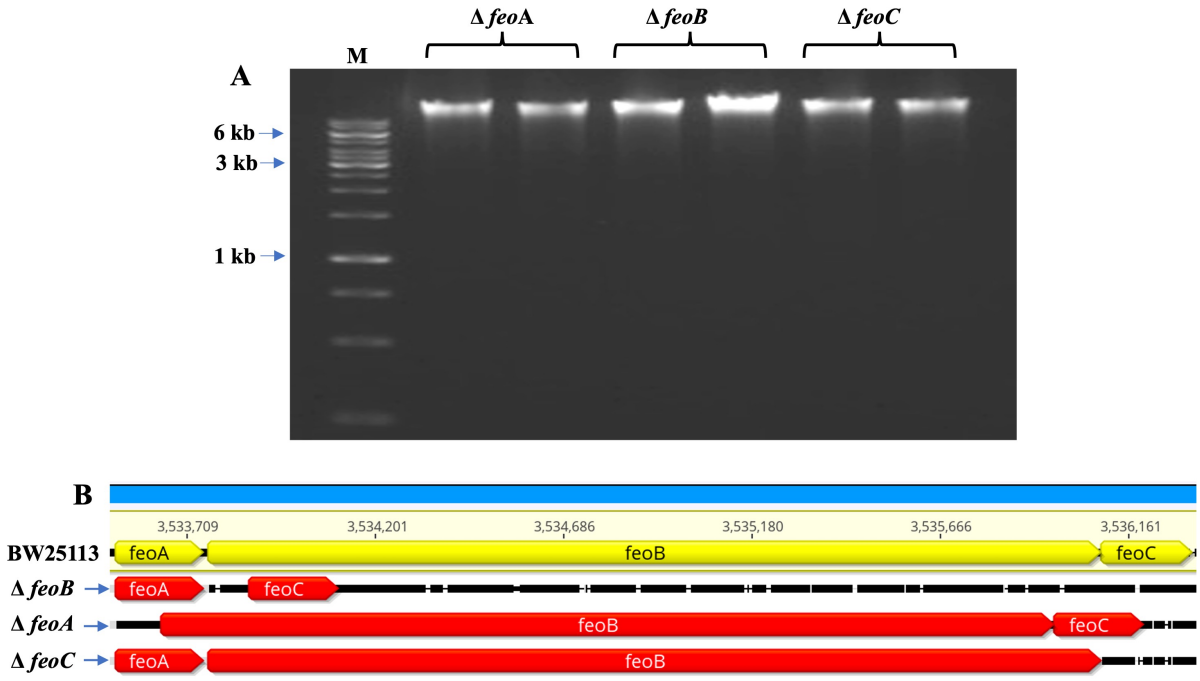

Figure 3.36: Confirmation of the Δ*feoA*, Δ*feoB* and Δ*feoC* status on the *kan*-cassette deletion mutants by NGS. (**A**) Agarose gel electrophoretic analysis of genomic DNA from the Δ*feoA,* Δ*feoB* and Δ*feoC* mutants used from whole-genome NGS. Lanes from left to right: M, GeneRuler 1kb ladder; 2-3, Δ*feo*A gDNA; 4-5, Δ*feo*B gDNA; 6-7, Δ*feo*C gDNA. (**B**)

Schematic comparison of the nucleotide sequences of the *feo* locus for the wildtype and *feo* mutants presented using Geneious Prime.

3.3 Discussion

3.3.1 Summary of the experimental approach.

In this chapter, the focus was the widely distributed FeoABC ferrous iron transporter – specifically, the role of FeoC. The function of FeoC is reported to be in protecting FeoB from proteolytic degradation under anaerobiosis to enable FeoB-mediated ferrous iron absorption (Guo *et al.,* 2011). Indeed, FeoC is found to interact with FeoB *in vivo* (Kim *et al.,* 2013). FeoC is thought to carry an Fe-S cluster under anaerobic conditions which renders it less sensitive to Lon-mediated proteolysis, enabling FeoC to protect FeoB against FtsH-mediated degradation anaerobically (Kim *et al.,* 2015; Al-Aidy, 2020).

The main aim of this chapter was to explore the role of FeoC in enabling Feo activity and to determine the role of FeoC in regulation of Feo activity under aerobic and anaerobic conditions. To progress this aim, it was necessary to isolate and confirm the *feoAB* and *feoABC* inducible expression plasmids which would be used to determine any requirement for FeoC in Feo activity (section 3.2). Following this, it was necessary to confirm the phenotype of the iron-uptake mutant, JC32, that would be used as host for the *feoAB* and *feoABC* inducible expression plasmids (sections 3.2.1 -3.2.2). It was also a requirement to confirm the Δ*feoABC* genotype for JC32 by PCR amplification of the corresponding locus (section 3.2.3). Further, it was necessary to compare the iron-restricted growth phenotypes of JC32 carrying the vector, pBADara-*feoAB* and pBADara-*feoABC* under iron restriction, both aerobically and anaerobically, to determine any impact of *feoC* status (sections 3.2.4 -3.2.5 -3.2.6). Thus, the impact of these three plasmids on iron-restricted growth was determined in order to assess any effect of *feoC* on Feo-dependent iron-restricted growth. Both aerobic and anaerobic conditions were considered along with pH control (buffered at pH 6) and the presence of reductant (where ferrous iron is expected to predominate over ferric iron). The results showed a clear role of

feoC in supporting Feo-mediated iron uptake under iron restricted, buffered, reducing conditions with DTPA, aerobically (Figs. 3.12B, 3.16A, 3.16B). Following this, the single mutants of each gene of the *feo* system (Δ*feoA*, Δ*feoB* and Δ*feoC*), with/without kanamycin cassette substitution, were compared with their parental 'wild type' strain, BW25113, under the conditions previously applied for the inducible *feoAB* and *feoABC* plasmid transformants in an attempt to confirm a role for the *feoC* gene in supporting aerobic Feo activity under reducing conditions aerobically with DTPA. The results illustrated a strong increased growth of BW25113 of 2.18-fold over 24 h with respect to the Δ*feoA*::*kan*, Δ*feoB*::*kan* and Δ*feoC*::*kan* (Fig. 3.20). These results were similar to those obtained by complementation under the same conditions (Fig. 3.16B). However, there was no difference in phenotype between the *feoA*, *feoB* and *feoC* mutants, which was unexpected for the *feoC* mutant. This may be due to the presence of other iron transporters that may impact the activity observed for the Feo system aerobically. In addition, under anaerobic conditions, BW25113 and the single Δ*feoA*::*kan*, Δ*feoB*::*kan* and Δ*feoC*::*kan* mutants showed similar growth with/without iron and with 200 μM bipyridyl (Fig. 3.21AB and 3.22, respectively). These results were similar to the results obtained by *feoAB* and *feoABC* complementation (Fig. 3.13 and 3.14). However, the addition of ascorbic acid under buffered low-iron anaerobic condition with the presence of 100 μM bipyridyl resulted in stronger growth of BW25113 with respect to the Δ*feoA*::*kan*, Δ*feoB*::*kan* and Δ*feoC*::*kan* strains (Fig. 3.24) (4.5 to 7.2-fold) and again the Δ*feoC*::*kan* mutant showed a strong defect phenotype which indicated that the Δ*feoC*::*kan* mutation did result in an inactive Feo system because all three single mutants showed similarly strong iron-restriction phenotypes. After that, the *kan* cassette was deleted by pCP20 and confirmed by PCR (section 3.2.11). Similar conditions were employed to test the phenotype of the *kan* deletion mutants. Under aerobic conditions in the absence of iron and addition of DTPA, Δ*feoA*, Δ*feoB* and Δ*feoC* mutants showed an iron-restriction growth defect with respect to the wildtype (Fig. 3.31), and this result

was similar to that seen with the *kan* substitution mutants (Fig. 3.18). These findings suggested that the growth defect of the *feo* single mutants was not related to the presence and absence of the *kan* cassette. Under buffered low-iron conditions with ascorbate and DTPA, aerobically, a growth defect for all the three mutants (Δ*feoA*, Δ*feoB* and Δ*feoC*) was observed (Fig. 3.33A). These findings were similar to those obtained with *feoAB* and *feoABC*- complementation (Fig 3.16) and with *kan* mutants (Fig. 3.20).

3.3.2 FeoC supports Feo-dependent iron-restricted growth aerobically in JC32 when tested using pBADara-*feoAB* and pBADara-*feoABC* complementation studies

The required inducible expression plasmids (pBADara- and pBADrha-based; Table 2.2) were isolated and confirmed (Figs. 3.1-3.3). In addition, JC32 was shown to display an iron-restricted phenotype (Fig. 3.5B; Fig. 3.6B) with DTPA under aerobic conditions as shown previously (Cao *et al.*, 2007). This was as expected given its genotype (Table 2.1) which results from absence of five major iron transporters (including *feo*), as well as absence of enterobactin production. In addition, the iron-restricted phenotype of JC32 was also tested under anaerobic growth conditions, since the Feo system is considered to function anaerobically, and a clear low-iron growth defect was observed, although this was not impacted by DTPA (Fig. 3.7B). The observed phenotype is thus consistent with the *feo*$^-$ status of the JC32 strain (Cao *et al.*, 2007; Al-Aidy, 2020). The mutation status with respect to the five major iron transporters of *E. coli* K-12 (including *feo*) for JC32 was confirmed by whole genome sequencing (Fig. 3.9C) and *feo*$^-$ status was further confirmed by PCR (Fig. 3.10).

To determine whether the inducible *feoABC* and *feoAB* plasmids can support the iron-restricted growth of the JC32 and thus complement the iron uptake defect of this strain, growth of corresponding JC32 transformants was compared under low-iron aerobic conditions with DTPA. Results showed that the *feoAB*- and *feoABC*-complemented strains had enhanced growth with respect to the vector control, with the *feoC* bearing strain showing a greater growth than the *feoC*$^-$ strain (Fig. 3.12B). Thus, under aerobic conditions, induction of *feoAB* or

feoABC enhanced iron-restricted growth (with DTPA) of the iron-uptake mutant and there was a significant increase in growth for the *feoABC*-complemented transformant with respect to that of the *feoAB*-complemented transformant; this difference can be attributed to *feoC* (Fig. 3.12B). These findings clearly indicate a role for FeoC in supporting Feo dependent iron-restricted growth aerobically.

Anaerobically, the *feoAB*- and *feoABC*-complemented JC32 mutant strains both showed greater growth than the vector control (Fig. 3.13A), but grew similarly, and DTPA had little impact (Fig. 3.13B & 3.14). Therefore, *feoAB* and *feoABC* provided a similar iron-restricted growth advantage anaerobically suggesting that FeoC may not have a role anaerobically, which contrasts with the case aerobically. Such findings contradict those of Kim *et al*. (2013) who found that FeoC supports FeoAB function anaerobically in *S. enterica*. The possibility of an aerobic function for FeoC in *S. enterica* was not considered by Kim *et al*. (2013).

The inclusion of ascorbic acid, as reductant, under buffered low-iron aerobic conditions with DTPA resulted in a major growth advantage for the *feoABC*-complemented strain with respect to the *feoAB*-complemented strain (Fig. 3.16B). Indeed, the growth of the *feoABC*-complemented strain resembled that of the wildtype suggesting that iron uptake under these conditions was almost entirely Feo dependent. An important observation is that FeoC is critical for Feo function under such conditions. These results thus show that the addition of ascorbate along with DTPA, and controlling the pH at 6, increase the aerobic growth difference between the *feoABC*- and *feoAB*-complemented strains (17-fold difference; 0.83 and 0.05 OD units at 24 h, respectively). These parameters were thus considered to represent excellent growth conditions for exploring the role of FeoC in Feo function.

3.3.3 Phenotype of Δ*feoA*::*kan*, Δ*feoB*::*kan* and Δ*feoC*::*kan* compared with BW25113

The previous results that obtained using the inducible *feoAB* and *feoABC* plasmids showed an important role of *feoC* under aerobic condition; in contrast there was no role of *feoC* under

anaerobic conditions. Therefore, similar conditions were used to compare single-gene *feo* replacement mutants (Δ*feoA*::*kan*, Δ*feoB*::*kan* and Δ*feoC*::*kan*) with the parental wildtype strain (BW25113) to determine whether the *feoC* phenotype obtained via complementation under inducible conditions can be confirmed using the single-gene, chromosomal *feo* mutants. The results showed a significantly increased growth for BW25113 of 2.18-fold over 24 h with respect to the Δ*feoA*::*kan*, Δ*feoB*::*kan* and Δ*feoC*::*kan* under aerobic condition in the absence of iron and inclusion of DTPA and reductant (Fig. 3.20). These findings are similar to those obtained by complementation under the same conditions (Fig. 3.16B) indicating that Feo can support growth under iron-restricted conditions aerobically. However, the *feoC* mutant gave a similar phenotype to the *feoA* and *feoB* mutants, which was unexpected (Fig. 3.20). The results suggest that the Δ*feoC*::*kan* mutation resulted in inactivation of the Feo system producing a similarly strong phenotype to that observed for the *feoA* and *feoB* single mutants. Importantly, the results illustrate that the inclusion of ascorbate with DTPA, along with the control of the pH at 6, enhanced the aerobic growth difference between the wild type (BW25113) and the *feo* mutants (Δ*feoA*::*kan*, Δ*feoB*::*kan* and Δ*feoC*::*kan* showing an approximately 8-fold significant difference at 24 h. A similar effect was observed when comparing the *feoAB* and *feoABC* complemented JC32 strain.

Anaerobically, the BW23115 and the single Δ*feoA*::*kan*, Δ*feoB*::*kan* and Δ*feoC*::*kan* mutants showed similarly growth with/without iron (Fig. 3.21AB), even with absence of iron and presence of 200 μM bipyridyl (Fig. 3.22), which is similar to the results obtained for the *feoAB* and *feoABC* complementation studies (Fig. 3.13 and 3.14). However, the inclusion of ascorbic acid under buffered low-iron anaerobic conditions, along with 100μM bipyridyl, showed a significant growth advantage for BW25113 with respect to the Δ*feoA*::*kan*, Δ*feoB*::*kan* and Δ*feoC*::*kan* strains (Fig. 3.24) (4.5 to 7.2-fold). Thus, the Δ*feoC*::*kan* mutant again showed a strong iron-restricted phenotype (this time anaerobically) further indicating that the Δ*feoC*::*kan*

mutation had resulted in inactivation of the Feo system such the three single mutants gave similar iron-restriction phenotypes.

3.3.4 Phenotype of the Δ*feoA*, Δ*feoB* and Δ*feoC* strains

The results with the Δ*feo*::*kan* cassette substitution mutants indicated an iron-restriction growth defect for the Δ*feoC*::*kan* mutant under both aerobic and anaerobic conditions under reducing, pH 6 conditions with Bip, that was similar to that of the corresponding *feoA* and *feoB* mutants. To determine whether the *kan* cassette insertion had any impact on the phenotypes observed, it was considered necessary to delete the cassette to generate unmarked deletion mutants and then determine whether the phenotypes previously observed are retained. Therefore, the pCP20 plasmid was isolated (Fig. 3.26 and 3.27) and employed for removal of the *kan* cassette; the resultant *kan* deletants were confirmed by PCR (Fig. 3.29). After that, similar conditions were used to test the phenotype of the Kan^S deletion mutants.

Aerobically, in the absence of iron and presence of DTPA (Fig. 3.31), the Δ*feoA*, Δ*feoB* and Δ*feoC* mutants displayed an iron-restriction growth defect with respect to the wildtype, similar to that seen for the *kan* replacement mutants (Fig. 3.18). Thus, the growth defect of the *feo* single mutants appears to not be overly impacted by the presence/absence of the *kan* cassette.

The inclusion of ascorbic acid, under buffered low-iron aerobic conditions along with DTPA, resulted in a stronger growth defect for the Δ*feoA*, Δ*feoB* and Δ*feoC* mutants (Fig. 3.33A) of 2.3- to 3.3-fold (Fig. 3.33B). These results were similar those obtained by *feoAB*- and *feoABC*-complementation (Fig. 3.16) and with the *kan*-replacement mutants (Fig. 3.20) in that a clear aerobic iron-restriction growth advantage was associated the presence of *feo*. In addition, the strong phenotype for the *feoC* mutant is apparent both with and without the *kan* cassette.

In summary, the results obtained by complementation with the inducible *feoAB* and *feoABC* constructs indicated a clear role for *feoC* in supporting Feo-dependent iron-restricted growth aerobically, but not anaerobically – particularly in the presence of chelator, buffer at pH 6 and

reductant. However, the results with the single-gene *feo* mutants did not show any distinct aerobic role for *feoC* in supporting Feo-dependent low-iron growth aerobically, with respect to the *feoA* and *feoB* mutants. Instead, all three *feo* mutants (*feoA*, *feoB* and *feoC*) gave similar strong growth restrictions under low-iron conditions both aerobically and anaerobically (particularly with reductant, buffer at pH 6 and chelator). The reason for this difference is unclear but may be related to differences in expression (controlled induction versus oxygen and iron dependent regulation), genetic background (presence or absence of defects in other iron transporters), and/or defects in the function of the *feoAB* genes deriving from the *feoC* mutation.

Chapter 4: The role of the "C-terminal region" of FeoB in supporting FeoC-dependent enhanced Feo iron-uptake activity; a site-directed mutagenesis approach

Introduction

Iron is an important element for nearly all organisms (Lau *et al*., 2013). The Feo system is the primary ferrous iron (Fe^{2+}) transport system found in both pathogenic and non-pathogenic bacteria. The *feo* system consists of three proteins FeoA, FeoB and FeoC. FeoA is small (75-85 residues) cytoplasmic protein and its precise function is not yet known, but it is absolutely important for Feo-mediated uptake in *E. coli* and it is likely to interact with the N-terminal G-protein domain of FeoB (Cartron *et al.*, 2006; Lau *et al*., 2013). The FeoB protein is considered to be the main ferrous-iron permease, and contains two main regions: an N-terminal cytoplasmic G-protein domain and C-terminal polytopic transmembrane domain. In addition, there is a short C-terminal extension within the FeoB proteins of the *Gammaproteobacteria* designated the "C-terminal region" (CFeoB, residues 747-773 of the FeoB of *E. coli*). CFeoB is predicted to be cytoplasmic and is rich in conserved Cys and His residues. Its function is unclear (Cartron *et al.*, 2006; Orzel *et al.*, 2025). FeoC, which is the third protein, is a small (78 residues), cytoplasmic protein. FeoC is not universally conserved in Feo systems and appears to be largely restricted to the *Gammaproteobacteria* (Lau *et al*., 2015). This suggests that it may interact with CFeoB (Lau *et al*., 2015). Indeed, in *V. cholera* and *S. enterica*, FeoC has been found to interact with FeoB *in vivo* (Kim *et al*., 2013; Weaver *et al.*, 2013). FeoC was discovered in *S. enterica* to protect FeoB from the FtsH protease under anaerobiosis (Kim *et al*., 2013). FeoC is believed to contain an Fe-S cluster under anaerobic circumstances which renders it less sensitive to Lon-mediated proteolysis (Kim *et al*., 2015).

The previous chapter focused on the role of FeoC and found that induction of *feoABC* enhances aerobic iron-restricted growth with DTPA and this effect is very much enhanced by the presence of *feoC*. This effect was particularly strong under reducing and buffered condition aerobically.

Chapter 4

This chapter further focuses on the role of FeoC by considering a possible interaction between FeoC and the unique C-terminal region of FeoB (CFeoB) within the *Gammaproteobacteria* that may explain the FeoC-enhanced low-iron growth observed aerobically in Chapter 3. To progress this aim, it was necessary to accurately identify the amino acid residues that correspond to the unique C-terminal extension of FeoB (CFeoB), as found in the *Gammaproteobacteria*. This was achieved by using multiple amino acid sequence alignment and structure prediction approaches. Once the CFeoB region had been defined, stop codons were introduced into *feoB* at various positions within the CFeoB-encoding region, using site-directed mutagenesis. This approach allowed the generation of a serial set of FeoB C-terminal truncations in which all or part of the CFeoB region was deleted. The mutants thus generated were confirmed by Sanger sequencing. The mutations were produced in both pBADara-*feoAB* and pBADara-*feoABC* plasmids to enable comparison of the resulting effect on aerobic, iron-restricted growth in the absence and presence of FeoC. As in Chapter 3, growth tests were performed using *E. coli* JC32 transformants. This allowed any detection of the impact of the CFeoB disruptions on FeoC-enhanced aerobic, iron-restricted growth with DTPA.

In addition, an attempt was made to interfere with FeoC activity by overexpressing the CFeoB region. The aim was to utilise the overexpressed CFeoB to titrate FeoC away from FeoB, and thus suppress the predicted ability of FeoC to enhance aerobic Feo-dependent iron uptake. Thus, the CFeoB-encoding region (*CfeoB*) was cloned into pBADrha in inducible format, in three forms: N-terminal Flag-tag; C-terminal Flag-tag; and no Flag-tag. Flag-tags were included to enable confirmation of expression. All constructs were confirmed by Nanopore 30 whole-plasmid sequencing. All *CfeoB* constructs were then transferred into JC32 transformants carrying pBADara-*feoAB* or pBADara-*feoABC* to investigate whether *CfeoB* expression caused any disruption of the ability of *feoC* to enhance iron-restricted growth aerobically with DTPA.

Chapter 4

4.1 Identifying the C-terminal region (CFeoB) of FeoB of *E. coli*

The UniProt database was used to obtain FeoB protein sequences from the *Gammaproteobacteria* and other classes of bacteria, including Gram-positive bacteria. Thus, 22 protein sequences were selected from different classes. The CFeoB region was previously found to be conserved only in the *Gammaproteobacteria* (Orzel *et al.*, 2025). The 22 selected protein sequences were aligned using Geneious Prime (the Geneious alignment, global alignment option, default parameters) to identify the CFeoB region of *E. coli* (Fig. 4.1A). The multiple alignment showed that the CFeoB region is only conserved in *Gammaproteobacteria* and that it contains conserved cysteine and histidine residues suggestive of metal binding (red box in Fig. 4.1B) (Orzel *et al.*, 2023, 2025).

PyMOL was then used to display the predicted structure of FeoB, as provided by the AlphaFold Protein Structure Database (accession no. AF-P33650-F1-v4) (Jumper *et al*., 2021), to further identify the extent of the C-terminal region. The two major domain of FeoB protein are clearly apparent: the N-terminal cytoplasmic G-protein domain region and the C-terminal polytopic transmembrane domain (Fig. 4.1C). In addition, a C-terminal extension (located from residues 747 to 773) is also apparent, orientated towards the cytoplasm (in red, Fig. 4.1C), that is distinct from the rest of the C-terminal domaim. This extension matches the region highlighted in Fig. 4.1B that corresponds to the unique 'CFeoB' residues in FeoB of the *Gammaproteobacteria*.

Thus, on the basis of the structural prediction and multiple alignment, it was decided to generate five CFeoB truncations, as follows:

S747Δ, deletion of the entire CFeoB region (residues 747-773);

D750Δ, deletion of the C-terminal region beyond the short linker sequence;

A755Δ, retention of the first short alpha helix but loss of the remaining parts of CFeoB;

V760Δ, deletion of the loop preceding the second helix and the conserved CC motif; and

A765Δ, deletion of residues 765-773 predicted to form a random coil, that include the C-

terminal CH motif (Fig. 4.1C). Fig. 4.1D shows the CFeoB amino acid sequence of *E. coli* with the location of the five CFeoB truncations indicated.

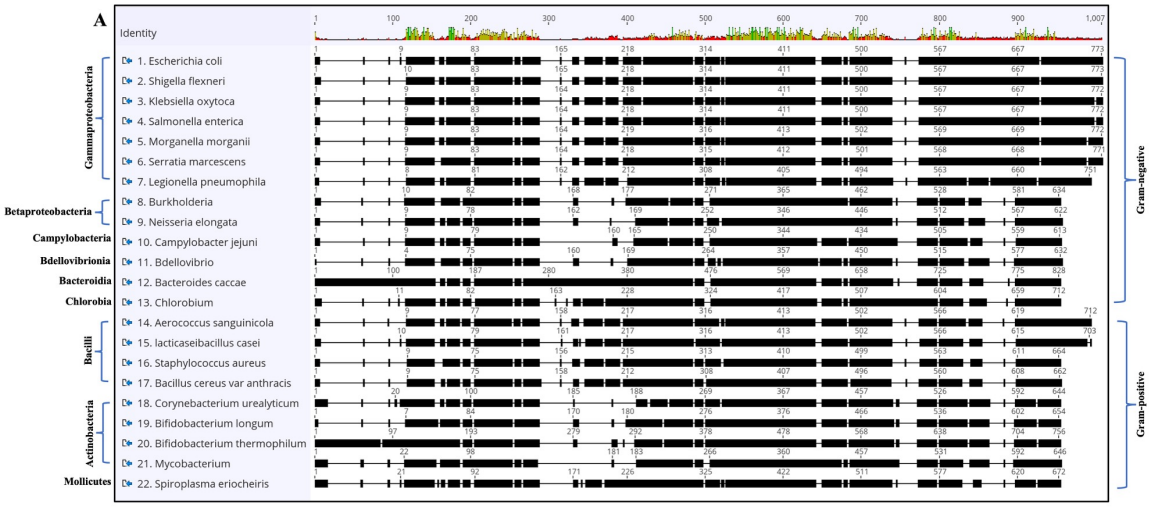
A
Identity
1. Escherichia coli
2. Shigella flexneri
3. Klebsiella oxytoca
4. Salmonella enterica
5. Morganella morganii
6. Serratia marcescens
7. Legionella pneumophila
8. Burkholderia
9. Neisseria elongata
10. Campylobacter jejuni
11. Bdellovibrio
12. Bacteroides caccae
13. Chlorobium
14. Aerococcus sanguinicola
15. lacticaseibacillus casei
16. Staphylococcus aureus
17. Bacillus cereus var anthracis
18. Corynebacterium urealyticum
19. Bifidobacterium longum
20. Bifidobacterium thermophilum
21. Mycobacterium
22. Spiroplasma eriocheiris
Gammaproteobacteria
Betaproteobacteria
Campylobacteria
Bdellovibrionia
Bacteroidia
Chlorobia
Bacilli
Actinobacteria
Mollicutes
Gram-negative
Gram-positive

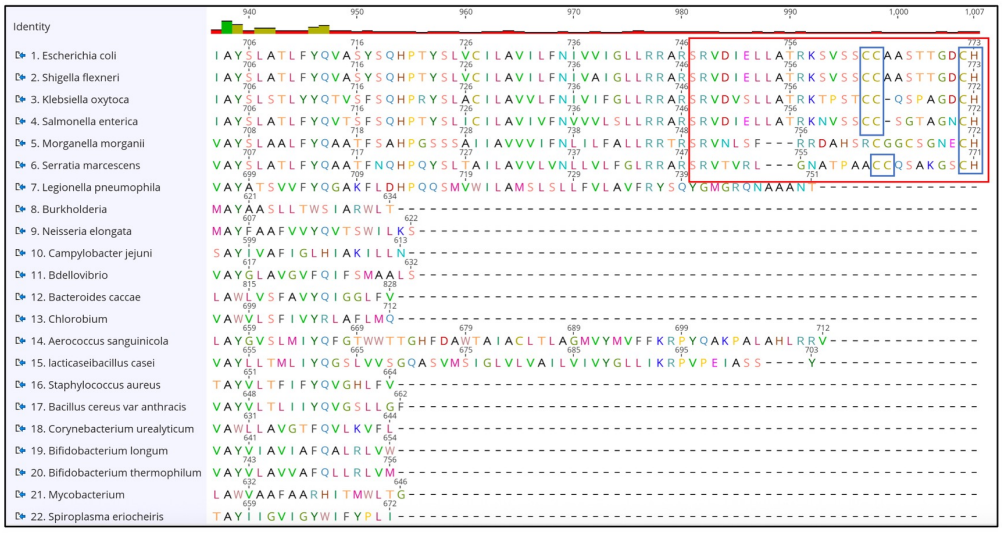
B
Identity
1. Escherichia coli
2. Shigella flexneri
3. Klebsiella oxytoca
4. Salmonella enterica
5. Morganella morganii
6. Serratia marcescens
7. Legionella pneumophila
8. Burkholderia
9. Neisseria elongata
10. Campylobacter jejuni
11. Bdellovibrio
12. Bacteroides caccae
13. Chlorobium
14. Aerococcus sanguinicola
15. lacticaseibacillus casei
16. Staphylococcus aureus
17. Bacillus cereus var anthracis
18. Corynebacterium urealyticum
19. Bifidobacterium longum
20. Bifidobacterium thermophilum
21. Mycobacterium
22. Spiroplasma eriocheiris

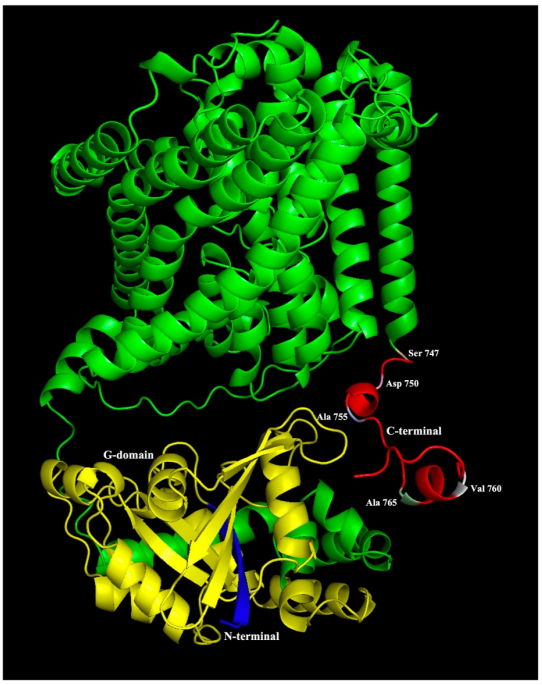
C
Ser 747
Asp 750
Ala 755
C-terminal
G-domain
Val 760
Ala 765
N-terminal


D
E. coli CFeoB amino acid 747-773
S R V D I E L L A T R K S V S S C C A A S T T G D C H
ΔSer 747
ΔAsp 750
ΔAla 755
ΔVal 760
ΔAla 765

Figure 4.1: The C-terminal region of FeoB. (A) Summary of the multiple alignment of the FeoB amino acid sequences for different bacteria species (from the *Gammaproteobacteria* and other classes, as indicated) generated using Geneious Prime (Geneious alignment; global alignment). Identity/similarity are indicated in Logo format. Black blocks indicate conserved segments of the corresponding sequence. **(B)** The alignment of the C-terminal region of the FeoB proteins (from A) showing the CFeoB is only conserved in *Gammaproteobacteria* from 747 to 773 in red box and rich of cysteine with histidine residues in blue box. **(C)** The predicted *E. coli* K-12 FeoB protein structure from the AlphaFold database (accession no. AF-P33650-F1-v4) visualised using PyMOL. Two main regions in the structure are indicated: the N-terminal cytoplasmic (blue) G-protein domain (yellow); and C-terminal polytopic transmembrane domain (green/yellow). In red, located from 747 to 773, is the location of the CFeoB region with the five residues targeted for truncation by SDM indicated. **(D)** The *E. coli* CFeoB amino acid sequence is shown with the location of the five CFeoB truncations provided: ΔSer747; ΔAsp750; ΔAla755; ΔVal760; and ΔAla765.

4.2 Site-directed mutagenesis of pBADara-*feoAB* and pBADara-*feoABC*

4.2.1 Isolation of plasmid DNA

In order to progress with the SDM of *feoB*, it was necessary to isolate sufficient pBADara-*feoAB* and pBADara-*feoABC* DNA for use as SDM templates. As indicated above, the aim was to introduce in-frame stop codons into the *CfeoB* region in order to generate a series of C-terminally truncated FeoB variants (see Fig. 3.3). For this purpose, the TAA/UAA (ochre) stop codon was selected as this is recognised by both *E. coli* release factors (RF1 and RF2) (Baggett *et al*., 2017). Plasmid DNA was extracted using the GeneJET plasmid Miniprep kit (Methods 2.11). The identities of the plasmids were confirmed by agarose gel electrophoresis and plasmid digestion by restriction enzymes (Methods 2.12 & 2.13), as shown in Fig. 4.2.

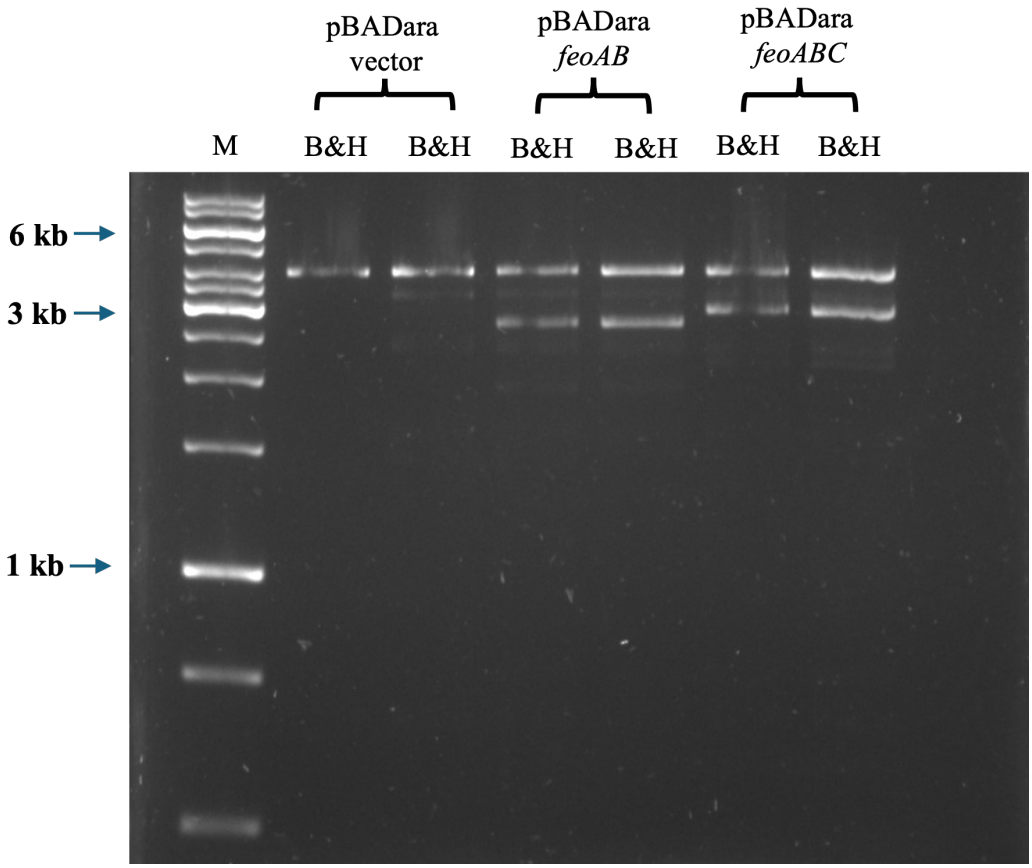

Figure 4.2: Agarose electrophoretic analysis of pBADara, pBADara-*feoAB* and pBADara-*feoABC* DNA with restriction digestion. M, GeneRule 1 kb ladder (Fig. 2.1); H&B, *Hin*dIII and *Bam*HI digested.

For the three plasmids (Fig. 4.2), the expected sizes and restriction fragments were observed indicating the presence of the 2.8 and 4.1 kb *feoAB* and *feoABC* inserts, respectively).

4.2.2 Site-directed mutagenesis

The Quikchange II XL Site-directed Mutagenesis kit from Agilent was used according to the manufacturer's instructions. The primers (complementary forward and reverse) were designed to be 25-45 nucleotides in length with the mismatch(es) directing the corresponding mutation position in the middle (Table 2.4). The PCR was performed according to the manufacturer's instructions (Methods 2.17; Table 2.8) and successful PCR amplification was determined by agarose gel electrophoresis (Methods 2.12). In all cases, the expected amplification product sizes were generated (Fig. 4.3).

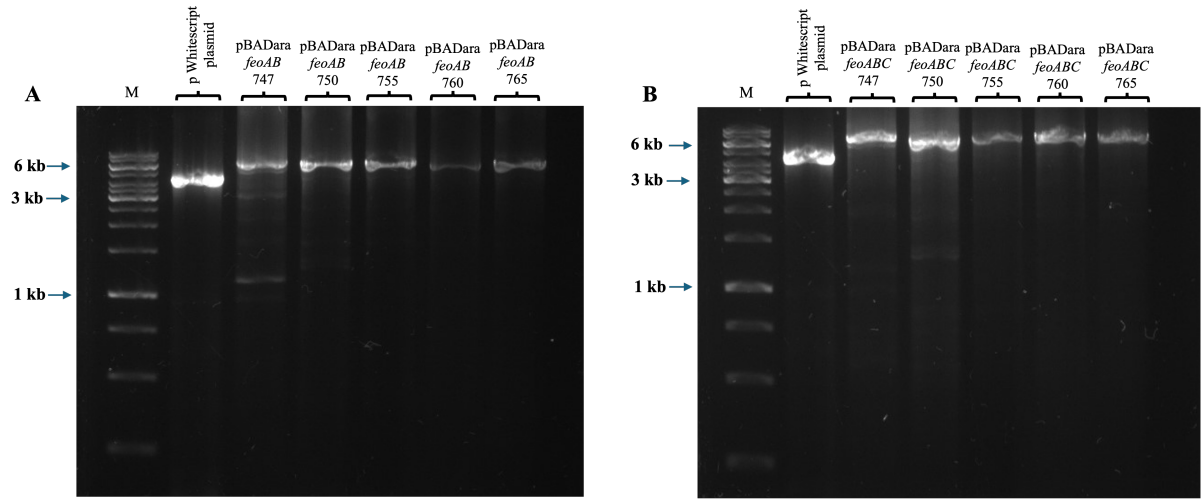

Figure 4.3: Agarose gel electrophoretic analysis confirming the amplification of the templates during SDM. M, GeneRuler 1 kb ladder (Fig. 2.1). pWhitescript plasmid was used as control to ensure the efficiency of mutated plasmid generation, with the expected PCR fragment size (~4.5 kb) observed. **(A)** PCR amplification of pBADara-*feoAB* plasmid with expected sizes (~6.65 kb) obtained for all mutation. **(B)** PCR amplification of pBADara-*feoABC* plasmid with expected sizes (~6.9 kb) observed for all mutations.

Following confirmation of PCR products by gel electrophoresis, the PCR products were treated by *Dpn*I (as per manufacturer's instructions) to digest methylated template DNA, ensuring that only the mutated plasmid DNA was retained for transformation. The results show that PCR product of the expected size was retained in all cases (Fig. 4.4).

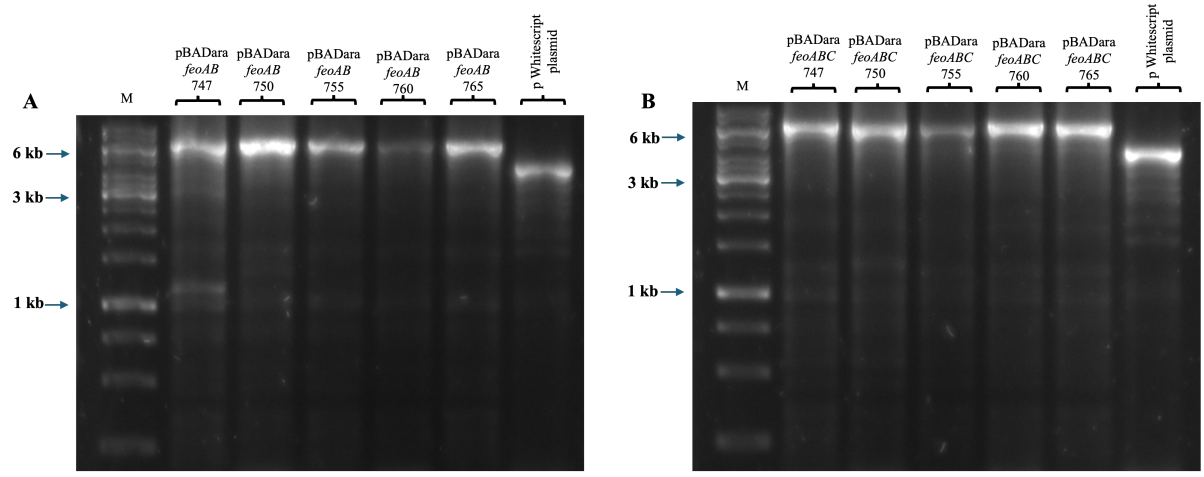

Figure 4.4: Agarose gel electrophoresis analysis confirming the SDM PCR products after *Dpn*I digestion. M, GeneRule 1 kb ladder (Fig. 2.1). *Dpn*I-treated pBADara-*feoAB* **(A)** and pBADara-*feoABC* (**B**) PCR products.

In the next step, 2 µl of each *Dpn*I-treated PCR-amplified DNA sample were used to transform XL 10-Gold ultracompetent cells (Methods 2.17). Transformants (Ap^R) were thus obtained in all cases (Fig. 4.5).

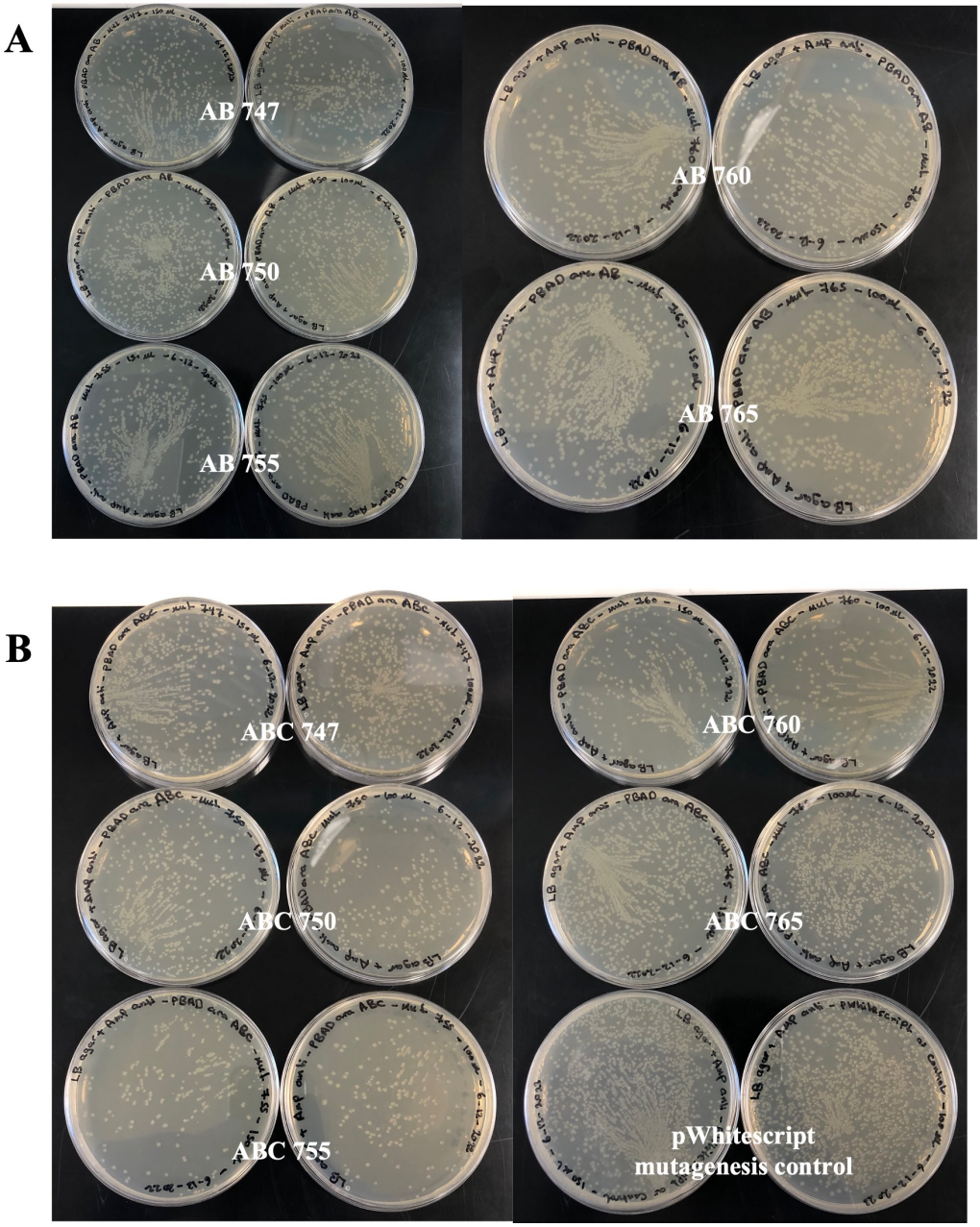

Figure 4.5: Transformation of the SDM-treated plasmid into XL 10-Gold ultracompetent cells. The pBADara-*feoAB* (**A**) and pBADara *feoABC* (**B**) mutant (TAA replacement at codons 747, 750, 755, 760 and 765) transformants. Controls are pWhitescript transformants.

The transformants were subject to plasmid isolation using the GeneJET plasmid Miniprep kit (Methods 2.11) and the isolated plasmid DNA was assessed by agarose gel electrophoresis

(Fig. 4.6). Those samples that exhibited the expected size on electrophoresis were submitted to Eurofins Scientific for Sanger sequencing using forward and reverse primers designed to anneal ~50 bp up and downstream of the mutation site region (F-*feoABC* and *R-feoABC*; Table 2.9). The Sanger sequencing results showed that all mutations were successfull for both plasmids (Fig. 4.7).

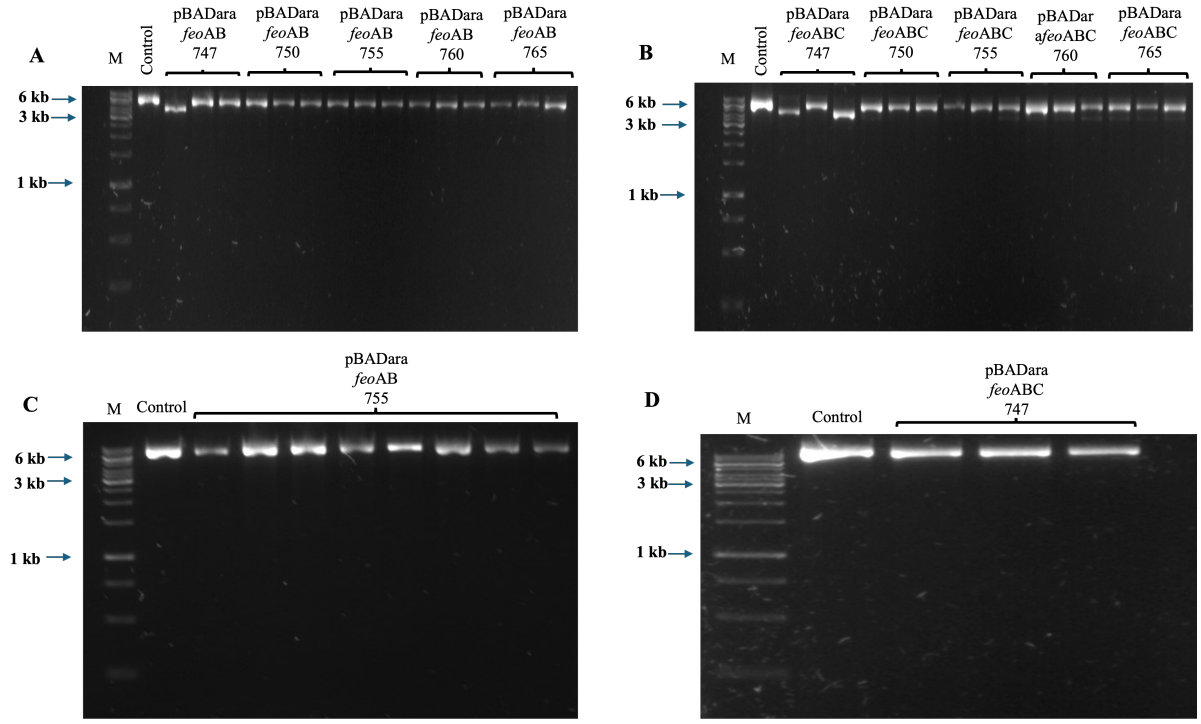

Figure 4.6: Agarose electrophoretic analysis of purified SDM plasmid DNA. Controls were the non-mutated pBADara-*feoAB* (A & C) and pBADara-*feoABC* (B & D). **(A)** pBADara-*feoAB* mutants; three isolates for each mutation. **(B)** pBADara-*feoABC* mutants; three isolates for each mutation. **(C)** Repeated plasmid isolations for pBADara-*feoAB* (755). **(D)** Repeat plasmid isolations for of pBADara-*feoABC* (747). Repeat isolation were performed where plasmid DNA size was incorrect or where Sanger sequencing indicated that the desired mutation had not been generated.

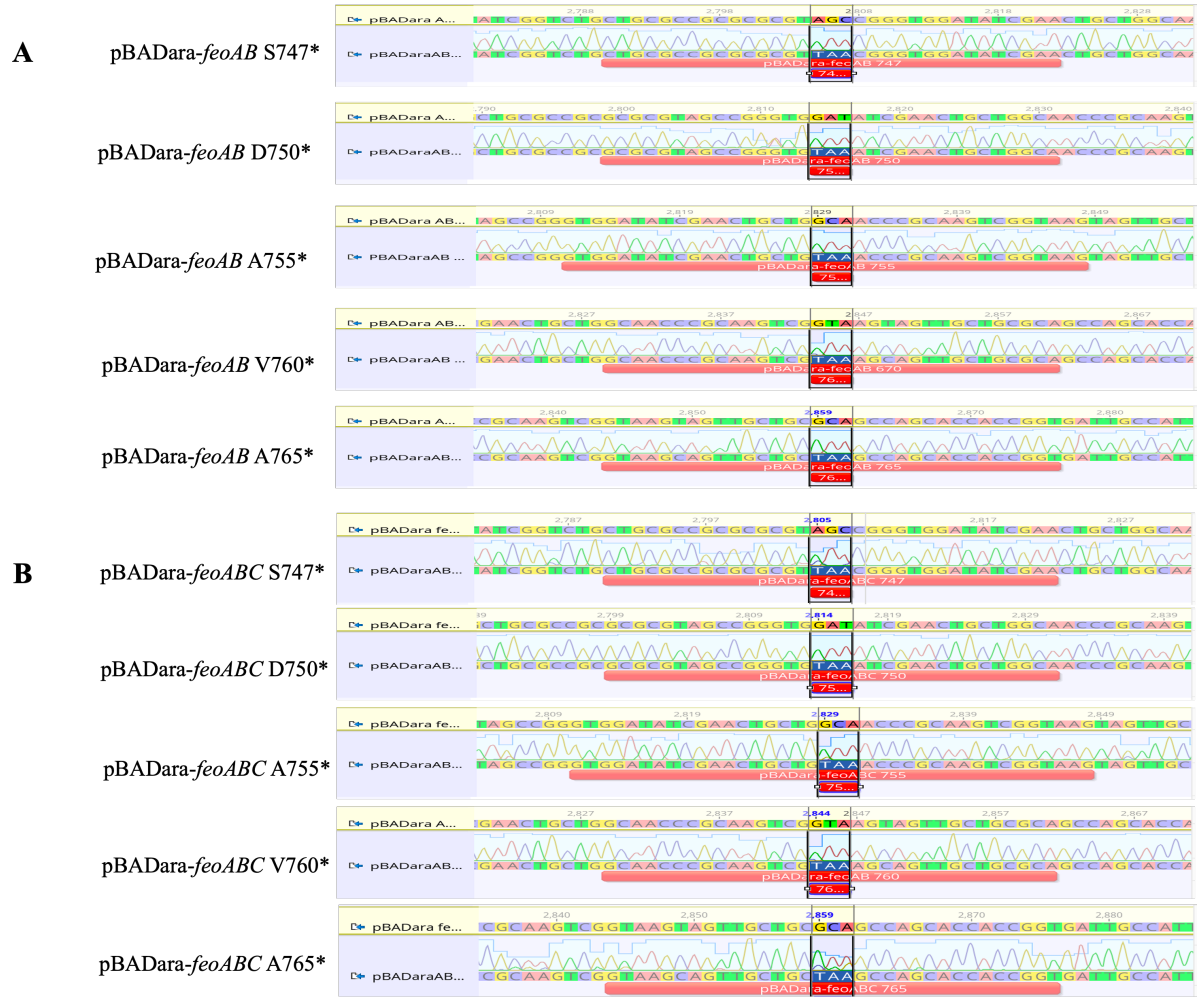

Figure 4.7: Summary of the Sanger sequencing results. The pBADara-*feoAB* **(A)** and pBADara-*feoABC* **(B)** sequencing data are shown with each mutated sequence aligned to the nonmutated sequence of the parent/template.

4.2.3 Phenotypic analysis of JC32 with pBADara-*feoAB* and pBADara-*feoABC* carrying the CFeoB mutations: effect on iron-restricted growth with DTPA under aerobic conditions

Once the mutations had been confirmed in both plasmids, the mutated plasmids were introduced into *E. coli* JC32 by transformation to enable investigation of their impact on FeoC-dependent Feo iron-uptake capacity. The growth was performed under aerobic conditions in 96-well plates using a Stratus Cerillo plate reader in 200 µl of M9 medium with 0.4% glucose, without ferric citrate (Fig. 4.8). The results illustrate that under aerobic, low-iron conditions, the *feoAB* plasmid offered no advantage, and indeed resulted in a slightly weaker growth than that seen for the vector control (Fig. 4.8AC). The *feoAB* variants all caused weaker growth than

that seen for the *feoAB* plasmid or vector control; these reductions in growth were significant and were similar for all five variants (Fig. 4.8AC). Thus, the CFeoB truncations all resulted in lower growth. However, since the vector control outgrew all of the *feoAB* transformants, this suggests that the FeoAB system was not providing any benefit in countering lack of iron under the conditions tested. The reduced growth observed for the CFeoB truncation mutants thus likely reflect a negative impact of the corresponding plasmids on growth.

For the *feoABC* transformants, a similar effect was observed (Fig. 4.8BD). The vector control outperformed all of the *feoABC* transformants, again indicating that the Feo system was not providing any advantage under the conditions tested (Fig. 4.8B). The non-mutated *feoABC* plasmid showed a greater growth (which was significant in two cases) than the CFeoB truncation strains, which again suggests that the truncations had a negative impact on growth (unlikely to be iron related). The five *feoABC* CFeoB mutant strains grew similarly to each other, except for the D750Δ strain which showed growth similar to that of the non-mutated *feoABC* strain and significantly superior to that of two of the other four CFeoB truncation strains (Fig. 4.8D).

In summary, since the Feo system provided no advantage, it was not possible to determine whether the CFeoB truncations had any impact on iron-restricted growth.

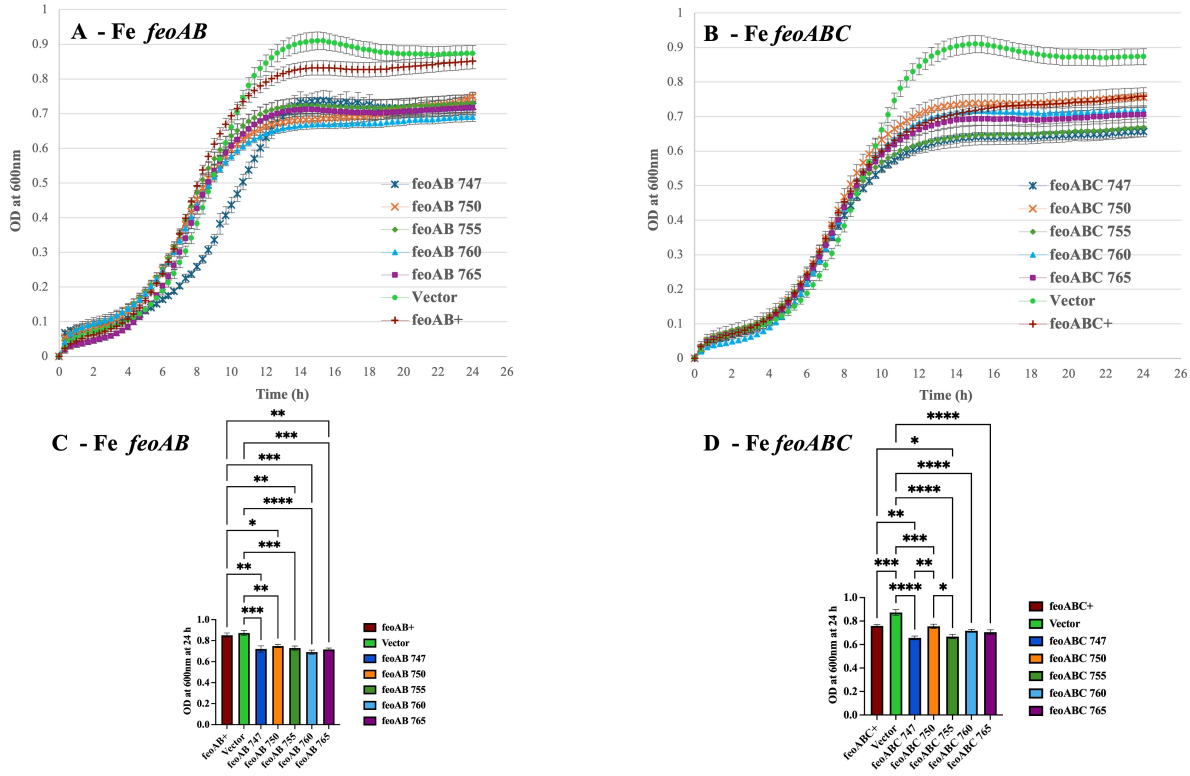

Figure 4.8: Effect of CFeoB truncations on *feoAB*- and *feoABC*-dependent iron-restricted growth in JC32 under aerobic conditions. JC32 transformants carrying pBADara-*feoAB* and pBADara-*feoABC* with/without CFeoB truncations, or carrying the pBADara as vector control, were grown overnight in 5 ml of M9 medium with 0.4% glucose containing 100 µg/ml ampicillin and 20 µM of ferric citrate in test tubes on a shaker at 37 °C and 250 rpm. The following day, the overnight was harvested by centrifugation (an Eppendorf Centrifuge 5804 R) at 4 °C and 5000 rpm and then the pellets were washed twice with fresh M9 to remove any residue of iron. The washed overnight cultures where then used to inoculate fresh M9 minimal medium with 0.4% glucose, antibiotic and 0.2% arabinose, without ferric citrate, under aerobic condition in a 96-well plate. See Methods 2.10 for further details. (**A**) and (**B**) show growth curves for *feoAB* and *feoABC* transformants, respectively. (**C**) and (**D**) summarise growth achieved at 24 h; data derived from (A) and (B), respectively. P-value were calculated by one-way ANOVA and generated by GraphPad Prism (*, P <0.05; **, P <0.01; ***, P <0.001; ****, P <0.0001).

In Chapter 3, a clearer aerobic, iron-restricted growth advantage for the *feoABC* strain was obtained when DTPA was included (Fig. 3.12B). Therefore, growth comparisons were repeated as in Fig. 4.8, but with the addition of 1 µM DTPA (Fig. 4.9). The results show that *feoAB* strains largely grew similarly to the vector control, with no significant differences in

most cases (Fig. 4.9AC). However, the V760Δ mutant showed a greater growth than all the other strains, and in three cases (including the vector control), this was significant (Fig. 4.9C). Furthermore, the S747Δ mutant displayed weaker growth than all the other strains (including the vector control) which was significant in all cases. Indeed, this strain also exhibited slower growth than any other strain in the absence of DTPA (Fig. 4.8A). This result suggests that the complete loss of the CFeoB region negatively impacts Feo function in a manner that impairs growth (in the absence of FeoC). However, although the non-mutated *feoAB* stain outgrew the vector control, this effect was not significant and thus the FeoAB system was not shown to offer an advantage under the aerobic iron-restriction conditions employed in this experiment. This was not the case for the V760Δ mutant, which showed a clear growth advantage. The reason for this effect is unclear.

For the *feoABC* transformants (Fig. 4.9B), the non-mutated *feoABC* strain exhibited a major growth advantage with respect to both the vector control (2.1-fold at 24 h; $P < 0.0001$; Fig. 4.9D) and the non-mutated *feoAB* strain (1.81-fold at 24 h; $P < 0.0001$; Fig. 4.9C). This result indicates that the growth conditions were suitable for displaying the aerobic, iron-restricted growth advantage offered by the Feo system when FeoC is included (as observed in Chapter 3, Fig. 3.12B). All five CFeoB-truncation *feoABC* strains showed a significantly reduced growth advantage with respect to the non-mutated *feoABC* strain. This indicates that the CFeoB region supports Feo-enhanced growth, in the presence of FeoC, under the aerobic, iron-restricted conditions (1 μM DTPA) employed (Fig. 4.9). This result thus supports the hypothesis that FeoC interacts with CFeoB in order to enhance Feo-dependent growth aerobically. The growth curve (Fig. 4.9B) shows that the A765Δ mutation had the lowest impact on FeoABC-dependent aerobic iron-restricted growth (17.5% lower at 24 h cf. the non-mutated *feoABC* strain) with respect to that of the other four CFeoB mutant strains (30-52.5% lower). This is presumably because the A765 mutation generates the smallest CFeoB truncation (loss of the last nine

residues). The greatest impact on growth (52.5% reduction) was caused by the A755Δ mutation, resulting in growth similar to that of the vector control. This suggests that the growth advantage provided by FeoC under the conditions employed was entirely eliminated by the A755Δ mutation. This is surprising since this mutation results in loss of 19 amino acids, whereas S747Δ and D750Δ cause larger deletions (24 and 27 residues) and so might be expected to result in similar (or greater) degrees of growth reduction. Nevertheless, the data clearly indicate that the CFeoB region is required for optimal FeoC enhanced growth under aerobic, iron restriction. Thus the data support the notion that the ability of FeoC to promoter FeoAB iron uptake activity aerobically is, at least partly, mediated via CFeoB.

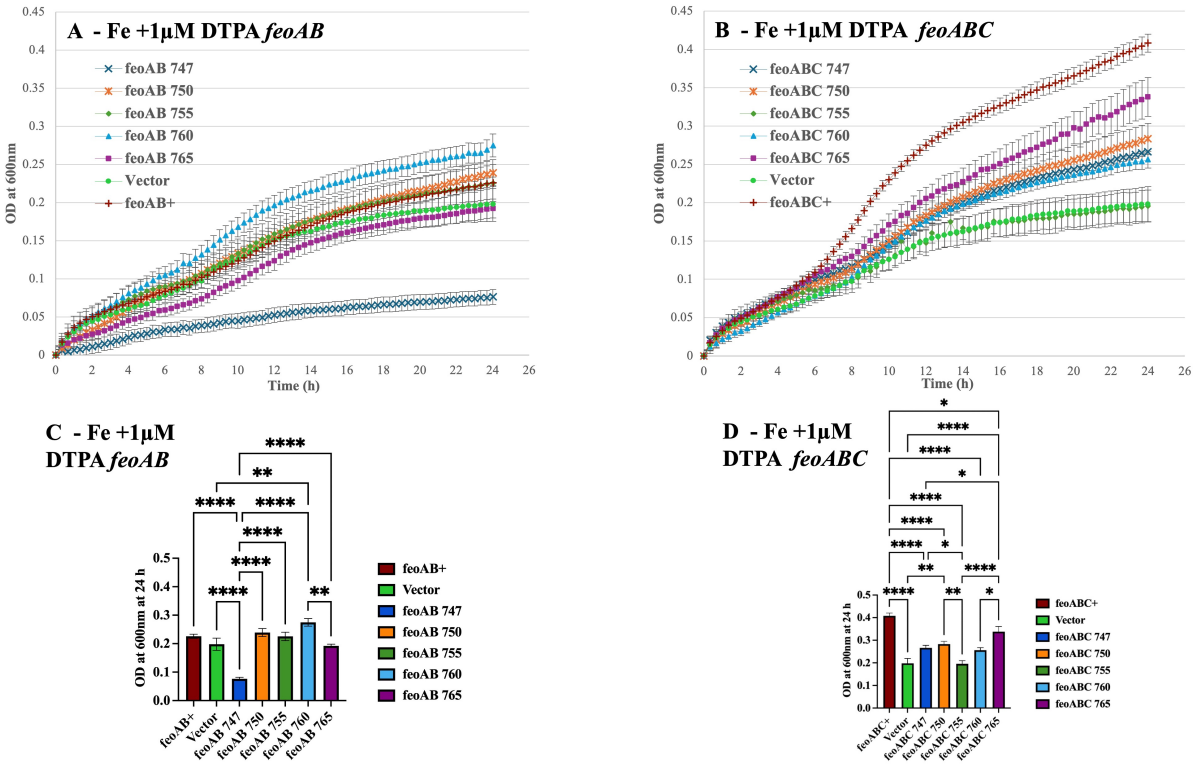

Figure 4.9: Effect of CFeoB truncations on *feoAB*- and *feoABC*-dependent DTPA-enhanced, iron-restricted growth in JC32 under aerobic conditions. Details are as for Fig. 4.8, except for the inclusion of 1 µM DTPA for the growth comparison. (**C** & **D**) ODs at 24 h are presented from (**A**) and (**B**), respectively. P-value were calculated by one-way ANOVA and generated by GraphPad Prism (*, P <0.05; **, P <0.01; ****, P <0.0001).

4.2.4 Phenotypic analysis of JC32 with pBADara-*feoAB* and pBADara-*feoABC* carrying the CFeoB mutations: effect on iron-restricted growth under aerobic, and buffered conditions

A major *feoC*-dependent growth difference under aerobic, iron-restricted conditions was also observed in the previous chapter when reductant and pH control were applied (Fig. 3.15AB and Fig. 3.16AB). Therefore, the growth experiment above was repeated in 0.4% glucose M9 medium with 100 mM MES (pH 6). The results showed (Fig. 4.10A) a significant growth advantage for the unmutated *feoAB* strain with respect to the vector control indicating that FeoAB supports aerobic iron-restricted growth at pH 6. The five *feoAB* CFeoB mutants displayed significantly weaker growth than the unmutated *feoAB* strain, indicating that (in the absence of FeoC) the CFeoB truncations have a negative impact of FeoAB function. Furthermore, although four of the five CFeoB mutants outgrew the vector control in the early stages of growth, all five CFeoB mutants displayed a weaker final growth density (significant in three cases). This matches the data above (Fig. 4.8A) indicating that the CFeoB mutations results in deleterious growth effects. In addition, the *feoAB* S747Δ strain again showed much weaker growth than that of the other four CFeoB mutants (Fig. 4.10AC), confirming the findings above (Fig. 4.9A) suggesting that complete truncation of CFeoB (in absence of FeoC) causes a major growth defect due to FeoAB toxicity effects.

In the case of the *feoABC* strains (Fig. 4.10B), all five CFeoB mutants grew similarly to the unmutated *feoABC* strain (Fig. 4.10D). However, the vector control showed a delay in growth, but achieved a higher final growth density than the other strains. Thus, no clear growth advantage was apparent for the *feoABC* strains under the growth conditions employed suggesting that FeoABC was not supporting iron restricted growth. The lack of a significant growth difference between the unmutated *feoABC* strain and the CFeoB mutants further supports this view.

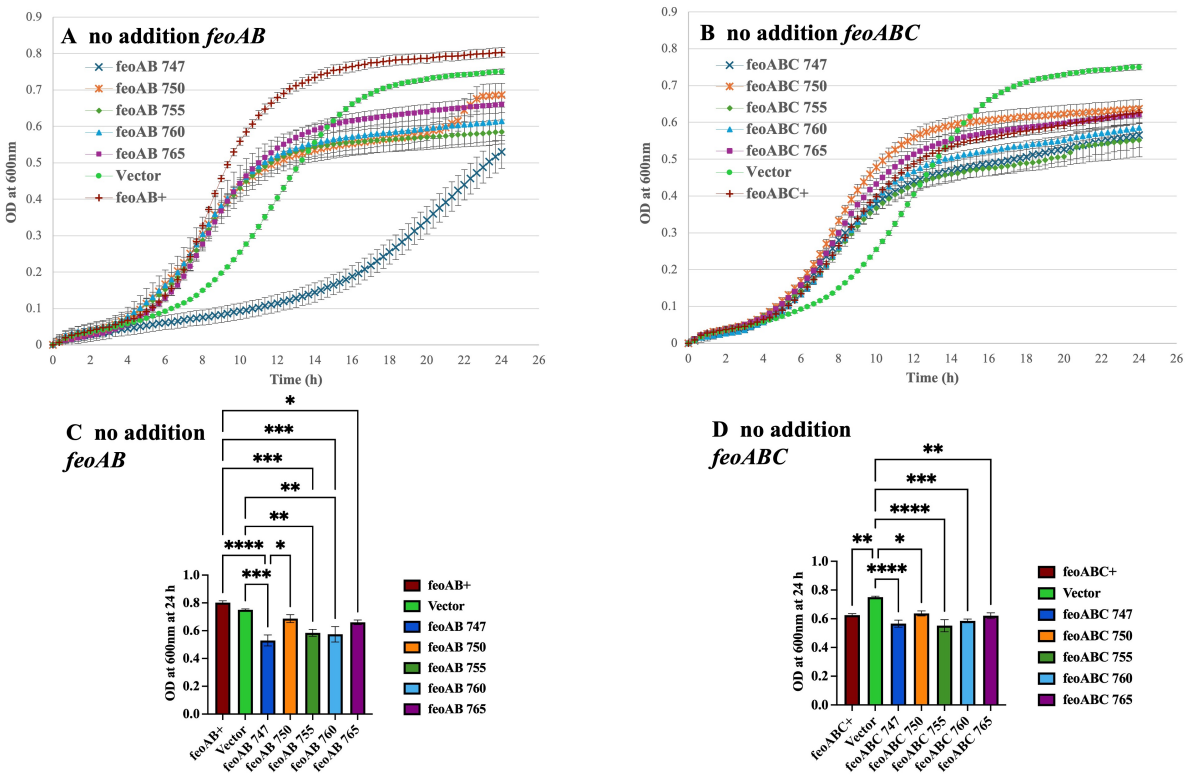

Figure 4.10: Effect of CFeoB truncations on *feoAB*- and *feoABC*-dependent iron-restricted growth in JC32 under aerobic conditions with <u>100 mM MES (pH 6)</u>. Details are as for Fig. 4.8, except for the inclusion of 100 mM MES (pH 6).

In an attempt to provide a *feoC*-dependent growth difference, the above experiment was repeated with 1 µM DTPA (as in Fig. 3.15B) since this was previously effective under buffer-free conditions (Fig. 4.9B). Thus, all strains were grown as above (Fig. 4.10) but with the inclusion of 1 µM DTPA. The results show that the unmutated *feoAB* outgrew the vector control, although the difference was not significant (Fig. 4.11AC). Four of the five CfeoB's mutants showed lower growth than the unmutated *feoAB* strain, although the differences were not significant (Fig 4.11AC). The S747Δ strain again showed the weakest growth, confirming the previous observations (Fig. 4.9A).

For the *feoABC* strains (Fig 4.11BD), the unmutated *feoABC* strain showed a significantly 170% greater growth than the vector and a 68.7% better growth than the unmutated *feoAB* strain. This indicates that inclusion of *feoC* improved the Feo-dependent increase in aerobic iron restricted growth at pH 6 with DTPA. All five of the CFeoB's mutants showed weaker

growth than the unmutated *feoABC* strain (Fig. 4.11BD), but this was only significant in one case (A755Δ) where growth was similar to that of the vector control. Thus, although truncation of the CFeoB region diminished FeoABC-enhanced growth, the effect was largely insignificant.

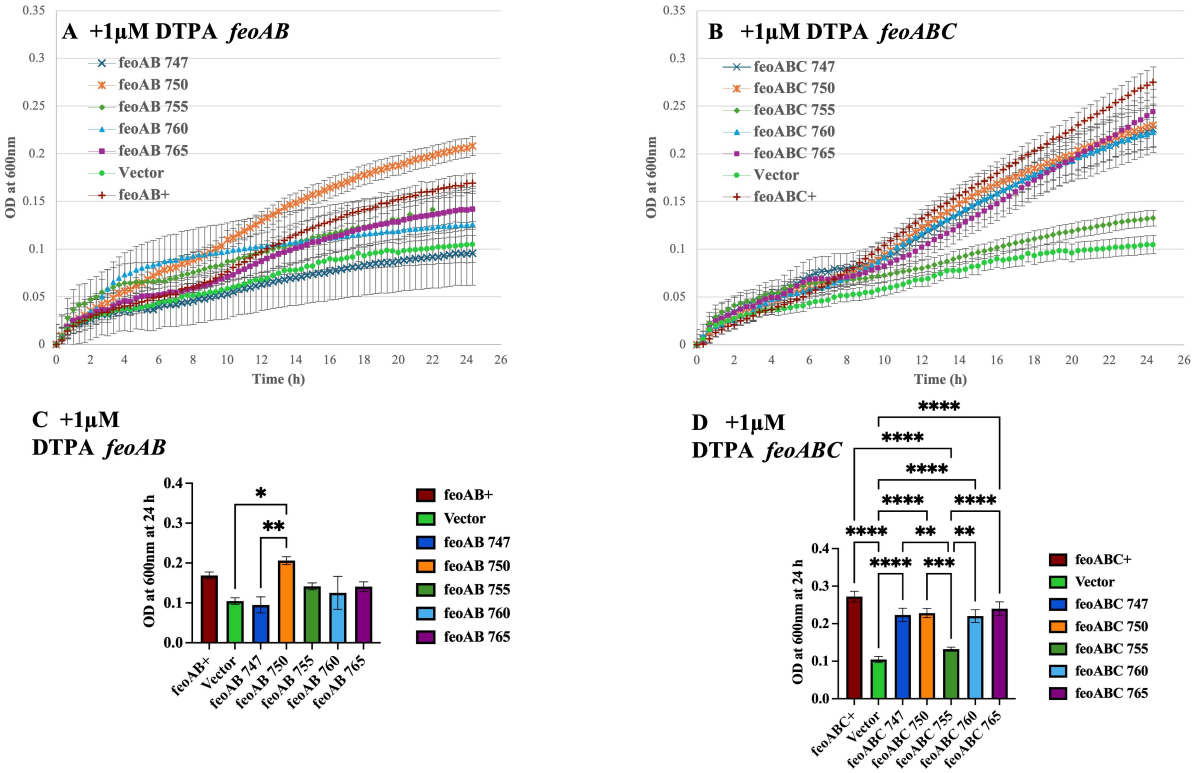

Figure 4.11: Effect of CFeoB truncations on *feoAB*- and *feoABC*-dependent iron-restricted growth in JC32 under aerobic conditions with 100 mM MES (pH 6) and 1 μM DTPA. Details are as for Fig. 4.10, except for the inclusion of 1 μM DTPA for the growth comparison.

In summary, the above results indicate that truncation of the CFeoB region has a negative impact on Feo-meditated growth (as a proxy for Feo-mediated iron uptake) under aerobic conditions with DTPA (Fig. 4.11). However, such effects vary between the five truncation mutants and are observed both in the presence and absence of FeoC. However, a significant reductions as a result of CFeoB truncations was only obtained in the FeoABC strain in the case of the Δ755 truncation, not for the FeoAB strain. Thus, the evidence suggests that the CFeoB

truncations result in impaired FeoAB function aerobically, but the evidence is not sufficient to show that this linked to the presence of FeoC.

4.3 Effect of CFeoB expression on FeoC-dependent growth enhancement under aerobic iron-restriction conditions

4.3.1 Introduction

The possibility that the CFeoB region of FeoB is involved in FeoC-mediated enhancement of Feo iron-uptake activity under aerobiosis was further explored by determining the effect of CFeoB overexpression. The prediction was that excess CFeoB would titrate FeoC and thus inhibit its positive impact on aerobic low-iron growth. The AlphFold-predicted structure of FeoB (Fig. 4.1) was used to define the CFeoB region (as above). The corresponding coding sequence was then utilised to design synthetic CFeoB-encoding DNA for introduction into a compatible inducible plasmid, as described below.

4.3.2 Design for expression the C-terminal region of *feoB* (*CfeoB*)

The CFeoB-encoding region (*CfeoB*) was synthesized by GeneArt in three formats:

1. with an 8-codon Flag-tag sequence (DYKDDDDK) at the N-terminus;

2. with an 8-codon Flag-tag sequence at the C-terminus; and

3. without any Flag-tag.

All the three synthetic *CfeoB* sequences included flanking regions to enable Gibson cloning into the multiple-cloning site of the inducible plasmid pBADrha (compatible with pBADara) in order to allow the expression of *CfeoB* from the rhamnose-inducible promotor. In addition, a start codon was placed at the beginning of each *CfeoB* gene with two consecutive stop codons at the end. In addition, *Nde*I and *Hin*dIII sites were placed at the up and down-stream flanking regions respectively (Methods 2.18.1). The synthetic constructs were received from GeneArt within the pMA-T vector (Amp^R) and were designed: pMA:Flag-*CfeoB*; pMA:*CfeoB*-Flag; and pMA:*CfeoB* (Appendix Figs. A.1-A.6). Each plasmid was used to transform TOP10 to enable isolation of plasmid DNA as source of DNA for cloning purposes. The pBADrha plasmid was

digested with *Nde*I and *Hin*dIII (Fig. 4.12A) (Methods 2.13), and the linearised plasmid was then purified from an agarose gel (Fig. 4.12B) (Methods 2.18.2). The pBADrha (6.1 kb) uncut DNA had a mobility similar to that of the 4 kb marker because the plasmid was in supercoiled form. Digested pBADrha gave a band of ~6.1 kb, as expected for the for the linearised plasmid. Thus, the expected size was observed.

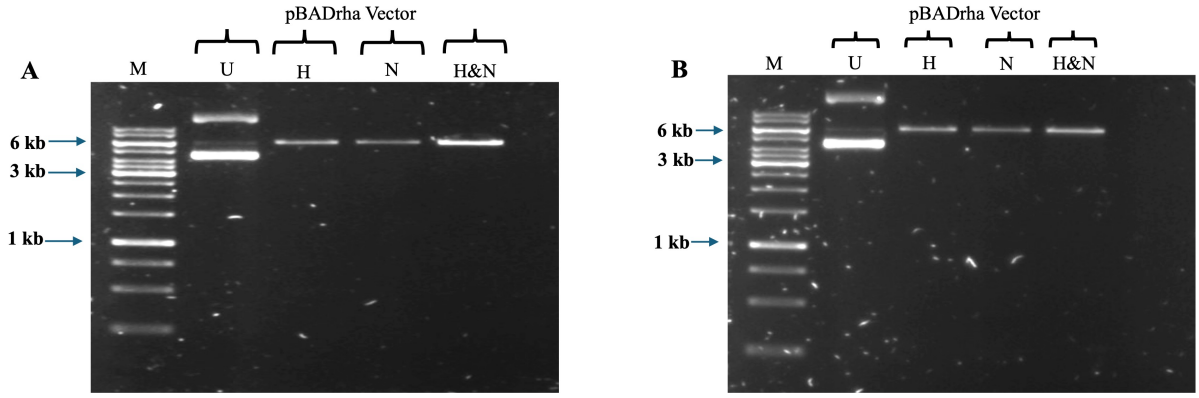

Figure 4.12: Agarose gel electrophoretic analysis of pBADrha plasmid DNA digestion and isolation. (**A**) Digestion of pBADrha. M, GeneRule 1 kb ladder (Fig. 2.1); U, undigested DNA; H, *Hin*dIII digested; N, *Nde*I digested; and H&N, *Hin*dIII and *Nde*I digested. (**B**) Purified, *Hin*dIII and *Nde*I digested pBADrha.

When the three synthetic constructs were received from GeneArt, 1 µl of each construct sample was introduced into TOP10 for triplicate plasmid DNA extraction (Methods 2.2, 2.3 and 2.11) and then the DNA was analysed by agarose gel electrophoresis (Methods 2.12) (Fig. 4.13).

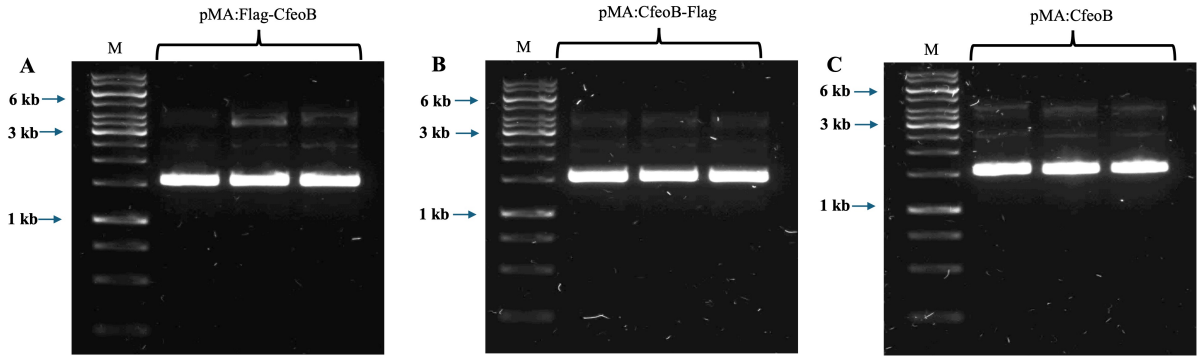

Figure 4.13: Agarose gel electrophoretic analysis of uncut plasmids for pMA:Flag-*CfeoB* (A), pMA:*CfeoB*-Flag (B) and pMA:*CfeoB* (C). M, GeneRule 1 kb ladder (Fig. 2.1).

Fig. 4.13 shows that the uncut pMA plasmids (~2.5 kb) had a mobility similar to that of the 1.5 kb marker because the plasmids were in supercoiled form. However, the single and double digested plasmids gave bands of 2.5 kb, which is as expected for the linearised plasmid (Fig. 4.17). One isolate for each plasmid was subject to restriction fragment analysis (Fig. 4.14) and the expected restriction pattern was observed in each case.

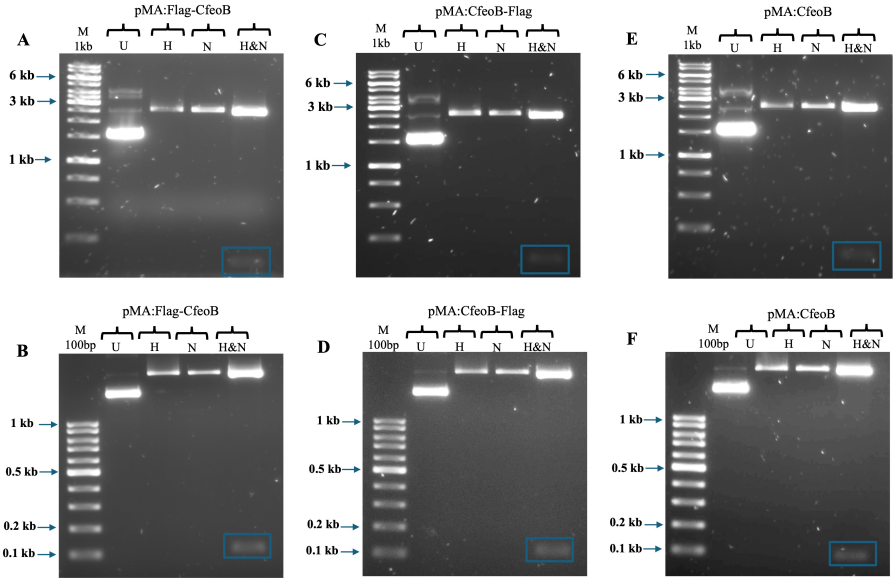

Figure 4.14: Agarose gel electrophoretic analysis of pMA:Flag-*CfeoB* (A & B), pMA:*CfeoB*-Flag (C & D) and pMA:*CfeoB* (E & F) with and without digestion. M, GeneRule 1 kb ladder for (**A**, **C** and **E**) and M, GeneRule 100bp ladder for (**B**, **D** and **F**) (Fig. 2.1). U, undigested; H, *Hin*dIII; N, *Nde*I; and H&N, *Hin*dIII and *Nde*I digested. The blue boxes indicate the CFeoB inserts (164, A-B; 164, C-D; or 140 bp, E-F).

The *CfeoB* target genes (insert DNA) were then prepared for cloning by digestion with *Nde*I and *Hin*dIII (Fig. 4.14). Ligation was then achieved with T4 DNA ligase by applying the manufacturer's (ThermoFisher) protocol for sticky-end ligation. The reaction mixture thus included the linearised vector (20-100 ng of DNA) and the insert DNA at 1:1, 3:1, 5:1 molar ratios (insert:vector) (Methods 2.18.3).

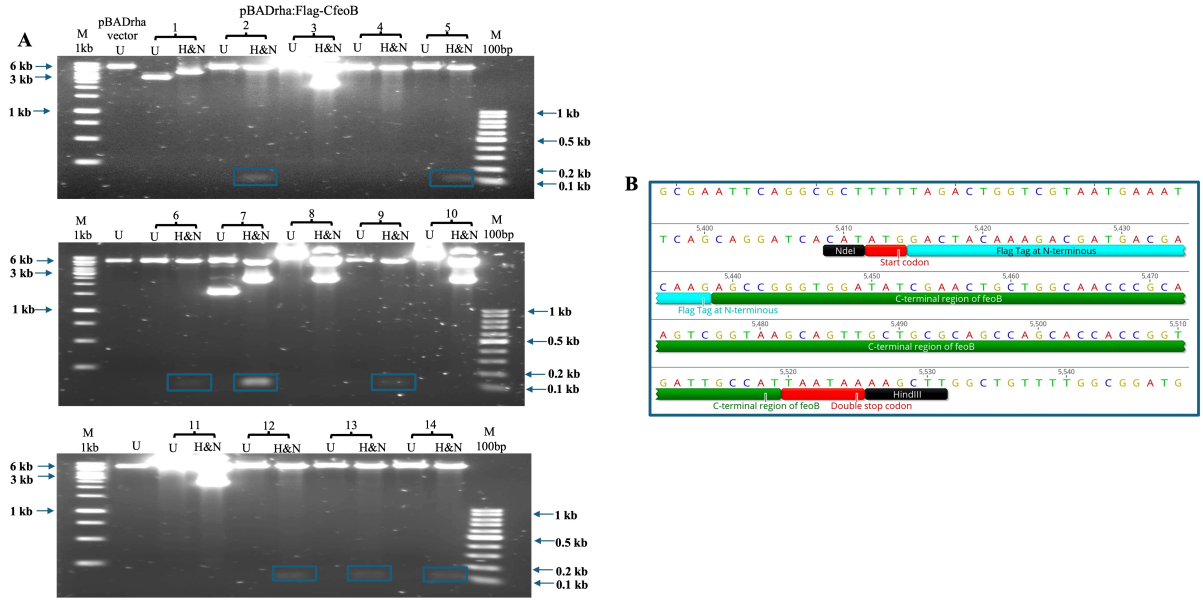

Figure 4.15: Agarose gel electrophoretic analysis of pBADrha:Flag-*CfeoB* and NGS analysis. (**A**) Gel electrophoresis. M, GeneRule 1 kb ladder (left); M, GeneRule 100bp ladder (right) (Fig. 2.1). U, undigested; H&N, *Hin*dIII and *Nde*I digested. A total of 14 isolates were analysed of which 8 had the anticipated restriction digestion pattern. (**B**) Confirmation of successful cloning by Nanopore 30 sequencing. Only the insert sequence is shown for just one of the two sequenced samples, with key regions highlighted (restrictions sites, black boxes; Flag-tag region, cyan; start and stop coding, red; CfeoB region, green).

Fig. 4.15A shows 14 samples of candidate pBADrha:Flag-*CfeoB* plasmid DNA that were extracted by GeneJET Plasmid Miniprep kit (Methods 2.11), double-digested with *Hin*dIII and *Nde*I (Method 2.13) and analysed by agarose gel electrophoresis (Methods 2.12). As shown in Fig. 4.15A, eight gave the expected digestion pattern: two bands of ~6.1 kb and 164 bp. Two of these were submitted to Source Biosciences for Nanopore 30 NGS which confirmed that the expected insert was present (Fig. 4.15B).

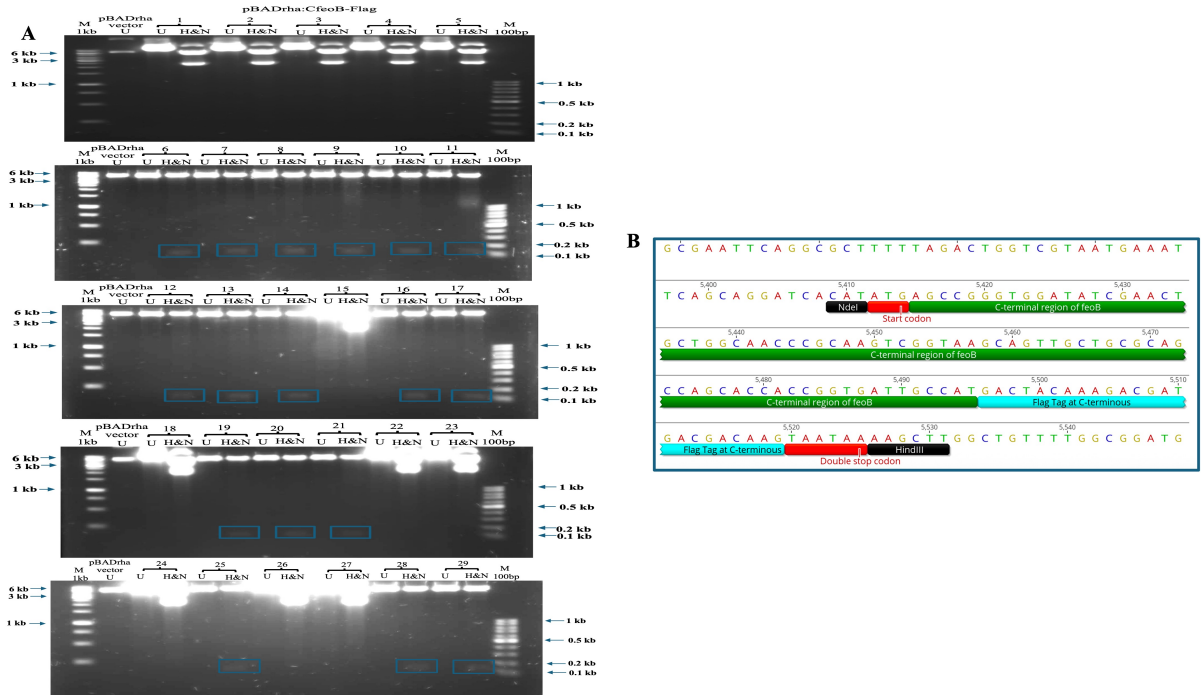

Figure 4.16: Agarose gel electrophoretic analysis of pBADrha:*CfeoB*-Flag and NGS analysis. Details are as above (Fig. 4.15) except that pBADrha:*CfeoB*-Flag was the construct analysed, and 29 isolates were explored.

Fig. 4.16A illustrates that of the 29 potential pBADrha:*CfeoB*-Flag isolates analysed (as above) 17 gave the expected fragmentation pattern (two bands of ~6.1 kb and 164 bp). Again, two of the 17 successful plasmid isolates were subjected to Nanopore 30 sequencing (Fig. 4.16B) which confirmed their identity.

Fig. 4.17A shows that of seven potential pBADrha:*CfeoB* isolates analysed, three had the anticipated restriction fragment pattern (~6.1 kb and 140 bp). Two were sequenced (as above) and were found to carry the expected nucleotide sequence (Fig. 4.17B). Thus, all three *CfeoB* constructs were successfully generated.

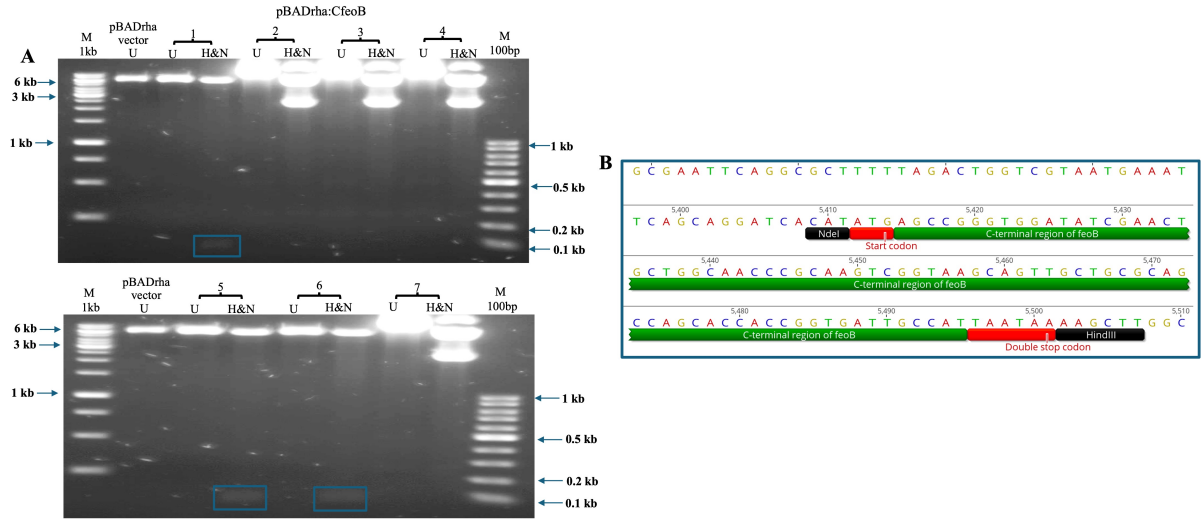

Figure 4.17: Agarose gel electrophoretic analysis of pBADrha:*CfeoB* and NGS analysis. Details are as above (Fig. 4.15) except that pBADrha:*CfeoB* was the construct analysed, and 7 isolates were explored.

4.3.3 Detecting the Flag-tagged protein constructs

In order to determine whether the CFeoB protein was produced in *E. coli* upon induction, an anti-Flag tag western blotting experiment was performed. Thus, pBADrha, pBADrha:Flag-*CfeoB*, pBADrha:*CfeoB*-Flag and pBADrha:*CfeoB* TOP10 transformants were grown aerobically and anaerobically in LB medium supplemented with 0.2% rhamnose as inducer and 50µM chloramphenicol for plasmid selection. In addition, a positive control was also included (pBADrha:*feoAB*-Flag-tag-transformants) which had previously given positive results for FeoB detection by anti-Flag-tag western blotting (Al-Aidy, 2020). The cultures were incubated at 37 °C with shaking (aerobic) or in syringes anaerobically until the bacterial cultures reached an of OD 0.5. The cultures were then harvested by centrifugation, and the cells were resuspended and lysed using 1X SDS digestion buffer followed heating at 100 °C for 10 min. Following a 5 min centrifugation, the samples were subjected to SDS-PAGE (Methods 2.19.1). Three types of acrylamide gels were used in attempt to resolve and detect the Flag-Tag constructs: 15% acrylamide freshly made in the lab; premade 4 to 20% acrylamide gradient gels in Tris-glycine; and 16% acrylamide in Tris-Tricine. The SDS-PAGE was used to separate proteins using a BioRad miniProtean III system. Duplicate gels were produced; one

was stained with Coomassie Brilliant Blue R-250 (Methods 2.19.2; Figs 4.18- 4.22) and the other was subjected to anti-Flag tag western blotting.

Following SDS-PAGE, the unstained gel was used to transfer the resolved proteins to a nitrocellulose membrane using a BioRad Transblot Turbo and then the nitrocellulose membrane was stained by Ponceau red to make sure all the proteins were transferred to the nitrocellulose before proceeding the western blotting steps. The stain was then removed by treatment with 0.1% NaOH for 5 min followed by three washes in qH_2O (Figs. 4.18-4.22). The blots were then immunostained with anti-Flag-tag primary antibody and HRP-conjugated goat anti-mouse IgG, as described in (Methods 2.19.3) (Fig. 4.22C). The anti-Flag tag western blotting gave the expected results for the positive control: ~73 kDa for FeoB-Flag which match the results obtained by Al-Aidy (2020). The lower bands could be degraded fragments from the above band. However, no positive staining could be detected for the CFeoB Flag-tag constructs. This might be because of the small molecular weight (~3.94 kDa) of CFeoB or due to instability.

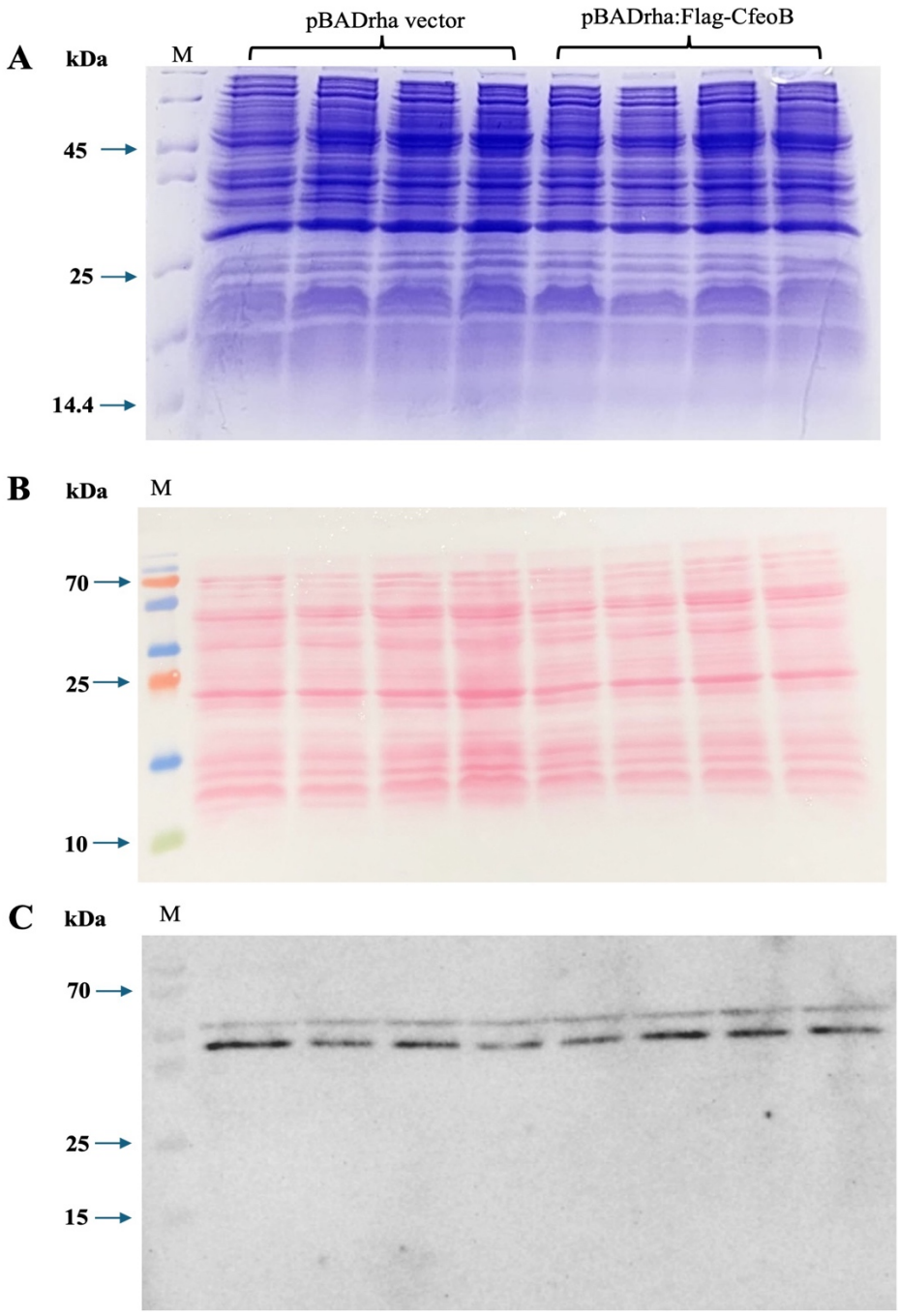

Figure 4.18: Flag-CFeoB detection by western blotting using 15% acrylamide gels. (**A**) SDS-PAGE analysis of pBADrha and pBADrha:Flag-*CfeoB* (Methods 2.19.2); M, Marker 14.4-116 kDa (ThermoFisher un-stained protein marker) (Fig. 2.2A). (**B**) Blot stained with Ponceau red; M, Marker 10-250 kDa (ThermoFisher pre-stained protein marker) (Fig. 2.2B). (**C**) Western blot analysis of pBADrha and pBADrha:Flag-*CfeoB* (Methods 2.19.3).

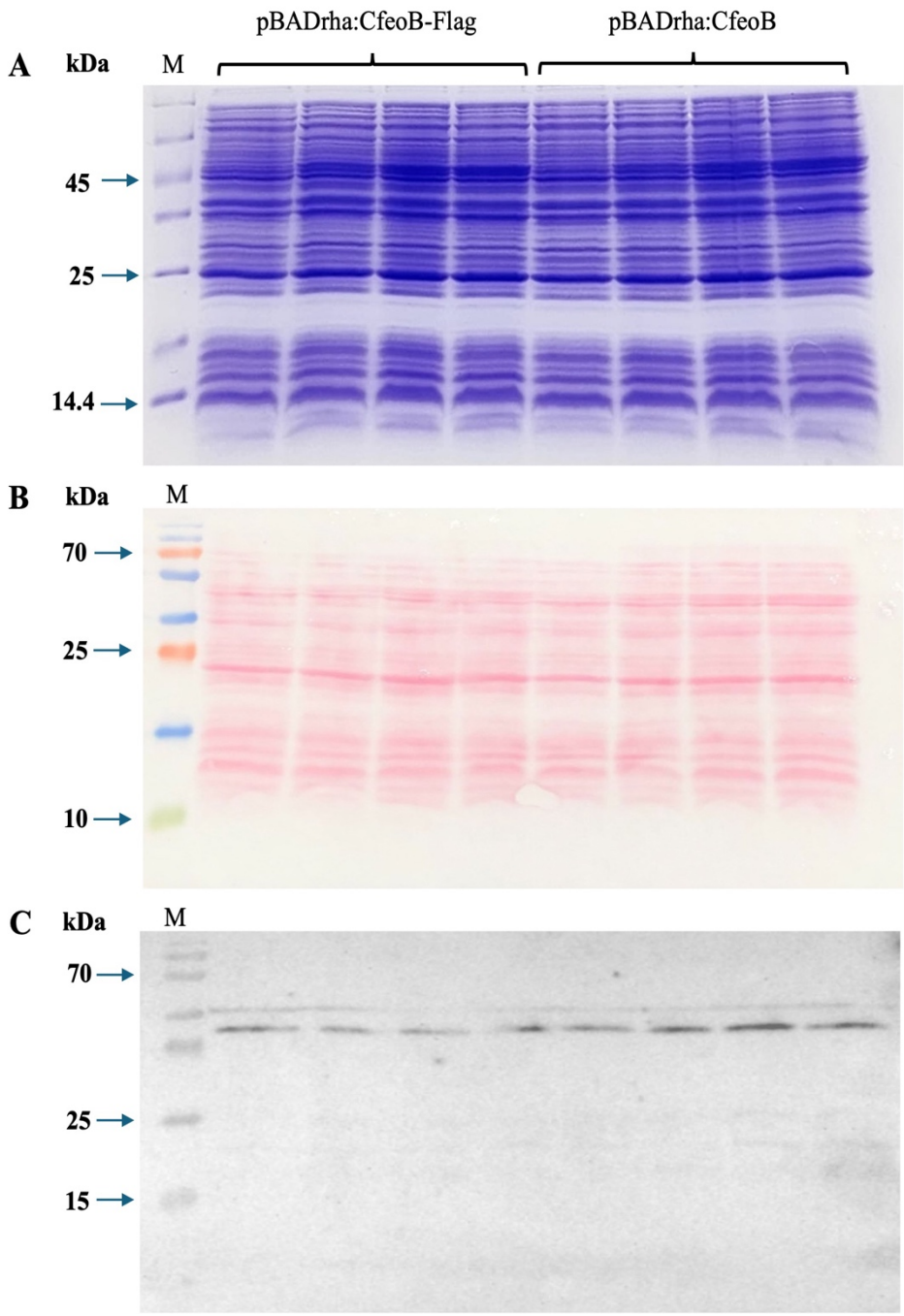

Figure 4.19: CFeoB-Flag detection by western blotting using 15% acrylamide gels. (**A**) SDS-PAGE analysis of pBADrha:*CfeoB*-Flag and pBADrha:*CfeoB*; M, Marker 14.4-116 kDa (ThermoFisher un-stained protein marker). (**B**) Blot stained with Ponceau red; M, Marker 10-250 kDa (ThermoFisher pre-stained protein marker). (**C**) Western blot analysis of pBADrha:*CfeoB*-Flag and pBADrha:*CfeoB*.

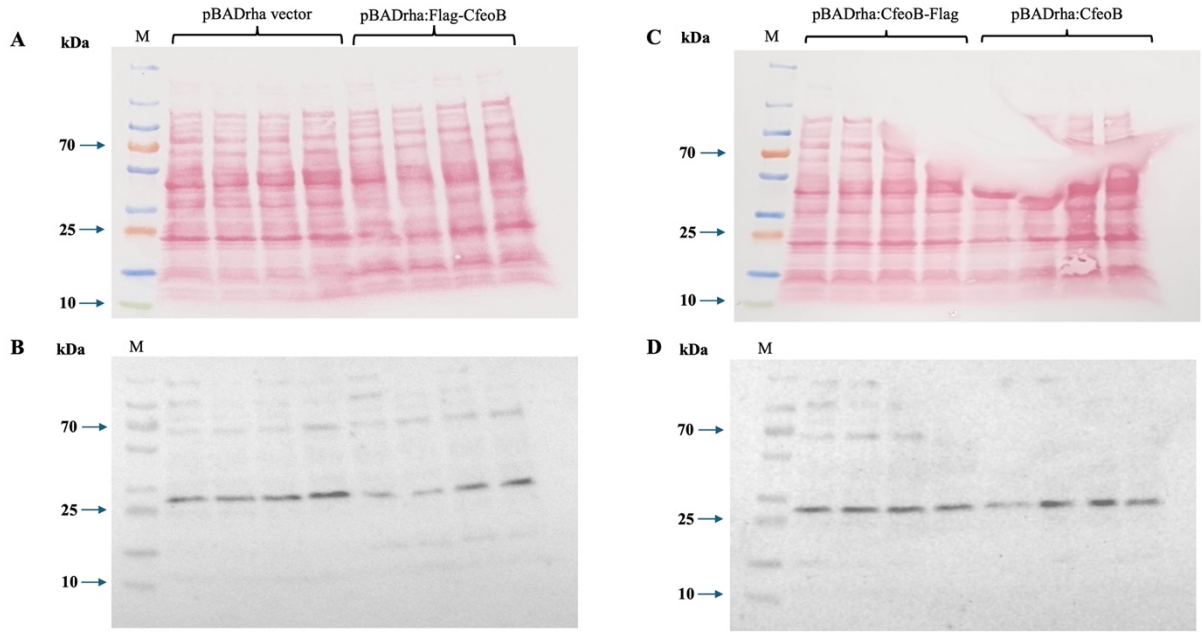

Figure 4.20: Western blot analysis of CFeoB using gradient (4 to 20%) Tris-glycine gels (BioRad). (**A&B**) Western blot analysis of pBADrha and pBADrha:Flag-*CfeoB*; M, Marker 10-250 kDa. (**C&D**) Western blot analysis of pBADrha:*CfeoB*-Flag and pBADrha:*CfeoB*; M, Marker 10-250 kDa. A and C are Ponceau red stained blots; B and D are the anti-Flag tag western blots.

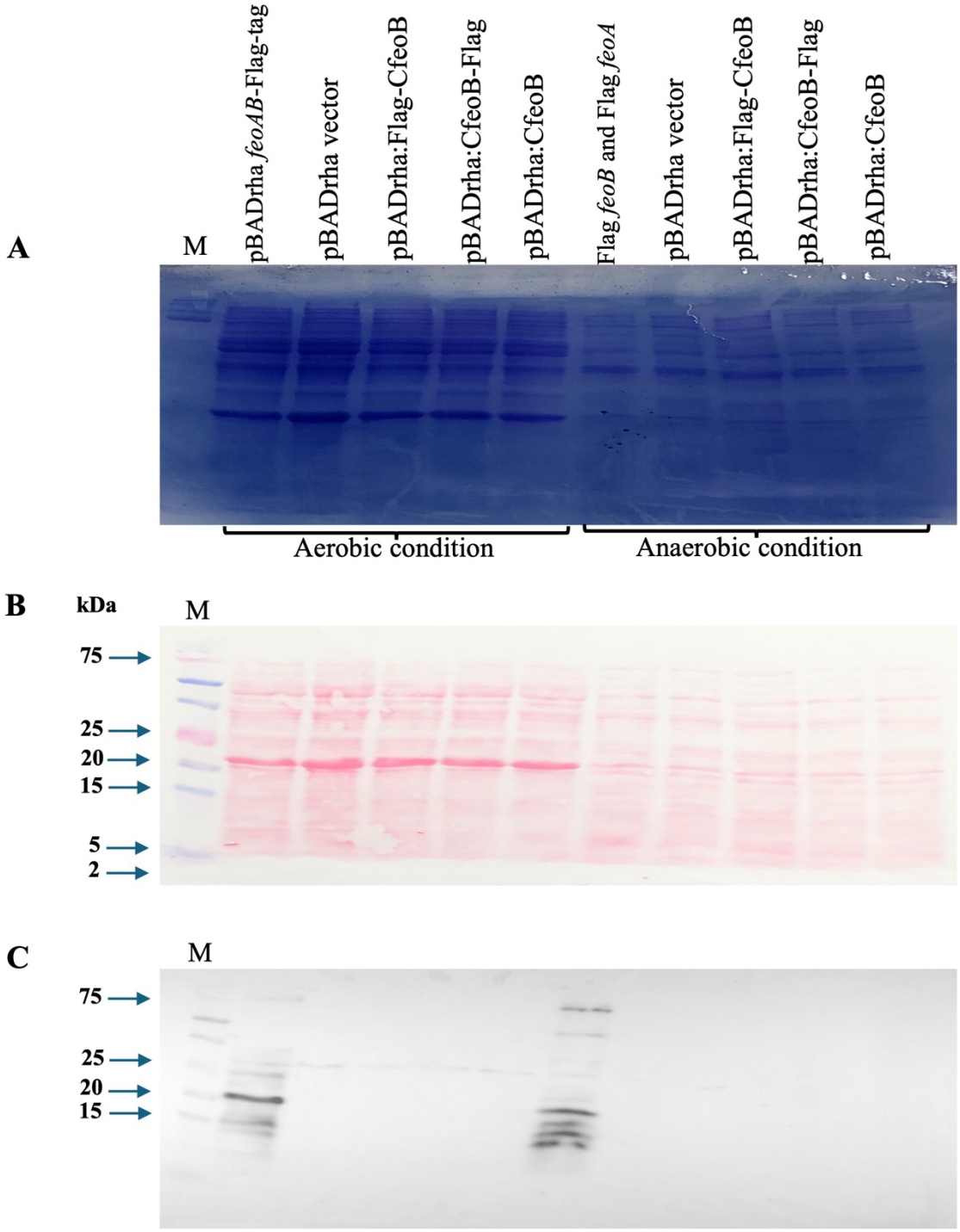

Figure 4.21: SDS-PAGE analysis of Flag-tag constructs with the pBADrha:*feoAB*-Flag-tag positive control using 16% acrylamide Tris-Tricine gels. (**A**) Coomassie strained gel. (**B**) Blot stained with Ponceau red. (**C**) Anit-Flag tag Western blot. M, Marker 14.4-116 kDa. M, Marker 2-250 kDa (BioRad precision plus protein™ dual xtra pre-stained protein standards) (Fig. 2.2C); TOP10 transformants carrying pBADrha:*feoAB*-Flag-tag, pBADrha, pBADrha:Flag-*CfeoB*, pBADrha:*CfeoB*-Flag and pBADrha:*CfeoB* grown aerobically and anaerobically.

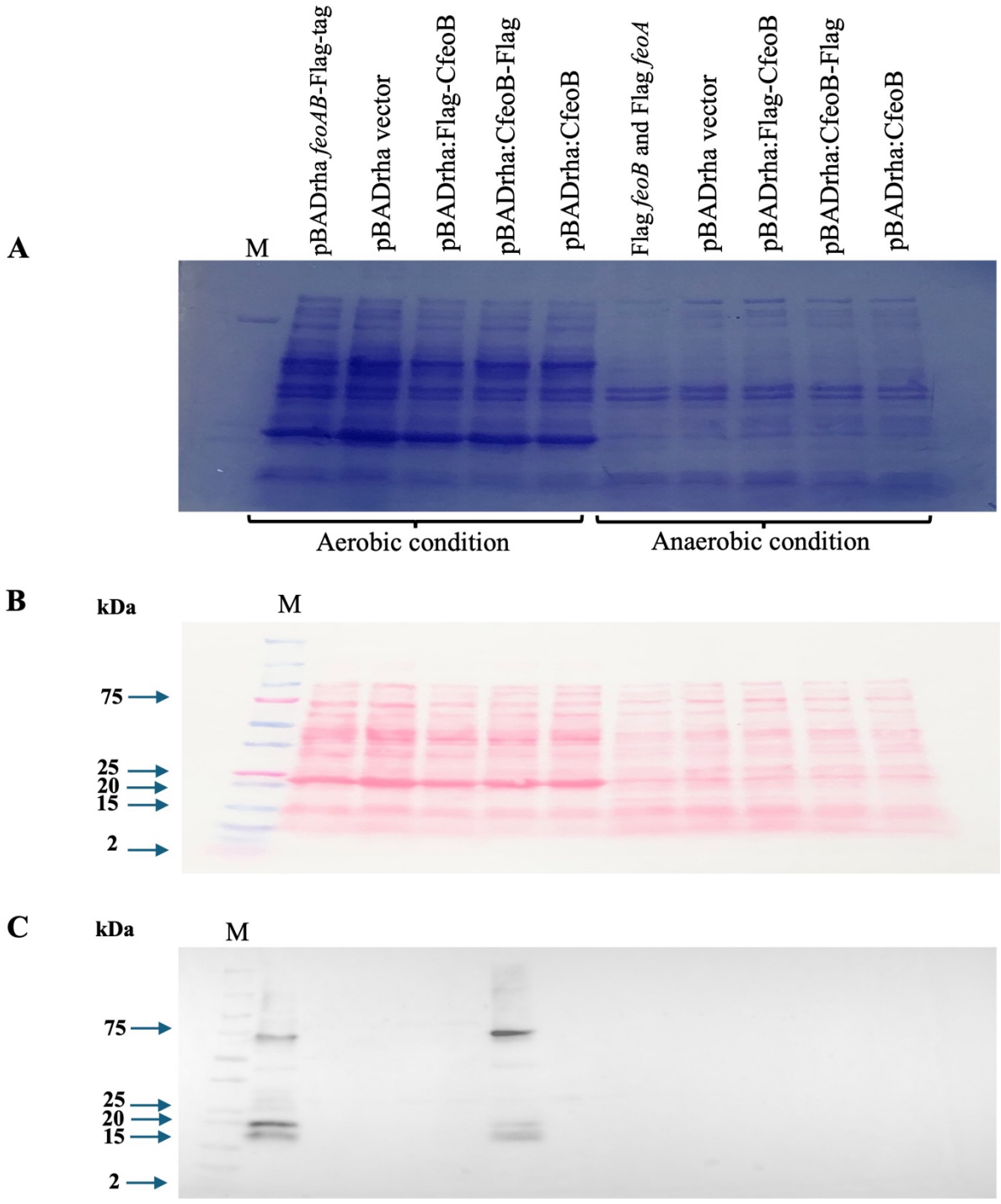

Figure 4.22: SDS-PAGE analysis of Flag-tag constructs with the pBADrha:*feoAB*-Flag-tag positive control using 4-20% gradient Tris-glycine gels. Details are as above except for the use of a gradient acrylamide gel in place of the 16% acrylamide gel in Fig. 4.21.

4.3.4 Phenotypic analysis of JC32 with pBADara-*feoAB* and pBADara-*feoABC* carrying the pBADrha:CfeoB constructs: effect on iron-restricted aerobic growth under buffered conditions

Despite the failure to detect CFeoB expression by western blotting, the *CfeoB* constructs were utilised in an attempt to inhibit FeoC-stimulated FeoAB iron uptake (enhanced growth under iron restriction). Thus, it was necessary to transfer the plasmids (pBADrha, pBADrha:Flag-*CfeoB*, pBADrha:*CfeoB*-Flag and pBADrha:*CfeoB*) into the pBADara-*feoAB* and pBADara-*feoABC* (Methods 2.2) JC32 transformants. Once achieved, growth was performed under aerobic conditions in 96-well plates using a Stratus Cerillo plate reader in 200 µl of M9 medium with 0.4% glucose without ferric citrate (Fig. 4.23).

The results show that, when the iron was absent (Fig. 4.23A) the pBADara-*feoABC*/pBADrha transformant gave greater growth compared to the pBADara-*feoABC*/pBADrha:*CfeoB* and *feoABC*/pBADrha:Flag-*CfeoB* transformants (a significant ~21-28% better growth at 24 h; Fig. 4.23D). This is consistent with a CFeoB inhibition of FeoC-enhancement of FeoAB-mediated iron uptake. However, there was no notable difference seen for the CFeoB-Flag containing strain with respect to the vector control. In addition, comparison of the growths for the FeoABC and FeoAB strains shows that there was a weaker (~22%) aerobic, iron-restricted growth for the FeoABC strains cf. the FeoAB strains (Fig. 4.23DE). This indicates that, under the conditions utilised, FeoC had offered no growth advantage for the FeoABC strains, and had indeed resulted in inhibited growth. Thus, the experiment did not allow any potential impact of CFeoB on FeoABC dependent iron-restricted growth to be determined. Furthermore, the pBADara vector controls gave better growth than either the FeoABC or FeoAB strains (by 73 and 35%, respectively), which indicates that iron restriction was not sufficient to allow opportunity for Feo-enhanced growth.

When considering the impact of the CFeoB constructs, the effects on growth were variable. For the FeoABC strain, in two cases the CFeoB constructs caused significant growth reduction,

and in one case a significant (but weak) growth increase (Fig. 4.23D). For the FeoAB strain, no effect or very modest effects were seen in two cases, but the Flag-CFeoB construct resulted in a clear and significant 15% increase in growth (Fig. 4.23E). A similar effect was observed in the vector control (pBADara), although the CFeoB construct resulted in a slight (but significant) reduced growth (Fig. 4.23F).

In summary, the lack of a Feo-dependent growth increase results in inability to determine any impact of the CFeoB constructs on FeoABC-dependent growth. Thus, growth conditions were revised in order to enable the display of a FeoC enhancement in FeoAB dependent iron-restricted growth.

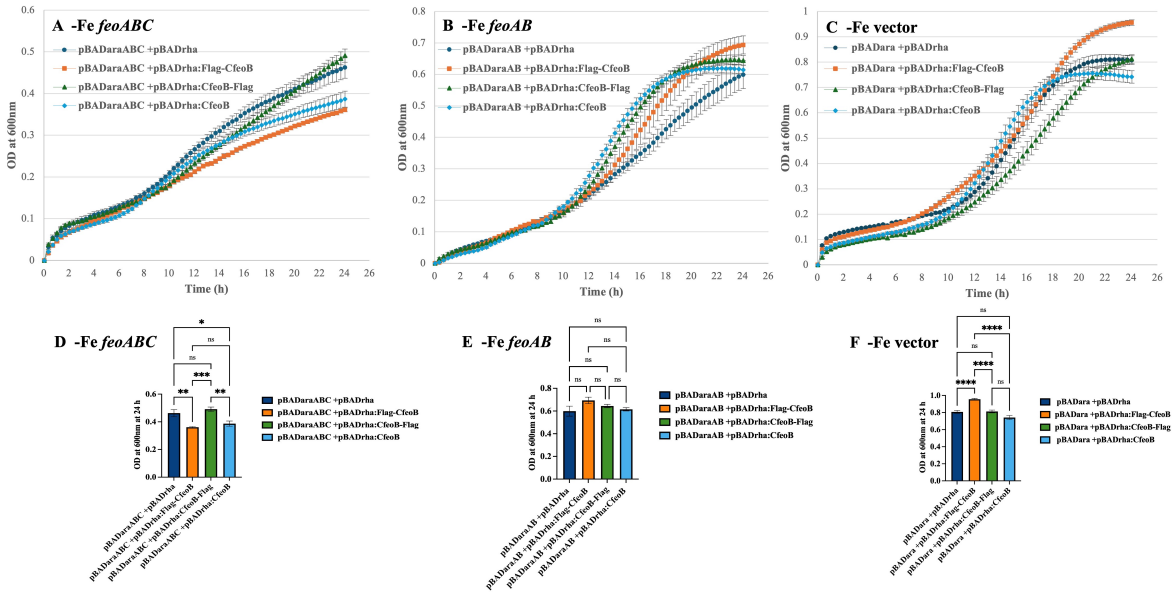

Figure 4.23: Effect of CFeoB expression on *feoAB* and *feoABC* aerobic growth under low-iron. JC32 transformants carrying pBADara-*feoABC* (**A**), pBADara-*feoAB* (**B**) or pBADara (**C**), with either pBADrha, pBADrha:Flag-CfeoB, pBADrha:CfeoB-Flag or pBADrha:CfeoB, were grown overnight in 5 ml of M9 medium with 0.4% glucose containing 100 µg/ml ampicillin, 50 µg/ml chloramphenicol and 20 µM of ferric citrate in test tubes on a shaker at 37 °C and 250 rpm. The following day, the overnight was harvested by centrifuge and the washed cell pellets where then used to inoculate fresh M9 minimal medium with 0.4% glucose, antibiotics, 0.2% arabinose and 0.2% rhamnose, without ferric citrate, under aerobic condition in a 96-well plate (Methods 2.10). The ODs at 24 h for A-C are presented as bar charts (**D-F**,

respectively). P-value were calculated by one-way ANOVA and generated by GraphPad Prism (*, P <0.05; **, P <0.01; ***, P <0.001; ****, P <0.0001).

Previous growth comparisons showed a stronger impact of FeoAB and FeoABC with the addition of DTPA (Fig. 3.12B). Therefore, a set of growth comparisons was performed as in Fig. 4.18, but with 1 μM DTPA included (Fig. 4.24). The results show that the FeoABC strain had a growth advantage (~18%) over the FeoAB strain, and that both strains had superior growth with respect to the vector control (by ~73 and 46%, respectively; Fig. 4.24). Thus, growth was Feo supported and this effect was enhanced by the presence of FeoC. Interestingly, the presence of CFeoB Flag-tag constructs resulted in a significant and substantial reduction in the growth of the FeoABC strain by ~38% (Fig. 4.24D). A similar effect was observed for the CFeoB construct (without a Flag-tag) but this was more modest (~11.5%) and was not significant. In contrast, the CFeoB constructs caused the opposite effect in the vector control strain (Fig. 4.24F), i.e. nonsignificant increases in growth were observed (13-26%). For the FeoAB strain, the CFeoB constructs had a relatively modest and insignificant effect on growth (Fig. 4.24E).

Thus, in summary, the results are somewhat consistent with the notion that FeoC enhances FeoAB-dependent growth under aerobic, iron restricted conditions, and that this FeoC-dependent enhancement can be countered by provision of CFeoB (Flag tagged) in trans.

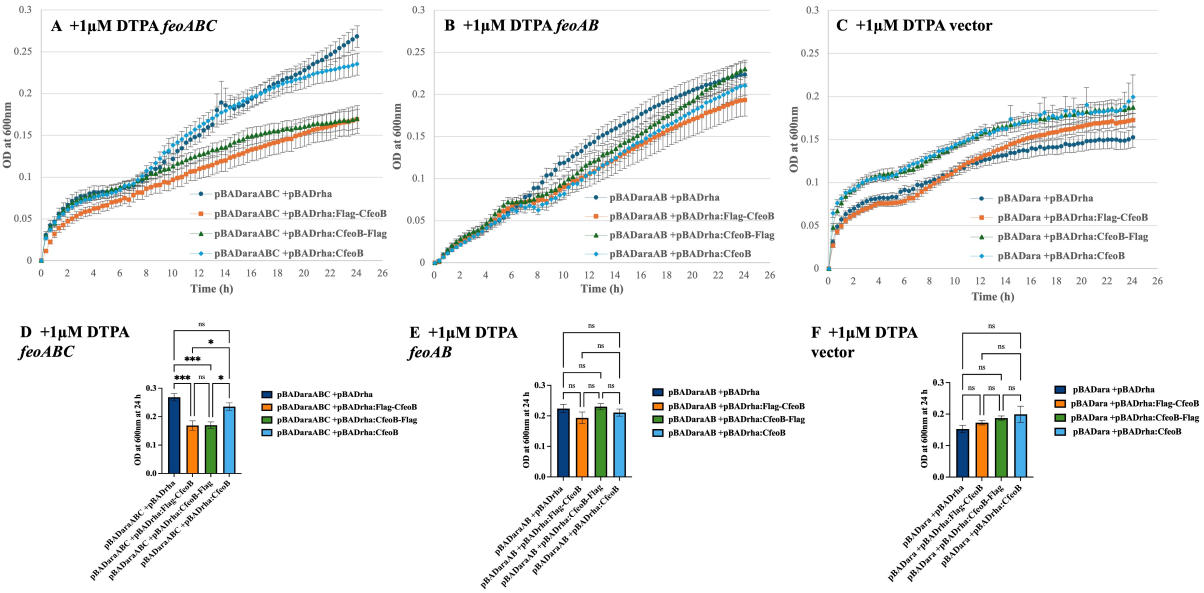

Figure 4.24: Effect of CFeoB expression on *feoAB* and *feoABC* aerobic growth under low-iron with <u>DTPA</u>. Details are as for Fig. 4.18, except for the inclusion of 1 µM DTPA for the growth comparison.

4.4 Discussion

This chapter further focused on the role of FeoC and a potential interaction between FeoC and the C-terminal extension region of FeoB (CFeoB) in enhancing FeoAB-dependent iron restricted growth under aerobiosis. As mentioned above, FeoC is a small, cytoplasmic protein (78 residues) that is thought to form an Fe-S cluster. FeoC is homologous with bacterial helix-turn-helix transcriptional regulators, although there is no evidence that FeoC regulates *feoABC* expression (Kim *et al*., 2013). However, its potential interaction with the C-terminal region of FeoB has been suggested (Lau *et al*., 2015). Thus, FeoC has been found to interact with FeoB *in vivo* in *V. cholera* and *S. enterica* (Kim *et al*., 2013; Weaver *et al.*, 2013). The C-terminal extension region of FeoB is only conserved in *Gammaproteobacteria* and its function is unclear (Cartron *et al.*, 2006; Orzel *et al.*, 2025). Therefore, this chapter was concentrated mainly on the potential role of the CFeoB region in interaction between FeoC and FeoB.

4.4.1 Effect of the *CfeoB* truncation on Feo-mediated iron-restricted growth in the presence and absence of FeoC

Firstly, it was important to accurately define the C-terminal extension region of FeoB in order to target it for deletion without disruption of the FeoB membrane embedded domain. This was achieved by performing a multiple alignment of FeoB amino acid sequences from diverse bacteria within and outside the *Gammaproteobacteria* class (Fig. 4.1A) together with structure-based analysis using the Alphafold prediction (Fig. 4.1C). Thus, a region of CFeoB amino acids (residues 747-773) was defined that was predicted to be cytoplasm located and contained a conserved Cys-Cys and Cys-His motif (Fig. 4.1B). Five distinct site-directed mutations were introduced at different positions along the CFeoB-encoding region, whereby an amino acid codon was substitute for a stop codon. In this way, five CFeoB truncations were generated that were designed to explore the importance of specific regions within CFeoB. The mutations were generated in pBADara:*feoAB* and pBADara:*feoABC* to enable comparison of their effects in the presence and absence of FeoC. All mutations were confirmed by Sanger sequencing (sections 4.3.2). Once confirmed, all 10 constructs carrying *CfeoB* truncation mutations were transferred into the JC32 strain to allow phenotypic analysis (aerobic growth under iron restriction). The results showed that, when iron was absent, no *feoAB* and or *feoABC* enhanced growth was apparent (compared to the vector control) (Fig. 4.8). In addition, the CFeoB mutations had little impact on growth. Thus, growth conditions were modified to enhance iron restriction by including 1 μM DTPA. The results showed a very clear growth advantage for the *feoABC* strain, but not the vector control for *feoAB* strain (Fig. 4.9). In addition, all five CFeoB truncations resulted in a significantly subdued FeoC-enhanced growth for the FeoABC strain (Fig. 4.9D). These results are consistent with a role for FeoC in enhancing FeoAB dependent iron-restricted growth aerobically, and a role for CFeoB in mediating this effect.

Under iron-restricted aerobic growth in the presence of 100 mM MES (pH 6), again there was little difference between the vector control and the FeoAB/FeoABC strains (Fig. 4.10). This

indicates that iron-restricted growth had not been achieved and thus no advantage of Feo could be observed. The CFeoB truncations had significant, but relatively modest negative impacts on growth. It is unclear how such an effect could be mediated, but it is possible that the truncations resulted in a FeoB impairment that caused toxicity. Interestingly, the S747Δ mutation (full CFeoB deletion) resulted in a major delay/reduction in growth for the FeoAB strain, but not the FeoABC strain (Figs. 4.9A and 4.10A).

When both 1 μM DTPA and MES buffer were included in the growth medium, a clear growth advantage of the FeoABC strain was observed with respect to both the FeoAB and vector control strains (Fig. 4.11), indicating that the conditions of growth had enabled the FeoC-enhancement effect on FeoAB-supported growth to be realised. The CFeoB mutations had an overall negative impact on Feo-dependent growth. For the FeoAB strain, the average CFeoB-truncation growth reduction was ~12%, whereas that for the FeoABC strain was ~19%. These findings indicate the CFeoB truncations negatively affected FeoAB dependent growth both in the presence and absence of FeoC, although the effect was greater when FeoC was included. The only significant effect of the CFeoB truncations was obtained for the FeoABC strain carrying the A755Δ mutation. Thus, the data are suggestive of a possible impact of the CFeoB truncations on FeoABC dependent aerobic, iron-restricted growth, but further experiments (e.g. growth comparisons) are required in order to obtain a clearer picture of the degree and validity of the effect indicated.

4.4.2 Effect of the CFeoB expression on FeoAB-dependent aerobic and iron-restricted growth in the presence and absence of FeoC

The possibility that cytosolic CFeoB is able to interact with FeoC when provided independently of the FeoB protein, and thus inhibit the FeoC-growth advantage observed above, was investigated. The predicted location of the CFeoB region had already been defined (residues 747-773) by structure prediction and multiple amino acid alignment (sections 4.2). Thus, synthetic DNA encoding *CfeoB* was synthesized by GeneArt in three formats (with an N-

terminal Flag-tag, with a C-terminal Flag-tag and with no Flag-tag. The three synthetic *CfeoB* gene fragments were then subcloned from the pMA-T vector into pBADrha (compatible with pBADara) to enable rhamnose-induced expression (section 4.4.2; Appendix Figs. A.1-A.6). The identity of the plasmids thus generated was confirmed by restriction mapping and Nanopore 30 whole plasmid sequencing (Figs. 4.15- 4.17).

Once all three constructs had been successfully generated, an attempt was made to detect Flag-CFeoB and CFeoB-Flag by anti-Flag tag western blotting. However, the Flag-tagged proteins could not be detected, which might be because of low molecular weight (~3.94 kDa) for the Flag-tagged CFeoB proteins or due to lack of stability since the constructs were unnatural and may not fold to form a well assembled structure, which could promote rapid turnover (section 4.3.3). However, despite the failure to detect CFeoB by western blotting, the impact of induction of the three CFeoB plasmids on FeoABC-dependent growth (under aerobiosis and iron restriction) was explored. Thus, pBADrha, pBADrha:Flag-*CfeoB*, pBADrha:*CfeoB*-Flag and pBADrha:*CfeoB* were transferred into the pBADara-*feoAB* and pBADara-*feoABC* JC32 transformants.

Under aerobic conditions in the absence of iron, the presence of the FeoAB and FeoABC constructs appears deleterious, and thus no Feo-growth advantage was apparent (Fig. 4.23). The CFeoB constructs had no significant impact on growth for the vector control and FeoAB strain. However, a significant negative impact was observed for two of the three CFeoB constructs in the FeoABC strain (Fig. 4.23). It is unclear how this effect was achieved given that FeoABC was inhibiting, not promoting, growth under the conditions utilised. When 1 μM DTPA was also included, a clear growth advantage for the FeoABC strain was apparent (Fig. 4.24), indicating the growth was Feo promoted and FeoC enhanced. The CFeoB constructs resulted in a reduction in the FeoABC promoted growth observed, and this was significant in two cases (Fig. 4.24D). The CFeoB constructs also caused a slight overall

reduction in FeoAB-supported growth (Fig. 4.24E), but this was not significant. For the vector control, the CFeoB constructs caused an enhanced growth (Fig. 4.24F) – although it is unclear how this might be mediated. The findings thus suggest that the FeoC-enhancement of FeoAB-dependent aerobic, iron-restricted growth can be inhibited by provision of CFeoB (in Flag-tagged form). This is consistent with the proposed interaction of FeoC with the CFeoB region of FeoB. It should note that the presence of ascorbic as reductant agent was tested on the CFeoB truncation and pBADrha:CFeoB constructs on FeoAB/ABC dependent growth but the results were inconsistent and so have not been reported herein.

Chapter 5: The role of FeoC in global gene expression; an RNAseq approach

5.1 Introduction

In order to further investigate the role of FeoC, RNA sequencing (RNAseq) was performed to explore the effect of *feoC* on global gene expression during *in vitro* growth in the presence and absence of FeoC. RNAseq (RNA sequencing) was first reported two decades ago (Bainbridge *et al.*, 2006) and it has since been become a common technique in molecular biology for the study of the transcriptome. RNAseq is mostly utilized for studying and analyzing differential gene expression (DGE). Such DGE studies involve RNA isolation followed by mRNA purification and/or rRNA removal, cDNA synthesis and sequencing library preparation. Then the library is sequenced via NGS methodology to generate deep reads for each sample, usually using an Illumina platform. This is followed by data analysis steps, such as read alignment, transcript quantification, normalization and application of statistics to determine which genes are significantly differentially expressed (Stark *et al*., 2019). The aim of this chapter is to utilize RNAseq to identify genes/transcripts that are influences by FeoC that might indicate a regulatory functional role for FeoC in gene control.

5.2 Growth conditions for RNAseq

As indicated in the previous chapters, induction of *feoABC* expression supports aerobic iron-restricted growth with DTPA (as well as under reducing and buffered conditions) and this effect is very much enhanced by the presence of *feoC*. In order to determine suitable conditions for growth of the JC32 transformants in 250 ml flasks (for RNA isolation), the growth comparisons (previously performed in microtiter plates) was repeated aerobically in 250 ml acid-washed flasks containing 50 ml of M9 minimal medium with 0.4% glucose (Fig. 5.1). In the presence of reductant (2 mM ascorbate), the *feoABC* strain showed slightly better growth (14% at 24 h; $p < 0.0001$) than the *feoAB* strain, and both the *feoABC* and *feoAB* strains showed better growth than the vector control strain (by 2.2-fold at 10 h; $p < 0.0001$; Fig. 5.1A). This effect was not observed in the presence of iron, with all three strains growing equivalently and more strongly

than in the absence of added iron (by 1.8- and 2.6-fold at 12 h; p <0.0001 and <0.0001, respectively; Fig. 5.1B). However, when both 2 mM ascorbate and 1 µM DTPA were included, the *feoABC* strain showed strong growth whereas very weak growth was seen for the *feoAB* and vector control strains (Fig. 5.1C). Thus, it was decided to utilize the two conditions where all three strains showed good growth, where a clear iron-dependence was apparent, where the presence of FeoC positively impacted growth, and where the FeoAB and FeoABC strains showed a growth advantage under iron restriction. Thus, two conditions were used to perform the RNAseq expression study: the first condition without iron and with ascorbate (Fig. 5.1A), at two time points (OD 0.5 and 0.8); and the second condition was with iron (Fig. 5.1B), at two time points (OD 0.5. and 1.0). Unfortunately, the cultures grown in the presence of DTPA and ascorbate had to be excluded due to the very poor growth of two of the transformant strains, which would be expected to greatly affect gene expression.

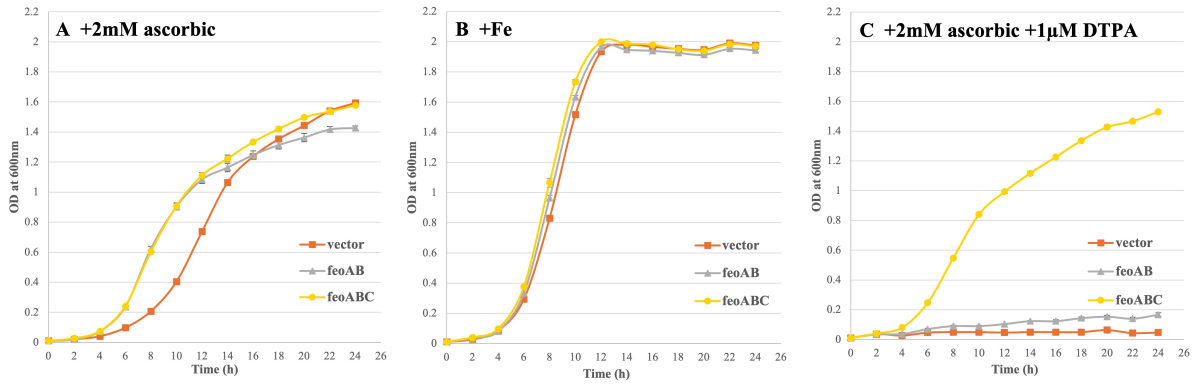

Figure 5.1: Effect of *feoAB* and *feoABC* induction on iron-restricted aerobic growth of *E. coli* JC32 with 2 mM ascorbate and 1 µM DTPA. JC32 transformants carrying pBADara-*feoABC*, pBADara-*feoAB* and pBADara were grown overnight in 5 ml of M9 medium with 0.4% glucose containing 100 µg/ml ampicillin and 20 µM of ferric citrate in test tubes on a shaker at 37 °C and 250 rpm. The following morning, the overnight cultures were harvested by centrifugation (an Eppendorf Centrifuge 5804 R) at 4 °C and 5000 rpm and then the pellets were washed twice with fresh M9 to remove any residual iron. The washed overnight cultures where then used to inoculate fresh M9 minimal medium with 0.4% glucose, antibiotic and 0.02% arabinose, with either 2 mM ascorbate **(A),** 20 µM ferric citrate **(B)** or 1 µM DTPA and 2 mM ascorbate **(C)** under aerobic condition in 250 ml acid-washed flasks.

5.2.1 RNA extraction

Growth experiments were performed in M9 minimal medium under two conditions, as above: 2 mM ascorbate; and 20 μM ferric citrate. Samples were collected in RNA-free sterile 50 ml Falcon tubes and two volumes of RNALater were added. All samples were equivalent to 0.8 OD units (Methods 2.20.1). The RNAprotect Bacteria Reagent kit (Qiagen) was then used to extract the total RNA (Methods 2.20.2) and turbo DNA-free kit was applied to all the RNA samples to remove any contamination of DNA (Methods 2.20.3).

5.3 Integrity of RNA analysis

5.3.1 Quality check of RNA

Once the total RNA had been extracted and treated by the turbo DNA-free kit to remove any residues of DNA, it was then necessary to check the quality and quantity of the RNA. A good RNA integrity should meet the following criteria (Imbeaud *et al.*, 2005):

- Free of genomic DNA and protein (absorbance at 260:280 nm of greater than 1.8 indicates pure RNA)
- no degradation on agarose gel electrophoresis and the ratio between (23S: 16S) should be 2.0 which indicates pure and intact RNA
- RNA integrity number (RIN) range between 1-10, 1 is fully degraded RNA and 10 is considered to be high quality RNA

Bacteria possess three types of rRNA (5S, 16S and 23S rRNA; Giuliano and Engl, 2021). The Agilent 4200 TapeStation was used to check quality and quantity of RNA (Figs. 5.2-5.5) (Methods 2.20.4) prior to submission for RNAseq. The quality and quantity of all 36 samples were considered sufficient for RNAseq (Table 5.1) and so were submitted to Novogene for RNAseq.

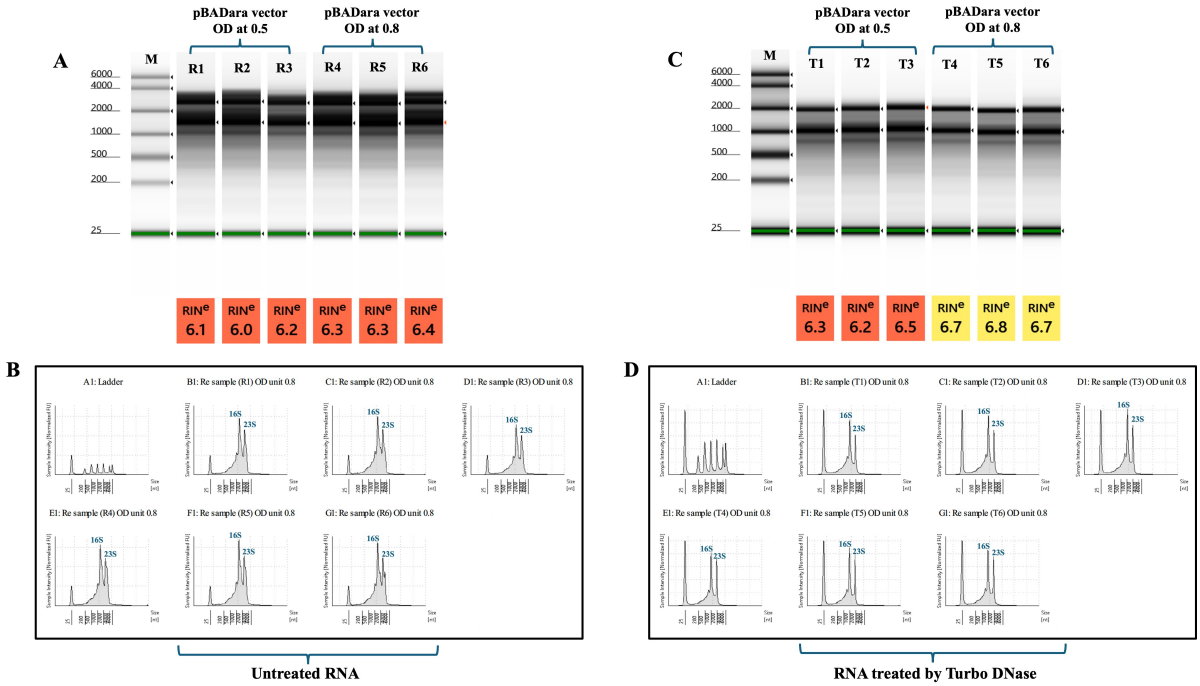

Figure 5.2: Electrophoretic analysis of total RNA for JC32(pBADara) grown with ascorbate (without iron) using an Agilent 4200 TapeStation. M, RNA screen tape ladder. **(A & C)** TapeStation electrophoresis of total RNA samples extracted from three different cultures of JC32(pBADara) harvested at OD 0.5 and 0.8 with ascorbate before (A) and after (B) Turbo-treatment. The resulting RNA integrity number (RIN) is shown. **(B & D)** The corresponding electropherograms for A and C, respectively, indicating the two peaks for 16S and 23S rRNA. Images were generated by the Agilent 4200 TapeStation and manually edited.

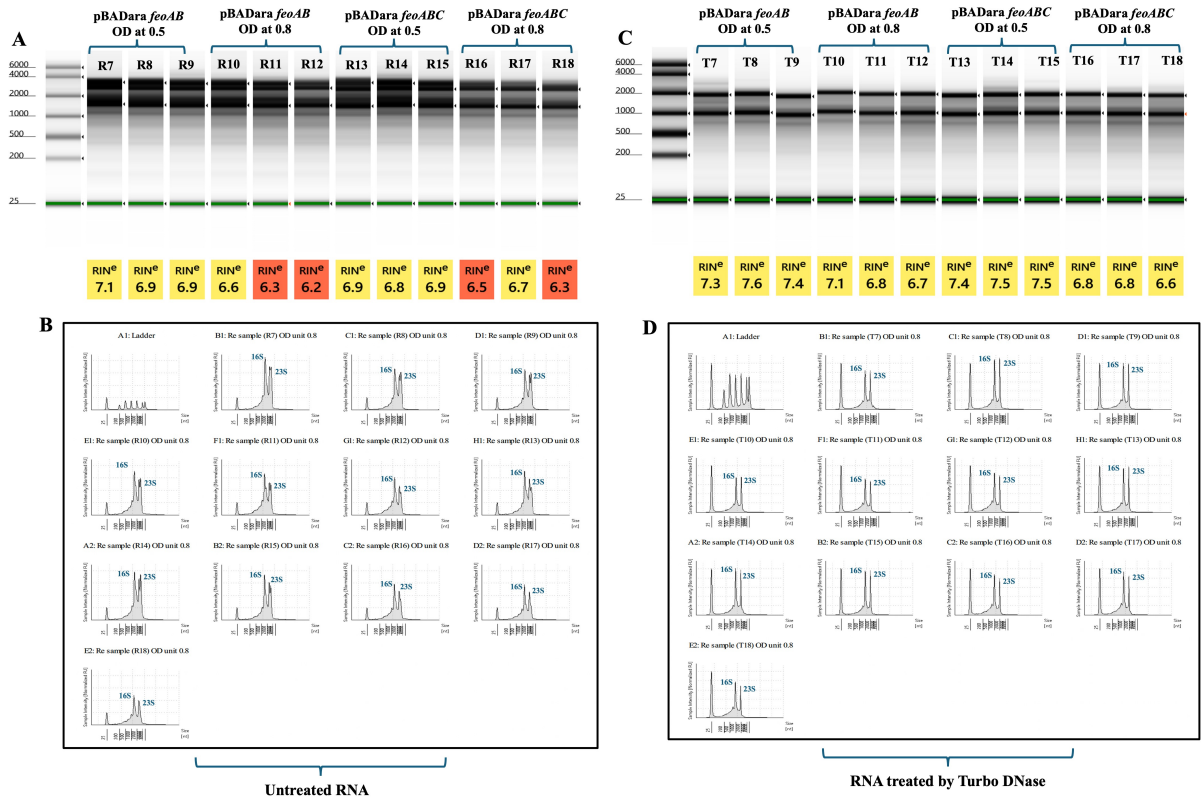

Figure 5.3: Electrophoretic analysis of total RNA for JC32(pBADara-*feoAB*) and JC32(pBADara-*feoABC*) grown with ascorbate (without iron) using an Agilent 4200 TapeStation. M, RNA screen tape ladder. **(A & C)** TapeStation electrophoresis of total RNA samples extracted from three different cultures of JC32 (pBADara-*feoABC*) and JC32 (pBADara-*feoAB*) harvested at OD 0.5 and 0.8 with ascorbate before (A) and after (B) Turbo-treatment. The resulting RNA integrity number (RIN) is shown. **(B & D)** The corresponding electropherograms for A and C, respectively, indicating the two peaks for 16S and 23S rRNA. Images were generated by the Agilent 4200 TapeStation and manually edited.

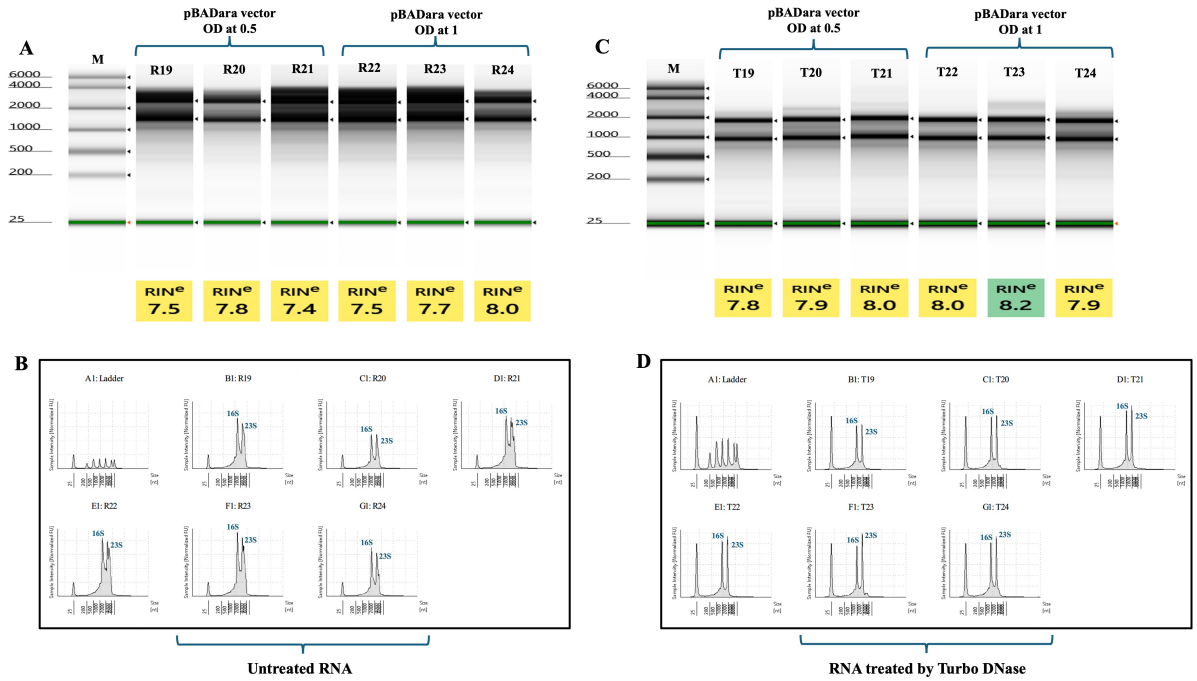

Figure 5.4: Electrophoretic analysis of total RNA for JC32(pBADara) grown with iron using an Agilent 4200 TapeStation. M, RNA screen tape ladder. **(A & C)** TapeStation electrophoresis of total RNA samples extracted from three different cultures of JC32 (pBADara) harvested at OD 0.5 and 1.0 with iron before (A) and after (B) Turbo-treatment. The resulting RNA integrity number (RIN) is shown. **(B & D)** The corresponding electropherograms for A and C, respectively, indicating the two peaks for 16S and 23S rRNA. Images were generated by the Agilent 4200 TapeStation and manually edited.

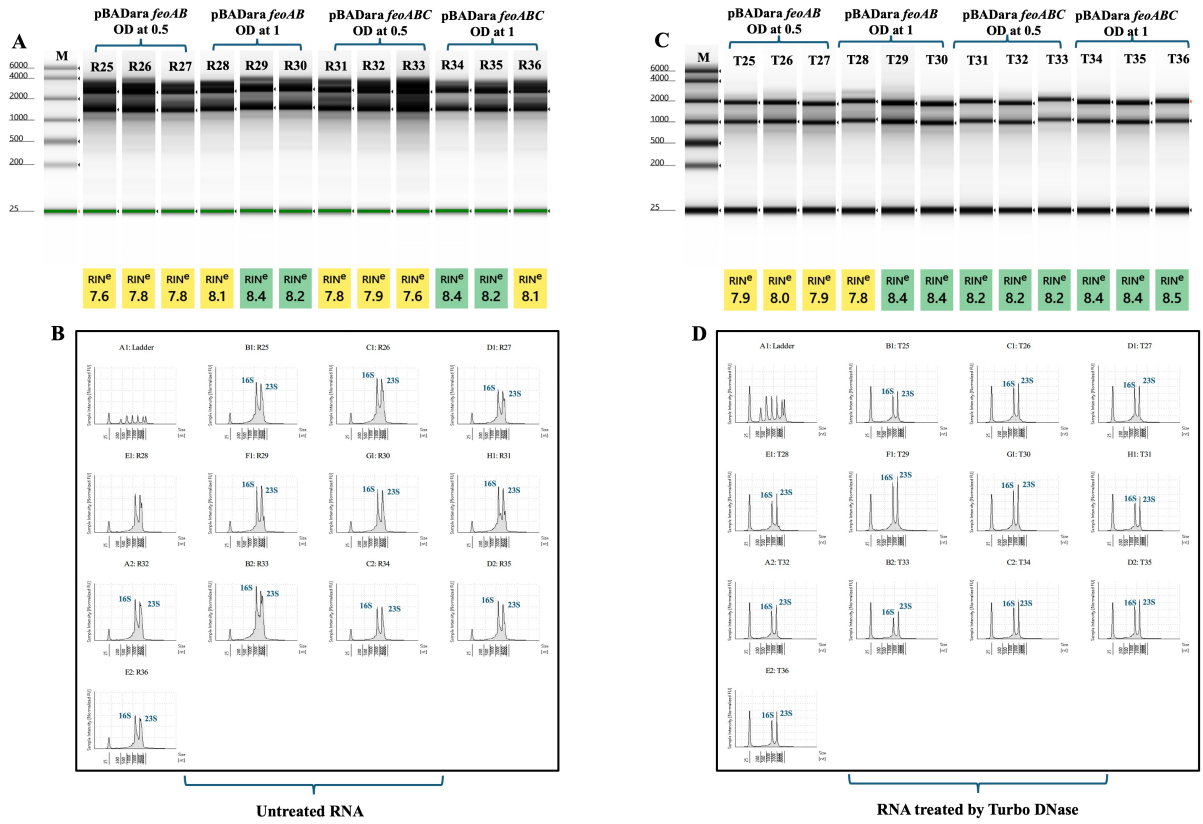

Figure 5.5: Electrophoretic analysis of total RNA for JC32(pBADara-*feoAB*) and JC32(pBADara-*feoABC*) grown with iron using an Agilent 4200 TapeStation. M, RNA screen tape ladder. **(A & C)** TapeStation electrophoresis of total RNA samples extracted from three different cultures of JC32 (pBADara-*feoABC*) and JC32 (pBADara-*feoAB*) harvested at OD 0.5 and 1.0 with iron before (A) and after (B) Turbo-treatment. The resulting RNA integrity number (RIN) is shown. **(B & D)** The corresponding electropherograms for A and C, respectively, indicating the two peaks for 16S and 23S rRNA. Images were generated by the Agilent 4200 TapeStation and manually edited.

5.3.2 Quality check of RNA by Novogene

Following sample submission for RNAseq, Novogene re-checked the quality of the RNA samples provided before committing them to cDNA generation. Thus, two steps were followed, sample quantity was measured by Nanodrop (Table 5.1; Fig. 5.6-5.8). These analyses indicated that the quality and quantity of the samples was sufficient for RNAseq to progress.

Table 5.1: The concentration and the RNA integrity number (RIN) as determined by Novogene.

No.	Sample Name	Nucleic Acid ID	Concentration (ng/ul)	Integrity value
1	Vector_asc_05_1	FKRN240354904-1A	101	7.00
2	Vector_asc_05_2	FKRN240354905-1A	107	6.80
3	Vector_asc_05_3	FKRN240354906-1A	131	6.90
4	Vector_asc_08_4	FKRN240354907-1A	114	7.30
5	Vector_asc_08_5	FKRN240354908-1A	129	7.40
6	Vector_asc_08_6	FKRN240354909-1A	87	6.90
7	*feoAB*_asc_05_7	FKRN240354910-1A	130	8.70
8	*feoAB*_asc_05_8	FKRN240354911-1A	102	8.20
9	*feoAB*_asc_05_9	FKRN240354912-1A	108	8.10
10	*feoAB*_asc_08_10	FKRN240354913-1A	134	7.70
11	*feoAB*_asc_08_11	FKRN240354914-1A	119	7.30
12	*feoAB*_asc_08_12	FKRN240354915-1A	123	7.20
13	*feoABC*_asc_05_13	FKRN240354916-1A	168	8.20
14	*feoABC*_asc_05_14	FKRN240354917-1A	128	8.10
15	*feoABC*__asc_05_15	FKRN240354918-1A	101	8.40
16	*feoABC*_asc_08_16	FKRN240354919-1A	113	7.00
17	*feoABC*_asc_08_17	FKRN240354920-1A	156	7.50
18	*feoABC*_asc_08_18	FKRN240354921-1A	144	7.60
19	Vector_Fe_05_19	FKRN240337010-1A	123	8.80
20	Vector_Fe_05_20	FKRN240337011-1A	158	6.00
21	Vector_Fe_05_21	FKRN240337012-1A	179	9.10
22	Vector_Fe_1_22	FKRN240337013-1A	168	8.70
23	Vector_Fe_1_23	FKRN240337014-1A	168	9.60
24	Vector_Fe_1_24	FKRN240337015-1A	127	9.20
25	*feoAB*_Fe_05_25	FKRN240337016-1A	180	9.80
26	*feoAB*_Fe_05_26	FKRN240337017-1A	164	9.70
27	*feoAB*_Fe_05_27	FKRN240337018-1A	206	9.40
28	*feoAB*_Fe_1_28	FKRN240337019-1A	186	9.90
29	*feoAB*_Fe_1_29	FKRN240337020-1A	158	9.30
30	*feoAB*_Fe_1_30	FKRN240337021-1A	186	9.80
31	*feoABC*_Fe_05_31	FKRN240337022-1A	106	6.20
32	*feoABC*_Fe_05_32	FKRN240337023-1A	143	9.10
33	*feoABC*_Fe_05_33	FKRN240337024-1A	152	9.00
34	*feoABC*_Fe_1_34	FKRN240337025-1A	168	9.60
35	*feoABC*_Fe_1_35	FKRN240337026-1A	149	9.40
36	*feoABC*_Fe_1_36	FKRN240337027-1A	167	8.10

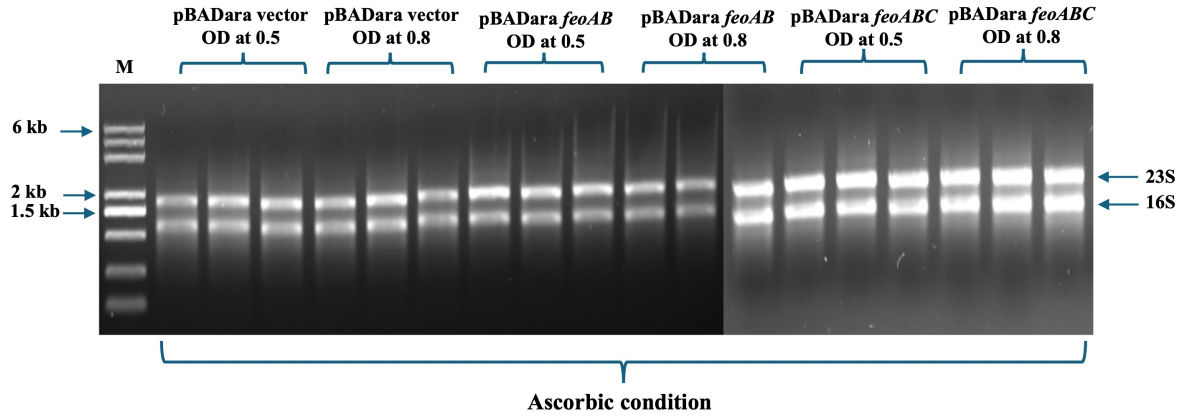

Figure 5.6: Agarose gel electrophoretic analysis of total RNA samples from cultures grown with added ascorbate (by Novogene). M, RiboRuler high range RNA ladder. Total RNA samples were subjected to electrophoresis which showed the two rRNA bands (16S and 23S rRNA) at high intensity for all samples.

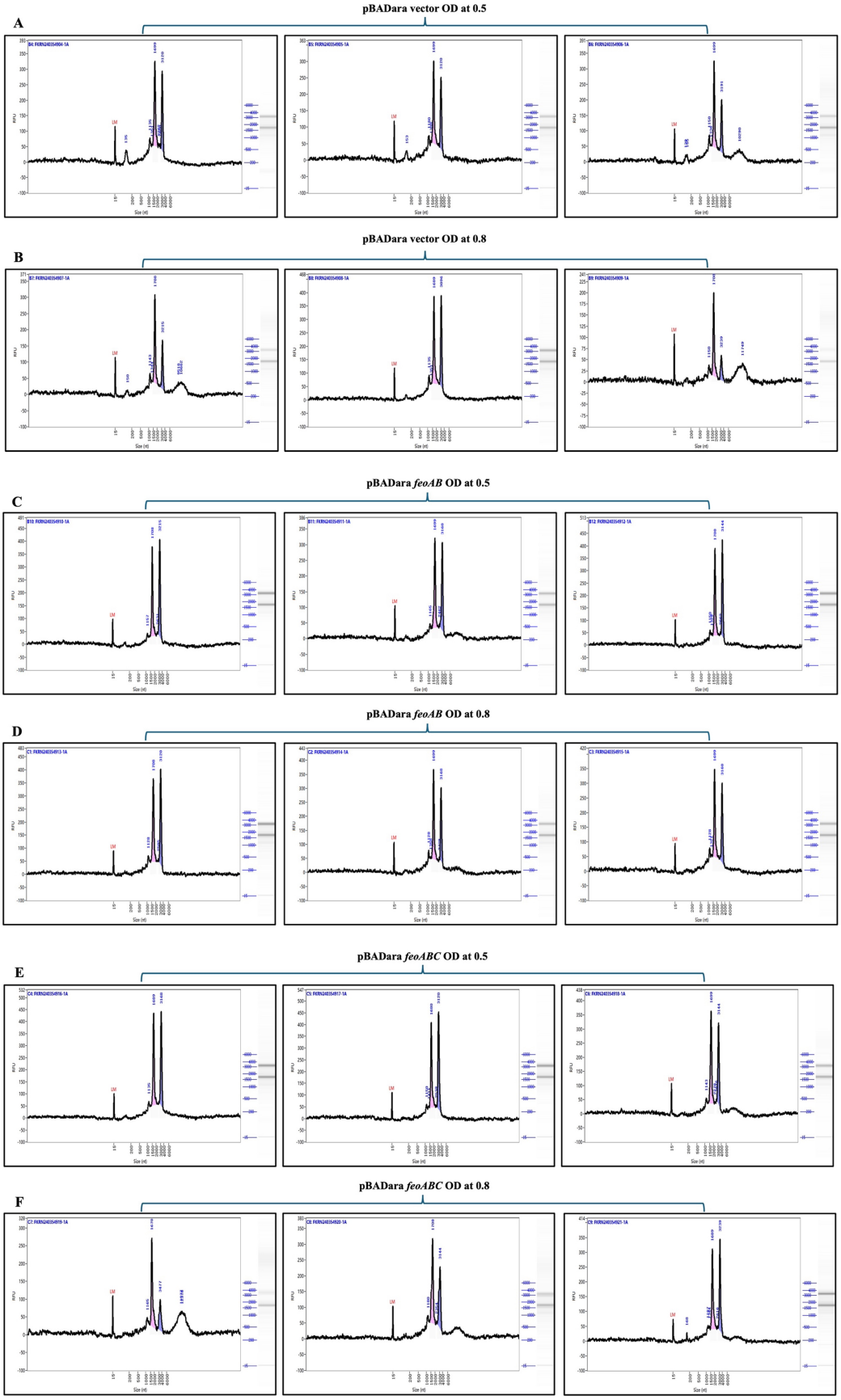

Figure 5.7: Electropherograms of the total RNA for samples grown with ascorbate.

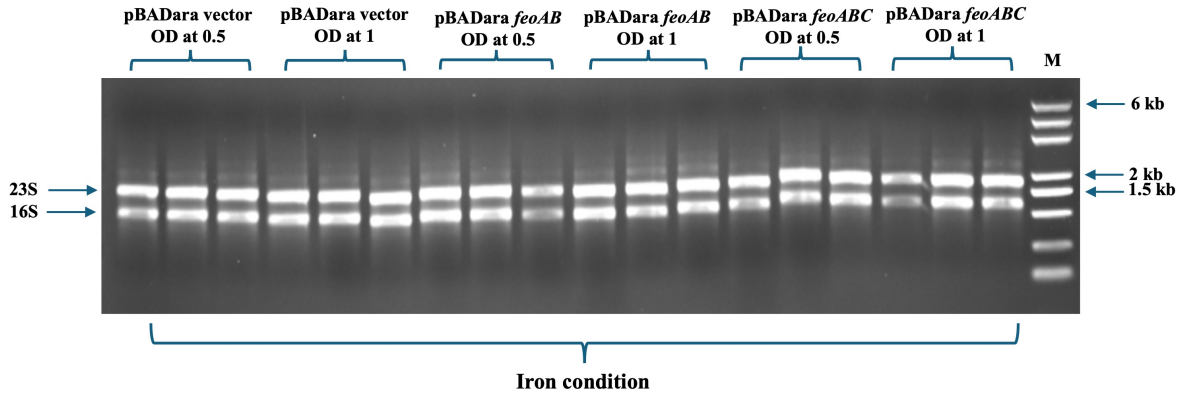

Figure 5.8: Agarose gel electrophoretic analysis of total RNA samples from cultures grown with added iron (by Novogene). M, RiboRuler high range RNA ladder.

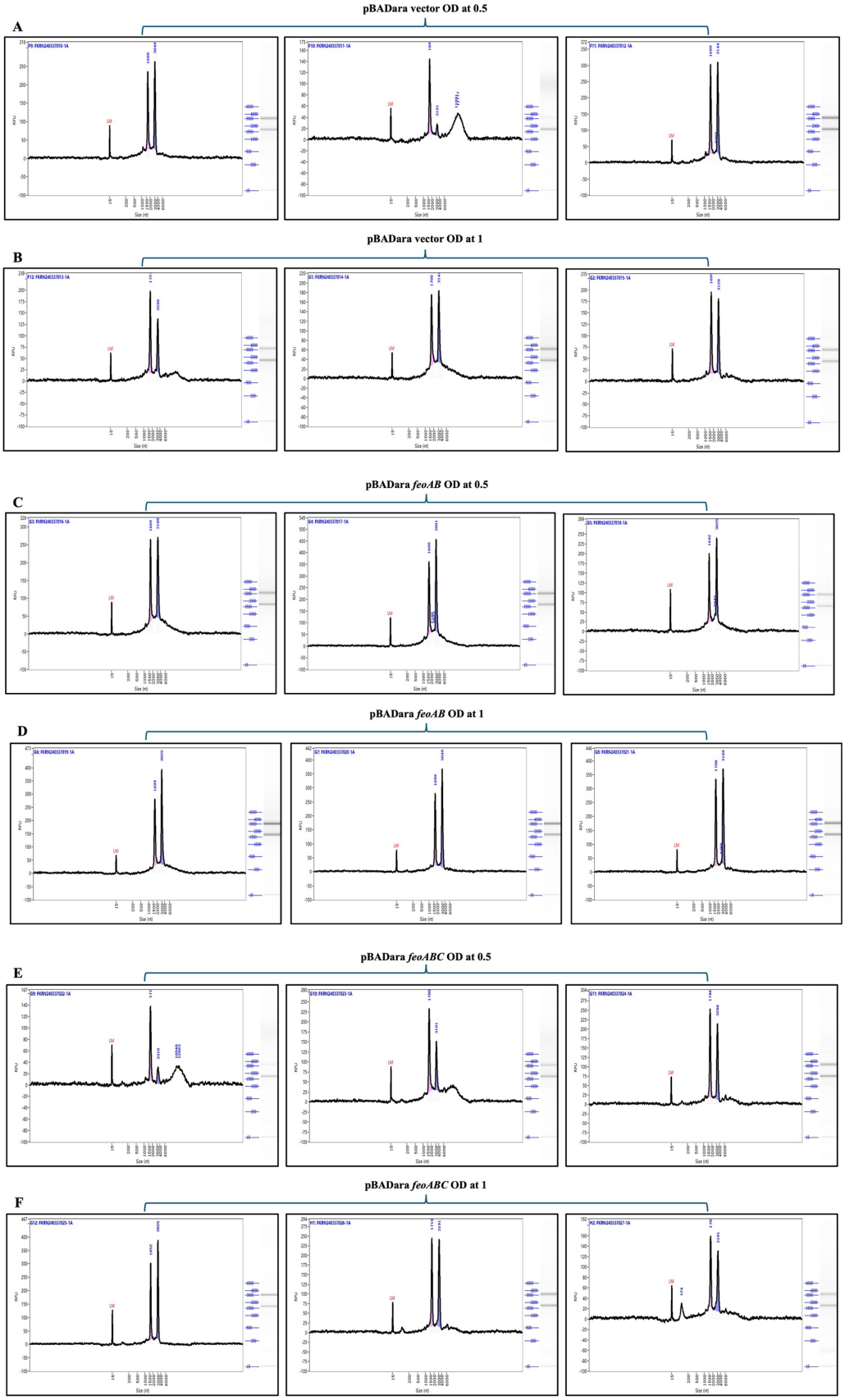

Figure 5.9: Electropherograms of the total RNA samples grown with iron.

5.4 RNAseq data

5.4.1 Data processing and quality

The raw reads were filtered to eliminate low quality data and adapters (representing ~1% of reads). The quality of the RNAseq read data was considered high: error rates were below 0.01%, GC content was at ~52% as expected; and raw reads had low error rates (Appendix Fig. A.7). The quality of the reads for all 36 samples is provided in the Appendix (Table A.1). Reads were mapped using Bowtie2 to the *E. coli* W3110 genome (4646332 bp; GenBank accession no. AP009048.1) sequence and ~96% of reads were thus successfully mapped (Appendix Fig. A.9; Table A.2). There was a relatively low level of reads mapping to multiple sites which indicates successful rRNA depletion. Within the data set as a whole, a total of 2807 genes were mapped to the RNAseq reads generated. These genes were categorized into 38 GO term categories (Appendix Fig. A.8). Pearson correlation analysis was used to compare the similarity between the read data produced by each of the 36 samples (Appendix Fig. A.10). Triplicate samples generally showed a high degree of correlation, however three sets of triplicates showed differences (v-Fe_05, v_Fe_1 and ABCFe_1) indicative of experimental variability. A strong correlation is apparent for all those samples treated with ascorbate, and a low correlation is obtained when comparing samples with ascorbate to those without ascorbate.

5.4.2 Confirmation of *feoAB* and *feoABC* expression

To confirm that the induction of *feoAB* and *feoABC* had occurred, the read data were combined into three groups corresponding to all 36 samples (12 samples each for the vector control, the *feoAB* strain and the *feoABC* strain) and subjected to volcano plot analysis (Fig. 5.10). The results show that the *feo* genes were appropriately highly (and significantly) induced in the *feoAB* and *feoABC* strains, by 8.8- to 18.4 log2-fold. This change in expression was far higher than that observed for any other gene, excluding a "unidentified" gene (00420) that corresponds to a *feoA-feoB* transcript. The RNAseq data thus show that induction of the *feo* genes had been

successful which suggests that any impact of the *feo* gene products on global gene expression should be revealed.

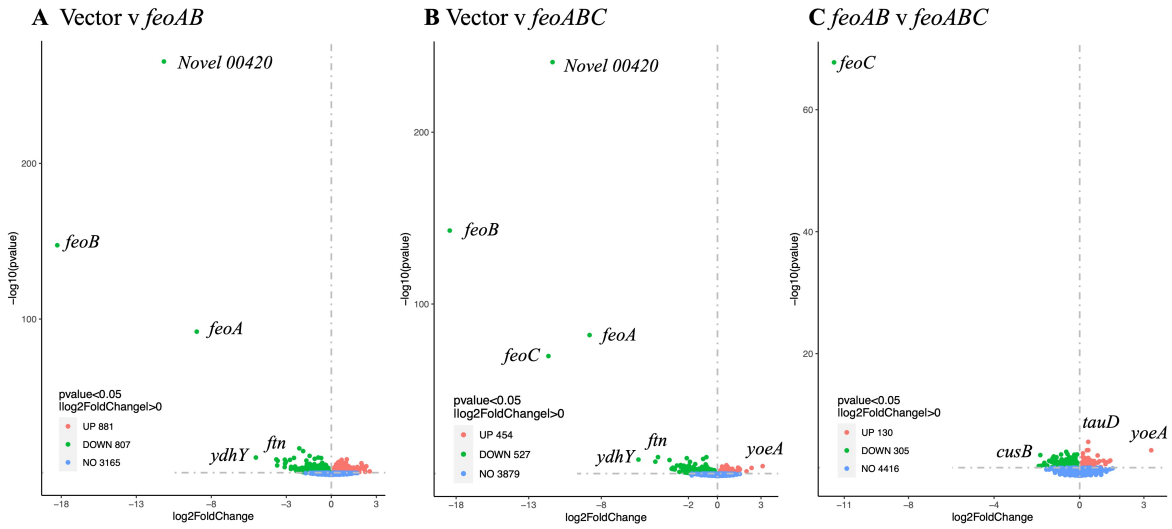

Figure 5.10: Volcano plot of differentially expressed genes in response to *feoAB* and *feoABC* induction. (**A**) Vector versus *feoAB*. (**B**) Vector versus *feoABC*. (**C**) *feoAB* versus *feoABC*. The identities of the *feoA*, *feoB* and *feoC* reads are indicated, and the number of significantly (>2 fold) induced and repressed transcripts is also provided as determined by DESeq2. Highly differentially regulated genes are annotated, including "Novel 00420" which corresponds to a *feoAB* transcript.

Therefore, in order to determine the effect of FeoAB and FeoC on global gene expression under aerobiosis, differential expression was considered for the vector control in comparison with either the *feoAB* or *feoABC* strain, in the presence of either ascorbate or ferric citrate.

5.4.3 Impact of FeoAB in the presence of ascorbate

Fig. 5.11 shows a volcano plot indicating the impact *feoAB* induction at two points in the growth curve (OD 0.5 and 0.8) in the presence of ascorbate. The results show that *feoAB*, *feoA* and *feoB* were strongly induced by 10.2- to 18.3 log2 fold (Fig. 5.11). At both OD 0.5 and 0.8, a large number of genes were induced (~900-1100) and repressed (~900) by *feoAB* induction (Fig. 5.11). Table 5.2 and 5.3 show the 40 most highly induced and suppressed genes, respectively, at OD 0.5. For the 40 most strongly FeoAB-induced genes, a large proportion (13 genes, 32%) were associated with anaerobic nitrite/nitrate respiration. This indicates a targeted

regulatory response. In addition, three FeoAB-induced genes specify anaerobic C_4-dicarboxylate transport systems and three encode hydrogenase 2 associated components (Table 5.2).

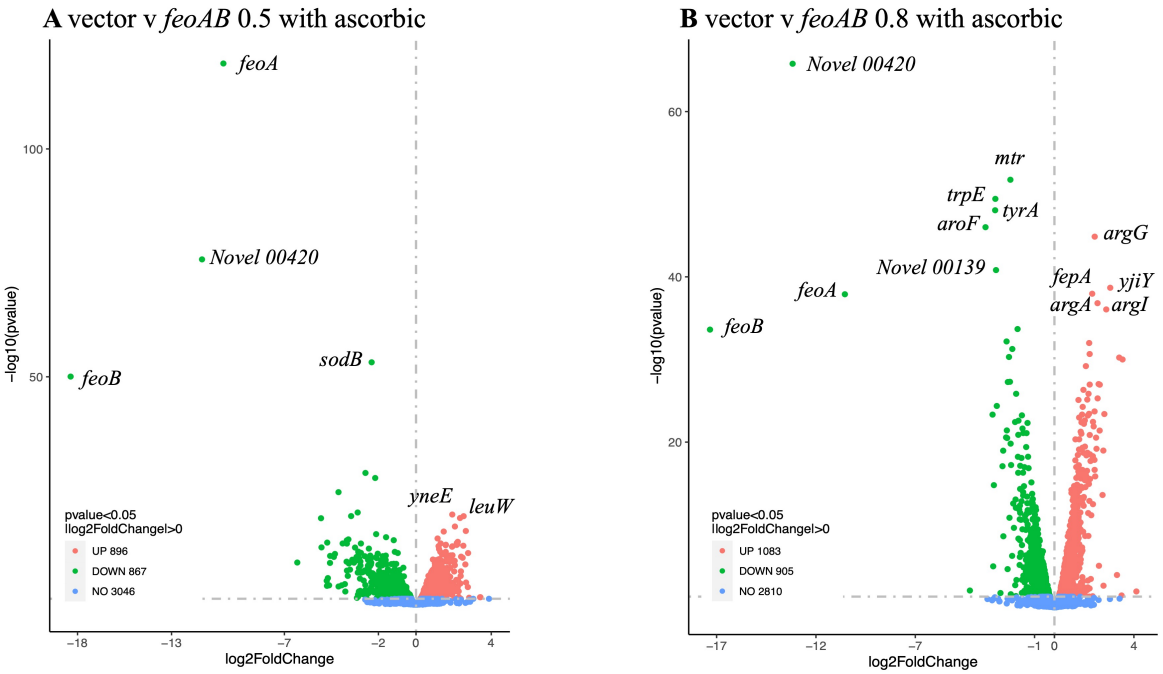

Figure 5.11: Volcano plot of differentially expressed genes in response to *feoAB* induction with ascorbate. (**A**) Vector versus *feoAB* at OD 0.5. (**B**) Vector versus *feoAB* at OD 0.8. The identities of the *feoA* and *feoB* reads are indicated, as are several other genes showing marked expression effects. The total number of significantly >2 fold up/down regulated genes is indicated, as determined by DESeq2. "Novel 00139" corresponds to a nitrate reductase gamma subunit (4Fe-4S dicluster domain transcript).

This pattern again indicates a coordinated regulatory response to FeoAB production. Of the remaining 18 genes, most (14) encode genes of unknown function. Thus, the regulatory response is suggestive of an induction of genes associated with anaerobic energy generation. Such an effect could be theoretically achieved by FeoAB-mediated delivery of additional iron supporting Fur-induction of iron-protein genes involved in energy generation (Massé and Gottesman, 2002; McHugh *et al.*, 2003). Alternatively, raised FeoAB levels may exert a direct gene regulation effect through interaction with relevant global regulators such as FNR and Fur.

Indeed, the induction of anaerobic functions is consistent with an FNR regulatory response (Grainger *et al.*, 2007).

For the 40 most FeoAB-repressed genes at OD 0.5 (Table 5.3), the functional categories were distinct to those identified in Table 5.2. Eight suppressed genes either specified tRNA transcripts or tRNA modification enzymes. Other categories repressed were as follows: seven encoded proteins involved in amino acid biosynthesis; four in nucleotide metabolism; three in sulphur transport; and three encode TCA cycle components (Table 5.3). Thus, systems involved in anabolism were suppressed. Indeed, the TCA cycle is known to be down regulated anaerobically. This correlates with the induction of anaerobic energy-generating components described above, and suggests an anaerobiosis regulatory response has been imposed by *feoAB* induction. Interestingly, the *efeU* and *efeO* genes were also repressed. These genes encode components of the EfeUOB ferrous iron transporter that is induced by iron restriction and acidity (Cao *et al.*, 2007) and their repression may be related to excess cellular iron arising from FeoAB activity combined with acidity due to mixed-acid fermentation of glucose (Sawers *et al*., 2004). Of the remaining 13 most strongly suppressed genes, 5 encode genes of unknown function and the remaining eight are associated with distinct cell functions.

Fig. 5.11B shows the same conditions as in Fig. 5.11A except that the OD of the cultures employed was at ~0.8 (rather than 0.5). Again, *feoA*, *feoB* and *feoAB* were far more highly induced than any other gene (Table 5.4). In addition, four *ara* genes were included in the top 40 list. As the regulatory *araC* gene is carried by the pBADara vector and arabinose is provided, it is possible that this raised expression is an artefact. Of the remaining 40 most FeoAB-induced genes, only three (*napD*, *napF* and *yehD*) were also induced at OD 0.5. This suggests that any regulatory effect of FeoAB is influenced by growth phase and/or growth condition. Nine of the top 40 FeoAB-induced genes are involved in amino acid generation. However, the identities of these genes are distinct from the seven amino acid metabolism genes

suppressed by FeoAB at OD 0.5 (Table 5.3), which again indicates distinct regulatory effects according to growth phase/conditions. Only two anaerobic nitrite/nitrate respiration genes were induced at OD 0.8, compared to 13 at OD 0.5. In addition, eight genes involved in carbon catabolism were induced at OD 0.8, and these were not included in the top-40 induced gene list at OD 0.5. Four toxin/antitoxin genes were also in the top-40 upregulated set, unlike at OD 0.5. Thus, the top 40 gene expression sets at OD 0.5 and 0.8 give distinct patterns. Interestingly, the *sodB* gene was included in the top-40 induced gene set. This encodes the iron-dependent SOD enzyme known to be iron induced via the Fur/RyhB pathway (Massé and Gottesman, 2002). Its induction would be consistent with a raised cellular iron content (via FeoAB) or a direct impact of FeoAB on Fur-dependent gene expression.

Table 5.2: The top 40 FeoAB-induced genes at OD 0.5 with ascorbate. Highlights indicate *feo* genes (yellow), nitrate/nitrate respiration genes (light brown), hydrogenase genes (mid-brown) and anaerobic C4-dicarbioxylate transport genes (brown).

gene_name	log2 Fold Change	pvalue log10	start	end	strand	length	description
feoB	-18.4	-50.1	4097688	4100009	-	2322	*feoB*
feoAB	-11.4	-75.8	4097550	4100265	+	2716	*feoAB*
feoA	-10.2	-118.7	4100026	4100253	-	228	*feoA*
nirD	-6.3	-9.3	4143539	4143865	-	327	nitrite reductase, small subunit, Rieske-like [2Fe-2S] domain
Novel00132	-5.1	-19.0	1281686	1288619	-	6934	Nitrate reductase, narK-I locus
narH	-5.0	-12.6	1285181	1286719	+	1539	nitrate reductase beta (Fe-S) subunit 4Fe-4S dicluster domain
nirC	-4.7	-5.2	4142607	4143413	-	807	Formate/nitrite transporter
nirB	-4.7	-4.1	4143862	4146405	-	2544	nitrite reductase large subunit BFD-like [2Fe-2S] binding domain,4Fe-4S domain
dcuC	-4.7	-13.6	653806	656390	-	2585	anaerobic C4-dicarboxylate transport
narI	-4.7	-5.8	1287426	1288103	+	678	nitrate reductase gamma (cytochrome b) subunit
narG	-4.6	-4.2	1281441	1285184	+	3744	nitrate reductase alpha subunit|Molydopterin dinucleotide binding domain
Novel00149	-4.6	-9.2	1549555	1550359	-	805	fdnG, nitrate dependent formate dehydrogenase
narJ	-4.6	-10.7	1286716	1287426	+	711	molybdenum-cofactor-assembly chaperone subunit (delta subunit) of nitrate reductase
yoeA	-4.4	-10.5	2070772	2071164	+	393	CP4-44 prophage region, predicted disrupted hemin or colicin receptor, TonB-dependent Receptor Plug Domain
ynfK	-4.3	-11.1	1668238	1668933	-	696	predicted dethiobiotin synthetase
napF	-4.1	-24.7	2306337	2306831	-	495	ferredoxin-type protein periplasmic nitrate reductase 4Fe-4S dicluster domain
yhbU	-4.1	-4.0	3301340	3302335	+	996	predicted peptidase
fdnG	-4.0	-4.2	1549115	1552162	+	3048	formate dehydrogenase-N alpha subunit Molybdopterin oxidoreductase Fe4S4 domain
yhbV	-3.9	-13.4	3302344	3303222	+	879	predicted protease Ubiquinone biosynthesis protein UbiV
yehC	-3.8	-4.5	2194260	2194979	-	720	predicted periplasmic pilin chaperone
yfiD	-3.8	-2.9	2714722	2715105	-	384	pyruvate formate lyase subuni GRCA Autonomous glycyl radical cofactor
yehD	-3.7	-9.4	2195014	2195556	-	543	predicted fimbrial-like adhesin protein
yjjI	-3.7	-14.1	4620195	4621745	-	1551	conserved hypothetical protein of unknown function (DUF3029)
hybO	-3.7	-13.4	3143799	3144917	-	1119	hydrogenase 2 C small subunit NiFe/NiFeSe hydrogenase small subunit
yliH	-3.7	-7.5	878670	879053	+	384	hypothetical protein BSSR Biofilm regulator
sRNA00018	-3.6	-6.3	1991229	1991284	-	56	sRNA
napD	-3.6	-14.3	2306084	2306347	-	264	assembly protein for periplasmic nitrate reductase
hybA	-3.6	-9.0	3142810	3143796	-	987	hydrogenase 2 4Fe-4S ferredoxin-type componen, 4Fe-4S dicluster domain
yfcC	-3.5	-7.7	2422527	2424047	+	1521	predicted inner membrane protein, Putative basic amino acid antiporter, C4-dicarboxylate anaerobic carrier
ybjM	-3.5	-19.4	890511	890888	+	378	predicted inner membrane protein
yecH	-3.4	-9.9	1991388	1991627	-	240	hypothetical protein of unknown function (DUF2492)
ydjY	-3.3	-9.2	1835830	1836507	+	678	hypothetical protein
Novel00152	-3.3	-9.4	1668286	1668936	+	651	ynfK
hypB	-3.2	-12.5	2849657	2850529	+	873	GTP hydrolase involved in nickel liganding into hydrogenases
dcuB	-3.2	-10.5	4352082	4353422	-	1341	Anaerobic C4-dicarboxylate transporter
insB_3	-3.1	-1.5	289873	290376	-	504	IS1 transposase Ins AB
napA	-3.1	-20.2	2303601	2306087	-	2487	nitrate reductase periplasmic large subunit Molybdopterin oxidoreductase Fe4S4 domai
yjdK	-3.1	-7.0	4357262	4357558	+	297	hypothetical protein GHOS Endoribonuclease antitoxin
hcr	-3.1	-9.7	911604	912572	-	969	HCP oxidoreductase NADH-dependent, Fe-2S iron-sulfur cluster binding domain
hisL	-3.1	-2.2	2092133	2092183	+	51	his operon leader peptide-

Table 5.3: The top 40 FeoAB-repressed genes at OD 0.5 with ascorbate. Highlights indicate iron metabolism genes (Fur regulated, yellow), tRNA genes (light blue), amino acid metabolism genes (mid-plum), nucleotide (light plum), TCA cycle genes (light green) and sulphur transport (mid blue).

gene_name	log2FoldChange	pvalue log10	start	end	strand	length	description
racC	3.42	-1.64	1419202	1419477	-	276	hypothetical protein
argZ	3.40	-1.64	2816715	2816791	-	77	tRNA-Arg
cysP	2.82	-1.53	2547958	2548974	-	1017	thiosulfate transporter subunit extracellular solute-binding protein
lysY	2.77	-11.33	781569	781644	+	76	tRNA-Lys-
yeeE	2.75	-3.86	2086604	2087662	-	1059	predicted inner membrane protein, Sulphur transport
sdhC	2.66	-4.86	755599	755988	+	390	succinate dehydrogenase membrane subunit cytochrome b556 subunit Succinate dehydrogenase/Fumarate reductase transmembrane subunit
yigI	2.65	-16.17	3631984	3632451	+	468	conserved hypothetical protein, Thioesterase superfamily
efeU	2.62	-8.84	1081778	1082607	+	830	predicted membrane protein Putative inactive ferrous iron permease EfeU Iron permease FTR1 family
leuW	2.53	-19.42	697385	697469	-	85	tRNA-Leu
lysW	2.51	-12.94	781265	781340	+	76	tRNA-Lys
pps	2.48	-10.30	1786448	1788826	-	2379	phosphoenolpyruvate synthase, Pyruvate phosphate dikinase, PEP/pyruvate binding domain
yegQ	2.40	-10.54	2167805	2169166	+	1362	predicted peptidase, tRNA hydroxylation protein
paaA	2.39	-7.31	1455641	1456570	+	930	predicted multicomponent oxygenase/reductase subunit for phenylacetic acid degradation
yciW	2.38	-1.30	1350694	1351821	-	1128	predicted oxidoreductase
ydcI	2.37	-6.29	1495862	1496785	-	924	predicted DNA-binding transcriptional regulator
yceA	2.36	-4.66	1118384	1119436	+	1053	conserved hypothetical protein, TRHO tRNA uridine(34) hydroxylase O Rhodanese-like domain, acylphosphatase like domain
yejG	2.34	-19.02	2281227	2281571	-	345	hypothetical protein
purE	2.31	-4.55	551814	552323	-	510	N5-carboxyaminoimidazole ribonucleotide mutase
sdhD	2.27	-1.71	755982	756329	+	348	Succinate dehydrogenase/Fumarate reductase transmembrane subunit
mqo	2.27	-2.94	2308442	2310088	-	1647	malate dehydrogenase FAD/NAD(P)-binding domain, Probable malate:quinone oxidoreductase, Malate:quinone oxidoreductase (Mqo)
metK	2.23	-5.43	3085362	3086516	+	1155	S-adenosylmethionine synthase
glnW	2.22	-13.79	697178	697252	-	75	tRNA-Gln
yeeF	2.21	-3.85	2087841	2089199	-	1359	predicted amino-acid transporter, Low-affinity putrescine importer PlaP
suhB	2.21	-3.87	2662098	2662901	+	804	inositol monophosphatas, Nus factor SuhB, Inositol monophosphatase family, ribosome interaction
argH	2.20	-13.25	3478458	3479831	-	1374	argininosuccinate lyase
purM	2.19	-3.63	2619853	2620890	+	1038	phosphoribosylaminoimidazole synthetase
glcC	2.17	-13.53	3126928	3127692	+	765	DNA-binding transcriptional dual regulator, glycolate-binding regulatory proteins, gntR family
metU	2.16	-13.11	697086	697162	-	77	tRNA-Met
lysP	2.15	-2.98	2250397	2251866	-	1470	lysine transporter
mhpR	2.14	-5.44	366811	367758	-	948	DNA-binding transcriptional activator, degradation of the aromatic compound 3-(3-hydroxyphenyl)propionic acid
ndk	2.09	-3.12	2643089	2643520	-	432	multifunctional nucleoside diphosphate kinase, apyrimidinic endonuclease
efeO	2.09	-3.82	1082665	1083792	+	1128	conserved hypothetical protein Iron uptake system component Cupredoxin-like domain and Imelysin domain
argA	2.07	-17.15	2947898	2949229	+	1332	fused acetylglutamate kinase homolog (inactive) and amino acid N-acetyltransferase
metN	2.06	-8.66	221614	222645	-	1032	DL-methionine transporter subunit
metA	2.06	-9.63	4217870	4218799	+	930	Homoserine O-succinyltransferase
carA	2.05	-1.43	29651	30799	+	1149	carbamoyl phosphate synthetase small subunit glutamine amidotransferase
yicE	2.04	-3.10	3810079	3811470	-	1392	predicted transporter Xanthine permease XanP O
yeeD	2.04	-4.11	2086363	2086590	-	228	conserved hypothetical protein Putative sulfur carrier protein YeeD Sulfurtransferase TusA
gpt	2.03	-7.30	255977	256435	+	459	guanine-hypoxanthine phosphoribosyltransferase, Xanthine-guanine phosphoribosyltransferase
fadB	2.02	-3.08	3605710	3607899	+	2190	Fatty acid oxidation complex subunit alpha

Table 5.4: The top 40 FeoAB-induced genes at OD 0.8 with ascorbate. Highlights indicate *feo* genes and *sodB* gens (Fur regulated, yellow), nitrate/nitrate respiration genes (light brown), amino acid metabolism genes (mid-plum), carbohydrate metabolism genes (red text), *ara* genes (light yellow), antitoxin/toxin (dark orange text) and tRNA genes (light blue). Those in bold were also in the top-40 up regulated list at OD 0.5 (Table 5.2).

gene_name	log2FoldChange	pvalue log10	start	end	strand	length	description
feoB	-17.33	-33.62	4097688	4100009	-	2322	*feoB*
feoAB	-13.17	-65.79	4097550	4100265	+	2716	*feoAB*
feoA	-10.54	-37.89	4100026	4100253	-	228	*feoA*
fruA reverse transcript	-4.25	-2.04	2263616	2263833	+	218	Fructose uptake
aroF	-3.47	-46.01	2738736	2739806	-	1071	3-deoxy-D-arabinoheptulosonate-7-phosphate synthase, tyrosine-repressible, amino acid biosytnthesis
csrC	-3.11	-23.33	3585401	3585645	-	245	CsrC is a small regulatory RNA controlling central carbon metabolism, biofilm formation and motility
napD	-3.08	-4.97	2306084	2306347	-	264	assembly protein for periplasmic nitrate reductase
csrC reverse transcript	-3.05	-14.79	3585439	3585620	+	182	CsrC is a small regulatory RNA controlling central carbon metabolism, biofilm formation and motility
tyrA	-2.98	-48.06	2737604	2738725	-	1122	fused chorismate mutase T and prephenate dehydrogenase; Prephenate dehydrogenase; tyrosine biosynthesis
trpE	-2.97	-49.44	1323098	1324660	-	1563	Anthranilate synthase component 1
trpCDE	-2.94	-40.82	1320667	1324668	+	4002	tryptophan biosynthesis
araB	-2.90	-24.37	68348	70048	-	1701	L-ribulokinase, carbohydrate kinases
isrC	-2.71	-1.74	2073452	2073655	+	204	small regulatory RNA
sgrS	-2.61	-17.09	77367	77593	+	227	Putative inhibitor of glucose uptake transporter SgrT
ygiUT rev trabscript	-2.58	-18.96	3166552	3167175	+	624	Motility quorum-sensing regulator, Antitoxin component of bacterial toxin-antitoxin system, MqsA
pheL	-2.57	-8.60	2736255	2736302	+	48	pheA gene leader peptide, amino acid biosynthesis, attenuator for pheA
glcD	-2.43	-20.57	3125178	3126677	-	1500	glycolate oxidase subunit, Glycolate oxidase subunit G, FAD linked oxidases
ygiU	-2.41	-32.18	3166904	3167200	-	297	predicted cyanide hydratase, MQSR mRNA interferase toxin MqsR, Motility quorum-sensing regulator, toxin of MqsA
araA	-2.39	-21.42	66835	68337	-	1503	L-arabinose isomerase
glcE	-2.38	-20.49	3124126	3125178	-	1053	Glycolate oxidase subunit
yehD	-2.36	-4.63	2195014	2195556	-	543	predicted fimbrial-like adhesin protein
araD	-2.34	-27.27	65855	66550	-	696	L-ribulose-5-phosphate 4-epimerase
pheA	-2.29	-30.30	2736401	2737561	+	1161	fused chorismate mutase P and prephenate dehydratase, Bifunctional chorismate mutase/prephenate dehydratase
ibpB	-2.26	-10.85	3773518	3773946	+	429	heat shock chaperone, Hsp20/alpha crystallin family
ygiT	-2.24	-27.30	3166507	3166902	-	396	predicted DNA-binding transcriptional regulator, Antitoxin MqsA
mtr	-2.22	-51.75	3304428	3305672	-	1245	tryptophan transporter of high affinity
trpD	-2.20	-19.81	1321503	1323098	-	1596	fused glutamine amidotransferase (component II) of anthranilate synthase and anthranilate phosphoribosyl transferase
ypdH	-2.19	-1.59	2513362	2513688	-	327	PTS system, Lactose/Cellobiose specific IIB subunit
glcF	-2.18	-17.23	3122892	3124115	-	1224	glycolate oxidase iron-sulfur subunit, 4Fe-4S dicluster domain
napF	-2.13	-6.23	2306337	2306831	-	495	ferredoxin-type protein periplasmic nitrate reductase 4Fe-4S dicluster domain
antisense tRNA transcript -	-2.12	-31.27	696989	697569	+	581	leuW-metT-glnUWV-metU antisense
rmf	-2.07	-12.57	1016137	1016304	+	168	ribosome modulation factor
antisense yciI	-2.04	-9.62	1312304	1312582	+	279	Hypothetical
ryeA	-1.98	-22.43	1924780	1925028	+	249	Also called sraC, sRNA, toxin-antitoxin system in S phase
antisense yfgO	-1.97	-2.68	2614278	2614459	+	182	transporter, unknown function
glcG	-1.95	-13.06	3122483	3122887	-	405	glycolate utilisation
araC	-1.94	-12.05	70387	71265	+	879	Arabinose operon regulatory protein
insB	-1.94	-1.37	2411473	2411976	-	504	Insertion element IS1 1 protein InsB
sodB	-1.93	-25.85	1737092	1737673	+	582	Superoxide dismutase [Fe]
insH	-1.91	-3.31	2068442	2069458	-	1017	IS5 transposase and trans-activator H for insertion sequence element IS5H

For the 40-most FeoAB repressed genes at OD 0.8 with ascorbate, the most abundant functional category was amino acid biosynthesis and uptake (16 genes). This suggests that FeoAB expression resulted in a reduced demand for amino acids indicative of a slower rate of growth. This suggestion is supported by the reduced expression of eight nucleotide metabolism and three tRNA genes (Table 5.5). One iron uptake gene, *fepA*, was also in the top-40 most supressed gene set. This gene is repressed by the Fe-Fur complex and the observed regulation is consistent with the induction of *sodB* since this gene is Fe-Fur induced (Table 5.4) (McHugh *et al.*, 2003).

Table 5.5: The top 40 FeoAB-repressed genes at OD 0.8 with ascorbate. Highlights indicate tRNA genes (light blue), amino acid metabolism genes (mid-plum), nucleotide metabolism (light plum), sulphur transport (mid blue), carbohydrate metabolism genes (red text) and TCA cycle and related genes (light green). Those in bold were also in the top-40 down regulated list at OD 0.5 (Table 5.3).

gene_name	log2FoldChange	pvalue log10	start	end	strand	length	description
gltT	4.12	-1.93	3468234	3468309	-	76	tRNA-Glu
pyrB	3.43	-30.00	4476140	4477075	-	936	aspartate carbamoyltransferase, Aspartate/ornithine carbamoyltransferase, carbamoyl-P binding domain
gltW	3.38	-1.44	2728025	2728100	-	76	tRNA-Glu
pyrI	3.26	-30.23	4475666	4476127	-	462	aspartate carbamoyltransferase regulatory subunit , metal binding domain
ygaW	3.15	-3.92	2797820	2798269	+	450	predicted inner membrane protein, L-alanine exporter AlaE
yjiY	2.81	-38.68	4593809	4595959	-	2151	predicted inner membrane protein, Pyruvate/proton symporter BtsT, Carbon starvation protein CstA
argI	2.61	-36.06	4481987	4482991	-	1005	ornithine carbamoyltransferase subunit I
argF	2.51	-23.40	288525	289529	-	1005	ornithine carbamoyltransferase 2 chain F, carbamoyl-P binding domain
yhhQ	2.47	-2.62	4030533	4031198	-	666	conserved inner membrane protein, QPTR Queuosine precursor transporter, Putative vitamin uptake transporter
carA	2.46	-18.98	29651	30799	+	1149	carbamoyl phosphate synthetase small subunit C glutamine amidotransferase
asnA	2.42	-13.60	3708534	3709526	-	993	asparagine synthetase, Aspartate--ammonia ligase
yjgF	2.28	-26.95	4475207	4475593	-	387	ketoacid-binding protein, RIDA iminobutanoate/2-iminopropanoate deaminase, Endoribonuclease L-PSP. Isoleucine biosynthesis
uraA	2.28	-21.40	2617527	2618816	-	1290	uracil transporter, Uracil permease
yeeE	2.24	-5.03	2086604	2087662	-	1059	predicted inner membrane protein, Sulphur transport
argD	2.23	-27.03	4150236	4151456	+	1221	bifunctional acetylornithine aminotransferase and succinyldiaminopimelate aminotransferase
artJ	2.17	-25.29	900266	900997	-	732	arginine transporter subunit, extracellular solute-binding proteins
argA	2.17	-36.81	2947898	2949229	+	1332	fused acetylglutamate kinase homolog (inactive) and amino acid N-acetyltransferase
yraQ	2.12	-19.19	3296953	3297993	-	1041	predicted permease
argC	2.10	-20.54	3480676	3481680	-	1005	N-acetyl-gamma-glutamylphosphate reductase NAD(P)-binding
aceE	2.05	-15.85	123017	125680	+	2664	pyruvate dehydrogenase, decarboxylase component, thiamin-binding, E1 component middle domain
argG	2.03	-44.87	3318492	3319835	+	1344	argininosuccinate synthetase, Argininosuccinate synthase
aceF	2.02	-16.64	125695	127587	+	1893	pyruvate dehydrogenase, dihydrolipoyltransacetylase component E2, Biotin-requiring enzyme
carB	2.02	-23.72	30817	34038	+	3222	carbamoyl-phosphate synthase large subunit, ATP binding domain. first step in pyrimidine and arginine biosynthesis
codB	2.01	-17.85	354146	355405	+	1260	cytosine permease
argH	1.98	-21.90	3478458	3479831	-	1374	argininosuccinate lyase, &
pta	1.94	-22.45	2420193	2422337	+	2145	Phosphate acetyl/butaryl transferase, acetate metabolism
pyrD	1.94	-12.49	1005190	1006200	+	1011	FMN-linked Dihydroorotate dehydrogenase (quinone) OS=Escherichia coli
argB	1.93	-18.29	3479892	3480665	-	774	acetylglutamate kinase
mqo	1.93	-18.27	2308442	2310088	-	1647	malate dehydrogenase FAD/NAD(P)-binding domain, Probable malate:quinone oxidoreductase, Malate:quinone oxidoreductase (Mqo)
pinH	1.92	-1.35	2781721	2781864	-	144	predicted invertase fragment
fepA	1.90	-37.96	609477	611717	-	2241	iron-enterobactin outer membrane transporter,TonB-dependent Receptor
lysY	1.85	-11.15	781569	781644	+	76	tRNA-Lys
ydjN	1.83	-3.44	1812648	1814039	+	1392	predicted transporter, L-cystine transporter TcyP
upp	1.82	-17.71	2618902	2619528	-	627	uracil phosphoribosyltransferase
yeiH	1.79	-15.54	2253051	2254100	+	1050	conserved inner membrane protein
marA	1.79	-18.52	1621288	1621671	+	384	DNA-binding transcriptional dual regulator, Multiple antibiotic resistance protein MarA
purF	1.78	-20.86	2434167	2435684	-	1518	amidophosphoribosyltransferase
artQ	1.78	-26.96	901956	902672	-	717	arginine transporter subunit, ABC transporter permease
guaB	1.77	-30.66	2631260	2632726	-	1467	IMP dehydrogenase,
yeeD	1.77	-2.29	2086363	2086590	-	228	conserved hypothetical protein Putative sulfur carrier protein YeeD Sulfurtransferase TusA

5.4.4 Impact of FeoAB in the presence of iron

The expression effect of FeoAB in the presence of 20 µM ferric citrate at OD 0.5 and 1.0 is summarised in Fig. 5.12. The results show that ~1200 and ~600 genes were upregulated, and that ~1000 and 500 genes were down-regulated, respectively, with ~twice as many genes differentially regulated at OD 0.5 than at OD 1.0. This difference may reflect a reduced degree of growth at the higher OD resulting in a general suppression of gene expression. The *feoAB*, *feoA* and *feoB* genes were induced by 6.7- to 19 log2 fold which confirms that the *feoAB* locus had been successfully induced, as in Fig. 5.11. Consideration of the 40 most FeoAB-induced genes at OD 0.5 shows that the major functional category affected is for those involved in anaerobic energy generation and fermentation (17 genes; Table 5.6), four of which were also induced under the identical conditions with ascorbate (Table 5.2). Two *cus* genes involved in copper export were also induced suggestive of excess copper, as were four amino acid metabolism genes and the *ftn* gene which is indicative of an excess cellular iron effect imposed

by FeoAB activity. For the 40 must repressed genes at OD 0.5, the vast majority (32) were Fe-Fur repressed genes with roles in iron uptake, iron release or substitution of iron-dependent functions (Table 5.7). This largescale repression of Fur repressed genes suggests that the induction of *feoAB* results in raised cellular iron that thus raises the degree of Fe-Fur repression when excess is available for FeoAB to import. Alternatively, FeoAB could directly impact Fe-Fur dependent gene expression through interaction with Fe-Fur in a fashion that enhances repression activity of Fe-Fur. It should be noted that with ascorbate only two Fe-Fur repressed genes were further repressed at OD 0.5 (*efeU* and *efeO*; Table 5.3). Thus, the repression of the Fe-Fur regulon was much greater when ferric citrate was provided than in the presence of ascorbate.

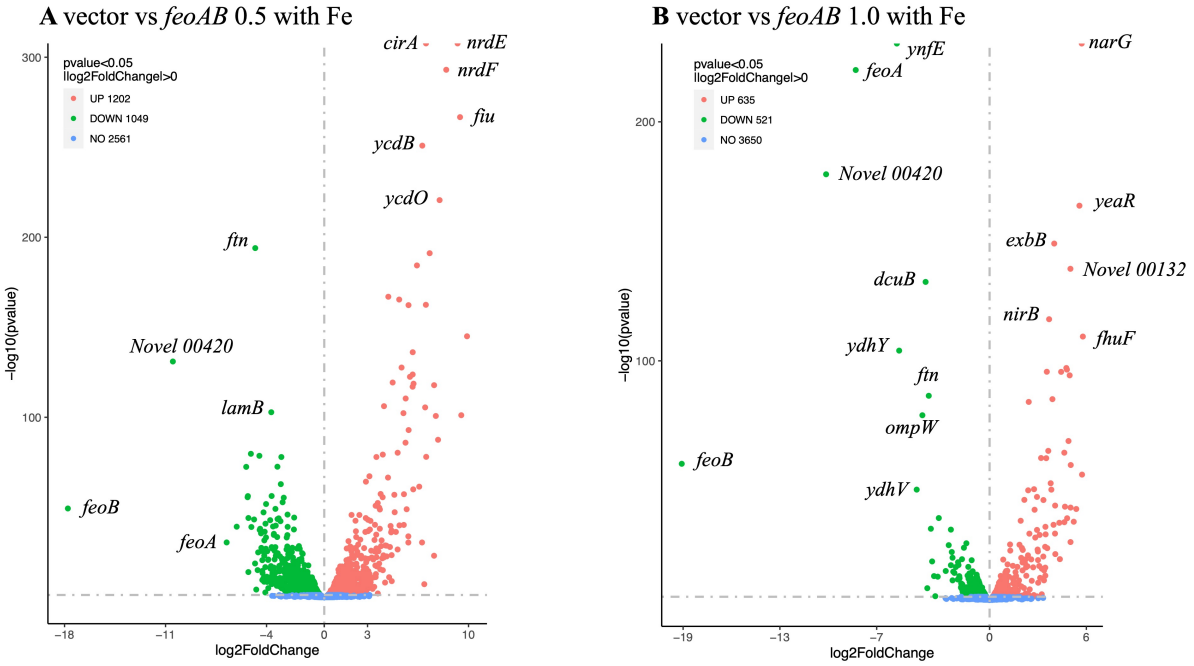

Figure 5.12: Volcano plot of differentially expressed genes in response to *feoAB* induction with iron. (**A**) Vector versus *feoAB* at OD 0.5. (**B**) Vector versus *feoAB* at OD 1.0. The identities of the *feoA* and *feoB* reads are indicated, and the number of significantly (>2 fold) induced and repressed transcripts is also provided as determined by DESeq2. "Novel 00420" is *feoAB* and "Novel 00132" is *narK*. Other highly regulated genes, or those with a high significance score, are also labelled; many are Fur regulated.

Table 5.6: The top 40 FeoAB-induced genes at OD 0.5 with ferric citrate. Highlights indicate *feo* genes and *ftn* gene (yellow), nitrate/nitrate respiration genes (light brown), amino acid metabolism genes (mid-plum), carbohydrate metabolism genes (red text), anaerobic C4-dicarbioxylate transport genes (brown), hydrogenase genes (mid-brown) and other metals (orange). Those in bold were also in the top-40 up regulated list at OD 0.5 (Table 5.2).

gene_name	log2FoldChange	pvalue log10	start	end	strand	length	description
feoB	-17.77	-49.35	4097688	4100009	-	2322	*feoB*
feoAB	-10.49	-131.00	4097550	4100265	+	2716	*feoAB*
feoA	-6.76	-30.49	4100026	4100253	-	228	*feoA*
nirD	-6.07	-39.23	4143539	4143865	-	327	nitrite reductase, small subunit, Rieske-like [2Fe-2S] domain
ykgE	-5.41	-72.47	320832	321551	+	720	predicted oxidoreductase, putative lactate utilization oxidoreductase
nrfB	-5.31	-55.61	4292835	4293401	+	567	nitrite reductase, formate-dependent, penta-heme cytochrome c
nirC	-5.29	-56.23	4142607	4143413	-	807	Formate/nitrite transporter
dcuC	-5.26	-14.03	653806	656390	-	2585	anaerobic C4-dicarboxylate transport
nrfC	-5.26	-44.06	4293398	4294069	+	672	formate-dependent nitrite reductase, 4Fe-4S dicluster domain
yebN/mntP	-5.08	-79.72	1907402	1907968	+	567	conserved inner membrane protein, Probable manganese efflux pump MntP
hybA	-5.05	-39.07	3142810	3143796	-	987	hydrogenase 2 4Fe-4S ferredoxin-type component
adiY	-4.86	-43.25	4341846	4342607	-	762	DNA-binding transcriptional activator
nrfA	-4.80	-18.80	4291354	4292790	+	1437	nitrite reductase, formate-dependent, Cytochrome c-552
ftn	-4.78	-193.99	1990853	1991350	+	498	cytoplasmic ferritin iron storage protein
cusC	-4.71	-4.31	594823	596196	+	1374	copper/silver efflux system, outer membrane component
flu	-4.62	-15.12	2073676	2076795	+	3120	antigen 43 (Ag43), phase-variable biofilm formation autotransporter, Adhesin of bacterial autotransporter system, probable stalk
napB	-4.58	-24.97	2301603	2302052	-	450	nitrate reductase small, cytochrome C550 subunit
artJ	-4.50	-78.61	900266	900997	-	732	arginine transporter subunit
yohK	-4.47	-37.44	2234353	2235048	+	696	predicted inner membrane protein, export of 3-hydroxypropanoate
narJ	-4.44	-38.08	1286716	1287426	+	711	molybdenum-cofactor-assembly chaperone subunit (delta subunit) of nitrate reductase
narI	-4.38	-35.53	1287426	1288103	+	678	nitrate reductase gamma (cytochrome b) subunit
hypC	-4.36	-27.47	2850520	2850792	+	273	protein required for maturation of hydrogenases 1 and 3
yqeC	-4.33	-25.75	3012943	3013713	-	771	selenium cofactor biosynthesis protein
nrfD	-4.30	-14.65	4294066	4295022	+	957	formate-dependent nitrite reductase
ybcV	-4.29	-9.63	578407	578817	-	411	hypothetical protein, DUF1398
yjiM	-4.29	-20.64	4569379	4570530	-	1152	predicted 2-hydroxyglutaryl-CoA dehydratase, D-component
flgB	-4.28	-13.48	1132595	1133011	+	417	flagellar component of cell-proximal portion of basal-body rod
hybO	-4.21	-10.66	3143799	3144917	-	1119	hydrogenase 2 C small subunit
yohJ	-4.21	-47.20	2233958	2234356	+	399	conserved inner membrane protein, efflux pump for the microcin J25 antibiotic
fruB	-4.17	-8.67	2265699	2266829	-	1131	fused fructose-specific PTS enzyme IIA component and HPr component
argI	-4.16	-23.14	4481987	4482991	-	1005	Aspartate/ornithine carbamoyltransferase
ygaW	-4.16	-9.23	2797820	2798269	+	450	predicted inner membrane protein, L-alanine exporter AlaE
hypD	-4.15	-31.63	2850792	2851913	+	1122	protein required for maturation of hydrogenases
narH	-4.13	-36.45	1285181	1286719	+	1539	nitrate reductase 1, beta (Fe-S) subunit
ygfJ	-4.09	-16.78	3013816	3014394	+	579	conserved hypothetical protein, MOCA_ECOLI Molybdenum cofactor cytidylyltransferase
cusF	-4.08	-2.70	596354	596686	+	333	periplasmic copper-binding protein, Cation efflux system protein
ykgF	-4.07	-40.90	321562	322989	+	1428	predicted amino acid dehydrogenase with NAD(P)-binding domain and ferridoxin-like domain
yjjW	-4.05	-26.99	4619360	4620223	-	864	predicted pyruvate formate lyase activating enzyme, 4Fe-4S single cluster domain
fruK	-4.04	-33.26	2264761	2265699	-	939	fructose-1-phosphate kinase
ydhY	-4.03	-51.82	1755565	1756191	-	627	predicted 4Fe-4S ferridoxin-type protein, predicted anaerobic oxidoreductase complex

Table 5.7: The top 40 FeoAB-repressed genes at OD 0.5 with ferric citrate. Highlights indicate Fe-Fur repressed genes (yellow), amino acid metabolism genes (mid-plum) and carbohydrate metabolism genes (red text).

gene_name	log2FoldChange	pvalue Log10	start	end	strand	length	description
nrdH	9.90	-145.0	2799379	2799624	+	246	glutaredoxin-like protein, ribonucleotide reductase
nrdI	9.50	-101.2	2799621	2800031	+	411	ribonucleotide reduction, Flavodoxin like,
fiu	9.41	-266.7	839671	841953	-	2283	predicted iron outer membrane transporter, catecholate siderophore receptor, TonB-dependent Receptor
nrdE	9.24	0.0	2800004	2802148	+	2145	ribonucleoside-diphosphate reductase alpha subunit, Ribonucleotide reductase
nrdF	8.46	-293.0	2802158	2803117	+	960	ribonucleoside-diphosphate reductase 2, beta subunit, ferritin-like, Ribonucleotide reductase, small chain
efeO	7.99	-220.6	1082665	1083792	+	1128	Iron uptake system component Cupredoxin-like domain and Imelysin domain
fepA	7.89	-87.5	609477	611717	-	2241	iron-enterobactin outer membrane transporter, TonB-dependent Receptor
fes	7.73	-100.7	612038	613162	+	1125	enterobactin/ferric enterobactin esterase
yncE	7.61	-117.8	1525021	1526082	+	1062	conserved hypothetical protein, YNCE, Fe-Fur repressed
ybdZ	7.61	-23.1	613165	613383	+	219	conserved hypothetical protein, Enterobactin biosynthesis protein, MbtH-like protein
fhuF	7.31	-191.1	4609555	4610343	-	789	ferric iron reductase involved in ferric hydroximate transpor
entB	7.07	-78.0	626917	627774	+	858	isochorismatase, Enterobactin synthase component
cirA	7.05	0.0	2248112	2250103	-	1992	ferric iron-catecholate outer membrane transporter, &TonB dependent receptor
entE	7.04	-162.5	625293	626903	+	1611	3-dihydroxybenzoate-AMP ligase component of enterobactin synthase multienzyme complex
ybdA	6.99	-105.5	621523	622773	+	1251	predicted transporter,Enterobactin exporter EntS
fecA	6.93	-7.3	4519033	4521357	-	2325	ferric citrate outer membrane transporter, onB dependent receptor
efeB	6.80	-250.9	1083798	1085069	+	1272	EfeB peroxidase EfeB, Dyp-type peroxidase family
yjjZ	6.78	-30.5	4610484	4610720	+	237	Uncharacterized protein (DUF1435)
yjiY	6.58	-61.5	4593809	4595959	-	2151	predicted inner membrane protein, Pyruvate/proton symporter BtsT Carbon starvation protein CstA
entF	6.42	-184.4	613380	617261	+	3882	enterobactin synthase multienzyme complex component
fecI	6.19	-118.7	4522394	4522915	-	522	RNA polymerase sigma factor 19, regulation of fec genes (ferric citrate uptake)
fepC	6.17	-60.0	618607	619422	-	816	iron-enterobactin transporter subunit, ABC transporter
fepB	6.13	-136.1	622777	623733	-	957	iron-enterobactin transporter subunit, periplasmic binding protein
ybiX	6.13	-123.8	838952	839629	-	678	conserved hypothetical protein,PKHD-type hydroxylase YbiX 2OG-Fe(II) oxygenase superfamily, Fe-Fur repressed
fhuE	6.12	-117.0	1160939	1163128	-	2190	ferric-rhodotorulic acid outer membrane transporter, TonB-dependent Receptor
entA	5.94	-122.5	627774	628520	+	747	3-dihydro--dihydroxybenzoate dehydrogenase, enterobactin biosynthesis
fepG	5.85	-92.9	619419	620411	-	993	iron-enterobactin transporter subunit
phoH	5.84	-162.3	1085414	1086478	+	1065	nucleoside triphosphate hydrolase domain, phosphate regulon, mamagement of phosphate
yddA	5.83	-33.9	1579371	1581056	-	1686	putative multidrug efflux ABC transporter
bfd	5.83	-30.4	4173425	4173619	+	195	bacterioferritin-associated ferredoxin, [2Fe-2S] binding domain, iron release from Bfr
puuA	5.71	-48.9	1361204	1362622	-	1419	gamma-Glu-putrescine synthase, Glutamine synthetase, catalytic domain
fepD	5.64	-110.4	620408	621412	-	1005	iron-enterobactin transporter subunit
fecR	5.63	-85.9	4521444	4522397	-	954	transmembrane signal transducer for ferric citrate transport
csgF	5.53	-57.3	1101952	1102368	-	417	predicted transport protein, Curli production assembly/transport component Type VIII secretion system
csgE	5.51	-40.2	1102393	1102782	-	390	predicted transport protein, Curli production assembly/transport component
yqjH	5.49	-102.3	3214383	3215147	-	765	predicted siderophore reductase, FAD-binding domain
sufB	5.36	-127.6	1764236	1765723	-	1488	component of SufBCD complex, FeS cluster assembly system, Fe-Fur repressed
puuP	5.21	-40.0	1359516	1360901	-	1386	putrescine importer, Amino acid permease
sufC	5.20	-165.4	1763480	1764226	-	747	component of SufBCD complex, iron-sulphur cluster biosynthesis, Fur repressed
ybdB	5.09	-80.3	628523	628936	+	414	Proofreading thioesterase EntH, enterobactin production

At OD 1.0, the *feoAB* genes were again the most highly induced, as expected (Table 5.8). From the top 40 FeoAB-induced genes, the most abundant category was the anaerobic energy generation gene set (12 genes). These may be induced through an FNR activation effect (Kang *et al.*, 2005) or the induction may be related to the high iron-dependence of the encoded proteins (Fe-S cluster rich) whereby iron-rationing genes are subject to Fe-Fur induction under high iron through RyhB. This suggestion is supported by the FeoAB-related up regulation of *ftn* and *ompW* (Fe-Fur induced genes; (McHugh *et al*., 2003; Table 5.8). No other major functional categories were apparent. For the 40-most FeoAB repressed genes at OD 1 (Table 5.9), a clear pattern was apparent similar to that seen at OD 0.5 (Table 5.7). As at OD 0.5, the major functional category effected was the iron-metabolism genes (25 genes involved in iron acquisition and combating iron restriction were down regulated). Many of these genes were the same as those seen at OD 0.5 (Table 5.7); indeed, 20 of the top 40 most FeoAB-repressed genes at OD 1 were also included in the top 40 most FeoAB repressed genes at 0.5 OD. This indicates good consistency between the two datasets. The only other significant category of genes affected were those involved in anaerobic energy generation, many of which encode iron-containing proteins and would thus be expected to be induced by any iron delivered by FeoAB, not repressed. Thus, the FeoAB-repression effect observed is unlikely to be related to FeoAB-mediated iron delivery. Indeed, 12 anaerobic energy generating genes were induced by FeoAB (Table 5.8). This regulatory effect may relate to the nitrate/nitrite expression dependence of the anaerobic energy generation genes that are repressed by FeoAB and so the effect could be caused by the NarXL/NarQP (Stewart and Bledsoe, 2003) two-component regulators. Such an effect was not seen at OD 0.5 (Tables 5.6 and 5.7).

Table 5.8: The top 40 FeoAB-induced genes at OD 1.0 with ferric citrate. Highlights indicate Fur-regulated genes (iron metabolism, yellow), nitrate/nitrate respiration genes (light brown), carbohydrate metabolism genes (red text), anaerobic C4-dicarbioxylate transport genes (brown), nucleotide metabolism (light plum) and genes involved in metabolism of other (not iron) metals (orange). Those in bold were also in the top-40 up regulated list at OD 0.5 (Table 5.6).

gene_name	log2FoldChange	pvalue Log10	start	end	strand	length	description
feoB	-19.08	-56.9	4097688	4100009	-	2322	*feoB*
feoAB	-10.13	-178.1	4097550	4100265	+	2716	*feoAB*
feoA	-8.30	-221.7	4100026	4100253	-	228	*feoA*
ynfE	-5.75	0.0	1659783	1662209	+	2427	oxidoreductase subunit, Putative dimethyl sulfoxide reductase chain, Molydopterin dinucleotide binding domain, Fe4S4 domain
ydhY	-5.61	-104.3	1755565	1756191	-	627	predicted 4Fe-4S ferridoxin-type protein
ydhV	-4.52	-46.1	1753442	1755544	-	2103	predicted oxidoreductase, Aldehyde ferredoxin oxidoreductase
ompW	-4.17	-77.2	1315734	1316372	+	639	outer membrane protein, porin, Fe-Fur induced
dcuB	-3.97	-133.0	4352082	4353422	-	1341	Anaerobic c4-dicarboxylate transporter
flu	-3.86	-4.9	2073676	2076795	+	3120	antigen 43 (Ag43) phase-variable biofilm formation autotransporte, Adhesin of bacterial autotransporter system, probable stalk
ftn	-3.77	-85.4	1990853	1991350	+	498	cytoplasmic ferritin iron storage protein &
ynfF	-3.64	-29.8	1662270	1664693	+	2424	oxidoreductase subunit, Probable dimethyl sulfoxide reductase chain, Molybdopterin oxidoreductase. Fe4S4 domain
yeeR	-3.56	-16.1	2076916	2078448	+	1533	predicted membrane protein
isrC	-3.44	-9.9	2073452	2073655	+	204	sRNA
ydaC	-3.37	-1.5	1415245	1415454	-	210	hypothetical protein, RCBA, Double-strand break reduction protein
ydhY reverse	-3.21	-9.7	1755689	1756248	+	560	ydhY encoding a 4Fe-4S ferredoxin, antisense transcript
frmB	-3.15	-34.2	4350358	4352004	-	1647	anaerobic class I fumarate hydratase, anaerobic
yeeS	-2.72	-12.1	2078445	2078891	+	447	predicted DNA repair protein, RadC-like JAB domain
yeiT	-2.53	-22.9	2237367	2238605	+	1239	predicted oxidoreductase, NAD-dependent dihydropyrimidine dehydrogenase subunit PreT, pyridine nucleotide-disulphide oxidoreductase, 4Fe-4S cluster. Degradation of pyrimidine bases
mbN	-2.40	-14.5	1907402	1907968	+	567	Probable manganese efflux pump MntP
adhE	-2.40	-29.4	1297023	1299698	-	2676	Aldehyde dehydrogenase family, Iron-containing alcohol dehydrogenase, adhE antisense
adhE antisense	-2.34	-20.0	1296954	1299847	+	2894	Aldehyde dehydrogenase family, Iron-containing alcohol dehydrogenase
frdA	-2.30	-17.6	4385190	4386998	-	1809	fumarate reductase (anaerobic)
ydhW	-2.29	-8.2	1752791	1753438	-	648	hypothetical protein, FNR induced
yqeC	-2.25	-11.8	3012943	3013713	-	771	selenium cofactor biosynthesis protein
ynfG	-2.18	-11.3	1664704	1665321	+	618	oxidoreductase Fe-S subunit , Probable anaerobic dimethyl sulfoxide reductase chain
dmsA	-2.09	-13.8	941381	943825	+	2445	dimethyl sulfoxide reductase, anaerobic subunit, Molydopterin dinucleotide binding domain
frd	-1.97	-8.5	4383721	4387064	+	3344	Fumarate reductase flavoprotein, 4Fe-4S dicluster domain, 2Fe-2S iron-sulfur cluster binding domain
yeiA	-1.96	-15.7	2238599	2239834	+	1236	predicted oxidoreductase, NAD-dependent dihydropyrimidine dehydrogenase subunit PreA ,4Fe-4S dicluster domain
puuE	-1.93	-14.6	1367264	1368529	+	1266	GABA aminotransferase, putrascine utilisation
puuC	-1.88	-9.9	1364457	1365944	+	1488	gamma-Glu-gamma-aminobutyraldehyde dehydrogenase, NADP/NAD-dependent aldehyde dehydrogenase. putrascine utilisation
puuB	-1.86	-9.1	1365946	1367226	+	1281	gamma-Glu-putrescine oxidase, putrascine utilisation
ydhX	-1.77	-5.1	1752059	1752727	-	669	predicted 4Fe-4S ferridoxin-type protein, Uncharacterized ferredoxin-like protein
citC	-1.77	-5.4	650021	651079	-	1059	citrate lyase synthetase,
frdB	-1.76	-6.9	4384463	4385197	-	735	fumarate reductase (anaerobic) Fe-S subunit
phoH	-1.73	-4.7	1085414	1086478	+	1065	nucleoside triphosphate hydrolase domain, phosphate regulon, mamagement of phosphate
sRNA00018	-1.71	-17.0	1991229	1991284	-	56	sRNA between sdiA and yecC
frdC	-1.70	-6.6	4384057	4384452	-	396	fumarate reductase (anaerobic) membrane anchor subunit
yqeB	-1.69	-6.4	3011270	3012895	-	1626	conserved hypothetical protein with NAD(P)-binding Rossman fold, selenium-dependent purine catabolism
pntA reverse	-1.67	-3.4	1678050	1679626	+	1577	pyridine nucleotide transhydrogenase
ymgB	-1.64	-2.6	1217946	1218212	+	267	hypothetical protein, Regulatory protein AriR, Biofilm development protein YmgB/AriR

Table 5.9: The top 40 FeoAB-repressed genes at OD 1.0 with ferric citrate. Highlights indicate genes involved in iron acquisition (yellow) and nitrate/nitrate respiration genes (light brown). Those in bold were also in the top-40 down regulated list at OD 0.5 (Table 5.7).

gene_name	log2FoldChange	pvalue Log10	start	end	strand	length	description
fhuF	5.78	-110.2	4609555	4610343	-	789	ferric iron reductase involved in ferric hydroximate transport
narH	5.73	-52.4	1285181	1286719	+	1539	nitrate reductase beta (Fe-S) subunit 4Fe-4S dicluster domain
narG	5.71	0.0	1281441	1285184	+	3744	nitrate reductase alpha subunit|;Molydopterin dinucleotide binding domain
yeaR	5.57	-164.9	1881303	1881662	-	360	Uncharacterized protein (DUF1971). Nitrate and nitrite induced anaerobically by NarL
ybdZ	5.37	-38.0	613165	613383	+	219	conserved hypothetical protein, Enterobactin biosynthesis protein, MbtH-like protein
narJ	5.22	-32.7	1286716	1287426	+	711	molybdenum-cofactor-assembly chaperone subunit (delta subunit) of nitrate reductase
narK	5.03	-56.4	1279534	1280925	+	1392	nitrate/nitrite transporter
fes	5.02	-38.6	612038	613162	+	1125	ferric enterobactin esterase, iron release from ferric enterobactin, Fur repressed
nirC	5.02	-24.2	4142607	4143413	-	807	Formate/nitrite transporter
Novel00132	5.01	-138.5	1281686	1288619	-	6934	Nitrate reductase, narK-I locus
fepC	4.97	-93.9	618607	619422	-	816	iron-enterobactin transporter subunit
yoaG	4.89	-66.5	1881117	1881299	-	183	hypothetical protein, DUF1869. Nitrate and nitrite induced anaerobically by NarL
yncE	4.81	-34.1	1525021	1526082	+	1062	conserved hypothetical protein, Fur repressed
fepD	4.80	-96.3	620408	621412	-	1005	iron-enterobactin transporter subunit
fepG	4.76	-97.0	619419	620411	-	993	iron-enterobactin transporter subunit
narI	4.67	-39.0	1287426	1288103	+	678	nitrate reductase gamma (cytochrome b) subunit
fiu	4.64	-32.5	839671	841953	-	2283	predicted iron outer membrane transporter, Catecholate siderophore receptorTonB dependent receptor|PF07715:TonB-dependent
ybdA	4.63	-61.6	621523	622773	+	1251	Enterobactin exporter EntS
fdnG	4.44	-95.4	1549115	1552162	+	3048	formate dehydrogenase-N, alpha subunit, nitrate-inducible, Molydopterin dinucleotide binding domain
yoeA	4.36	-17.0	2070772	2071164	+	393	predicted disrupted hemin or colicin receptor, &TonB-dependent Receptor
bfd	4.32	-32.2	4173425	4173619	+	195	bacterioferritin-associated ferredoxin, [2Fe-2S] binding domain, release of iron from Bfr
cirA	4.08	-19.2	2248112	2250103	-	1992	ferric iron-catecholate outer membrane transporter,TonB dependent receptor
nirD	4.06	-39.5	4143539	4143865	-	327	nitrite reductase, small subunit, Rieske-like [2Fe-2S] domain
efeO	4.06	-27.7	1082665	1083792	+	1128	conserved hypothetical protein Iron uptake system component Cupredoxin-like domain and Imelysin domain
exbB	4.01	-149.1	3149906	3150640	-	735	membrane spanning protein in TonB-ExbB-ExbD complex, ferrisiderophore uptake
anti-fdnG	3.96	-31.4	1549555	1550359	-	805	anti-sense fdnG, notrate dependent formate dehydrogenase
fepB	3.90	-84.0	622777	623733	-	957	iron-enterobactin transporter subunit, Periplasmic binding protein
exbD	3.83	-46.1	3149474	3149899	-	426	membrane spanning protein in TonB-ExbB-ExbD complex, &ferri-siderophore uptake
yojI	3.79	-48.8	2310306	2311949	-	1644	fused predicted multidrug transport subunits and membrane component and ATP-binding component of ABC superfamily
nirB	3.69	-117.4	4143862	4146405	-	2544	nitrite reductase large subunit BFD-like [2Fe-2S] binding domain,4Fe-4S domain
entF	3.64	-62.3	613380	617261	+	3882	enterobactin synthase multienzyme complex component,Thioesterase domain
entE	3.58	-21.6	625293	626903	+	1611	3-dihydroxybenzoate-AMP ligase component of enterobactin synthase multienzyme complex
fecR	3.55	-95.4	4521444	4522397	-	954	transmembrane signal transducer for ferric citrate transport regulation
fecI	3.51	-59.3	4522394	4522915	-	522	RNA polymerase sigma 19 factor, ferric citrate uptake regulator
nrdE	3.47	-27.4	2800004	2802148	+	2145	ribonucleoside-diphosphate reductase alpha subunit, Fe-Fur repressed
anti-exbBD	3.46	-30.6	3149308	3150636	+	1329	exbBD antisense - iron uptake across outer membrane, TonB dependent
nrfD	3.46	-10.1	4294066	4295022	+	957	formate-dependent nitrite reductase, membrane subunit
efeB	3.45	-13.5	1083798	1085069	+	1272	conserved hypothetical protein, peroxidase EfeB, Dyp-type peroxidase family
ydiE	3.44	-22.2	1791327	1791518	+	192	Hemin uptake protein hemP, Fe-Fur repressed
nrdH	3.38	-12.3	2799379	2799624	+	246	glutaredoxin-like protein H- Fe-Fur repressed ribonucleotide reductase

5.4.5 Impact of FeoABC on global gene expression in the presence of ascorbate

Fig. 5.13 summarizes the effect of *feoABC* induction at OD 0.5 and 0.8 in the presence of ascorbate. The results confirm that the *feoABC* genes were greatly induced (10.3 to 18.7 log2 fold) with respect to the vector control (Fig. 5.13), supporting the possibility that any regulatory response to FeoABC induction may be detectable. Roughly equal numbers of genes were up and down regulated by FeoABC, with slightly higher (20%) total numbers at OD 0.8 (Fig. 5.13).

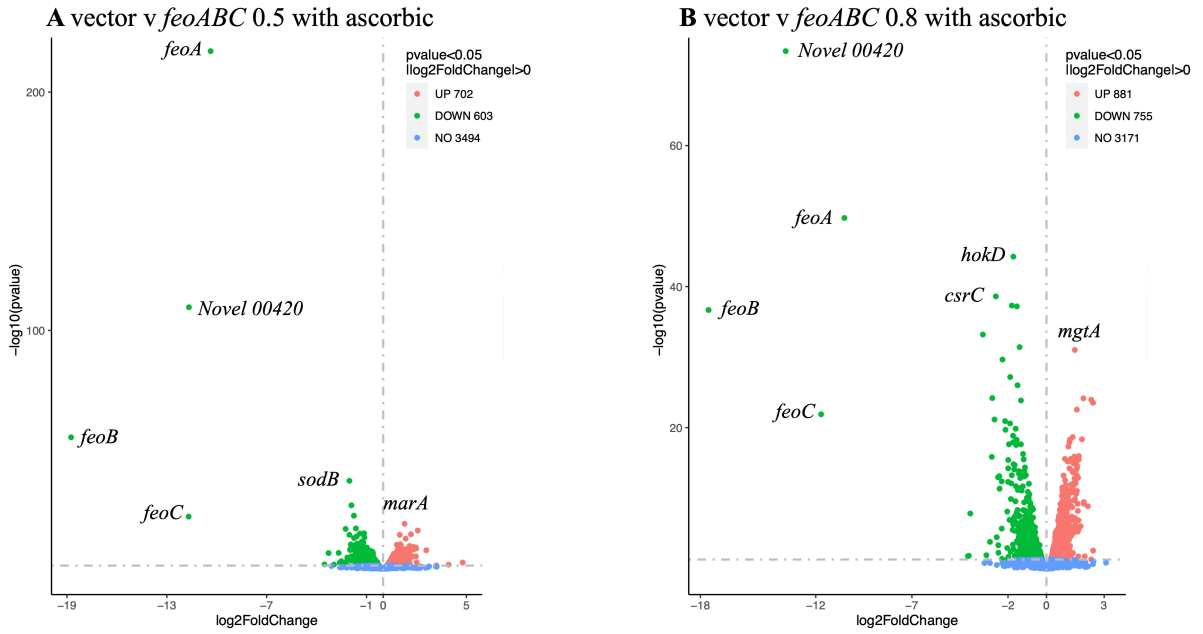

Figure 5.13: Volcano plot of differentially expressed genes in response to *feoABC* induction with ascorbate. (**A**) Vector versus *feoABC* at OD 0.5. (**B**) Vector versus *feoABC* at OD 0.8. The identities of the *feoA*, *feoB* and *feoC* reads are indicated, and the number of significantly (>2 fold) induced and repressed transcripts is also provided as determined by DESeq2. "Novel 00420" corresponds to a *feoAB* transcript.

The top 40 FeoABC-induced and -suppressed genes in the presence of ascorbate at OD 0.5 and 0.8 are shown in Table 5.10. The results show that the *feoC* gene is now also strongly induced (11.7 log2 fold increase), alongside *feoA* and *feoB*, with respect to the vector control. Thus, results should be similar to those presented in Table 5.2 for *feoAB*. No major effect on any functional gene category was apparent in the FeoABC-induced gene list, although the *sodB* Fe-

Fur induced gene was included in the top 20 which is consistent with raised cellular iron levels mediated by FeoABC activity. An *sufB* (a Fe-Fur repressed gene) antisense transcript also showed raised levels, although it is unclear what the biological significance of this transcript might be. Interestingly, unlike for the FeoAB induced gene set (Table 5.2), no anaerobic energy generation genes were included (Table 5.10) suggesting differences between the responses observed in the presence and absence of FeoC. For the top 20 most FeoABC-repressed genes, the major functional category affected was amino acid metabolism (eight genes; Table 5.10). This resembles the findings with FeoAB induction where seven such genes were suppressed, along with eight tRNA related genes (Table 5.3). Indeed, two tRNA genes were also suppressed in the FeoABC data (Table 5.10). Another similarity was the suppression of *efeU* in both cases, a known Fe-Fur repressed (and acid induced) gene involved in iron uptake. The second and third most FeoABC repressed genes specified 23S rRNA transcripts which should have been largely removed by the ribosome depletion treatment.

Table 5.10: The top 40 FeoABC-induced and repressed genes at OD 0.5 with ascorbate. Highlights indicate *feo* genes and iron metabolism genes (Fur regulated, yellow), amino acid metabolism genes (mid-plum), tRNA genes (light blue) and sulphur transport (mid blue). Those in bold were also in the top-40 down regulated list at OD 0.5 (Table 5.3).

gene_name	log2FoldChange	pvalue log10	start	end	strand	length	description
feoB	-18.75	-55.16	4097688	4100009	-	2322	*feoB*
yhgG	-11.69	-21.87	4097452	4097688	-	237	*feoC*
feoAB	-11.67	-109.72	4097550	4100265	+	2716	*feoAB*
feoA	-10.37	-217.20	4100026	4100253	-	228	*feoA*
insH	-3.53	-1.81	3128834	3129850	+	1017	IS5 transposase and trans-activator
isrC	-3.28	-6.56	2073452	2073655	+	204	sRNA
ydcC	-2.96	-1.75	1533530	1534666	+	1137	conserved hypothetical protein, H repeat-associated putative transposase. Transposase DDE domain
Novel00163	-2.68	-6.64	1765435	1765548	+	114	sufB antisense
flu	-2.61	-2.52	2073676	2076795	+	3120	antigen 43 (Ag43), phase-variable biofilm formation autotransporter, Adhesin of bacterial autotransporter system, probable stalk
yeeT	-2.58	-1.87	2078954	2079175	+	222	hypothetical protein (DUF987)
yeeR	-2.52	-3.16	2076916	2078448	+	1533	predicted membrane protein
yciG	-2.35	-1.58	1317570	1317749	-	180	hypothetical protein, Stress-induced bacterial acidophilic repeat motif
ibpB	-2.26	-16.68	3773518	3773946	+	429	heat shock chaperone, Hsp20/alpha crystallin family
pheL	-2.20	-3.03	2736255	2736302	+	48	pheA gene leader peptide, phenylalanine synthesis
yeeS	-2.16	-4.70	2078445	2078891	+	447	predicted DNA repair protein, RadC-like JAB domain
sodB	-2.03	-36.87	1737092	1737673	+	582	superoxide dismutase [Fe]
Novel00053	-2.03	-14.22	574804	576050	+	1247	antisense prophage gene transcript (insH-nmpC)
Novel00408	-1.99	-8.12	3964335	3965629	+	1295	yhjE antisense. Major Facilitator Superfamily, Sugar (and other) transporter
Novel00193	-1.98	-7.83	2009887	2010127	+	241	yedD antisense, YedD-like protein
Novel00139	-1.94	-10.18	1320667	1324668	+	4002	antisense trpCDE, trytophan biosynthesis

gene_name	log2FoldChange	pvalue log10	start	end	strand	length	description
ykiB	4.78	-2.60	389121	389339	-	219	hypothetical protein
rrlB	3.93	-1.68	3465137	3468040	-	2904	23S ribosomal RNA
rrlA	3.19	-1.37	3596258	3599162	-	2905	23S ribosomal RNA-
ygaW	2.59	-7.75	2797820	2798269	+	450	predicted inner membrane protein, L-alanine exporter AlaE
lysY	2.08	-16.03	781569	781644	+	76	tRNA-Lys
yeeE	2.01	-2.59	2086604	2087662	-	1059	predicted inner membrane protein, Sulphur transport
argC	1.98	-8.54	3480676	3481680	-	1005	N-acetyl-gamma-glutamylphosphate reductase, Arg biosynthesis
argF	1.97	-5.15	288525	289529	-	1005	ornithine carbamoyltransferase
yraQ	1.97	-8.87	3296953	3297993	-	1041	predicted permease
argD	1.83	-9.15	4150236	4151456	+	1221	bifunctional acetylornithine aminotransferase and succinyldiaminopimelate aminotransferase
efeU	1.83	-8.08	1081778	1082607	+	830	Putative inactive ferrous iron permease EfeU, Iron permease FTR1 family
argA	1.80	-8.50	2947898	2949229	+	1332	fused acetylglutamate kinase homolog (inactive) and amino acid N-acetyltransferase
asnA	1.76	-5.18	3708534	3709526	-	993	asparagine synthetase, Aspartate--ammonia ligase
lysW	1.67	-14.45	781265	781340	+	76	tRNA-Lys
cysJ	1.63	-1.34	2888755	2890554	-	1800	sulfite reductase alpha subunit flavoprotein
rbsA	1.63	-8.17	3701398	3702903	-	1506	fused D-ribose transporter subunits and ATP-binding components ABC superfamily Ribose import ATP-binding protein, ABC transporter
yeeD	1.60	-4.38	2086363	2086590	-	228	conserved hypothetical protein Putative sulfur carrier protein YeeD Sulfurtransferase TusA
adiY	1.58	-2.09	4341846	4342607	-	762	DNA-binding transcriptional activator, a regulatory protein that controls adiA, which produces biodegradative arginine decarboxylase, for acid resistance.
ydjX	1.58	-2.50	1835115	1835825	+	711	predicted inner membrane protein,
artP	1.58	-9.51	903428	904156	-	729	arginine transporter subunit, ABC transporter

For the samples collected at OD 0.8, a summary of the 40 most FeoABC-induced and -suppressed genes is provided in Table 5.11. The results show that of the 20 top FeoABC induced genes, eight (excluding *feo* genes) were also included in the equivalent FeoAB data set (Table 5.4), which indicates good correspondence between the two data sets, as expected. The amino acid metabolism group was the most abundant gene category induced; all four of which were also induced by FeoAB (Table 5.4). In addition, of the four carbon metabolism genes induced by FeoABC at OD 0.8, three were also upregulated by FeoAB (Table 5.4). Thus, there is good agreement between the FeoAB and FeoABC data at OD 0.8 with ascorbate. For the top 20 most FeoABC suppressed genes (Table 5.11), 17 were also included in the corresponding gene set for FeoAB (Table 5.5) which indicates a very strong correlation between the FeoAB and FeoABC expression data. Indeed, the major gene categories suppressed where the amino acid metabolism (8 genes) and the nucleotide metabolism (5 genes) genes, as was the case for the FeoAB data (Table 5.5). The only Fur repressed gene that was down regulated was *efeU*. This gene was not included in the FeoAB dataset but another Fur repressed iron transporter was included (*fepA*), suggestive of a modest suppression of iron uptake genes in both dataset.

Table 5.11: The top 40 FeoABC-induced and repressed genes at OD 0.8 with ascorbate. Highlights indicate *feo* genes and *efeU* (yellow), carbohydrate metabolism genes (red text), amino acid metabolism genes (mid-plum), nucleotide metabolism (light plum), sulphur transport (mid blue) and tRNA genes (light blue). Those in bold were also in the top-40 up and down regulated list at OD 0.8 (Table 5.4 and Table 5.5).

gene_id	log2FoldChange	pvalue log10	start	end	strand	length	description
feoB	-17.57	-36.68	4097688	4100009	-	2322	*feoB*
feoAB	-13.56	-73.39	4097550	4100265	+	2716	*feoAB*
yhgG	-11.72	-21.90	4097452	4097688	-	237	*feoC*
feoA	-10.51	-49.74	4100026	4100253	-	228	*feoA*
Novel00151	-4.09	-1.78	1643001	1643404	+	404	Cold-shock' DNA-binding domain, antisense cspB
Novel00212	-4.04	-1.83	2263616	2263833	+	218	fruA antisense transcript
isrC	-3.96	-7.83	2073452	2073655	+	204	sRNA
rspA	-3.31	-33.21	1655641	1656855	-	1215	predicted dehydratase, Starvation-sensing protein RspA , Mandelate racemase / muconate lactonizing enzyme
Novel00144	-3.13	-1.92	1365133	1365306	-	174	Aldehyde dehydrogenase family, antisense puuC. Putrescene metabolism
flu	-2.94	-3.81	2073676	2076795	+	3120	antigen 43 (Ag43), phase-variable biofilm formation autotransporter, Adhesin of bacterial autotransporter system, probable stalk
aroF	-2.84	-15.86	2738736	2739806	-	1071	3-deoxy-D-arabinoheptulosonate-7-phosphate synthase, tyrosine-repressible, amino acid biosytnthesis
rspB	-2.82	-24.19	1654610	1655629	-	1020	predicted oxidoreductase, Zn-dependent and NAD(P)-binding, Starvation-sensing protein RspB
Novel00363	-2.70	-21.16	3585439	3585620	+	182	csrC antisense (sRNA, controlling cental C metabolism, biofilm formation and motility)
csrC	-2.63	-38.61	3585401	3585645	-	245	sRNA, controlling cental C metabolism, biofilm formation and motility
ynfP	-2.58	-4.47	1654442	1654552	-	111	hypothetical protein,
Novel00139	-2.52	-12.97	1320667	1324668	+	4002	Antisense trpCDE. Tryptophan biosynthesis. Anthranilate synthase component I, chorismate binding enzyme,Glutamine amidotransferase class, Indole-3-glycerol phosphate synthase
yeeR	-2.50	-3.33	2076916	2078448	+	1533	predicted membrane protein,
ypdH	-2.50	-2.26	2513362	2513688	-	327	predicted enzyme IIB component of PTS, Lactose/Cellobiose specific IIB subunit
tyrA	-2.45	-13.13	2737604	2738725	-	1122	fused chorismate mutase T and prephenate dehydrogenase, Prephenate dehydrogenase
trpE	-2.44	-11.35	1323098	1324660	-	1563	Anthranilate synthase component I

gene_name	log2FoldChange	pvalue log10	start	end	strand	length	description
codB	1.62	-9.21	354146	355405	+	1260	cytosine transporter, Permease for cytosine/purines, uracil, thiamine, allantoin
argF	1.63	-5.26	288525	289529	-	1005	ornithine carbamoyltransferase
purF	1.63	-8.19	2434167	2435684	-	1518	amidophosphoribosyltransferase
oppA	1.65	-12.88	1302896	1304527	+	1632	oligopeptide transporter subunit
yeeD	1.66	-1.75	2086363	2086590	-	228	conserved hypothetical protein Putative sulfur carrier protein YeeD Sulfurtransferase TusA
argI	1.67	-6.86	4481987	4482991	-	1005	ornithine carbamoyltransferase
ynfM	1.67	-5.58	1671413	1672666	+	1254	predicted transporter, potential arabinose exporter
argG	1.68	-15.47	3318492	3319835	+	1344	argininosuccinate synthetase
yjgF	1.68	-15.98	4475207	4475593	-	387	catalyzes the deamination of enamine/imine intermediates to yield 2-ketobutyrate and ammonia. It is required for the detoxification of reactive intermediates of IlvA
lysY	1.78	-6.03	781569	781644	+	76	tRNA-Lys
yraQ	1.84	-18.35	3296953	3297993	-	1041	predicted permease,
uraA	1.92	-24.16	2617527	2618816	-	1290	uracil transporter, Uracil permease
efeU	1.94	-9.45	1081778	1082607	+	830	Putative inactive ferrous iron permease EfeU, Iron permease FTR1 family
carA	1.95	-9.21	29651	30799	+	1149	carbamoyl phosphate synthetase small subunit C glutamine amidotransferase
yeeE	1.99	-1.74	2086604	2087662	-	1059	predicted inner membrane protein, Sulphur transport
asnA	2.15	-8.87	3708534	3709526	-	993	asparagine synthetase
pyrI	2.33	-23.96	4475666	4476127	-	462	aspartate carbamoyltransferase, regulatory subunit, metal binding domain
ygaW	2.33	-1.32	2797820	2798269	+	450	predicted inner membrane protein, L-alanine exporter AlaE
pyrB	2.42	-23.53	4476140	4477075	-	936	aspartate carbamoyltransferase
yhhQ	2.43	-2.57	4030533	4031198	-	666	conserved inner membrane protein, QPTR Queuosine precursor transporter, Putative vitamin uptake transporter

5.4.6 Impact of FeoABC on global gene expression in the presence of ferric citrate

Fig. 5.14 summarizes the differentially regulated genes in response to *feoABC* induction in the presence of iron at OD 0.5 and 1.0. The results showed that the *feoABC* genes were induced by 6.4- to 19-log2 fold. The number of differentially regulated genes was higher at OD 0.5 and OD 1.0 (2060 and 329, respectively), which may reflect the impact of more rapid growth at lower OD upon global gene expression, as suggested above.

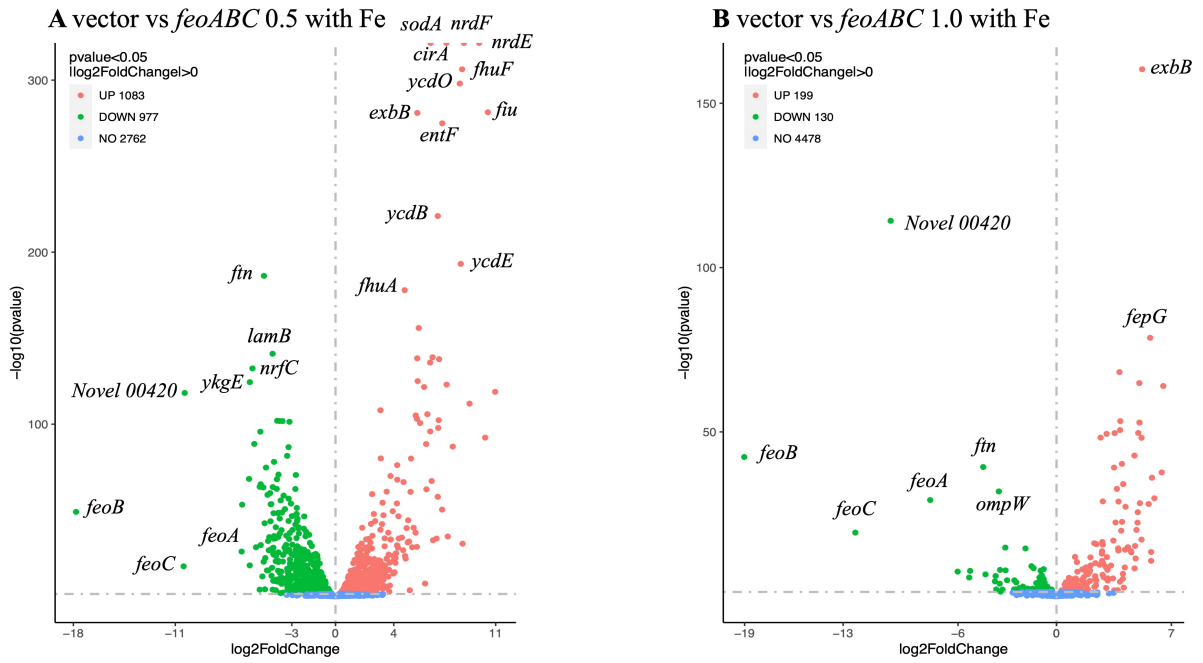

Figure 5.14: Volcano plot of differentially expressed genes in response to *feoABC* induction with iron. (**A**)Vector versus *feoABC* at OD 0.5. (**B**) Vector versus *feoABC* at OD 1.0. The identities of the *feoA*, *feoB* and *feoC* reads are indicated, and the number of significantly (>2 fold) induced and repressed transcripts is also provided as determined by DESeq2. "Novel 00420" corresponds to a *feoAB* transcript.

In the presence of iron at OD 0.5 (Table 5.12), 15 of the top-20 FeoABC-induced genes (ignoring the four *feo* genes) were also included in the equivalent FeoAB-induced gene list (Table 5.6), which again indicates close correlation between the *feoC*$^{+/-}$ data sets. The major category affected was the anaerobic energy metabolism genes, mostly involving nitrate/nitrite respiration systems. This reinforces the impact of the *feo* genes on gene expression as highlighted above (Table 5.6) in upregulation of such anaerobic energy generation systems. In addition, the *ftn* gene was induced, as for FeoAB (Table 5.6), which suggests an increased cellular iron content is afforded by *feoABC* induction. For the top 20 FeoABC repressed genes at OD 0.5 with iron, all 20 were also induced in the corresponding FeoAB data set (Table 5.7). This again shows a very close match between these highly related data sets. Of the 20 genes listed, 19 are known to be Fur repressed. As stated above, this effect likely arises though

increased cellular iron content as stimulated by *feoABC* induction. However, it is possible that the effect is mediated directly by interaction of Feo components with Fur.

Table 5.12: The top 40 FeoABC-induced and repressed genes at OD 0.5 with ferric citrate. Highlights indicate Fur regulated genes (yellow), nitrate/nitrate respiration genes (light brown), anaerobic C4-dicarbioxylate transport genes (brown), carbohydrate metabolism genes (red text) and other metal metabolism genes (orange). Those in bold were also in the top-40 up and down regulated list at OD 0.5 (Table 5.6 and Table 5.7).

gene_name	log2FoldChange	pvalue log10	start	end	strand	length	description
feoB	-17.81	-49.0	4097688	4100009	-	2322	*feoB*
yhjG	-10.43	-17.4	4097452	4097688	-	237	*feoC*
feoAB	-10.36	-118.2	4097550	4100265	+	2716	*feoAB*
feoA	-6.45	-26.0	4100026	4100253	-	228	*feoA*
nirD	-6.41	-53.2	4143539	4143865	-	327	nitrite reductase, small subunit, Rieske-like [2Fe-2S] domain
nirC	-5.94	-68.2	4142607	4143413	-	807	Formate/nitrite transporter
dcuC	-5.89	-17.9	653806	656390	-	2585	anaerobic C4-dicarboxylate transport
yhjE	-5.88	-124.5	320832	321551	+	720	predicted oxidoreductase, Cysteine-rich domain. Putative L-lactate utilisation component
nrfC	-5.70	-132.4	4293398	4294069	+	672	formate-dependent nitrite reductase, 4Fe4S subunit
nrfB	-5.57	-88.6	4292835	4293401	+	567	nitrite reductase, formate-dependent, penta-heme cytochrome c
fruK	-5.46	-28.5	2264761	2265699	-	939	fructose-1-phosphate kinase
citD	-5.20	-3.8	649710	650006	-	297	citrate lyase, Citrate lyase acyl carrier protein, Malonate decarboxylase delta subunit (MdcD)
narJ	-5.20	-63.6	1286716	1287426	+	711	molybdenum-cofactor-assembly chaperone subunit (delta subunit) of nitrate reductase
yehN	-5.16	-95.6	1907402	1907968	+	567	conserved inner membrane protein, Probable manganese efflux pump
narI	-5.14	-65.1	1287426	1288103	+	678	nitrate reductase gamma (cytochrome b) subunit
nrfD	-5.13	-29.7	4294066	4295022	+	957	formate-dependent nitrite reductase
fruB	-5.02	-11.5	2265699	2266829	-	1131	fused fructose-specific PTS enzyme IIA component and HPr component
narH	-4.96	-63.2	1285181	1286719	+	1539	nitrate reductase 1 beta (Fe-S) subunit
nrfA	-4.93	-20.0	4291354	4292790	+	1437	nitrite reductase, formate-dependent cytochrome c552
ftn	-4.91	-186.2	1990853	1991350	+	498	cytoplasmic ferritin iron storage protein

gene_name	log2FoldChange	pvalue log10	start	end	strand	length	description
nrdH	10.96	-118.8	2799379	2799624	+	246	glutaredoxin-like protein, &ribonucleotide reductase, Fur repressed
fiu	10.46	-281.3	839671	841953	-	2283	predicted iron outer membrane transporter, Catecholate siderophore receptor,TonB-dependent Receptor
nrdI	10.28	-92.2	2799621	2800031	+	411	protein that stimulates ribonucleotide reduction&&sp|P0A774|NRDI_ECO57 Protein NrdI OS=Escherichia coli O157:H7 OX=83334 GN=nrdI PE=3 SV=1 && PF07972:NrdI Flavodoxin like
nrdE	9.87	0.0	2800004	2802148	+	2145	ribonucleoside-diphosphate reductase alpha subunit
fes	9.20	-112.0	612038	613162	+	1125	ferric enterobactin esterase
nrdF	8.82	0.0	2802158	2803117	+	960	ribonucleoside-diphosphate reductase beta subunit
ybdZ	8.73	-30.6	613165	613383	+	219	conserved hypothetical protein, Enterobactin biosynthesis protein YbdZ, MbtH-like protein
fhuF	8.69	-306.3	4609555	4610343	-	789	ferric iron reductase involved in ferric hydroximate transport
yncE	8.60	-193.2	1525021	1526082	+	1062	conserved hypothetical protein, Fur repressed
efeO	8.53	-298.0	1082665	1083792	+	1128	Iron uptake system component EfeO, Cupredoxin-like domain, Imelysin
fepA	8.05	-87.0	609477	611717	-	2241	iron-enterobactin outer membrane transporter,TonB-dependent Receptor
yjjZ	7.71	-34.7	4610484	4610720	+	237	hypothetical protein (DUF1435), a Ser/Thr protein kinase and its primary protein substrates are the ribosomal protein RpmE (L31) and the carbon storage regulator CsrA, gene associated with a Fur binding site - adjacent to fhuF
ybdA	7.63	-123.0	621523	622773	+	1251	predicted transporter, Enterobactin exporter EntS
cirA	7.62	0.0	2248112	2250103	-	1992	ferric iron-catecholate outer membrane transporter, TonB dependent receptor
entF	7.33	-274.9	613380	617261	+	3882	enterobactin synthase multienzyme complex component
entB	7.32	-50.4	626917	627774	+	858	isochorismatase, Enterobactin synthase component
entE	7.12	-137.8	625293	626903	+	1611	3-dihydroxybenzoate-AMP ligase component of enterobactin synthase multienzyme complex
fepG	7.09	-102.3	619419	620411	-	993	iron-enterobactin transporter subunit
fepD	7.05	-97.8	620408	621412	-	1005	iron-enterobactin transporter subunit
ycdB	7.02	-221.0	1083798	1085069	+	1272	EfeUOB iron transporter, peroxidase EfeB Dyp-type peroxidase family

At OD 1.0, a similar correlation between the FeoAB (Table 5.8 & 5.9) and FeoABC (Table 5.13) data sets was observed. Indeed, 15 of the 16 most FeoABC-induced genes (excluding the *feo* genes) were also included in the corresponding FeoAB data set (Table 5.8). The induced gene set for both FeoAB and FeoABC included the *ydhYVWX* operon of unknown function that possibly plays a role in anaerobic energy generation. Indeed, five well defined anaerobic energy generation genes were also included in the FeoABC (and FeoAB) induced list, such that this was the major gene category induced by both FeoAB and FeoABC at OD 1 with iron. Two Fe-Fur induced genes (*ompW* and *ftn*) were included, suggesting a FeoABC mediated increase in cellular iron. The raised expression of the anaerobic energy generation genes may be related to raised cellular iron and Fe-Fur induction or to an effect on Fnr dependent gene expression. Of the 20 most FeoABC-repressed genes at OD 1 with iron (Table 5.13), 19 were also included in the FeoAB-repressed list (Table 5.9), again showing tight similarity between the related FeoAB and FeoABC data sets. The major gene category affected was for genes

involved in combating iron restriction (15/20) followed by genes involved in anaerobic energy generation via nitrate/nitrite respiration. These effects suggest repression by the ferrous-Fur complex of iron-restriction systems due to raised iron uptake mediated by FeoABC, and also a suppression of nitrate/nitrite respiration processes.

Table 5.13: The top 40 FeoABC-induced and repressed genes at OD 1.0 with ferric citrate. Highlights indicate genes involved in iron metabolism (Fur regulated, yellow), nitrate/nitrate respiration (light brown), anaerobic C4-dicarbioxylate transport (brown), other metal metabolism (orange) and nucleotide metabolism (light plum). Those in bold were also in the top-40 FeoAB up or down regulated list at OD 1.0 (Table 5.8 and Table 5.9).

gene_name	log2FoldChange	pvalue log10	start	end	strand	length	description
feoB	-19.02	-42.4	4097688	4100009	-	2322	*feoB*
yhgG	-12.26	-19.4	4097452	4097688	-	237	*feoC*
feoAB	-10.10	-114.2	4097550	4100265	+	2716	*feoAB*
feoA	-7.69	-29.3	4100026	4100253	-	228	*feoA*
ydhY	-6.02	-7.5	1755565	1756191	-	627	predicted 4Fe-4S ferridoxin-type protein, 4Fe-4S dicluster domain, anaerobic function
ydhV	-5.32	-5.7	1753442	1755544	-	2103	predicted oxidoreductase, Aldehyde ferredoxin oxidoreductase
ynfE	-5.26	-7.7	1659783	1662209	+	2427	oxidoreductase subunit, &Putative dimethyl sulfoxide reductase chain
ftn	-4.46	-39.3	1990853	1991350	+	498	ferritin iron storage protein
ynfF	-4.33	-6.6	1662270	1664693	+	2424	oxidoreductase subunit, & Probable dimethyl sulfoxide reductase chain, Molybdopterin oxidoreductase Fe4S4 domain
ydhW	-3.75	-4.5	1752791	1753438	-	648	hypothetical protein
ynfG	-3.71	-6.2	1664704	1665321	+	618	oxidoreductase Fe-S subunit, Probable anaerobic dimethyl sulfoxide reductase chain YnfG
ydaC	-3.67	-2.1	1415245	1415454	-	210	hypothetical protein, Double-strand break reduction protein (DUF1187)
ompW	-3.51	-31.9	1315734	1316372	+	639	outer membrane protein, porin, Fur induced
ydhX	-3.46	-3.8	1752059	1752727	-	669	predicted 4Fe-4S ferridoxin-type protein
dcuB	-3.44	-8.0	4352082	4353422	-	1341	Anaerobic C4-dicarboxylate transporter
ninE	-3.41	-1.4	572144	572314	+	171	conserved hypothetical protein,Prophage NinE homolog
ydhY antisense	-3.29	-2.0	1755689	1756248	+	560	antisense ydhY
yebN	-3.12	-14.8	1907402	1907968	+	567	conserved inner membrane protein, Probable manganese efflux pump MntP
fumB	-3.10	-7.9	4350358	4352004	-	1647	anaerobic class I fumarate hydratase
yeiT	-3.01	-4.9	2237367	2238605	+	1239	predicted oxidoreductase, NAD-dependent dihydropyrimidine dehydrogenase subunit PreT, 4Fe-4S cluster. Production of 5,6-dihydrouracil (DHU) from uracil

gene_name	log2FoldChange	pvalue log10	start	end	strand	length	description
fhuF	6.50	-64.0	4609555	4610343	-	789	ferric iron reductase involved in ferric hydroximate transport
fepC	6.41	-37.7	618607	619422	-	816	iron-enterobactin transporter subunit
ybdZ	5.96	-29.8	613165	613383	+	219	Enterobactin biosynthesis protein YbdZ, MbtH-like protein
yeaR	5.82	-36.1	1881303	1881662	-	360	Uncharacterized protein (DUF1971). Nitrate and nitrite induced anaerobically by NarL
narK	5.77	-13.5	1279534	1280925	+	1392	nitrate/nitrite transporte
narG	5.76	-10.8	1281441	1285184	+	3744	nitrate reductase 1 alpha subunit, Molydopterin dinucleotide binding domain|PF00384:
fepG	5.70	-78.6	619419	620411	-	993	iron-enterobactin transporter subunit
fes	5.62	-28.1	612038	613162	+	1125	enterobactin/ferric enterobactin esterase, iron release
exbB	5.22	-160.3	3149906	3150640	-	735	membrane spanning protein in TonB-ExbB-ExbD complex, ferric siderophore uptake
ybdA	5.18	-48.2	621523	622773	+	1251	Enterobactin exporter EntS
nrdH	5.18	-17.2	2799379	2799624	+	246	glutaredoxin-like protein, Fur repressed ribonucleotide reductase
bfd	5.08	-28.3	4173425	4173619	+	195	bacterioferritin-associated ferredoxin, iron release from Bfr
yoaG	5.05	-52.8	1881117	1881299	-	183	hypothetical protein, DUF1869. Nitrate and nitrite induced anaerobically by NarL
fepD	5.05	-64.9	620408	621412	-	1005	iron-enterobactin transporter subunit
exbD	4.98	-49.7	3149474	3149899	-	426	membrane spanning protein in TonB-ExbB-ExbD complex, &ferri-siderophore uptake
fiu	4.95	-25.6	839671	841953	-	2283	predicted iron outer membrane transporter, TonB-dependent Receptor
nrdI	4.94	-22.4	2799621	2800031	+	411	protein that stimulates ribonucleotide reduction, NrdI Flavodoxin like
Novel00132	4.87	-20.2	1281686	1288619	-	6934	Antisense narGHJI, Nitrate reductase gamma subunit, 4Fe-4S dicluster domain, Respiratory nitrate reductase beta, Molydopterin dinucleotide binding domain
yncE	4.82	-11.5	1525021	1526082	+	1062	conserved hypothetical protein, periplasmic Fur repressed
yoeA	4.79	-15.3	2070772	2071164	+	393	prophage region, predicted disrupted hemin or colicin receptor, TonB-dependent Receptor n

5.4.7 Impact of FeoC in the presence of ascorbate

Fig. 5.15 summaries the effect of the *feoAB* versus *feoABC* induction at OD 0.5 and 0.8 in the presence of ascorbate. The results show that the *feoC* gene was induced by 10.1- to 11.7-log2 fold and this significant change in expression was greater than that for any other gene (Fig. 5.15). FeoC caused differential regulation of fewer genes (1090 and 208 at OD 0.5 and 0.8, respectively) than did FeoAB, with far greater numbers at the lower OD, as was observed above (Fig. 5.14).

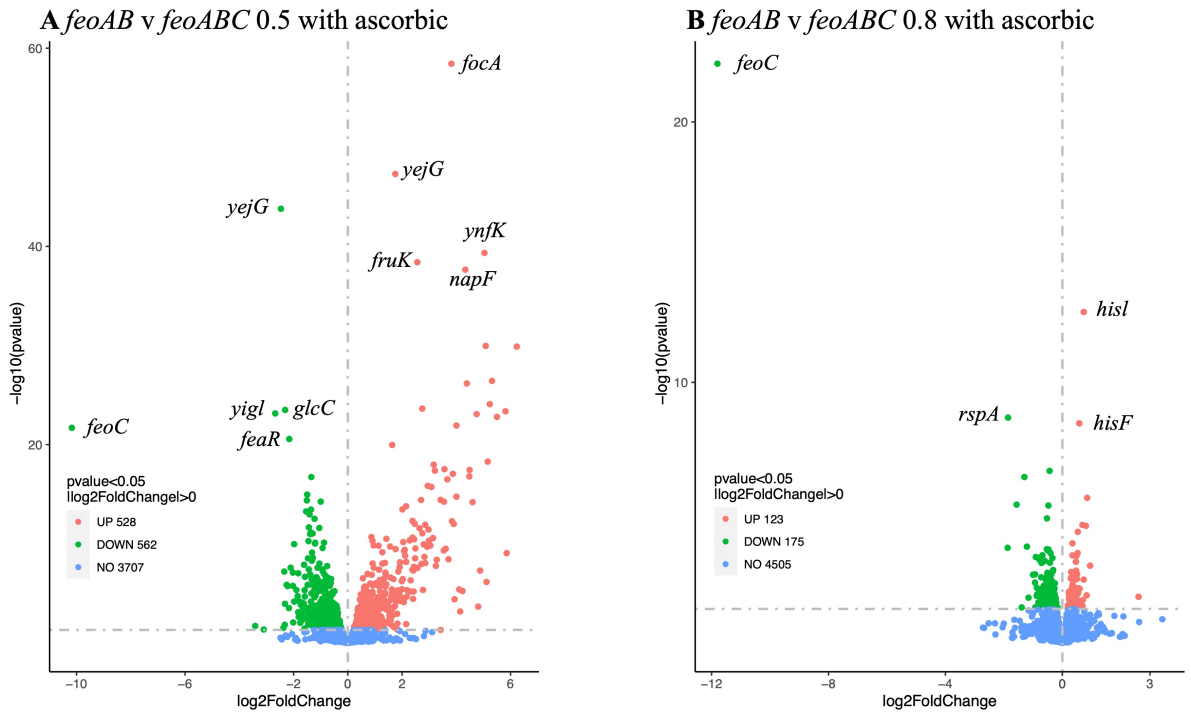

Figure 5.15: Volcano plot of differentially expressed genes in response to *feoC* induction with ascorbate. (**A**) *feoAB* versus *feoABC* at OD 0.5. (**B**) *feoAB* versus *feoABC* at OD 0.8. The identities of the *feoC* reads are indicated, and the number of significantly (>2 fold) induced and repressed transcripts is also provided as determined by DESeq2.

Consideration of the top-40 FeoC-induced and -repressed genes at OD 0.5 (Table 5.14) indicates only three (excluding *feoC*) were also regulated by FeoABC (Table 5.10). For the top 20 FeoC-induced genes, no major functional category was apparent. The two most abundant categories were carbon metabolism and amino acid metabolism (three and two genes, respectively. However, for the top-20 most FeoC repressed genes, 13 were in the anaerobic energy generation group with roles in nitrate/nitrite respiration, indicating that FeoC may be responsible for the down regulation of NarXL/NarQP dependent genes. A similar effect was observed for FeoAB with iron at OD 1.0 (Table 5.9). However, opposite effects (i.e. upregulation of such genes) were seen in three other cases (FeoAB with ascorbate and with iron at OD 0.5, and FeoABC with iron at OD 0.5; Tables 5.2, 5.6 & 5.12).

Table 5.14: The top 40 FeoC-induced and -repressed genes at OD 0.5 with ascorbate. Highlights indicate iron metabolism genes (yellow), amino acid metabolism genes (mid-plum), tRNA genes (light blue) nitrate/nitrate respiration genes (light brown), anaerobic C4-dicarbioxylate transport and carbohydrate metabolism genes (red text). Those in bold were also in the top-40 up and down regulated list at OD 0.5 (Table 5.10).

gene_name	log2FoldChange	pvalue log10	start	end	strand	length	description
yhgG	-10.17	-21.70	4097452	4097688	-	237	*feoC*
racC	-3.41	-1.70	1419202	1419477	-	276	hypothetical protein, RacC
argZ	-3.10	-1.34	2816715	2816791	-	77	tRNA-Arg
yigI	-2.68	-23.15	3631984	3632451	+	468	conserved hypothetical protein, Thioesterase superfamily, detergent-resistant phospholipase A
yejG	-2.47	-43.80	2281227	2281571	-	345	hypothetical protein,
insH	-2.38	-1.50	3128834	3129850	+	1017	IS5 transposase and trans-activator (DUF772)
mhpR	-2.34	-7.19	366811	367758	-	948	DNA-binding transcriptional activator, degradation or aromatic compounds
ydcC	-2.32	-1.82	1533530	1534666	+	1137	conserved hypothetical protein, H repeat-associated putative transposase
metF	-2.32	-3.94	3503175	3504065	-	891	5,10-methylenetetrahydrofolate reductase
glcC	-2.31	-23.50	3126928	3127692	+	765	DNA-binding transcriptional dual regulator, glycolate-binding
ydcI	-2.25	-5.85	1495862	1496785	-	924	predicted DNA-binding transcriptional regulator, acid stress resistance and induced biofilm formation
pstS	-2.22	-5.72	3725156	3726196	+	1041	phosphate transporter subunit n
sdhC	-2.17	-3.50	755599	755988	+	390	succinate dehydrogenase (Iron induced via the Fur/RyhB pathway
feaR	-2.16	-20.57	1448092	1448997	-	906	DNA-binding transcriptional regulator. Positive regulator of tynA/maoA and feaB/padA, the genes for 2-phenylethylamine catabolism
iscR	-2.11	-7.58	2660299	2660787	-	489	Regulation of Fe-S cluster biosynthesis
ymgB	-2.02	-5.74	1217946	1218212	+	267	hypothetical protein, Regulatory protein AriR O. Biofilm development protein YmgB/AriR
puuD	-2.02	-7.09	1362834	1363598	+	765	Gamma-glutamyl-gamma-aminobutyrate hydrolase PuuD . Putrescine degradation
ryjA	-2.01	-2.05	4281517	4281656	-	140	sRNA
hcaR	-1.98	-9.96	2666662	2667552	-	891	DNA-binding transcriptional regulator, Transcriptional activator of the hca operon for 3-phenylpropionic acid catabolism
metA	-1.98	-4.16	4217870	4218799	+	930	homoserine transsuccinylase

gene_name	log2FoldChange	pvalue log10	start	end	strand	length	description
nirB	6.23	-29.89	4143862	4146405	-	2544	nitrite reductase large subunit 4Fe-4S domain
nirD	5.86	-9.05	4143539	4143865	-	327	nitrite reductase small subunit, Rieske-like [2Fe-2S] domain
narK	5.81	-23.36	1279534	1280925	+	1392	nitrate/nitrite transporter
narG	5.50	-22.80	1281441	1285184	+	3744	nitrate reductase alpha subunit :Molydopterin dinucleotide binding domain
yfiD	5.32	-26.43	2714722	2715105	-	384	pyruvate formate lyase subunit,
yhbU	5.23	-24.08	3301340	3302335	+	996	predicted collagenase-like Ubiquinone biosynthesis protein UbiU
Novel00270	5.16	-18.29	2714693	2715159	+	467	Antisense of the FNR activated yfiD gene. Glycine radical, pyruvate formate lyase,
nirC	5.11	-6.14	4142607	4143413	-	807	Formate/nitrite transporter
yoeA	5.08	-29.96	2070772	2071164	+	393	CP4-44 prophage region, predicted disrupted hemin or colicin receptor,TonB-dependent Receptor Plug Domain
ynfK	5.04	-39.34	1668238	1668933	-	696	predicted dethiobiotin synthetase
narH	4.88	-7.29	1285181	1286719	+	1539	nitrate reductase beta (Fe-S) subunit 4Fe-4S discluster domain
ynfO	4.81	-3.66	1638470	1638703	+	234	hypothetical protein (DUF3950)
yliH	4.75	-23.08	878670	879053	+	384	conserved hypothetical protein, Biofilm regulator BssR
dcuC	4.60	-14.19	653806	656390	-	2585	anaerobic C4-dicarboxylate transport
Novel00132	4.49	-17.44	1281686	1288619	-	6934	Antisense narGHJI, Nitrate reductase gamma subunit, 4Fe-4S dicluster domain, Respiratory nitrate reductase beta, Molydopterin dinucleotide binding domain
fdnG	4.48	-16.79	1549115	1552162	+	3048	formate dehydrogenase, major subunit , Molybdopterin oxidoreductase Fe4S4 domain
ydjX	4.39	-26.17	1835115	1835825	+	711	predicted inner membrane protein
napF	4.33	-37.65	2306337	2306831	-	495	ferredoxin-type protein, role in electron transfer to periplasmic nitrate reductase, Ferredoxin-type protein
narJ	4.23	-5.23	1286716	1287426	+	711	molybdenum-cofactor-assembly chaperone subunit of nitrate reductase
ybcV	4.14	-3.16	578407	578817	-	411	hypothetical protein (DUF1398)

At OD 0.8, only one gene (excluding *feoC*) in the top-40 FeoC induced and repressed list (Table 5.15) was also included in the top-40 list for FeoABC induced genes under the same conditions (Table 5.11). In addition, the degree of differential expression was relatively modest indicating no major FeoC-induced regulatory change. No major pattern of FeoC-induced regulatory change was apparent in terms of functional categories affected, although four cold shock genes were found to be significantly down regulated by FeoC (Table 5.15).

Table 5.15: The top 40 FeoC-induced and repressed genes at OD 0.8 with ascorbate. Highlights indicate the *feoC* gene (yellow), amino acid metabolism genes (mid-plum), nucleotide metabolism (light plum), tRNA genes (light blue), carbohydrate metabolism genes (red text), *ara* genes (light yellow) and cold shock genes (light blue text). Those in bold were also in the top-40 up and down regulated list at OD 0.8 (Table 5.11).

gene_name	log2FoldChange	pvalue log10	start	end	strand	length	description
yhgG	-11.80	-22.24	4097452	4097688	-	237	*feoC*
ynfP	-1.87	-3.65	1654442	1654552	-	111	hypothetical protein
rspA	-1.86	-8.65	1655641	1656855	-	1215	predicted dehydratase Starvation-sensing protein RspA, Mandelate racemase / muconate lactonizing enzyme
rspB	-1.56	-5.31	1654610	1655629	-	1020	predicted oxidoreductase, Zn-dependent and NAD(P)-binding, Alcohol dehydrogenase, GroES-like domain, Zinc-binding dehydrogenase
yiaO	-1.39	-1.36	3893335	3894321	-	987	predicted transporter, 2,3-diketo-L-gulonate-binding periplasmic protein
yjiY	-1.30	-6.37	4593809	4595959	-	2151	predicted inner membrane protein, Pyruvate/proton symporter BtsT, Carbon starvation protein CstA
Novel00470	-1.21	-3.69	4594684	4595972	+	1289	Carbon starvation protein CstA, antisense
valY	-1.16	-1.73	2526619	2526694	+	76	tRNA-Val
pyrB	-1.00	-2.61	4476140	4477075	-	936	aspartate carbamoyltransferase
argI	-0.93	-2.31	4481987	4482991	-	1005	Aspartate/ornithine carbamoyltransferase
pyrI	-0.93	-2.63	4475666	4476127	-	462	aspartate carbamoyltransferase, regulatory subunit
yghF	-0.93	-1.36	3110710	3111576	-	867	predicted secretion pathway protein
Novel00054	-0.91	-3.30	583896	584864	+	969	OmpT antisense
argF	-0.88	-1.80	288525	289529	-	1005	ornithine carbamoyltransferase
nmpC	-0.87	-2.11	574981	576108	-	1128	DLP12 prophage region, truncated outer membrane porin
ygeO	-0.86	-1.86	2994618	2995043	-	426	hypothetical protein, Bacterial type III secretion apparatus protein
ompT	-0.83	-3.27	583903	584856	-	954	outer membrane protease
sRNA00032	-0.83	-1.39	3479474	3479533	+	60	argH antisense
Novel00053	-0.82	-1.55	574804	576050	+	1247	prophage genes, insH-nmpC antisense
borD	-0.78	-1.44	577823	578116	-	294	predicted lipoprotein, Prophage lipoprotein Bor

gene_name	log2FoldChange	pvalue log10	start	end	strand	length	description
insC	2.61	-1.77	4502907	4503317	+	411	IS2 insertion element repressor Transposase
cspI	0.95	-2.96	1640169	1640381	-	213	cold shock protein
araD	0.85	-5.57	65855	66550	-	696	L-ribulose-5-phosphate 4-epimerase
cspA	0.83	-1.82	3920154	3920366	-	213	major cold shock protein
yaiY	0.81	-4.49	398249	398557	-	309	predicted inner membrane protein (DUF2755)
hisI	0.73	-12.70	2098751	2099362	+	612	fused phosphoribosyl-AMP cyclohydrolase and phosphoribosyl-ATP pyrophosphatase
ddg	0.73	-2.43	2501091	2502011	+	921	palmitoleoyl-acyl carrier protein (ACP)-dependent acyltransferase, Lipid A biosynthesis palmitoleoyltransferase
Novel00407	0.70	-1.64	3920127	3920515	+	389	Cold-shock' DNA-binding domain, antisense
cspG	0.69	-1.42	1051883	1052095	+	213	DNA-binding transcriptional regulator 'Cold-shock' DNA-binding domain
ycgF	0.69	-4.53	1215841	1217052	-	1212	predicted FAD-binding phosphodiesterase, Blue light- and temperature-regulated antirepressor BluF
Novel00208	0.64	-1.45	2235839	2236419	-	581	Cytidine and deoxycytidylate deaminase zinc-binding region. sanA-cdd antisense
aroF	0.63	-1.38	2738736	2739806	-	1071	3-deoxy-D-arabinoheptulosonate-7-phosphate synthase tyrosine-repressible, amino acid biosynthesis
Novel00316	0.59	-2.08	3166552	3167175	+	624	Motility quorum-sensing regulator, toxin of MqsA, Antitoxin component of bacterial toxin-antitoxin system, MqsA. Antisense
araB	0.58	-1.50	68348	70048	-	1701	L-ribulokinase carbohydrate kinases
hisF	0.58	-8.43	2097981	2098757	+	777	imidazole glycerol phosphate synthase
gcvT	0.58	-2.09	3048229	3049323	-	1095	aminomethyltransferase, tetrahydrofolate-dependent subunit (T protein) of glycine cleavage complex Aminomethyltransferase folate-binding domain
araA	0.57	-2.09	66835	68337	-	1503	L-arabinose isomerase
yegS	0.54	-1.91	2170849	2171748	+	900	conserved hypothetical protein, Probable lipid kinase, Diacylglycerol kinase catalytic domain
ygiT	0.54	-2.06	3166507	3166902	-	396	predicted DNA-binding transcriptional regulator, Antitoxin component of bacterial toxin-antitoxin system, MqsA
yjbA	0.53	-4.26	4243915	4244325	+	411	predicted phosphate starvation inducible protein, PsiE, Phosphate-starvation-inducible E

5.4.8 Impact of FeoC on global gene expression in the presence of ferric citrate

Fig. 5.16 summaries the differential effect of *feoAB* and *feoABC* induction on global gene expression at OD 0.5 and 1.0 in the presence of iron. The results show that the *feoC* gene was induced by 11.1- to 12.4-log2 fold and this change in expression was higher than that of any other gene (Fig. 5.16). The number of significant regulated genes by FeoC was much lower than seen with FeoAB or FeoABC at 840 and 279 genes for OD 0.5 and 1.0, respectively, as was found in the presence of ascorbate (Fig. 5.15). The results again show a lower differential regulation effect at higher OD.

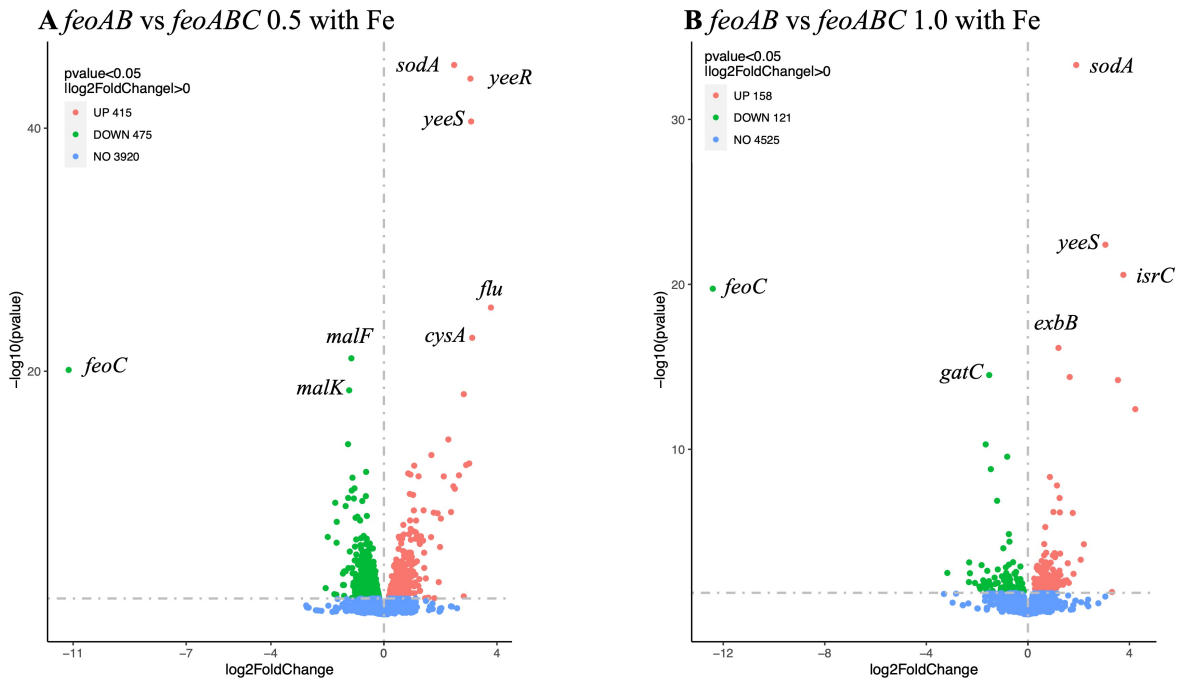

Figure 5.16: Volcano plot of differentially expressed genes in response to *feoC* with iron. (**A**) *feoAB* versus *feoABC* at OD 0.5. (**B**) *feoAB* versus *feoABC* at OD 1.0. The identities of the *feoC* reads are indicated, and the number of significantly (>2 fold) induced and repressed transcripts is also provided as determined by DESeq2.

The top-40 most FeoC-induced and repressed transcripts in the presence of iron at OD 0.5 are shown in Table 5.16. Only two (*citD* and *fruK*) of the FeoC-induced genes listed (excluding *feoC*) were also induced in the top-40 gene set for the corresponding FeoABC data set (Table 5.12), which might be considered as evidence for a genuine FeoC-induction effect. Indeed, the major category of FeoC-induced genes (six genes) was the carbon metabolism group, indicating an influence of FeoC on controlling such genes. Also, six genes involved in amino acid metabolism were up regulated, as were three hydrogenase genes contributing to anaerobic energy generation. However, the differential expression effect was modest in all cases (excluding *feoC*) at fourfold or less (Table 5.16) suggesting that any biological impact would be relatively weak. The top-20 FeoC-repressed gene set was entirely unique with respect to those genes induced under identical conditions by FeoABC (Table 5.12). This suggests that any FeoC effect in the FeoABC data set may have been obscured by the impact of FeoAB.

However, the degree of differential regulation for the FeoC-repressed genes (ranging from 14-fold) was greater than that seen for the FeoC-induced genes (no more than fourfold). In addition, a new major gene function category (seven genes) was apparent in the repressed gene set corresponding to genes involved in cysteine biosynthesis and sulphur assimilation (Table 5.16). This indicates a potential role for FeoC (an iron-sulphur helix-turn-helix motif protein) in regulating sulphur assimilation. Four motility genes were also repressed as was three co-operonic genes (*yeeRST*) of unknown function (Table 5.16). The Fe-Fur repressed *sodA* gene was also repressed by FeoC, alongside a predicted *sodA* antisense transcript. However, no other Fur-related regulatory effect was seen in the absence of FeoAB.

Table 5.16: The top 40 FeoC-induced and repressed genes at OD 0.5 with ferric citrate. Highlights indicate Fur regulated genes (yellow), amino acid metabolism genes (mid-plum), nitrate/nitrate respiration genes (light brown), carbohydrate metabolism genes (red text), cold shock genes (light blue text), cysteine biosynthesis (green) and motility genes (purple text). Those in bold were also in the top-40 up and down regulated list at OD 0.5 (Table 5.12).

gene_name	log2FoldChange	pvalue log10	start	end	strand	length	description
yhgG	-11.16	-20.11	4097452	4097688	-	237	*feoC*
citD	-2.06	-2.15	649710	650006	-	297	citrate lyase acyl carrier (gamma) subunit
hyaE	-1.99	-6.36	1036776	1037174	+	399	protein involved in processing of HyaA and HyaB proteins Hydrogenase-1 operon
asnA	-1.76	-1.65	3708534	3709526	-	993	asparagine synthetase
hisI	-1.72	-9.18	2098751	2099362	+	612	fused phosphoribosyl-AMP cyclohydrolase and phosphoribosyl-ATP pyrophosphatase&&s. Histidine biosynthesis bifunctional protein H
fruA	-1.68	-1.61	2263053	2264744	-	1692	fused fructose-specific PTS enzyme IIB'BC components PTS system fructose-specific EIIB'BC component
hisA	-1.68	-5.89	2097262	2097999	+	738	N-(5'-phospho-L-ribosyl-formimino)-5-amino-1-(5'-phosphoribosyl)-4-imidazolecarboxamide isomerase :Histidine biosynthesis protein
hisF	-1.67	-7.61	2097981	2098757	+	777	imidazole glycerol phosphate synthase: Histidine biosynthesis protein
nrfE	-1.45	-3.35	4295102	4296760	+	1659	heme lyase (NrfEFG) for insertion of heme into C subunit. Cytochrome c-type biogenesis protein CcmF
citC	-1.45	-2.41	650021	651079	-	1059	citrate lyase synthetase,
yggF	-1.44	-2.41	3073873	3074838	-	966	predicted hexoseP phosphatase Fructose-1,6-bisphosphatase 2 class 2 fructose-1,6-bisphosphatase, glpX-encoded
yjbI	-1.42	-2.41	4254545	4255873	+	1329	conserved hypothetical protein: SopA-like central domain: Pentapeptide repeats (9 copies)
hyaD	-1.41	-3.52	1036192	1036779	+	588	protein involved in processing of HyaA and HyaB proteins Hydrogenase 1 maturation protease
fruK	-1.41	-1.52	2264761	2265699	-	939	fructose-1-phosphate kinase
cspI	-1.35	-8.90	1640169	1640381	-	213	cold shock protein: 'Cold-shock' DNA-binding domain
hisH	-1.35	-3.55	2096672	2097262	+	591	imidazole glycerol phosphate synthase:Glutamine amidotransferase class-I
aspA	-1.27	-14.00	4371571	4373007	-	1437	aspartate ammonia-lyase
ycdQ	-1.27	-9.57	1086943	1088268	-	1326	predicted glycosyl transferase, Poly-beta-1,6-N-acetyl-D-glucosamine synthase pgaC: Glycosyl transferase family 2
hyaB	-1.26	-3.80	1033676	1035469	+	1794	hydrogenase 1 large subunit
malK	-1.23	-18.43	4250374	4251489	+	1116	fused maltose transport subunit

gene_name	log2FoldChange	pvalue log10	start	end	strand	length	description
flu	3.79	-25.2	2073676	2076795	+	3120	antigen 43 (Ag43), phase-variable biofilm formation autotransporter, Adhesin of bacterial autotransporter system, probable stalk
cysA	3.12	-22.8	2545163	2546260	-	1098	sulfate/thiosulfate transporter subunit
yeeS	3.09	-40.6	2078445	2078891	+	447	predicted DNA repair protein: RadC-like JAB domain
yeeR	3.06	-44.1	2076916	2078448	+	1533	predicted membrane protein
isrC	3.02	-12.4	2073452	2073655	+	204	small regulatory RNA
cysH	2.91	-12.3	2886234	2886968	-	735	3'-phosphoadenosine 5'-phosphosulfate reductase
Novel00243	2.83	-18.1	2545195	2546382	+	1188	cysA antisense
yfdR	2.83	-1.5	2480430	2480966	+	537	conserved hypothetical protein
cysI	2.66	-11.4	2887043	2888755	-	1713	sulfite reductase beta subunit, Nitrite and sulphite reductase 4Fe-4S domain
flgB	2.51	-10.3	1132595	1133011	+	417	flagellar component of cell-proximal portion of basal-body rod, Flagellar basal body rod protein FlgB
sodA	2.48	-45.2	3535251	3535871	-	621	superoxide dismutase [Mn] Fur repressed
flgC	2.46	-10.5	1133015	1133419	+	405	flagellar component of cell-proximal portion of basal-body rod
cysC	2.38	-8.4	2872043	2872648	-	606	adenosine 5'-phosphosulfate kinase
Novel00361	2.28	-14.4	3535219	3535906	+	688	Iron/manganese superoxide dismutases, sodA antisense
cysN	2.12	-11.3	2872648	2874075	-	1428	sulfate adenylyltransferase subunit
fliL	2.02	-7.9	2021755	2022219	+	465	flagellar biosynthesis protein
fliA	1.99	-5.5	2003207	2003926	-	720	RNA polymerase sigma 28 (sigma F) motility
yeeT	1.94	-2.6	2078954	2079175	+	222	hypothetical protein (DUF987)
cysD	1.90	-8.3	2874077	2874985	-	909	sulfate adenylyltransferase subunit
fixX	1.79	-1.3	45463	45750	+	288	predicted 4Fe-4S ferredoxin-type protein

At OD 1.0, no gene (excluding *feoC*) was found to be common between the FeoC and FeoABC top-20 induced genes in the presence of iron, again indicating that FeoAB may obscure any regulatory influence of FeoC in the FeoABC data set. The major categories induced were amino acid metabolism (seven genes) and nucleotide metabolism (four genes). There was no effect upon Fur-regulated genes, which is in contrast to the corresponding data set with

FeoABC (two Fe-Fur induced genes were upregulated; Table 5.13). In the case of the top-20 most FeoC repressed genes, three were also included in the corresponding FeoABC data set (Table 5.13). These three are well known Fe-Fur repressed genes. Indeed, Fe-Fur repressed genes was the only major category of FeoC down-regulated genes within the top 20 list (Table 5.17). For the equivalent FeoABC data set, 15 Fur repressed genes were included. The results indicate that FeoC may have some role to play in repressing Fur-supressed genes under high iron conditions. Again, the *yeeRST*(*U*) operon was FeoC repressed, as was the case at OD 0.5. However, the function of this operon is not defined and so any potential biological impact is unclear.

Table 5.17: The top 40 FeoC-induced and repressed genes at OD 1.0 with ferric citrate. Highlights indicate Fe-Fur regulated genes (yellow), genes with roles in metabolism of "other" metals (orange), amino acid metabolism genes (mid-plum), nucleotide metabolism (light plum), carbohydrate metabolism genes (red text), sulphur transport genes (mid blue) and antitoxin/toxin (dark orange text) genes. Those in bold were also in the top-40 up and down regulated list at OD 1.0 (Table 5.13).

gene_name	log2FoldChange	pvalue log10	start	end	strand	length	description
ybgG	-12.41	-19.74	4097452	4097688	-	237	*feoC*
cusB	-3.17	-2.51	596702	597925	+	1224	copper/silver efflux system
isrB	-2.32	-1.95	1989976	1990135	-	160	Uncharacterized protein AzuC
hisF	-2.31	-3.14	2097981	2098757	+	777	imidazole glycerol phosphate synthase
hisA	-2.28	-2.49	2097262	2097999	+	738	N-(5'-phospho-L-ribosyl-formimino)-5-amino-1-(5'-phosphoribosyl)-4-imidazolecarboxamide isomerase :Histidine biosynthesis protein
hisH	-2.08	-1.90	2096672	2097262	+	591	imidazole glycerol phosphate synthase; Glutamine amidotransferase class-I
yejG	-1.91	-1.68	2281227	2281571	-	345	hypothetical protein
cbl	-1.88	-1.65	2062101	2063051	-	951	DNA-binding transcriptional activator, transcription factor Cbl, for "cysB like," is a regulator involved in the expression of genes required for aliphatic sulfonate utilization and homeostatic response to sulfate starvation
Novel00051	-1.88	-1.55	550856	552272	+	1417	purEK antisense
purE	-1.86	-1.64	551814	552323	-	510	N5-carboxyaminoimidazole ribonucleotide mutase
hisI	-1.82	-2.98	2098751	2099362	+	612	fused phosphoribosyl-AMP cyclohydrolase and phosphoribosyl-ATP pyrophosphatase, Histidine biosynthesis bifunctional protein
lysA	-1.76	-1.75	2976293	2977555	-	1263	diaminopimelate decarboxylase, pyridoxal binding domain
ydhU	-1.76	-2.06	1751277	1752062	-	786	predicted cytochrome:Prokaryotic cytochrome b561
tsgA	-1.75	-1.72	4146667	4147848	-	1182	predicted transporter
gatD	-1.66	-10.30	2173970	2175010	-	1041	galactitol-1-phosphate dehydrogenase, 2C Zn-dependent and NAD(P)-binding:Alcohol dehydrogenase GroES-like domain: Zinc-binding dehydrogenase
yieG	-1.64	-1.48	3740072	3741409	+	1338	predicted inner membrane protein. Adenine permease AdeP
purN	-1.63	-1.58	2620890	2621528	+	639	phosphoribosylglycinamide formyltransferase
argH	-1.60	-2.63	3478458	3479831	-	1374	argininosuccinate lyase
tyrP	-1.60	-1.31	1991818	1993029	+	1212	tyrosine transporter:Tryptophan/tyrosine permease family
ydhT	-1.59	-1.91	1750461	1751273	-	813	conserved hypothetical protein -

gene_name	log2FoldChange	pvalue log10	start	end	strand	length	description
flu	4.23	-12.44	2073676	2076795	+	3120	antigen 43 (Ag43), phase-variable biofilm formation autotransporter, Adhesin of bacterial autotransporter system, probable stalk
isrC	3.76	-20.58	2073452	2073655	+	204	sRNA
yeeR	3.55	-14.20	2076916	2078448	+	1533	predicted membrane protein
Novel00163	3.31	-1.35	1765435	1765548	+	114	sufB antisense
yeeS	3.05	-22.40	2078445	2078891	+	447	predicted DNA repair protein: RadC-like JAB domain
yeeT	2.21	-4.25	2078954	2079175	+	222	hypothetical protein (DUF987)
yeeU	2.08	-3.31	2079249	2079617	+	369	antitoxin of the YeeV-YeeU toxin-antitoxin system, Cytoskeleton bundling-enhancing antitoxin CbeA
sodA	1.90	-33.30	3535251	3535871	-	621	superoxide dismutase [Mn]
nrdH	1.80	-2.45	2799379	2799624	+	246	glutaredoxin-like protein &ribonucleotide reductase Fur repressed
ykgM	1.77	-6.14	311598	312001	-	404	predicted ribosomal protein L31
Novel00361	1.65	-14.38	3535219	3535906	+	688	Iron/manganese superoxide dismutases, sodA antisense
nrdI	1.61	-1.90	2799621	2800031	+	411	protein that stimulates ribonucleotide reduction, Flavodoxin like
Novel00154	1.57	-3.10	1678050	1679626	+	1577	pntA antisense, NADH/NADPH transhyrogenase
insB	1.53	-2.06	19811	20314	-	504	IS1 transposase InsAB Insertion element IS1
fepC	1.44	-2.03	618607	619422	-	816	iron-enterobactin transporter subunit
insI	1.38	-1.79	269827	270978	+	1152	IS30 transposase InsI
livJ	1.28	-2.38	4040757	4041860	+	1104	leucine/isoleucine/valine transporter subunit:Periplasmic binding protein
nrdE	1.27	-3.68	2800004	2802148	+	2145	ribonucleoside-diphosphate reductase alpha subunit
ydeU	1.26	-1.95	1594379	1595779	-	1401	conserved hypothetical protein:Pertactin, Autotransporter beta-domain
Novel00194	1.26	-6.18	2074042	2077220	-	3179	antisense flu-yeeR, phage locus

5.5 Discussion

This chapter focused on the possibility that FeoC influences *E. coli* gene expression under conditions where FeoC enhances FeoAB-dependent iron restricted growth. Since FeoC carries a helix-turn-helix domain associated with transcription factors, a role for FeoC in gene control seemed plausible. Thus, RNAseq was utilised to explore the effect of induction of *feoC* on global gene expression during *in vitro* aerobic growth through comparison of *feoAB* and *feoABC* strains. Thus, this chapter concentrated on whether the Feo system affects gene expression, at the transcript level, through an RNAseq approach.

5.5.1 Growth conditions and RNA isolation

Two growth conditions were used to study to the role of FeoC in global gene expression; the first condition was with ascorbate (Fig. 5.1A), at two time points (OD 0.5 and 0.8); and the second condition was with iron (Fig. 5.1B), at two time points (OD 0.5. and 1.0) (section 5.2). One condition (with iron) acted as a control since the *feoAB* and *feoABC* strains grow similarly. The other (without iron, but with ascorbate) provided conditions that enabled a growth advantage for the *feoABC* strain over the *feoAB* strain, indicating FeoC functionality under the corresponding conditions. The strains deployed were JC32 (lacking iron uptake capacity) with the pBADrha, pBADrha-*feoAB* and pBADrha-*feoABC* plasmids, and growth was in minimal medium with inducer under aerobiosis.

5.5.2 RNAseq results

The quality of the isolated RNA was considered high and the read data was also considered to be of high quality (Fig. A.12; Table A.1) with 96% of reads successfully mapped to the *E. coli* W3110 genome (Fig. A.14; Table A.2). The read data showed that *feoAB* and *feoABC* were highly and significantly induced (8.8- to 18.4 log2-fold) within the corresponding transformants, with respect to the vector control. This demonstrated that *feo* induction had been successfully, and substantially, achieved.

5.5.2.1 The effect of FeoAB and FeoABC

Tables 5.2 and 5.3 showed that of the 40 most highly-induced genes by FeoAB at OD 0.5 with ascorbate, 19 were related to anaerobic energy generation of which 13 were associated with nitrite/nitrate respiration, and that for the 40 most highly-repressed genes, 15 were involved in translation or amino acid production. In addition, two iron-uptake genes *efeU* and *efeO* were repressed. At OD 0.8 with ascorbate, anaerobic energy generation genes were again induced but genes involved in amino acid generation and carbon catabolism were repressed. The Fe-Fur induced *sodB* gene was also induced (Table 5.4). In the FeoAB-repressed gene set at OD 0.8, 19 genes related to amino acid biosynthesis and translation, eight were related to nucleotide metabolism and one (*fepA*) was related to iron uptake. The data thus indicate a *feoAB*-dependent induction of anaerobic energy generation capacity combined with growth-phase dependent changes in protein production. In addition, there were modest changes in Fur-depndent gene expression indicative of FeoAB-mediated raised iron uptake.

Table 5.6 shows the 40 most highly-induced genes by FeoAB at OD 0.5 with iron. The most notable effects were the induction of 17 genes related to anaerobic energy generation and 4 involved in amino acid metabolism (as noted above). In addition, the Fe-Fur activated *ftn* gene was induced, which is indicative of an FeoAB-mediated increase in cellular iron. For the 40 most-highly FeoAB repressed genes at OD 0.5 with iron, 32 were Fe-Fur repressed genes with roles in iron restriction (Table 5.7). At OD 1.0 with iron, genes (12) involved in anaerobic energy generation were induced (as above) and two Fe-Fur activated genes (*ftn* and *ompW*) were also induced (Fe-Fur induced genes) (Table 5.8). At OD 1.0 with iron, 25 genes involved in combating iron restriction were down regulated as were 14 genes involved in anaerobic energy generation (Table 5.9). The results thus show a much greater impact of *feoAB* on iron homeostasis in the presence of iron than in its absence, and also indicated major changes in anaerobic energy generation in response to FeoAB. These effects resemble those obtained ascorbate in place of iron.

The effects of FeoABC on global gene expression resembled those for FeoAB, as discussed above.

5.5.2.2 The effect of FeoC

By comparing the *feoAB* and *feoABC* RNAseq data it was possible to determine the impact of FeoC on global genes expression. The differential abundance data clearly showed the *feoC* gene was induced (10.1- to 11.7-log2 fold) in the *feoABC* strain relative to the *feoAB*, such that any influence of FeoC on gene expression under the conditions utilized should be revealed within the differential expression data set. Indeed, the results also showed that 528 and 123 genes were upregulated, and that 562 and 175 genes were downregulated at both OD 0.5 and 0.8, respectively, in the presence of ascorbate. (Fig. 5.15). Table 5.14 shows the 40 most highly induced and repressed genes by FeoC at OD 0.5 with ascorbate. For the top 20 most FeoC induced genes, three were involved in carbon metabolism and two were involved in amino acid metabolism. For the top 20 most FeoC repressed genes, 13 were involved in anaerobic energy generation. For the 20 most highly-induced genes by FeoC at OD 0.8 with ascorbate, 3 were involved in amino acid metabolism, two in carbon metabolism and two in nucleotide metabolism (Table 5.15). For the top 20 most FeoC-repressed genes, four were involved in cold shock. Thus, FeoC appeared to induce a major induction in anaerobic energy generation capacity.

Tables 5.16 and 5.17 show the 40 most highly induced and repressed genes by FeoC at OD 0.5 and OD 1.0 with iron. For the top 20 most FeoC-induced genes, six were involved in carbon metabolism, six were involved in amino acid metabolism and three were associated with anaerobic energy generation. For the top 20 most FeoC-repressed genes, seven were involved in cysteine biosynthesis and sulphur assimilation, four were involved in motility. The Fur-repressed *sodA* gene was also down-regulated. This latter effect is consistent with a FeoC mediated increase in cellular iron levels. Table 5.17 shows the 40 most highly-induced and -

repressed genes by FeoC at OD 1.0 with iron. For the top 20 most FeoC-induced genes, seven were involved in amino acid metabolism and four in nucleotide metabolism. For the top 20 most FeoC-repressed genes, six were involved in countering iron restriction, and effect that is again consistent with a FeoC-mediated increase in cellular iron content. With respect to FeoC, the results thus suggest that FeoC enhances FeoAB-dependent iron uptake resulting in raised Fur regulatory activity. It also appears that FeoC may enhance expression of anaerobic energy-generation genes. These two effects were also apparent for FeoAB which would suggest that they are both associated with FeoAB-mediated raised cellular iron levels.

Chapter 6: General discussion

6.1 Introduction

Escherichia coli is a facultative Gram-negative bacterium that can propagate with (aerobic) or without (anaerobic) oxygen. *E. coli* is a common strain of the gut microbiota for humans and animals. Many *E. coli* strains are safe bacteria and do not cause disease in humans or animals when colonising their gastrointestinal tracts, but other strains are able to cause disease and are therefore classified as harmful or pathogenic (Lim, Yoon and Hovde, 2010). When the environment is aerobic and is at neutral to alkaline pH, iron is mainly in its oxidized, ferric form. Iron is stable in its reduced ferrous form only when the environment is microaerobic/anaerobic or at low pH. *E. coli* can transport both ferric and ferrous iron using distinct uptake systems (Mey *et al*., 2021). The main ferrous-iron transport system, found in both pathogenic and non-pathogenic, is FeoABC (Lau *et al*., 2015) which was the main focus of this study. The Feo system was first found in *E. coli* K-12 (Hantke, 1987; Cartron *et al.*, 2006). The Feo system is induced under anaerobic, low-iron conditions (Cartron *et al.*, 2006). The Feo system of *E. coli* is encoded by the *feoABC* operon. The *feoA* gene encodes the 75 amino acid residue, cytoplasmic FeoA protein that is essential to Feo-mediated ferrous-iron transport, although its specific purpose is not yet known. FeoA seems to interact with FeoB to stimulate its iron-uptake activity (Cartron *et al.*, 2006; Lau *et al*., 2015; Al-Aidy, 2020). FeoB is the main ferrous-iron permease. It is composed of 773 amino acid residues and two main domains: an N-terminal cytoplasmic G-protein domain and C-terminal polytopic transmembrane domain. The C-terminal tail of the *E. coli* FeoB protein is predicted to be cytoplasmic, and it possesses conserved cysteine and histidine residues suggestive of metal interaction, but it is only conserved in *Gammaproteobacteria* (Orzel *et al.*, 2023; 2025). FeoC contains 78 amino acid residues and is cytoplasmic. FeoC is found to be conserved only in *Gammaproteobacteria* and is suggested to interact with the C-terminal region of FeoB (Lau *et*

al., 2015). FeoC is believed to contain an Fe-S cluster under anaerobic conditions and protects FeoB from FtsH protease degradation under anaerobiosis. The Fe-S cluster is believed to become oxidized under aerobic conditions which results in loss of FeoC protection of FeoB against FtsH protease attack leading to loss of FeoB ferrous-iron uptake activity in *Salmonella enterica* (Kim *et al*., 2013, 2015). The aim here was to further explore the role of FeoC in supporting FeoAB activity using *E. coli* as the model.

6.2 The role of FeoC in supporting Feo iron-uptake activity under aerobic and anaerobic conditions

6.2.1 Complementation of JC32 with inducible *feoAB* and *feoABC*; *feoC* support *feoAB* dependent iron-restricted growth aerobically

In Chapter 3, the role of FeoC, using inducible *feoAB* and *feoABC* constructs, was explored under aerobic and anaerobic iron-restricted conditions. The *feoAB*/*ABC* inducible expression plasmids were confirmed as was the phenotype and genotype of the JC32 strain lacking iron transporters as JC32 would be used as the host strain. The approach was to compare the growth of complemented iron-uptake mutants carrying inducible *feoAB* and *feoABC* constructs (or the vector control) under iron restriction. Aerobically, when iron was absent with inclusion of DTPA, the results illustrated that the *feoABC*-complemented strain had greater growth than the *feoAB*-complemented strain and vector control (Fig. 3.12B); these findings clearly indicate a role for FeoC in supporting Feo-dependent iron-restricted growth aerobically. When ascorbate was included as reductant, under buffered low-iron aerobic conditions, along with DTPA, the *feoABC* strain showed an even stronger growth advantage with respect to the *feoAB*-complemented strain. Indeed, the *feoABC*-complemented strain grew similarly to the wildtype which suggested that iron uptake under these conditions was almost completely Feo dependent (Fig. 3.16B). This observation further indicates that the presence of FeoC supports aerobic FeoAB function under aerobic conditions.

Under anaerobic conditions, *feoAB*- and *feoABC*-complemented JC32 showed greater growth than the vector control, particularly with the absence of iron and addition of the DTPA (Figs. 3.13B and 3.14). Therefore, *feoAB* and *feoABC* gave a similar iron-restricted growth advantage anaerobically which suggested that FeoC may not have a role under anaerobic conditions, which contrasts with the results obtained under aerobic conditions. This findings contradicts those of Kim et al. (2013) who found that FeoC supports the function of FeoAB anaerobically in *Salmonella enterica*. The function of FeoC aerobically in *S. enterica* was not studied by Kim et al. (2013).

6.2.2 Phenotype of Δ*feoA*::*kan*, Δ*feoB*::*kan* and Δ*feoC*::*kan* BW25113 mutants; a clear iron transport defect for all three mutants

Studies using the inducible *feoAB* and *feoABC* plasmids in JC32 indicated a significant role for FeoC under aerobic conditions, but not under anaerobic conditions. Thus, similar conditions were used to test the single-gene *feo* replacement mutants (Δ*feoA*::*kan*, Δ*feoB*::*kan* and Δ*feoC*::*kan*) within the parental wild type (BW25113) background. The results were similar to those obtained with the inducible *feoAB* and *feoABC* plasmids. Under aerobic conditions when iron was absent and DTPA was included, the wildtype showed stronger growth than the Δ*feoA*::*kan*, Δ*feoB*::*kan* and Δ*feoC*::*kan* mutants which suggested that the presence of FeoC could play a role to support Feo dependent iron-restricted growth aerobically (Fig. 3.18B). Also, when ascorbic acid was included as a reductant (to generate ferrous iron) along with DTPA under aerobic conditions, BW25113 displayed a significantly increased growth with respect to the three mutants (Fig. 3.20B). These findings were similar to the results obtained with inducible *feoAB* and *feoABC* plasmids, and illustrated that Feo can support growth under iron-restricted conditions aerobically but the *feoC* mutant displayed a similar phenotype to *feoA* and *feoB* mutants, which was unexpected. The results indicated that the Δ*feoC*::*kan* mutation

caused an inactivation of the Feo system which leads to a similar phenotype for all three single mutants (Fig. 3.20B).

Under anaerobic conditions, BW25113 and the single Δ*feoA*::*kan*, Δ*feoB*::*kan* and Δ*feoC*::*kan* mutants showed similar growth with/without iron even with absence of iron and addition of bipyridyl (Figs. 3.21, 3.22 and 3.23) and these results were similar to the results obtained with inducible *feoAB* and *feoABC* plasmids (Figs. 3.13 and 3.14). However, when the addition of ascorbic acid along with bipyridyl, the wildtype showed a greater growth than the three mutants and the Δ*feoC*::*kan* mutant again gave an unexpected phenotype anaerobically indicating that the Δ*feoC*::*kan* mutation results in inactivation of the Feo system which leads to all three mutants giving a similar phenotype (Fig. 3.24).

6.2.3 Phenotype of Δ*feoA*, Δ*feoB* and Δ*feoC* compared with BW25113

In order to eliminate any influence of the *kan* cassette inserted in place of the deleted *feo* genes, the *kan* cassette was deleted. Under aerobic conditions in the absence of iron and presence of DTPA, BW25113 showed a growth advantage over the three mutants (Δ*feoA*, Δ*feoB* and Δ*feoC*) and these results were similar to those obtained for Δ*feo*::*kan* mutants which suggested that the presence and absence of *kan* cassette did not affect Feo activity (Fig. 3.31B). In the presence of ascorbate and DTPA, the Δ*feoA*, Δ*feoB* and Δ*feoC* mutants showed a strong growth defect (Fig. 3.33) and these results were similar to those obtained with inducible *feoAB* and *feoABC* plasmids and Δ*feo*::*kan* mutants (Fig. 3.16 and 3.20 respectively). Under anaerobic conditions, BW25113 and the single Δ*feoA*, Δ*feoB* and Δ*feoC* mutants showed similar growth with/without iron even with absence of iron and addition of bipyridyl and these results were similar to the results obtained with inducible *feoAB* and *feoABC* plasmids and Δ*feo*::*kan* cassette (Figs. 3.34 and 3.35).

To conclude, the inducible *feoAB* and *feoABC* constructs indicated a clear role for *feoC* in supporting Feo-dependent iron-restricted growth under aerobic conditions, but not under anaerobic conditions; specifically, the growth advantage was seen under reducing (ascorbic acid) and buffered (pH 6) conditions in the presence of the chelator DTPA. However, the results obtained from the single-gene *feo* mutants did not show any clear role for *feoC* in supporting Feo-dependent low-iron growth aerobically, and indeed the three mutants (Δ*feoA*, Δ*feoB* and Δ*feoC*) gave similar growth restrictions with ascorbic acid and DTPA (buffered at pH 6) under both aerobic and anaerobic conditions. The reason for this is unclear but it could be due to gene expression differences between the inducible plasmid borne *feo* genes, and the chromosomal *feo* genes. In addition, the presence of iron transporters in BW25113 (Feo, Ent, Fec, MntH, ZupT and EfeUOB), which are absent in JC32, could also provide a difference between the results obtained for the two different *feo* gene formats utilised.

In summary, these findings suggest that the role of FeoC depends on the experimental conditions and strain background. The inducible plasmid in JC32 indicated a clear role for FeoC under aerobic iron-restricted conditions (although this was not seen in BW25113) which indicates that FeoC may enhance Feo system activity. Also, it can be suggested that FeoC works as a supporting component of the Feo system improves the function of FeoB under aerobic low-iron conditions. However, under anaerobic conditions, FeoB appears to be functional without FeoC. These observations are based on growth experiments and do not confirm the exact mechanism of FeoC. The difference between JC32 and BW25113 is likely due to the presence of an array of other iron transport system in BW25113. The findings relayed here contrast with Kim et al. (2013) who found that FeoC plays a role of supporting the function of FeoAB anaerobically in *Salmonella enterica* but are consistent with Weaver et al. (2013) who indicated that FeoC is essential component for activating the Feo system in *Vibrio*

cholerae. The limitation of this is that the results are based on the growth experiment and do not directly show how the FeoC functions at the molecular level.

6.3 The role of CFeoB in supporting FeoC-dependent enhancement of FeoAB iron-uptake activity

6.3.1 Effect of the CFeoB mutation on Feo-mediated iron-restricted growth in the presence and absence of FeoC

In Chapter 4, studies on CFeoB were progressed by initially predicting residues from which this extension region is composed. This was achieved by sequence alignment and structure prediction. Thus, the CFeoB region was predicted which allowed the design of mutations aimed at disrupting CFeoB without affecting the FeoB membrane embedded domain. The identified region (residues 747-773) was predicted to be entirely located in the cytoplasm. It consisted of two conserved motifs of interest, a Cys-Cys and Cys-His amino acid pair, that may be able to act as metal ligands (Cartron *et al.*, 2006). Five distinct stop codon mutations were subsequently introduced at different positions of CFeoB by SDM, resulting in truncations that eliminated all or part of the CFeoB region. These SDMs were produced in pBADara:*feoAB* and pBADara:*feoABC* plasmids which allowed exploration of their effects in the presence and absence of FeoC. The results showed that, when the iron was absent, *feoAB* and *feoABC* did not show any growth advantages compared to the vector control. They also showed that the CFeoB mutations had little effect on growth (Fig. 4.8). However, in the presence of 1 μM DTPA, the results showed a very clear growth advantage for the *feoABC* strain with respect to the *feoAB* strain (as above). Moreover, all five CFeoB mutations showed a reduction in aerobic, iron restricted growth for the *feoABC* strain (Fig. 4.9). The results thus suggested a role of FeoC in supporting FeoAB-dependent iron-restricted growth under aerobic conditions and a role of CFeoB in mediating this impact.

When 100 mM MES (pH 6) was also included in the growth medium, there was a little difference between vector control and FeoAB/FeoABC strains which indicates that no iron-

restricted growth had been observed between the Feo strains (Fig. 4.10). The CFeoB truncations had a significant, but modest, negative effect which is possible that the truncations resulted in a FeoB impairment that caused toxicity. Interestingly, the S747Δ truncation (full CFeoB deletion) showed a major delay and decrease in growth for the *feoAB* strain but not the *feoABC* strain (Figs. 4.9A and 4.10A). When both 1 μM DTPA along with 100 mM MES were added to the growth medium, the *feoABC* strain showed a clear growth advantage with respect to the *feoAB* strain (Fig. 4.11) which indicates that the conditions of growth had achieved iron-restriction and had allowed the role of FeoC in supporting the Feo activity to be realised. The CFeoB truncations had an overall negative effect on Feo-dependent growth. For the FeoAB strain, the average growth reduction for the CFeoB truncations was ~12% whereas for the FeoABC strain this was ~19%. These findings showed that the CFeoB truncations negatively impacted FeoAB dependent growth both in the presence and absence of FeoC, but the effect was greater when the FeoC was present. The only significant impact of the CFeoB truncation on FeoABC strain was the A755Δ mutation which showed a delay and reduction in growth, but further growth analyses are required to obtain a clearer picture of this effect.

6.3.2 Effect of the CFeoB expression on FeoAB-dependent and iron-restricted growth in the presence and absence of FeoC under aerobic condition

In order to determine whether provision of CFeoB in trans could interfere with FeoC-mediated enhancement of FeoAB-dependent growth, the CFeoB-encoding region was synthesized in three formats: with a Flag-tag epitope peptide at the N-terminus; with Flag-tag at the C-terminus; and without any Flag-tag. The aim was to further explore whether CFeoB is able to interact with FeoC and interfere with the ability of FeoC to enhanced FeoAB mediated growth CFeoB is provided independently of the FeoB protein. Initially, an attempt was made to detect the Flag-CFeoB and CFeoB-Flag by anti-Flag tag western blotting when induced from the pBADrha plasmid. Unfortunately, the Flag-tagged proteins could not be detected which might be because of their low molecular weights (~3.94 kDa) or due to instability of the translation

products (Figs. 4.18-4.22). However, despite the unsuccessful attempts to detect the tagged CFeoB proteins by western blotting, the impact of all three CFeoB formats was tested on FeoABC-dependent growth under aerobic and iron-restricted conditions. The results showed that, in the absence of iron under aerobic condition, the presence of FeoAB and FeoABC constructs appears deleterious, and thus no Feo-growth advantage was apparent (Fig. 4.23). The CFeoB constructs had no effect on growth for the vector control and FeoAB strains, but two of the CFeoB constructs in the FeoABC strain caused a negative effect on growth. It is unclear how this effect was achieved given that FeoABC was inhibiting, not promoting, growth under the conditions utilised (Fig. 4.23). In the presence of 1 μM DTPA, the FeoABC strain gave a clear growth advantage indicative of FeoC-enhancement of FeoAB growth improvement. Induction of the CFeoB constructs in FeoABC-expressing strain resulted in a reduction of growth which was significant in two cases (Fig. 4.24D). However, induction of the CFeoB constructs in the FeoAB strain had a little effect on growth (Fig. 4.24E). Unexpectedly, expression of the CFeoB constructs in the vector control strain gave an increase in growth and the reason behind this effect is unclear (Fig. 4.24F). In summary, the findings thus suggest that the FeoC-improvement of FeoAB-dependent iron-limited growth can be inhibited by CFeoB (in Flag-tagged form) under aerobic and iron restricted growth. This is consistent with the suggestion that FeoC could interact with the CFeoB region of FeoB (Lau *et al*., 2015) in a manner that raises FeoAB activity.

In summary these finding suggest that the C-terminal region of FeoB contributes to support FeoC-dependent enhancement of FeoAB activity under aerobic low-iron conditions. Moreover, the reduction in growth was observed with CFeoB truncations in the presence of FeoC which indicates that this region may be essential for interaction between FeoC and FeoB. It can thus be suggested that CFeoB functions as a region of interaction with FeoC as the results shown here indicate that CFeoB reduces the ability of FeoC to enhance Feo activity. Indeed, the results

indicate that the expression of CFeoB in trans reduces growth in the FeoABC strain which supports the idea that CFeoB might interfere with FeoC function through competition or interaction. This is consistent with the previous proposal of Lau et al. (2015) who suggests that FeoC may interact with the C-terminal region of FeoB. In addition, it is an agreement with Al-Aidy (2020) who found that the FeoB C-terminal truncations in FeoB-C772S/H773G and –C763S/C764S enhanced Feo activity in the presence of FeoC under aerobic conditions, which led to the suggestion that FeoC interacts with C-terminal region of FeoB. Limitations relate to the reliance on growth experiments - the interaction between FeoC and CFeoB was not directly shown. Moreover, failure to detecting CFeoB by western blotting makes it unclear whether the protein was stably expressed. Therefore, the precise mechanism of CFeoB in FeoC role is still unclear.

6.4 The role of FeoC in global gene expression

In Chapter 5, the role of FeoC in global gene expression was explored by RNAseq. Two conditions were used; with ascorbate, at two time points (OD 0.5 and 0.8); and with iron, at two time points (OD 0.5. and 1.0). Fig. 5.10 confirms that *feoAB* and *feoABC* are highly and significantly induced by 8.8- to 18.4 log2-fold in the *feoAB* and *feoABC* strains, respectively.

6.4.1 Impact of FeoAB on global gene expression

With ascorbate, *feoAB*, *feoA* and *feoB* were induced by 10.2- to 18.3 log2 fold (Fig. 5.11). The major category of *feoAB*-induced genes was those involved in anaerobic nitrite/nitrate respiration, anaerobic C_4-dicarboxylate transport and hydrogenase 2 associated components (Table 5.2). The major category repressed were tRNA genes, amino acid biosynthesis, nucleotide metabolism, sulphur transport, the TCA cycle and ferrous iron transport (Table 5.3). At OD 0.8, the FeoAB-induced genes included those involved in amino acid generation, carbon catabolism, anaerobic nitrite/nitrate respiration, toxin/antitoxin genes and the Fur induced *sodB* gene (Table 5.4), whereas those repressed (Table 5.5) genes were involved in amino acid

biosynthesis, nucleotide metabolism and tRNA generation. In summary, for the FeoAB induction with ascorbate, three Fur-repressed genes were down regulated and one Fur-induced gene was up regulated, indicating to the FeoAB has moderately increased the cellular iron level resulting to Fe-Fur dependent function. The FeoAB induction of anaerobic energy metabolism genes may be due to the fast growth of FeoAB strain (Fig. 5.1) which may lead to decreased O_2 levels causing a switch to FNR-dependent induction anaerobic functions (Kang *et al.*, 2005). With 20 μM ferric citrate at OD 0.5, the major gene categories induced by FeoAB at OD 0.5 were anaerobic energy generation, copper export, amino acid metabolism and iron storage (which is related to an excess cellular iron) (Table 5.6). The major category repressed was 32 Fe-Fur repressed iron uptake genes (Table 5.7). At OD 1.0 with iron, the major category FeoAB-induced was 12 genes involved in anaerobic energy generation gene, and *ftn* and *ompW* (Fe-Fur induced genes) (Table 5.8). And the major category repressed was 25 genes involved in iron acquisition (and combating iron restriction) and 14 genes involved in anaerobic energy generation (Table 5.9). In summary, FeoAB induced anaerobic energy metabolism, amino acid metabolism (as with ascorbate), copper export and two Fe-Fur activated genes (Tables 5.6 & 5.8). FeoAB repressed a large number of Fur-repressed genes related to iron restriction and genes invovled in anaerobic nitrate/nitrite respiration (Tables 5.7 & 5.9). The results suggested that under aerobic and high iron conditions, FeoAB induction leads to excess iron accumulation causing a shift in Fe-Fur dependent gene control to decrease iron uptake and improve cellular-iron assimilation/storage.

6.4.2 Impact of FeoABC on global gene expression

For *feoABC* induction in the presence of ascorbate, no major functional category was apparent in the most highly FeoABC-induced genes at OD 0.5 (Table 5.10) but the major category repressed was that for amino acid metabolism (Table 5.10). At OD 0.8 with ascorbate (Table 5.11) the most highly FeoABC-induced category was amino acid metabolism (which were also

included in the FeoAB induction) and carbon metabolism. The major FeoABC repressed category was amino acid metabolism and nucleotide metabolism (some of these genes were also induced by FeoAB; Table 5.5). Only one gene related to Fur control was repressed (*efeU*) by FeoABC whereas *fepA* was repressed by FeoAB under the same conditions.

The differentially regulated genes in response to *feoABC* induction in the presence iron (Table 5.12) at OD 0.5 included nine genes involved in nitrate/nitrite respiration and *ftn*, which also induced by FeoAB under the same conditions (Table 5.6); this again suggested an excess cellular iron content resulting from *feo* induction. In addition, the major category repressed was 19 Fur-repressed genes, further indicating that *feo* induction leads to raised cellular iron uptake when excess iron is provided. The major category induced by FeoABC was the *ydhYVWX* operon possibly involved in anaerobic energy generation (Table 5.13) and two Fe-Fur induced genes (*ompW* and *ftn*) (Table 5.13); this further indicates that FeoABC mediated an increase in cellular iron in the presence of ferric citrate. The major category repressed was 15 genes involved in combating iron restriction; such effects again indicate a repression by Fe-Fur of iron-restriction systems because of an increased iron uptake mediated by FeoABC in the presence of iron.

6.4.3 Impact of FeoC on global gene expression

The *feoC* gene was induced by 10.1- to 11.7-log2 fold in the *feoABC* strain relative to the *feoAB* strain, indicating that *feoC* induction had been successful. With ascorbate at OD 0.5 (Table 5.14), FeoC caused a modest increase in carbon metabolism and genes involved in amino acid metabolism. The major category repressed was 13 genes involved in anaerobic energy generation which indicates that FeoC may play a role in down regulation of NarXL/NarQP dependent genes. At OD 0.8 with ascorbate (Table 5.15), the most abundant functional category induced by FeoC was amino acid metabolism and the major category repressed was four genes involved in cold shock. In the presence of iron at OD 0.5, the data suggest that FeoC

induced six genes involved in amino acid metabolism, six genes associated with carbon metabolism and three hydrogenase genes involved in anaerobic energy generation (Table 5.16). The major category repressed was seven and four genes involved in cysteine biosynthesis and sulphur assimilation, and motility, respectively. In addition, three genes (*yeeRST*) of unknown function and the *sodA* gene were repressed by FeoC. At OD 1.0 with iron, the major category induced by FeoC was seven genes involved in amino acid metabolism and four genes involved in nucleotide metabolism (Table 5.17). The major category repressed was six genes involved in iron acquisition. It should be noted that the *yeeRST*(*U*) operon was FeoC repressed at both OD 0.5 and 1.0, which indicates that FeoC may play a role in the repression of this operon.

In summary, these findings suggest that FeoC has a modest role in global gene expression but it can affect expression those genes involved in amino acid metabolism, carbon metabolism and anaerobic energy generation. The impacts of FeoC were less than those of FeoAB which which appears to act indirectly through its iron transport activity. Thus, it is likely that FeoC may not work as primary regulator but instead influences the gene expression indirectly by affecting FeoAB activity. In short, it can be suggested that the changes in gene expression with FeoC are likely associated with the impact on iron uptake which may change the intracellular iron level and thus affect the Fe-Fur regulated genes (Massé and Gottesman, 2002; McHugh *et al.*, 2003). Moreover, the changes in anaerobic energy metabolism may be related to oxygen availability and FNR dependent regulation (Kang *et al.*, 2005). The limitations are that the RNAseq data alone do not prove that FeoC directly regulates gene expression, or whether the observed effects are indirect. Moreover, the experiments were performed under only two conditions and two time points which may not entirely cover the role of FeoC in global expression. Thus, the role of FeoC in gene expression is still unclear and needs further research.

6.5 Conclusion and future work

To conclude, this research focused on the role of FeoC on the iron-uptake activity of the Feo system through performing comparisons under a range of iron-restriction conditions in the presence and absence of *feoC*, the interaction of FeoC with the C-terminal region of FeoB and investigating the potential regulatory role of FeoC on global gene expression by deploying an RNAseq approach. The findings indicate a clear role of FeoC in supporting Feo-mediated iron uptake aerobically but not anaerobically. In addition, the FeoB C-terminal truncations reduce FeoC-enhanced growth under iron-restricted conditions, supporting a functional interaction between FeoC and the FeoB C-terminal region. The RNA-seq analysis suggests that expression of FeoAB and FeoABC aerobically increases cellular iron levels, leading to Fur-associated regulation and enhanced expression of anaerobic energy generation genes, with FeoC potentially contributing to this effect. Further studies should investigate the complemented *feo* single mutants with pBADara- *feoA*, -*feoB* and *feoC* to confirm that *feoC* mutant does indeed impose a Feo-dependent iron-restriction growth defect. Repeating the experiments that involved Flag-tag constructs by utilising maltose-binding protein fusions instead might improve the stability of the FeoB C-terminal domain and allow its detection by western blotting. Site directed mutagenesis on the FeoC Fe-S ligands and key FeoB C-terminal residues (e.g. conserved Cys residues) would allow their role in FeoC-mediated enhancement of FeoAB iron uptake to be tested. Lastly, it would be interesting to test the effect of *feoC* expression (using a pBADara-*feoC* construct) aerobically and anaerobically on global gene expression (in a *feoC* mutant); this experiment would be supported by determining the effect of a *feoC* chromosomal mutation on global expression under a range of relevant conditions.

References

1. Al-Abri, S.S., Beeching, N.J. and Nye, F.J. (2005) 'Traveller's diarrhoea', *The Lancet infectious diseases*, 5(6), pp. 349–360.
2. Al-Aidy (2020) Molecular-genetic analysis of iron uptake in *E. coli*: Role and mechanism of Feo function and structural characterisation of target membrane protein transporter.
3. Allocati, N. *et al.* (2013) '*Escherichia coli* in Europe: an overview', *International journal of environmental research and public health*, 10(12), pp. 6235–6254.
4. Andrews *et al.* (2003) 'Bacterial iron homeostasis', *FEMS Microbiology Reviews*. Elsevier, pp. 215–237. Available at: https://doi.org/10.1016/S0168-6445(03)00055-X.
5. Andrews *et al.* (2013) 'Control of iron metabolism in Bacteria', *Metal Ions in Life Sciences*, 12, pp. 203–239. Available at: https://doi.org/10.1007/978-94-007-5561-1_7.
6. Andrews, S.C. (1998) 'Iron storage in bacteria', *Advances in microbial physiology*, 40, pp. 281–351.
7. Aslani, M.M. *et al.* (2011) 'Characterization of enteroaggregative *Escherichia coli* (EAEC) clinical isolates and their antibiotic resistance pattern', *International Journal of Infectious Diseases*, 15(2), pp. e136–e139.
8. Baba, T. *et al.* (2006) 'Construction of *Escherichia coli* K-12 in-frame, single-gene knockout mutants: The Keio collection', *Molecular Systems Biology*, 2. Available at: https://doi.org/10.1038/msb4100050.
9. Bachmann, B.J. (1972) 'Pedigrees of some mutant strains of *Escherichia coli* K-12', *Bacteriological reviews*, 36(4), pp. 525–557.
10. Baez, A. *et al.* (2022) 'Iron availability enhances the cellular energetics of aerobic Escherichia coli cultures while upregulating anaerobic respiratory chains', *New Biotechnology*, 71, pp. 11–20. Available at: https://doi.org/10.1016/j.nbt.2022.06.004.
11. Baggett, N.E., Zhang, Y. and Gross, C.A. (2017) 'Global analysis of translation termination in *E. coli*', *PLoS Genetics*, 13(3). Available at: https://doi.org/10.1371/journal.pgen.1006676.
12. Bainbridge, M.N. *et al.* (2006) 'Analysis of the prostate cancer cell line LNCaP transcriptome using a sequencing-by-synthesis approach', *BMC Genomics*, 7. Available at: https://doi.org/10.1186/1471-2164-7-246.

References

13. Bautista-De León, H. *et al.* (2013) 'Frequency of indicator bacteria, *Salmonella* and diarrhoeagenic *Escherichia coli* pathotypes on ready-to-eat cooked vegetable salads from M exican restaurants', *Letters in applied microbiology*, 56(6), pp. 414–420.
14. Bergthorsson, U. and Ochman, H. (1998) 'Distribution of chromosome length variation in natural isolates of *Escherichia coli*.', *Molecular Biology and Evolution*, 15(1), pp. 6–16.
15. Bilinski, P. *et al.* (2012) 'Public health hazards in Poland posed by foodstuffs contaminated with *E. Coli* O104: H4 bacterium from the recent European out break', *Annals of Agricultural and Environmental Medicine*, 19(1).
16. Blount, Z.D. (2015) 'The unexhausted potential of *E. coli*', *eLife*, 2015(4). Available at: https://doi.org/10.7554/eLife.05826.001.
17. Braun, V. (2001) 'Iron uptake mechanisms and their regulation in pathogenic bacteria', *International Journal of Medical Microbiology*, 291(2), pp. 67–79. Available at: https://doi.org/10.1078/1438-4221-00103.
18. Canizalez-Roman, A. *et al.* (2013) 'Prevalence and antibiotic resistance profiles of diarrheagenic *Escherichia coli* strains isolated from food items in northwestern Mexico', *International journal of food microbiology*, 164(1), pp. 36–45.
19. Cao, J. *et al.* (2007) 'EfeUOB (YcdNOB) is a tripartite, acid-induced and CpxAR-regulated, low-pH Fe^{2+} transporter that is cryptic in *Escherichia coli* K-12 but functional in *E. coli* O157:H7', *Molecular Microbiology*, 65(4), pp. 857–875. Available at: https://doi.org/10.1111/j.1365-2958.2007.05802.x.
20. Cartron *et al.* (2006) 'Feo - Transport of ferrous iron into bacteria', in *BioMetals*, pp. 143–157. Available at: https://doi.org/10.1007/s10534-006-0003-2.
21. Chervy, M., Barnich, N. and Denizot, J. (2020) 'Adherent-Invasive *E. coli*: Update on the Lifestyle of a Troublemaker in Crohn's Disease', *International Journal of Molecular Sciences*, 21(10), p. 3734.
22. Croxen, M.A. and Finlay, B.B. (2010) 'Molecular mechanisms of *Escherichia coli* pathogenicity', *Nature Reviews Microbiology*, 8(1), pp. 26–38.
23. Darfeuille-Michaud, A. (2002) 'Adherent-invasive *Escherichia coli*: a putative new E. coli pathotype associated with Crohn's disease', *International journal of medical microbiology*, 292(3–4), pp. 185–193.
24. Datsenko, K.A. and Wanner, B.L. (2000) 'One-step inactivation of chromosomal genes in *Escherichia coli* K-12 using PCR products', *Proceedings of the National Academy of Sciences*, 97(12), pp. 6640–6645.

References

25. Denamur, E. *et al.* (2021) 'The population genetics of pathogenic *Escherichia coli*', *Nature Reviews Microbiology*, 19(1), pp. 37–54.
26. Didelot, X. *et al.* (2012) 'Impact of homologous and non-homologous recombination in the genomic evolution of *Escherichia coli*', *BMC genomics*, 13(1), pp. 1–15.
27. Eren, E. *et al.* (2024) 'Encapsulated Ferritin-like Proteins: A Structural Perspective', *Biomolecules*. Multidisciplinary Digital Publishing Institute (MDPI). Available at: https://doi.org/10.3390/biom14060624.
28. Fetherston, J.D. *et al.* (2012) 'The Yfe and Feo transporters are involved in microaerobic growth and virulence of *Yersinia pestis* in bubonic plague', *Infection and immunity*, 80(11), pp. 3880–3891.
29. Ford, D.C. *et al.* (2014) 'Construction of an inducible system for the analysis of essential genes in *Yersinia pestis'*, *Journal of microbiological methods*, 100, pp. 1–7.
30. Gaschignard, J. *et al.* (2011) 'Neonatal bacterial meningitis: 444 cases in 7 years', *The Pediatric infectious disease journal*, 30(3), pp. 212–217.
31. Ge, R. and Sun, X. (2012) 'Iron trafficking system in *Helicobacter pylori*', *Biometals*, 25(2), pp. 247–258.
32. Giuliano, M.G. and Engl, C. (2021) 'The lifecycle of ribosomal RNA in bacteria', in *RNA Damage and Repair*. Springer International Publishing, pp. 27–51. Available at: https://doi.org/10.1007/978-3-030-76571-2_2.
33. Gómez-Garzón, C., Barrick, J.E. and Payne, S.M. (2022) 'Disentangling the Evolutionary History of Feo, the Major Ferrous Iron Transport System in Bacteria'. Available at: https://doi.org/10.6084/m9.figshare.17082758.
34. Good, N.E. and Izawa, S.B.T.-M. in E. (1972) '[3] Hydrogen ion buffers', in *Photosynthesis and Nitrogen Fixation Part B*. Academic Press, pp. 53–68. Available at: https://doi.org/https://doi.org/10.1016/0076-6879(72)24054-X.
35. Grainger, D.C. *et al.* (2007) 'Transcription factor distribution in *Escherichia coli*: Studies with FNR protein', *Nucleic Acids Research*, 35(1), pp. 269–278. Available at: https://doi.org/10.1093/nar/gkl1023.
36. Guo *et al.* (2011) 'Tn5AraOut mutagenesis for the identification of *Yersinia pestis* genes involved in resistance towards cationic antimicrobial peptides', *Microbial Pathogenesis*, 51(3), pp. 121–132. Available at: https://doi.org/10.1016/j.micpath.2011.04.010.

37. Hantke, K. (1987) 'Ferrous iron transport mutants in *Escherichia coli* K12', *FEMS Microbiology Letters*, 44(1), pp. 53–57. Available at: https://doi.org/10.1111/j.1574-6968.1987.tb02241.x.
38. Hantke, K. (2003) 'Is the bacterial ferrous iron transporter FeoB a living fossil?', *Trends in Microbiology* [Preprint]. Available at: https://doi.org/10.1016/S0966-842X(03)00100-8.
39. Hayashi, K. *et al.* (2006) 'Highly accurate genome sequences of *Escherichia coli* K-12 strains MG1655 and W3110', *Molecular systems biology*, 2(1), pp. 7–2006.
40. Hsueh, K.-L. *et al.* (2013) 'FeoC from *Klebsiella pneumoniae* contains a [4Fe-4S] cluster', *Journal of Bacteriology*, 195(20), pp. 4726–4734.
41. Hung *et al.* (2012) 'NMR structure note: The ferrous iron transport protein C (FeoC) from *Klebsiella pneumoniae*', *Journal of Biomolecular NMR*, 53(2), pp. 161–165. Available at: https://doi.org/10.1007/s10858-012-9633-6.
42. Ilari, A. *et al.* (2000) 'The dodecameric ferritin from *Listeria innocua* contains a novel intersubunit iron-binding site', *Nature Structural Biology*, 7(1), pp. 38–43.
43. Imbeaud, S. *et al.* (2005) 'Towards standardization of RNA quality assessment using user-independent classifiers of microcapillary electrophoresis traces', *Nucleic Acids Research*, 33(6), pp. 1–12. Available at: https://doi.org/10.1093/nar/gni054.
44. Johnson, E.E. and Wessling-Resnick, M. (2012) 'Iron metabolism and the innate immune response to infection', *Microbes and Infection*, 14(3), pp. 207–216.
45. Johnson, J.R. and Stell, A.L. (2000) 'Extended virulence genotypes of *Escherichia coli* strains from patients with urosepsis in relation to phylogeny and host compromise', *The Journal of Infectious Diseases*, 181(1), pp. 261–272.
46. Johnson, T.J. *et al.* (2007) 'The genome sequence of avian pathogenic *Escherichia coli* strain O1: K1: H7 shares strong similarities with human extraintestinal pathogenic *E. coli* genomes', *Journal of Bacteriology*, 189(8), pp. 3228–3236.
47. Jumper, J. *et al.* (2021) 'Highly accurate protein structure prediction with AlphaFold', *Nature*, 596(7873), pp. 583–589. Available at: https://doi.org/10.1038/s41586-021-03819-2.
48. Kallonen, T. *et al.* (2017) 'Systematic longitudinal survey of invasive *Escherichia coli* in England demonstrates a stable population structure only transiently disturbed by the emergence of ST131', *Genome research*, 27(8), pp. 1437–1449.
49. Kang, Y. *et al.* (2005) 'Genome-wide expression analysis indicates that FNR of *Escherichia coli* K-12 regulates a large number of genes of unknown function',

Journal of Bacteriology, 187(3), pp. 1135–1160. Available at: https://doi.org/10.1128/JB.187.3.1135-1160.2005.

50. Kaper *et al.* (2004) 'Pathogenic *Escherichia coli*', *Nature Reviews Microbiology*, 2(2), p. 123.
51. Kathayat, D. *et al.* (2021) 'Avian pathogenic *Escherichia coli* (APEC): an overview of virulence and pathogenesis factors, zoonotic potential, and control strategies', *Pathogens*, 10(4), p. 467.
52. Kim *et al.* (2012) 'The FeoA protein is necessary for the FeoB transporter to import ferrous iron', *Biochemical and Biophysical Research Communications*, 423(4), pp. 733–738. Available at: https://doi.org/10.1016/j.bbrc.2012.06.027.
53. Kim *et al.* (2013) 'The FeoC protein leads to high cellular levels of the Fe(II) transporter FeoB by preventing FtSH protease regulation of FeoB in *Salmonella enterica*', *Journal of Bacteriology*, 195(15), pp. 3364–3370. Available at: https://doi.org/10.1128/JB.00343-13.
54. Kim *et al.* (2015) 'Lon-mediated proteolysis of the FeoC protein prevents *Salmonella enterica* from accumulating the Fe(II) transporter FeoB under high-oxygen conditions', *Journal of Bacteriology*, 197(1), pp. 92–98. Available at: https://doi.org/10.1128/JB.01826-14.
55. Krewulak, K.D. and Vogel, H.J. (2008) 'Structural biology of bacterial iron uptake', *Biochimica et Biophysica Acta (BBA)-Biomembranes*, 1778(9), pp. 1781–1804.
56. Kumar, P. and Libchaber, A. (2013) 'Pressure and temperature dependence of growth and morphology of *Escherichia coli*: experiments and stochastic model', *Biophysical journal*, 105(3), pp. 783–793.
57. Lau *et al.* (2013) 'Solution structure of *Escherichia coli* FeoA and its potential role in bacterial ferrous iron transport', *Journal of Bacteriology*, 195(1), pp. 46–55. Available at: https://doi.org/10.1128/JB.01121-12.
58. Lau *et al.* (2015) 'Bacterial ferrous iron transport: The Feo system', *FEMS Microbiology Reviews*, 40(2), pp. 273–298. Available at: https://doi.org/10.1093/femsre/fuv049.
59. Lim, J.Y., Yoon, J.W. and Hovde, C.J. (2010) 'A brief overview of *Escherichia coli* O157: H7 and its plasmid O157', *Journal of Microbiology and Biotechnology*, 20(1), p. 5.

References

60. Lima, T. *et al.* (2009) 'HAMAP: a database of completely sequenced microbial proteome sets and manually curated microbial protein families in UniProtKB/Swiss-Prot', *Nucleic Acids Research*, 37(suppl_1), pp. D471–D478.
61. Liu, X. *et al.* (2020) 'The effects of kanamycin concentration on gene transcription levels in *Escherichia coli*', *3 Biotech*, 10(3). Available at: https://doi.org/10.1007/s13205-020-2100-2.
62. Lu, S. *et al.* (2016) 'Insights into the evolution of pathogenicity of *Escherichia coli* from genomic analysis of intestinal *E. coli* of Marmota himalayana in Qinghai–Tibet plateau of China', *Emerging Microbes & Infections*, 5(1), pp. 1–9.
63. Lukjancenko, O., Wassenaar, T.M. and Ussery, D.W. (2010) 'Comparison of 61 sequenced *Escherichia coli* genomes', *Microbial ecology*, 60(4), pp. 708–720.
64. Massé, E. and Gottesman, S. (2002) 'A small RNA regulates the expression of genes involved in iron metabolism in *Escherichia coli*', *Proceedings of the National Academy of Sciences*, 99(7), pp. 4620–4625.
65. McHugh, J.P. *et al.* (2003) 'Global iron-dependent gene regulation in *Escherichia coli*: A new mechanism for iron homeostasis', *Journal of Biological Chemistry*, 278(32), pp. 29478–29486. Available at: https://doi.org/10.1074/jbc.M303381200.
66. Messenger, A.J.M. and Barclay, R. (1983) 'Bacteria, iron and pathogenicity', *Biochemical Education*, 11(2), pp. 54–63.
67. Mey *et al.* (2021) *Iron Transport and Metabolism in Escherichia, Shigella, and Salmonella*. Available at: https://journals.asm.org/journal/ecosalplus.
68. Nataro, J.P. and Kaper, J.B. (1998) 'Diarrheagenic *Escherichia coli*', *Clinical Microbiology Reviews*, 11(1), pp. 142–201.
69. Nataro, J.P., Steiner, T. and Guerrant, R.L. (1998) 'Enteroaggregative *Escherichia coli*.', *Emerging Infectious Diseases*, 4(2), p. 251.
70. Negroni, A. *et al.* (2012) 'Characterization of adherent-invasive *Escherichia coli* isolated from pediatric patients with inflammatory bowel disease', *Inflammatory Bowel Diseases*, 18(5), pp. 913–924.
71. Noor, R. *et al.* (2013) 'Influence of temperature on *Escherichia coli* growth in different culture media', *J Pure Appl Microbiol*, 7(2), pp. 899–904.
72. Orzel, B. *et al.* (2023) 'Fe(II), Mn(II), and Zn(II) Binding to the C-Terminal Region of FeoB Protein: An Insight into the Coordination Chemistry and Specificity of the *Escherichia coli* Fe(II) Transporter', *Inorganic Chemistry*, 62(45), pp. 18607–18624. Available at: https://doi.org/10.1021/acs.inorgchem.3c02910.

References

73. Orzel, B. *et al.* (2025) 'The Coordination Chemistry of Two Peptidic Models of NFeoB and Core CFeoB Regions of FeoB Protein: Complexes of Fe(II), Mn(II), and Zn(II)', *Inorganic Chemistry* [Preprint]. Available at: https://doi.org/10.1021/acs.inorgchem.4c05111.
74. Parrow *et al.* (2013) 'Sequestration and scavenging of iron in infection', *Infection and immunity*, 81(10), pp. 3503–3514.
75. Paterson, J.R. *et al.* (2022) *Insights into the Antibacterial Mechanism of Action of Chelating Agents by Selective Deprivation of Iron, Manganese, and Zinc*. Available at: https://journals.asm.org/journal/aem.
76. Pouillot, F. *et al.* (2012) 'Efficacy of bacteriophage therapy in experimental sepsis and meningitis caused by a clone O25b: H4-ST131 *Escherichia coli* strain producing CTX-M-15', *Antimicrobial agents and chemotherapy*, 56(7), pp. 3568–3575.
77. Qadri, F. *et al.* (2005) 'Enterotoxigenic *Escherichia coli* in developing countries: epidemiology, microbiology, clinical features, treatment, and prevention', *Clinical Microbiology Reviews*, 18(3), pp. 465–483.
78. Rasko, D.A. *et al.* (2008) 'The pangenome structure of *Escherichia coli*: comparative genomic analysis of *E. coli* commensal and pathogenic isolates', *Journal of Bacteriology*, 190(20), pp. 6881–6893.
79. Rodriguez-Siek, K.E. *et al.* (2005) 'Comparison of *Escherichia coli* isolates implicated in human urinary tract infection and avian colibacillosis', *Microbiology*, 151(6), pp. 2097–2110.
80. Romeo, A.M. *et al.* (2001) 'Intracellular chelation of iron by bipyridyl inhibits DNA virus replication: Ribonucleotide reductase maturation as a probe of intracellular iron pools', *Journal of Biological Chemistry*, 276(26), pp. 24301–24308. Available at: https://doi.org/10.1074/jbc.M010806200.
81. Sambrook, J. and Russell, D.W. (2001) 'Molecular cloning: A laboratory manual, the third edition'. Cold spring harbor laboratory press, cold spring harbor, New York.
82. Sawers, R.G., Blokesch, M. and Böck, A. (2004) 'Anaerobic Formate and Hydrogen Metabolism', *EcoSal Plus*, 1(1). Available at: https://doi.org/10.1128/ecosalplus.3.5.4.
83. Servin, A.L. (2005) 'Pathogenesis of Afa/Dr diffusely adhering *Escherichia coli*', *Clinical Microbiology Reviews*, 18(2), pp. 264–292.

References

84. Stark, R., Grzelak, M. and Hadfield, J. (2019) 'RNA sequencing: the teenage years', *Nature Reviews Genetics*. Nature Publishing Group, pp. 631–656. Available at: https://doi.org/10.1038/s41576-019-0150-2.
85. Stewart, V. and Bledsoe, P.J. (2003) 'Synthetic lac operator substitutions for studying the nitrate- and nitrite-responsive NarX-NarL and NarQ-NarP two-component regulatory systems of *Escherichia coli* K-12', *Journal of Bacteriology*, 185(7), pp. 2104–2111. Available at: https://doi.org/10.1128/JB.185.7.2104-2111.2003.
86. Touchon, M. *et al.* (2009) 'Organised genome dynamics in the *Escherichia coli* species results in highly diverse adaptive paths', *PLoS genetics*, 5(1), p. e1000344.
87. Touchon, M. *et al.* (2020) 'Phylogenetic background and habitat drive the genetic diversification of *Escherichia coli*', *PLoS genetics*, 16(6), p. e1008866.
88. Weaver, E.A. *et al.* (2013) 'FeoA and FeoC are essential components of the *Vibrio cholerae* ferrous iron uptake system, and FeoC interacts with FeoB', *Journal of Bacteriology*, 195(21), pp. 4826–4835. Available at: https://doi.org/10.1128/JB.00738-13.
89. Weintraub, A. (2007) 'Enteroaggregative *Escherichia coli*: epidemiology, virulence and detection', *Journal of Medical Microbiology*, 56(1), pp. 4–8

Appendix

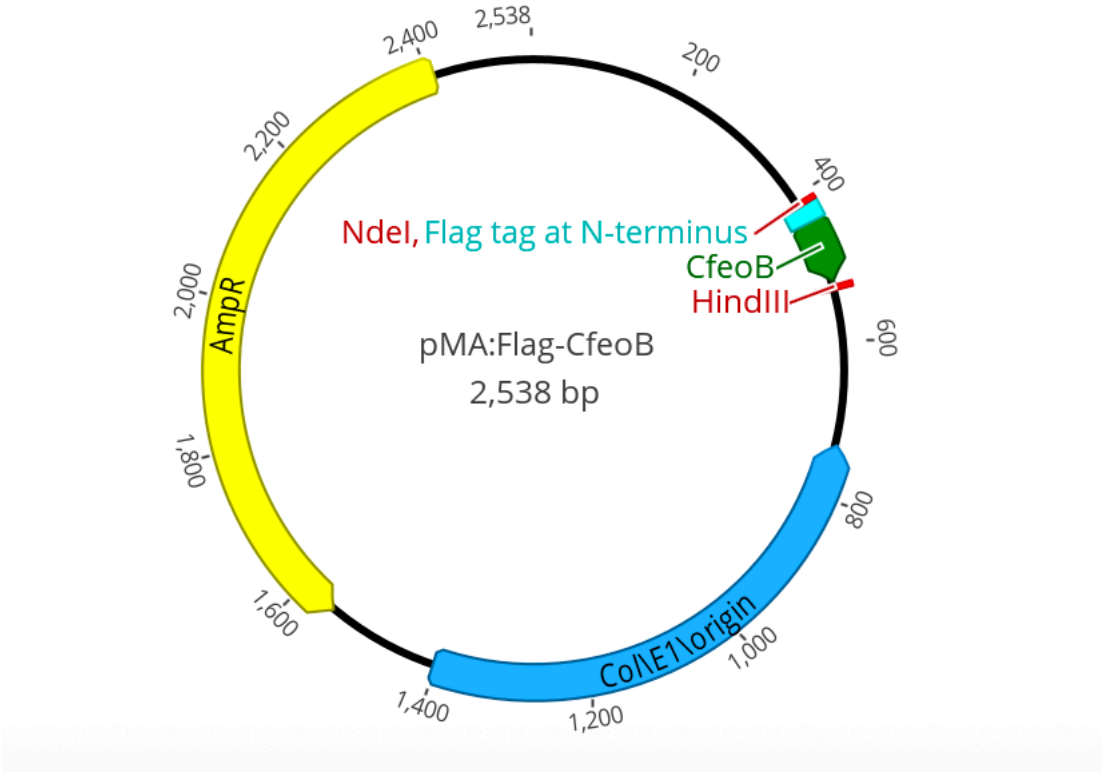

Figure A.1: Plasmid map of pMA:Flag-*CfeoB*. The C-terminal tail encoding region of *feoB* with Flag tag at the N-terminus (in green, 164 bp) cloned between *Nde*I and *Hin*dIII sites in pMA-T. Plasmid map generated using Geneious Prime.

I.
GTAATGAAATTCAGCAGGATCACATATGGACTACAAAGACGATGACGACAAGAGCCGGG
TGGATATCGAACTGCTGGCAACCCGCAAGTCGGTAAGCAGTTGCTGCGCAGCCAGCACC
ACCGGTGATTGCCATTAATAAAAGCTTGGCTGTTTTGGCGGATGAG

II.
MDYKDDDDKSRVDIELLATRKSVSSCCAASTTGDCH

Figure A.2: The synthetic Flag-tag-*CfeoB* sequence of pMA:Flag-*CfeoB*. I. Nucleotide sequence (164 bp). **II.** Amino acid sequence (~3.94 kDa). Flag-tag region in cyan; start/stop codons in red; CfeoB region in green; *Nde*I and *Hin*dIII sites, underscored.

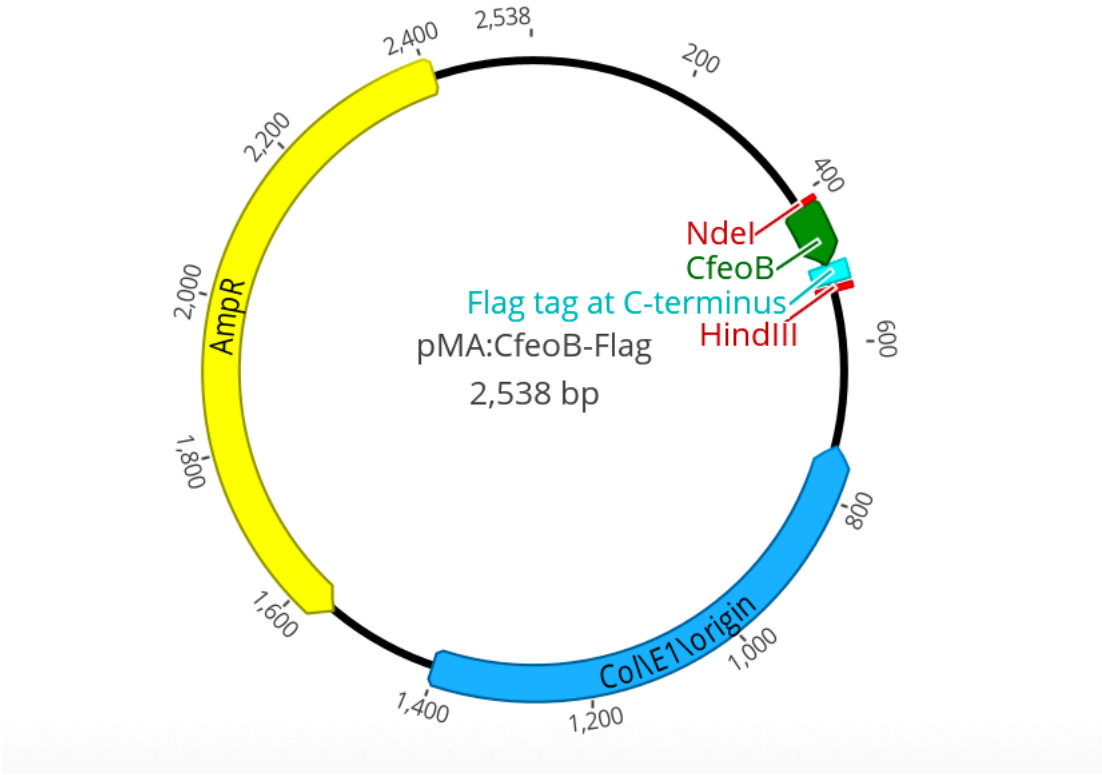

Figure A.3: Plasmid map of pMA:*CfeoB*-Flag. The C-terminal tail encoding region of *feoB* with Flag tag at the C-terminus (in green, 164 bp) cloned between *Nde*I and *Hin*dIII sites in pMA-T. Plasmid map generated using Geneious Prime.

I.
GTAATGAAATTCAGCAGGATCACATATGAGCCGGGTGGATATCGAACTGCTGGCAACCC
GCAAGTCGGTAAGCAGTTGCTGCGCAGCCAGCACCACCGGTGATTGCCATGACTACAAA
GACGATGACGACAAGTAATAAAAGCTTGGCTGTTTTGGCGGATGAG

II.
MSRVDIELLATRKSVSSCCAASTTGDCHDYKDDDDK

Figure A.4: The synthetic *CfeoB*-Flag-tag sequence of pMA:Flag-*CfeoB*. I. Nucleotide sequence (164 bp). **II.** Amino acid sequence (~3.94 kDa). Flag-tag region in cyan; start/stop codons in red; CfeoB region in green; *Nde*I and *Hin*dIII sites, underscored.

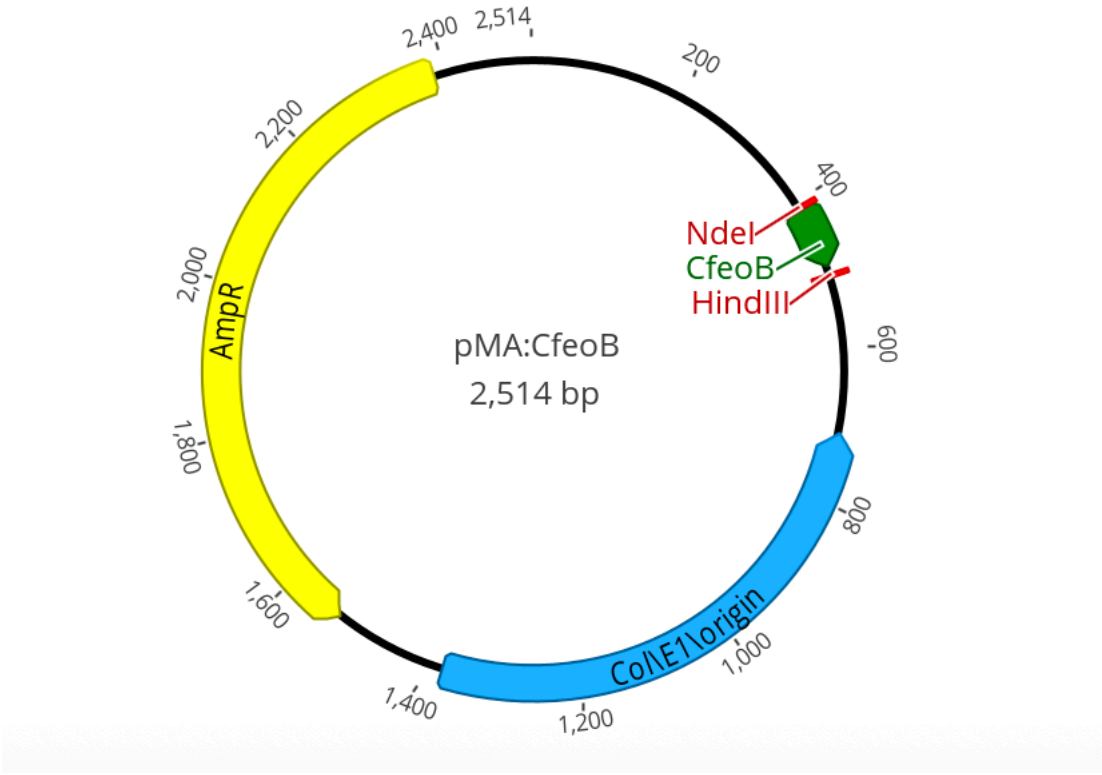

Figure A.5: Plasmid map of pMA:*CfeoB*. The C-terminal tail encoding region of *feoB* without any Flag tag (in green, 140 bp) cloned between *Nde*I and *Hin*dIII sites in pMA-T. Plasmid map generated using Geneious Prime.

I.
GTAATGAAATTCAGCAGGATCACATATGAGCCGGGTGGATATCGAACTGCTGGCAACCC
GCAAGTCGGTAAGCAGTTGCTGCGCAGCCAGCACCACCGGTGATTGCCATTAATAAAAG
CTTGGCTGTTTTGGCGGATGAG

II.
MSRVDIELLATRKSVSSCCAASTTGDCH

Figure A.6: The synthetic *CfeoB* sequence (no Flag tag) of pMA:*CfeoB*. I. Nucleotide sequence (140 bp). **II.** Amino acid sequence (~2.94 kDa). Start/stop codons in red; CfeoB region in green; *Nde*I and *Hin*dIII sites, underscored.

Appendix

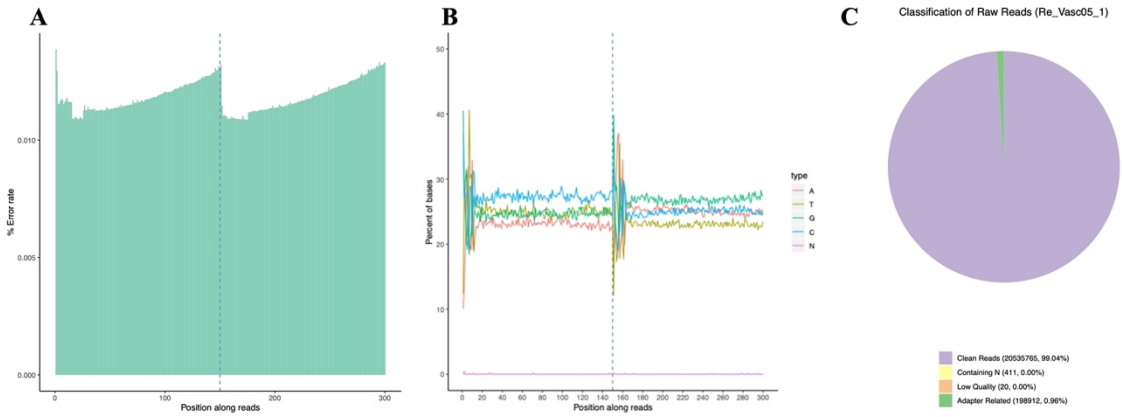

Figure A.7: Error rate and GC content of RNAseq reads. (A) Error rate for an example paired 150 nucleotide reads. (**B**) Base content for an example paired read. (**C**) Quality of raw reads. These data are representational and are for that of a single sample (Vasc05_1) only.

Table A.1: Summary of data quality. This table indicates the data quality for all 36 samples and includes the probability of incorrect base calling at 1 in 100 and 1 in 1000 sequencing reads (Q20 and Q30).

No	Sample name	Raw reads	Clean reads	Raw bases	Clean bases	Error rate (%)	Q20 (%)	Q30 (%)	GC content (%)
1	Re_Vasc05_1	41470216	41071530	6.2G	6.2G	0.01	98.77	96.35	51.94
2	Re_Vasc05_2	43875070	43274062	6.6G	6.5G	0.01	98.78	96.39	51.94
3	Re_Vasc05_3	45998654	45517690	6.9G	6.8G	0.01	98.74	96.25	52.07
4	Re_Vasc08_4	55850786	55265890	8.4G	8.3G	0.01	98.64	96.03	51.93
5	Re_Vasc08_5	43674786	43288152	6.6G	6.5G	0.01	98.75	96.27	51.94
6	Re_Vasc08_6	51388212	50863540	7.7G	7.6G	0.01	98.77	96.35	52.02
7	Re_ABasc05_7	54379372	52996228	8.2G	7.9G	0.01	98.74	96.32	51.99
8	Re_ABasc05_8	40473740	39668928	6.1G	6.0G	0.01	98.75	96.39	51.88
9	Re_ABasc05_9	50443688	49435152	7.6G	7.4G	0.01	98.74	96.36	51.85
10	ReABasc08_10	51144640	50307980	7.7G	7.5G	0.01	98.78	96.45	52.11
11	ReABasc08_11	49021288	48010024	7.4G	7.2G	0.01	98.74	96.37	52.27
12	ReABasc08_12	47060752	45760054	7.1G	6.9G	0.01	98.71	96.36	52.21
13	RABCasc05_13	45127162	44168034	6.8G	6.6G	0.01	98.74	96.34	51.96
14	RABCasc05_14	47248118	46493980	7.1G	7.0G	0.01	98.74	96.31	51.97
15	RABCasc05_15	48120148	46624612	7.2G	7.0G	0.01	98.73	96.35	52.09
16	RABCasc08_16	56206832	54904652	8.4G	8.2G	0.01	98.75	96.4	52.13
17	RABCasc08_17	57025492	55731312	8.6G	8.4G	0.01	98.74	96.37	52.1
18	RABCasc08_18	53419950	52653556	8.0G	7.9G	0.01	98.72	96.29	52.14
19	v_Fe_05_19	55903414	54431132	8.4G	8.2G	0.01	98.75	96.36	52.13
20	v_Fe_05_20	49708224	45354524	7.5G	6.8G	0.01	98.61	96.13	52.23
21	v_Fe_05_21	47624526	46688472	7.1G	7.0G	0.01	98.77	96.38	52.16
22	v_Fe_1_22	45072796	44520596	6.8G	6.7G	0.01	98.82	96.47	51.85

23	v_Fe_1_23	43030608	42360552	6.5G	6.4G	0.01	98.8	96.45	51.84
24	v_Fe_1_24	45266140	44601084	6.8G	6.7G	0.01	98.81	96.49	51.8
25	AB_Fe_05_25	44342402	43519240	6.7G	6.5G	0.01	98.79	96.42	51.89
26	AB_Fe_05_26	39348356	38561142	5.9G	5.8G	0.01	98.81	96.47	51.96
27	AB_Fe_05_27	44575794	43680130	6.7G	6.6G	0.01	98.81	96.46	52.02
28	ABFe_1_28	44534832	43607904	6.7G	6.5G	0.01	98.77	96.41	51.94
29	ABFe_1_29	50268520	49342558	7.5G	7.4G	0.01	98.79	96.4	51.78
30	ABFe_1_30	49044876	48330938	7.4G	7.2G	0.01	98.8	96.43	51.78
31	ABCFe05_31	58453558	56693384	8.8G	8.5G	0.01	98.77	96.4	51.96
32	ABCFe05_32	48876018	48220210	7.3G	7.2G	0.01	98.8	96.41	51.86
33	ABCFe05_33	46610848	46085280	7.0G	6.9G	0.01	98.8	96.42	51.86
34	ABCFe_1_34	51556346	51098270	7.7G	7.7G	0.01	98.75	96.32	51.95
35	ABCFe_1_35	47079820	46622960	7.1G	7.0G	0.01	98.79	96.38	51.84
36	ABCFe_1_36	44662790	44257320	6.7G	6.6G	0.01	98.79	96.38	51.79

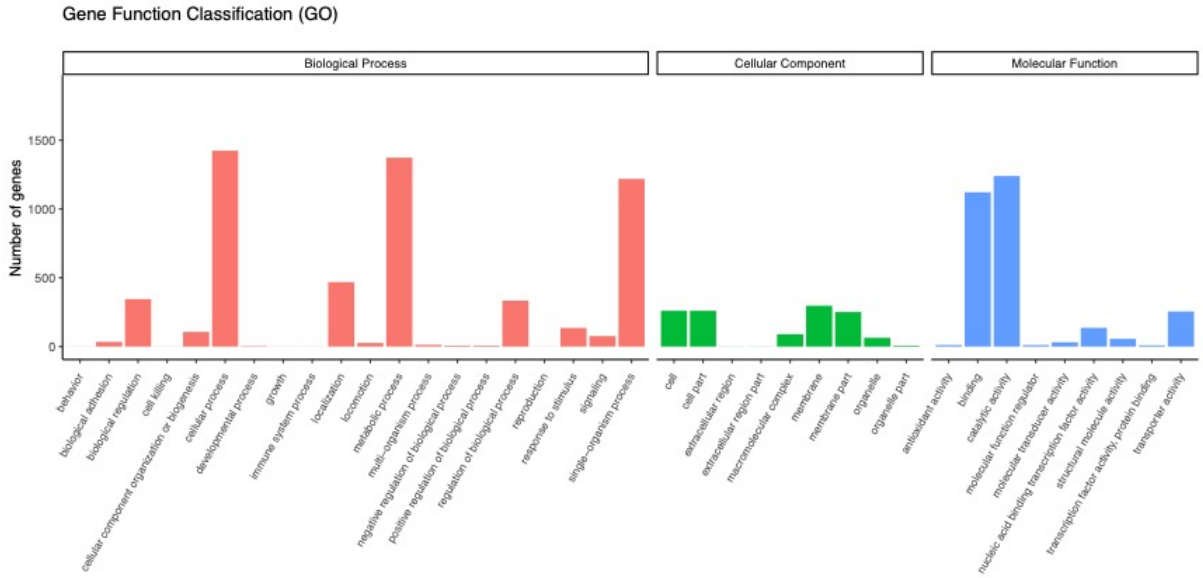

Figure A.8: Gene function classification (GO terms). This graph provides a summary of the functional classification for all 2807 genes that were annotated within the total data set, classified according to GO terms.

Appendix

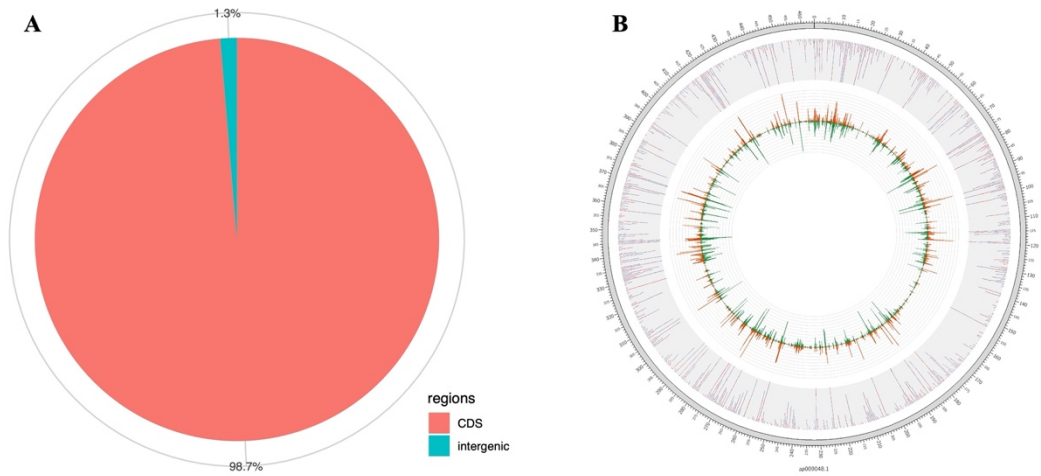

Figure A.9: Summary of transcripts mapped to genes in the E. coli W3110 genome. (**A**) Proportion of transcripts mapped >98%). (**B**) Position of mapped transcripts on the circular genome (scale give in 10^4 bp) together with relative read level. Data is for one representative sample (Vasc05_1).

Table A.2: Summary of mapping results for all 36 samples. This table indicates a high mapping rate (~94-98%) for all 36 samples with relatively low multiple mapping rates (as expected, due to rRNA depletion).

Sample name	Re_Vasc05_1	Re_Vasc05_2	Re_Vasc05_3	Re_Vasc08_4	Re_Vasc08_5	Re_Vasc08_6	Re_ABasc05_7	Re_ABasc05_8	Re_ABasc05_9	ReABasc08_10	ReABasc08_11	ReABasc08_12	RABCasc05_13	RABCasc05_14	RABCasc05_15	RABCasc08_16	RABCasc08_17	RABCasc08_18
Total reads	41071530	43274062	45517690	55265890	43288152	50863540	52996228	39668928	49435152	50307980	48010024	45760054	44168034	46493980	46624612	54904652	55731312	52653556
Total mapped reads	40371544	42532379	44562258	54269049	42605412	49901985	51727188	38483204	46900172	48546313	46332408	42848432	42148389	44626268	44779518	51491621	53039265	50365743
Uniquely mapped reads	39233351	41263277	43290620	52627167	41479348	48485920	50188518	37448871	45657342	47309720	45137480	41643960	40979021	43422335	43385215	50077494	51543120	48938941
Multiple mapped reads	1138193	1269102	1271638	1641882	1126064	1416065	1538670	1034333	1242830	1236593	1194928	1204472	1169368	1203933	1394303	1414127	1496145	1426802
Total mapping rate	98.30%	98.29%	97.90%	98.20%	98.42%	98.11%	97.61%	97.01%	94.87%	96.50%	96.51%	93.64%	95.43%	95.98%	96.04%	93.78%	95.17%	95.65%
Uniquely mapping rate	95.52%	95.35%	95.11%	95.23%	95.82%	95.33%	94.70%	94.40%	92.36%	94.04%	94.02%	91.01%	92.78%	93.39%	93.05%	91.21%	92.49%	92.95%
Multiple mapping rate	2.77%	2.93%	2.79%	2.97%	2.60%	2.78%	2.90%	2.61%	2.51%	2.46%	2.49%	2.63%	2.65%	2.59%	2.99%	2.58%	2.68%	2.71%

Sample name	v_Fe_05_19	v_Fe_05_20	v_Fe_05_21	v_Fe_1_22	v_Fe_1_23	v_Fe_1_24	AB_Fe_05_25	AB_Fe_05_26	AB_Fe_05_27	ABFe_1_28	ABFe_1_29	ABFe_1_30	ABCFe05_31	ABCFe05_32	ABCFe05_33	ABCFe_1_34	ABCFe_1_35	ABCFe_1_36
Total reads	54431132	45354524	46688472	44520596	42360552	44601084	43519240	38561142	43680130	43607904	49342558	48330938	56693384	48220210	46085280	51098270	46622960	44257320
Total mapped reads	53038947	44074127	45916846	43084718	41662213	43875509	42357664	37590292	42520935	42410100	47935313	46874184	55283212	47003830	44956474	49755136	45281498	43028700
Uniquely mapped reads	51524780	41874107	44813912	41999311	40542784	42732613	41217647	36600070	41354356	41185324	46722603	45667173	53708376	45855058	43888943	48391583	44081833	41955489
Multiple mapped reads	1514167	2200020	1102934	1085407	1119429	1142896	1140017	990222	1166579	1224776	1212710	1207011	1574836	1148772	1067531	1363553	1199665	1073211
Total mapping rate	97.44%	97.18%	98.35%	96.77%	98.35%	98.37%	97.33%	97.48%	97.35%	97.25%	97.15%	96.99%	97.51%	97.48%	97.55%	97.37%	97.12%	97.22%
Uniquely mapping rate	94.66%	92.33%	95.98%	94.34%	95.71%	95.81%	94.71%	94.91%	94.68%	94.44%	94.69%	94.49%	94.73%	95.10%	95.23%	94.70%	94.55%	94.80%
Multiple mapping rate	2.78%	4.85%	2.36%	2.44%	2.64%	2.56%	2.62%	2.57%	2.67%	2.81%	2.46%	2.50%	2.78%	2.38%	2.32%	2.67%	2.57%	2.42%

Appendix

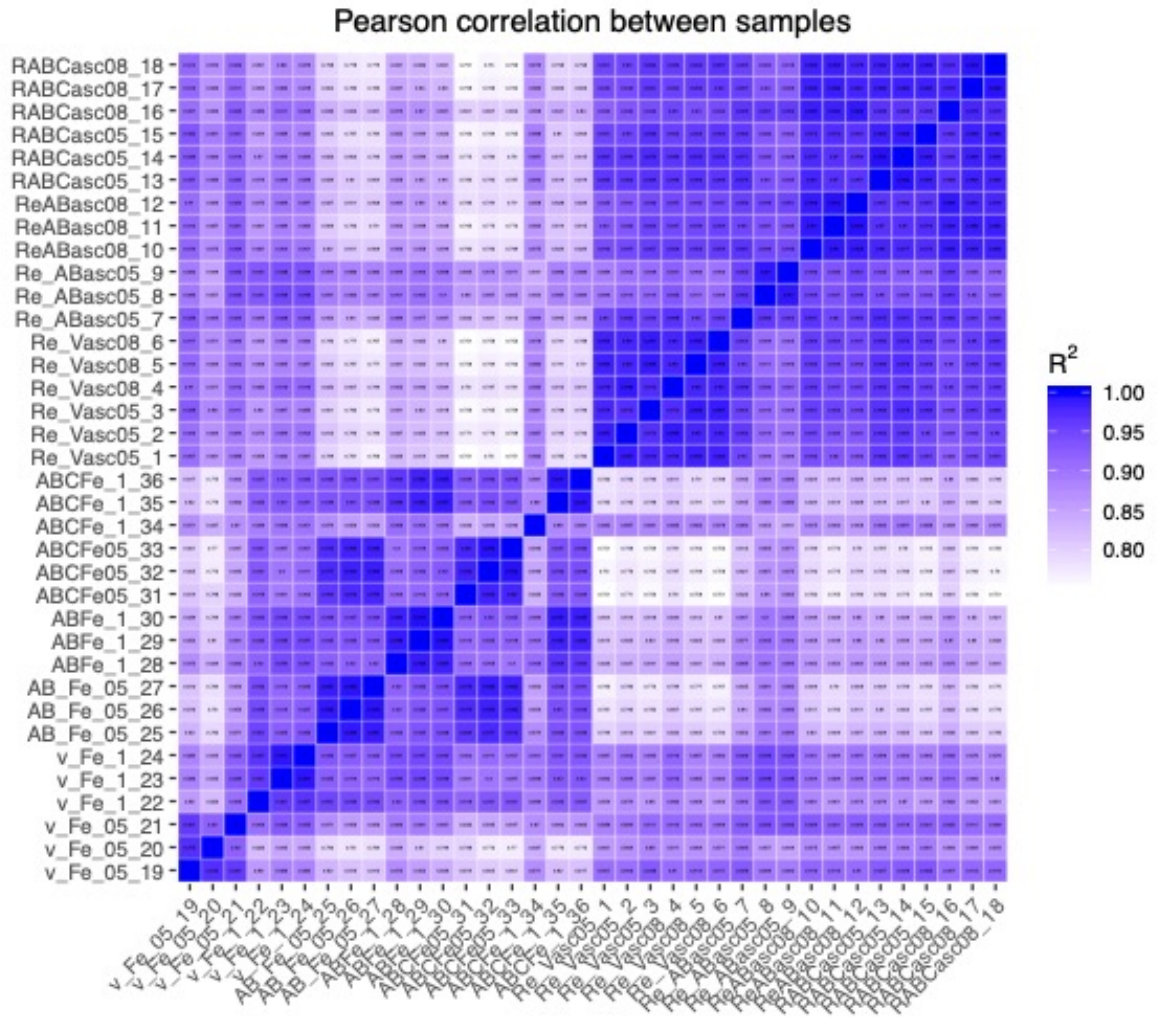

Figure A.10: Comparison of RNAseq sample data by Pearson correlation.